Modelling sleep-wake regulation:
The dynamics, bifurcations and applications of the two process model

Matthew Peter Bailey

Thesis submitted to the University of Surrey
for the degree of Doctor of Philosophy

Department of Mathematics
University of Surrey
Guildford GU2 7XH, United Kingdom

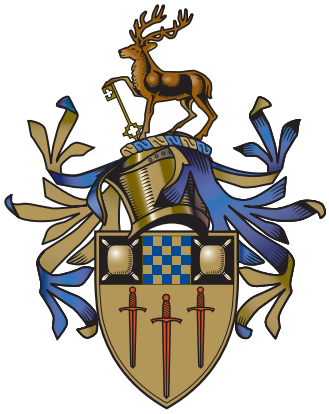

E-mail address: matthew.bailey@surrey.ac.uk

Declaration of originality

This thesis and the work to which it refers are the results of my own efforts. Any ideas, data, images or text resulting from the work of others (whether published or unpublished) are fully identified as such within the work and attributed to their originator in the text, bibliography or in footnotes. This thesis has not been submitted in whole or in part for any other academic degree or professional qualification. I agree that the University has the right to submit my work to the plagiarism detection service TurnitinUK for originality checks. Whether or not drafts have been so-assessed, the University reserves the right to require an electronic version of the final document (as submitted) for assessment as above.

Signed: _____ Date: _____

Matthew Peter Bailey

Abstract

Sleep is essential for most living things to function. Many features of sleep are not yet understood however, mathematical models are playing an important role in developing our understanding of many of the physiological properties of sleep. We introduce the most well-known model of sleep regulation, the two process model which proposes that sleep-wake cycles can be modelled by the interaction between two oscillators. This ostensibly simple model is an interesting example of a nonsmooth dynamical system whose rich dynamical structure has been relatively unexplored. A key aim of this work is to further understand how transitions between monophasic (one sleep a day) and polyphasic (many sleeps a day) sleep occur in the two process model.

The two process model can be framed as a one-dimensional map of the circle which, for some parameter regimes, has gaps. As is a feature of continuous circle maps the bifurcation set consists of saddle-node Arnold tongues. We show that border collision bifurcations that arise naturally in maps with gaps extend and supplement these tongues. We see how the periodic solutions that are created by saddle-node bifurcations in continuous maps transition to periodic solutions created by period-adding bifurcations as seen in maps with gaps. With this deeper understanding of the dynamics and bifurcation structure of the two process model we use modified versions of the model to explain two experimental data sets.

An ultradian rhythm is a recurrent period or cycle which repeats multiple times across the day. We consider the sleep wake patterns of a the common vole, *Microtus Arvalis*, which has ultradian rest activity and feeding patterns. By deriving parameters for the two process model from EEG data and sleep/ wake onset times we are able to simulate with high accuracy the key features of spontaneous sleep-wake patterns in the voles. However, to explain phenomena seen in sleep deprivation experiments we include a high amplitude ultradian oscillation alongside the circadian, the results allow us to give some physiological insight into the internal mechanisms which drive sleep/wake onset times in the common vole.

Across the human lifespan there are many changes in the physiological properties of sleep, sleep timing and sleep duration. In adolescence sleep timing is delayed and there is a reduction in slow wave sleep which continues into old age as sleep timing gradually becomes earlier. Using a modified two process model which incorporates a van der Pol oscillator driven by external light signals into the circadian process we show that changes in sleep timing and duration across the lifespan can be explained by varying parameters. Model simulation show that these changes can be understood by a simultaneous reduction in the amplitude of the circadian oscillator and the upper asymptote of the homeostatic sleep pressure.

Keywords: The two process model; Circadian rhythms and sleep; Maps of the circle; Bifurcations of limit cycles and periodic orbits; Dynamical systems in Biology; Ultradian rhythms and sleep.

Acknowledgements

Firstly, I owe a great deal of thanks to my supervisors Anne Skeldon and Gianne Derks for all of their advice and enthusiasm over the past three and a half years. I have really enjoyed working with them and am very grateful that they have been able to dedicate so much time to my project and for the opportunities they have given me. I'd like to also thank the Engineering and Physical Sciences Research Council for funding the project (grant number EP/M506655/1).

Alongside my supervisors, I have crossed paths with many interesting academics during the project. I am incredibly grateful to Daan Van Der Veen and Andreas Psomas for their collaboration and conversations on the sleep-wake patterns of the common vole and ultradian rhythmicity which aided a chapter of this work. This gratitude is extended to Paul Glendinning, Peter Achermann, Victoria Booth, Cecilia Diniz Behn and Derk-Jan Dijk for visiting and giving insightful talks in the Mathematics department at Surrey.

More generally, I would like to thank my colleagues at Surrey who have joined me in discussions about our academic work, played countless board games, shared accommodation and joined me at the bouldering wall.

Finally, I would like to acknowledge my family. In particular, my four parents and three siblings (Tamara, James and Louisa) for supporting me, always making me laugh and giving me encouragement throughout.

Contents

1. Introduction . . . 1
   - 1.1 Circadian rhythms and sleep . . . 1
     - 1.1.1 Sleep . . . 2
     - 1.1.2 Electroencephalography (EEG) . . . 4
     - 1.1.3 Stages of the sleep-wake cycle . . . 6
     - 1.1.4 Changes through lifespan . . . 7
     - 1.1.5 Light and modern society . . . 8
     - 1.1.6 Media and mobile applications . . . 10
   - 1.2 Mathematical models of sleep-wake regulation . . . 11
   - 1.3 One dimensional maps . . . 14
     - 1.3.1 Circle maps and Arnold tongues . . . 15
     - 1.3.2 One dimensional maps with gaps . . . 17
   - 1.4 Overview . . . 18
2. The two process model, its associated map and periodic solutions . . . 21
   - 2.1 General structure of the model . . . 21
     - 2.1.1 Model equations . . . 22
     - 2.1.2 Re-parametrization . . . 23
     - 2.1.3 Physiologically motivated assumptions . . . 26
     - 2.1.4 Symmetry in ODE solutions . . . 27
     - 2.1.5 Special case with zero amplitude circadian oscillator . . . 29
     - 2.1.6 Complex dynamics . . . 31
   - 2.2 The associated one-dimensional map . . . 32
     - 2.2.1 The composite map . . . 32
     - 2.2.2 Derivative of the map . . . 35
   - 2.3 Periodic solutions . . . 36
     - 2.3.1 Definition of a (p, q)-periodic solution . . . 37
     - 2.3.2 Analysis for $(1, q)$ periodic solutions . . . 38
     - 2.3.3 Small circadian amplitude approximation for $(1, q)$ periodic solutions . . . 40
3. Bifurcations of periodic solutions . . . 45
   - 3.1 Saddle node bifurcations . . . 45
     - 3.1.1 Calculation of general (p, q) tongues . . . 45
   - 3.2 Gaps in the map . . . 49
     - 3.2.1 Tangencies on the lower threshold . . . 49
     - 3.2.2 Using symmetry to find tangencies on the upper threshold . . . 58
     - 3.2.3 Discontinuities in the one dimensional map . . . 59
   - 3.3 Border collisions . . . 64
     - 3.3.1 Type I . . . 65
     - 3.3.2 Type II . . . 66
   - 3.4 Bifurcation set . . . 67
   - 3.5 Discussion . . . 71

4. The common vole and the two process model . . . 75
4.1 Biological data . . . 76
4.1.1 Electroencephalogram (EEG) data . . . 77
4.1.2 Finding sleep - wake onset times from scored EEG data . . . 78
4.2 Finding two process model parameters . . . 79
4.2.1 Using EEG data to find χ_s, χ_w . . . 79
4.2.2 Sleep-wake fitting for remaining parameters . . . 81
4.3 Comparison of the two process model with spontaneous data . . . 88
4.4 Modelling sleep deprivation . . . 95
4.4.1 Two process model predictions of sleep deprivation . . . 96
4.5 The hidden rhythm . . . 100
4.6 Parameter sensitivity . . . 106
4.6.1 Minimum wake length . . . 107
Results given a 40 minute minimum wake length . . . 107
4.6.2 Varying the sleep strength parameter, χ_s . . . 109
4.7 Arnold tongues for the common vole . . . 111
4.8 Discussion . . . 113
5. A modified two process model including an external zeitgeber . . . 117
5.1 Background . . . 117
5.2 A light inclusive model of the circadian pacemaker . . . 118
5.2.1 Process L . . . 119
5.2.2 Modified two process model . . . 120
5.3 Mid-sleep on free days (MSF) and sleep duration data . . . 123
5.4 Results . . . 124
5.5 Discussion . . . 126
6. Conclusions and future work . . . 129
6.1 The dynamics and bifurcations of the two process model . . . 129
6.1.1 Results . . . 129
6.1.2 Consequences . . . 131
6.2 Applications of the two process model . . . 132
6.2.1 The common vole and the two process model . . . 133
6.2.2 A modified two process model including an external zeitgeber . . . 135
6.3 Future Work . . . 136
Appendices . . . 141
A. The two process model, its associated map and periodic solutions . . . 141
A.1. Monotonicity of $\alpha(\tau)$ . . . 141
B. Bifurcations of periodic solutions . . . 143
B.1. The edge of the tangency existence region . . . 143
C. Voles and the two process model . . . 145
C.1. F-Test . . . 145
References . . . 148

1 Introduction

The purpose of this thesis is to give a deeper analysis than seen in the current literature of the complex dynamics of the two process model of sleep-wake regulation. We discuss in detail the bifurcation structure that exists within the two process model and apply modified versions of the two process model to two problems: predicting recovery sleep after sleep deprivation in the common vole; explaining changes in sleep patterns across the lifespan in humans.

1.1 Circadian rhythms and sleep

Most living things, from bacteria and fungi to plants and animals, experience some behavioural changes that follow a cycle of roughly one day. Natural oscillations in light intensity and temperature have promoted the evolution of approximately daily internal oscillators, these oscillators are known as circadian clocks (or circadian rhythms). Other external inputs such as population levels and societal pressure can also have an impact on these rhythms. The body is constantly reacting to these external stimuli in an attempt to maintain a stable condition, or homeostasis. An example of this is thirst, which is an important mechanism for an individual to maintain a relatively constant level of fluids in the body.

Many animals experience these clocks as cycles between sleepiness and alertness at regular intervals, the sleep-wake cycle. If an organism has synchronized its rhythms with the regular oscillations of the external stimuli it is said to be entrained. In humans it was not known until the late 1930's if their rhythms were internally generated or externally imposed. The forced desynchrony protocol of Kleitman [1] showed that despite having a forced sleep-wake period much longer than one day the internal temperature rhythm remained entrained to 24 hours. In the 1960's, so called "free-run" experiments, showed that rhythmicity also persists even when external stimuli are removed. Several of the experiments exploring autonomous rhythms under temporal isolation were performed by entraining participants to a normal light-dark (LD) cycle. The participants were then isolated, originally in bunkers [2–4] or natural

caves [1], from environmental time indicators. These studies could last for weeks or months at a time and participants were without clocks but were able to eat, sleep and turn on lights as they pleased. It was shown that subjects continued to experience roughly circadian oscillations in body temperature and melatonin levels.

For 99% of humans the intrinsic period of these oscillations lies between 23.5 hours and 24.7 hours, with a mean of 24.2 hours. Under normal conditions light signals adjust the length of the period to one solar day [5–7]. After many weeks the majority of participants experience Spontaneous Internal Desynchrony (SID), where the sleep-wake cycle becomes desynchronized from the autonomous circadian rhythms [2, 3]. In a large number of cases a free-running participant exhibiting SID will have a sleep-wake cycle between $30-50$ hours without being aware. A summary of results of many free-run experiments can be found in Czeisler [8,9] and Wever [4,10].

It is now known that circadian clocks are not just behavioural but are a result of complex biochemical oscillators. The internal mechanism that is considered to be most responsible for coordinating circadian rhythms is a group of around twenty thousand nerve cells called the suprachiasmatic nucleus (SCN). Some other regions of the brain which are involved in the regulation of sleep are illustrated in Figure 1.1 below. The SCN is a tiny region of the brain located in the hypothalamus, directly above the optic chiasm. Information about incoming light is relayed from the optic nerves to the hypothalamus, the SCN then regulates the level of melatonin in the body [11] through a direct neural connection to the pineal gland.

Melatonin is a biomarker for the circadian rhythms of the SCN, for example, during the night the brain produces higher levels of melatonin than during the day. Information is also sent to other hypothalamic nuclei to modulate body temperature and hormones such as: cortisol, which rises throughout sleep and peaks around wake onset, dissipating during the day [12]; and circadian prolactin, which begins rising in the late afternoon and peaks in the middle of the night.

1.1.1 Sleep

Sleep is essential for ensuring that the body's central and peripheral rhythms are synchronised, this helps maintain a healthy body and mind. During sleep many of the systems in the body are in an anabolic state, a state allowing for recovery of the immune [13], nervous, skeletal and muscular systems. Wound healing is also improved by 'good' sleep [14]. The brain in particular needs sleep for restoration, many other parts of the body are able to restore themselves during quiescent waking. Brain areas with reduced activity during sleep restore supplies of adenosine triphosphate (ATP), a molecule which can act as an energy current in the cell for both storage and transport [15]. Since ATP has hypnogenic properties [16, 17], ATP in the brain has been shown to support many of the functions involved in the regulation of sleep homeostasis and the

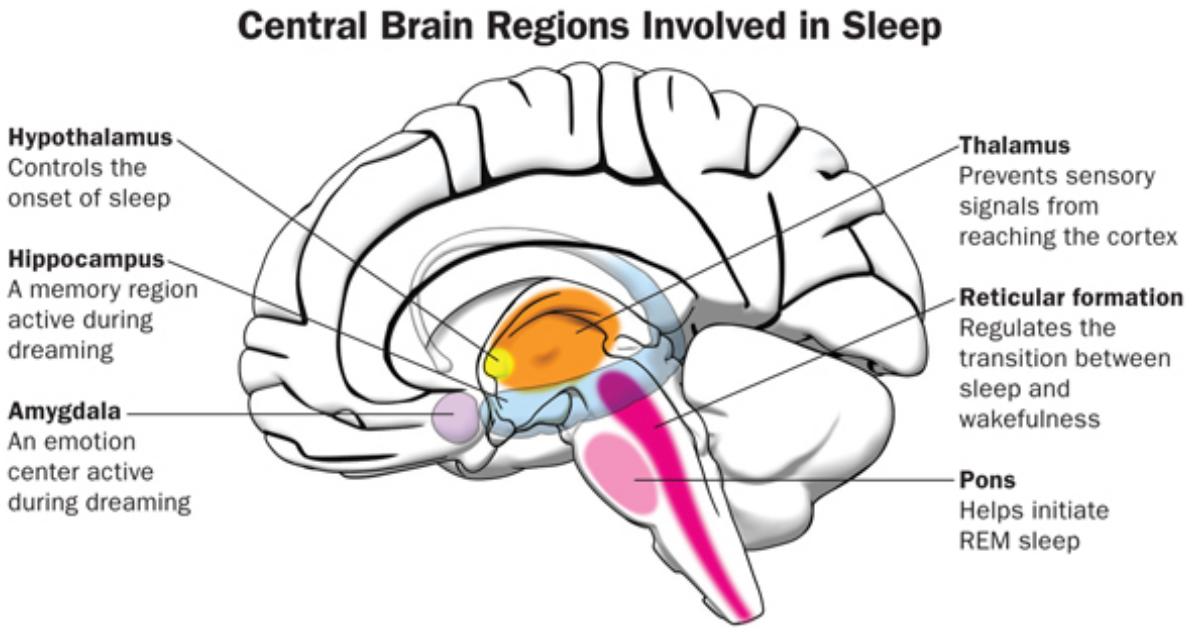

Figure 1.1: The regions of the brain which promote and regulate sleep-wake cycles
Source: www.nature.com/scientificamericanmind/journal/v24/n1/images/scientificamericanmind0313-12-13.jpg

sleep-wake cycle [18], including sleep duration.

There are many well documented sleep disorders which include dyssomnias (disorders related to initiating or maintaining sleep), such as insomnia, hypersomnia, narcolepsy, and sleep apnoea; parasomnias (disorders related to unusual behaviour of the nervous system during sleep), such as sleepwalking and sleep behavioural disorders; bruxism (involuntary grinding of teeth); and circadian rhythm sleep disorders (having a delayed sleep-wake phase).

When sleep is irregular or a sleep disorder is present, the carefully orchestrated circadian rhythms can become disorganised [19, 20]. Poor or mistimed sleep has been correlated with many health issues [21–23] such as: depression and psychotic disorders [24, 25]; cardiovascular disease [26, 27]; neurodegenerative conditions; disease progression in cancer [28–30]; obesity [31]; diabetes [32]. Due to the significant health risks associated with poor or mistimed sleep, it is important that we understand the biological mechanisms which regulate the sleep - wake cycle. To do this we must first define what sleep is and set out the fundamental properties of sleep.

Here we introduce the behavioural definition of sleep and the polysomnography (PSG) approach which includes the electroencephalographic (EEG) description of the various sleep stages. The original behavioural definition of sleep was given by Piéron in 1913 [33] and has since been extended [34, 35]. This definition proposes that a set of criteria need to be satisfied in order for a subject to be classified as asleep. These criteria are:

1. presence at a specific sleeping site;

2. typical body posture;
3. physical inactivity;
4. elevated arousal threshold;
5. rapid state reversibility (wakes up quickly from a big enough stimulus);
6. regulatory capacity (increased sleep quality and/or duration after sleep prevention).

Whilst these properties give a good visual indication as to whether the subject is awake or asleep they are not sufficient to categorize the stage/ type of sleep or give an explanation for the physiology which regulates the sleep-wake cycle. The behavioural definition is therefore usually considered alongside a PSG. Polysomnography (PSG) is the collection of various physiological measurements which indicate sleep, these include: electroencephalography (EEG) of brain waves, electrooculography (EOG) of eye movements, electromyography (EMG) of skeletal muscle activity, simplified electrocardiography (ECG) for cardiac activity and actigraphy for motor movements. Some sleep laboratories collect all measurements of the PSG simultaneously [36], this is usually in the diagnosis of a sleep disorder. Often sleep scoring will take place using only a few of the PSG measurements, in particular the sleep EEG.

1.1.2 Electroencephalography (EEG)

A conventional human scalp EEG recording is obtained by finding the difference in voltage between two electrode sites [37]. Each electrode on the scalp forms a pair with the common system reference electrode and each pair is connected to a differential amplifier. A differential amplifier amplifies the recorded voltages by between $1000 - 100000$ times. The amplified signal is then passed through an anti-aliasing filter and converted from analog to digital, allowing the data to be filtered for display. Typical filters that can be applied are a high-pass filter (0.5 - 1 Hz) and a low-pass filter (35 - 70 Hz). These filters are used to remove unwanted frequencies from movement, nerve and muscle signals and are also necessary to remove frequencies caused by mains power lines, around 50 Hz [38].

EEG recordings are usually represented by plotting time against the difference in voltages, as in Figure 1.2, these voltages produce sequences of waves referred to as EEG activity. The frequency of a wave refers to the number of times the wave completes a cycle in one second and the amplitude, measured in microvolts (μV), is given by comparing the height of the wave recorded to that of a calibration signal recorded with the same gain and applied filters. For example, if the height of an EEG wave measures 10mm and is compared to a calibration signal of $50\mu V$ measuring 5mm then the plotted amplitude is 100 μV.

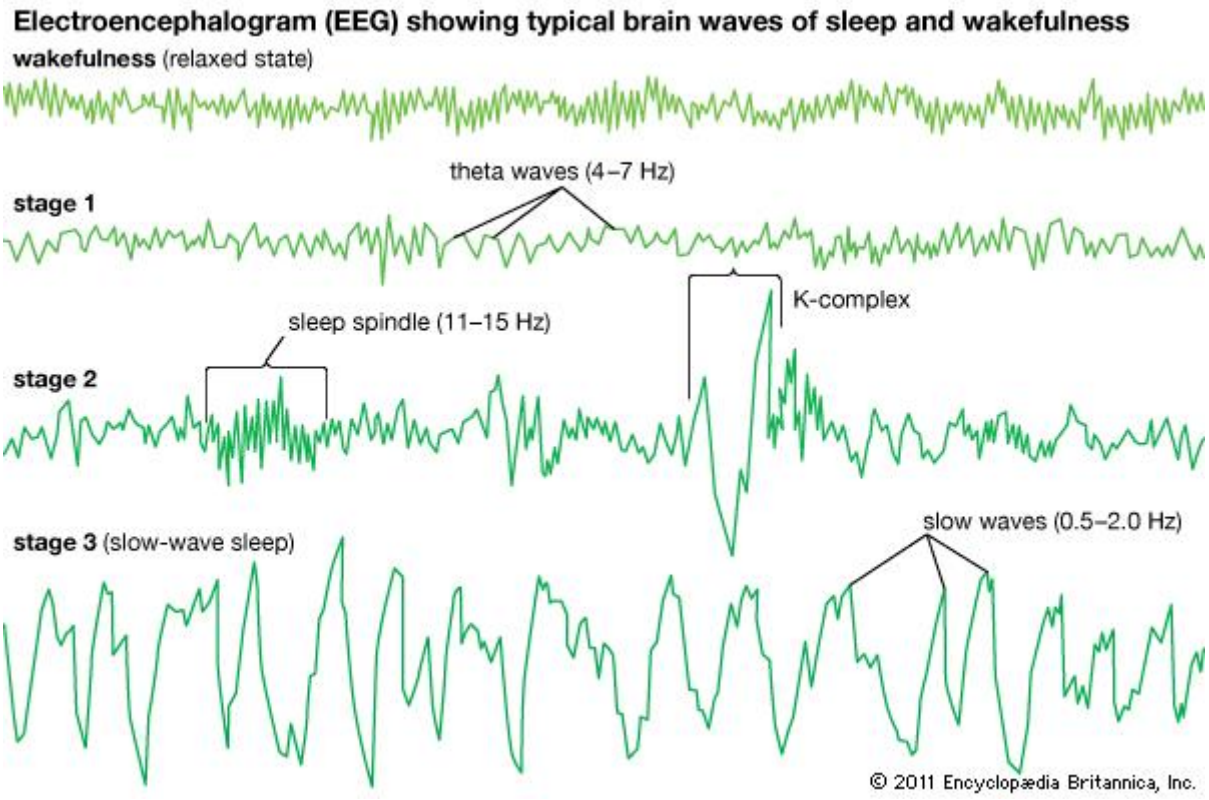

Figure 1.2: Various waveforms seen in the brain during wake and sleep.
Source: http://media-3.web.britannica.com/eb-media/77/144177-004-7621DE7D.jpg

The majority of signals observed in the scalp EEG lie within the 1-20Hz range and the waveforms are generally divided into four main bandwidths known as alpha, beta, theta and delta waves. In humans, frequencies in the range of 1-4 Hz are known as delta waves. These are the slowest waves and tend to have the highest amplitude in the sleep EEG.

Theta waves lie in the frequency range 4-7 Hz and are often seen in young children. Usually theta activity is seen during relaxed states such as drowsiness, arousal and even meditation.

Alpha waves were the first wave type to be categorised by Hans Berger, a German neurologist and the inventor of the EEG. Frequencies in the range 7-13Hz are known as alpha waves which correlate with closing of the eyes and relaxation. A phenomenon known as alpha blockage occurs when a subject opens their eyes, this is where alpha waves dissipate and beta waves in the frequency range 14-30Hz become prominent. Active movement or motor behaviour is closely linked to beta activity [39] and is therefore seen predominantly in the EEG during wakefulness.

Next, we discuss the various stages of sleep which can be categorised using the sleep EEG.

1.1.3 Stages of the sleep-wake cycle

The PSG, and in particular changes in the sleep EEG, have been used to divide sleep into various stages. Only a few years after its invention research projects were using EEG to study a whole-night sleep in humans, one of the first of such studies was led by Loomis. Loomis and his team were the first to describe many of the waveforms in the sleep EEG, namely sawtooth waves, sleep spindles, and random waves, later called K-complexes and slow waves [40,41]. Throughout sleep they noticed that there were changes in the features of the sleep EEG, this lead to the first categorization of sleep. This categorization consisted of 5 different sleep states in humans ranging from deep sleep to wakefulness with the level of arousability increasing through to wake [42,43]. As experimental equipment and our understanding of the physiology has improved other revised scoring systems have been developed.

It is now known that there are two broad types of sleep, nonrapid eye movement (NREM) sleep and rapid eye movement (REM) sleep. In humans, the sleep cycle alternates between NREM and REM sleep around $4-6$ times a night and each cycle takes an average of 90 minutes [44, 36]. NREM sleep occurs at the beginning of a sleep episode and was previously divided further, into 4 main stages [45]. However, this was reduced to three stages, N(I)-N(III), by the American Academy of Sleep Medicine in 2007 [46] where the previous stages 3 and 4 were combined. There are distinct characteristics seen in each stage:

- **Stage 1 (N1)** - Sometimes referred to as relaxed wakefulness, this stage occurs predominantly at the beginning of sleep with slow eye movements. In the sleep EEG alpha waves are seen dissipating and theta waves appear. The sleeper can be easily awakened from this stage and, if woken, often believe they have not been asleep at all.

- **Stage 2 (N2)** - No eye movements occur and the sleeper is still easily awakened. The sleep EEG shows sleep spindles and K-complexes during this stage.

- **Stage 3 (N3/ SWS)** - Otherwise known as deep sleep or slow-wave sleep (SWS). The sleep EEG shows an increase and then domination of delta waves during this stage. Dreaming is also more common in this stage than the other NREM stages.

There are other observable changes during NREM sleep,+ for example, the brain uses less energy and both heart rate and body temperature fall [47].

In REM sleep, rapid movements of the eyes occur and there is a loss of muscle tone or virtual paralysis of the body. REM sleep takes up only a small proportion of total sleep time and is often called paradoxical sleep due to physiological similarities to wakefulness including rapid, low-voltage desynchronized brain waves. Dreaming is predominant during the REM state but does also occur during NREM.

The sleep cycle usually follows the ordering N(I) → N(II) → N(III) or SWS → N(II) → REM, where REM occurs on a return to N(I) or N(II) from SWS. There is a higher proportion of SWS at the beginning of a sleep period which decreases through the night as the proportion of REM sleep increases [36].

For most people awakening means the end of sleep, however brief awakenings happen throughout sleep (usually around $1-2$ % of sleep duration in healthy teenagers and increasing into adulthood) to adjust body position or to survey the environment. Awakenings usually occur at the end of a REM sleep phase and wake onset occuring at the end of sleep is typically triggered by sufficient reduction of sleep need alongside internal circadian indicators. Wake onset coincides with an increase in electrical activity in the brain which begins in the thalamus and spreads through the cortex [48].

1.1.4 Changes through lifespan

As mentioned before, it has been shown that there are many health issues associated with poor or mistimed sleep. In terms of the sleep EEG one would expect to see disturbances in the continuity of sleep, decreased delta activity and changes in the distribution and density of eye movements [25] if the individual was not getting adequate sleep (dysregulated). Adequate sleep is considered to be when there are no periods of sleepiness/ drowsiness during daytime. The amount of sleep needed to achieve this varies through age and for each individual.

The periods of a human life with the highest proportion of sleep occur in the first 2 years namely: newborns (0 - 3 months old), infants (4 - 11 months old) and toddlers (1 - 2 years old). By the end of this first 2 years a baby's brain is almost the size of an adult sized brain [49] and sleep plays a clear role in this development. It has been shown that consolidated periods of sleep with few wake episodes in these early years influences a child's ability to perform cognitive tasks [50], learn languages [51], improve vocabulary [52] and have a calmer temperament [53]. The timing of sleep with respect to learning is also significant, with infants known to recall information and rules much better if they sleep within 4 hours of learning.

In these early years, sleep is polyphasic (many sleep-wake episodes each day), becoming monophasic (one sleep each day) by roughly ages 5-6 when a child reaches school age. Usually school age children have earlier sleep onset and wake onset times, with mid-sleep on free (non-work) days (MSF) occurring at approximately 03:00 am, which becomes later into the teenage years to 05:00 am. Into adulthood this shift in timing reverses and both sleep and wake onset become earlier again, approximately 03:30 am by age 60 [54]. The duration of sleep has been shown to decrease monotonically from teenage years to retirement and then level off [55, 56]. These variations of sleep can be seen directly in the sleep duration recommendations given by the National Sleep Foundation in the USA [57] shown below.

- Newborns (0 - 3 months) - 14 to 17 hours
- Infants (4 - 11 months) - 12 to 15 hours
- Toddlers (1 - 2 years) - 11 to 14 hours
- Preschoolers (3 - 4 years) - 10 to 13 hours
- School-age children (5 - 12 years) - 9 to 11 hours
- Teenagers (13 - 17 years) - 8 to 10 hours
- Adults (18 - 64 years) - 7 to 9 hours
- Older Adults (65 years and over) - 7 to 8 hours

The age related changes in sleep shown in MSF studies could be the result of both underlying physiological changes and environmental or societal pressures. In modern society there are many pressures that can alter human sleep patterns. For example, it has been suggested that changes in sleep timing are primarily a result of the modern light environment [58]. In the next section we discuss some of the societal pressures.

1.1.5 Light and modern society

Changes in light have an influence on the internal circadian clock, since light gives the circadian clock an idea of the time of day. It has been shown that exposure to even small amounts of light during night time can affect body temperature, melatonin secretion and cognitive ability. Pulses of light at the right time in a circadian cycle have a resetting effect on the internal clock [59].

The advent of electric light has substantially altered sleep timing in the developed world and this has an impact on the internal circadian clock, which can become desynchronized [7]. This circadian desynchrony can occur due to differences in weekday and weekend sleep patters, night time shift work [60], waking during the wrong sleep stage and looking at light emitting screens before bed [61]. All of this can lead people to have issues sleeping even when tired, or difficulty waking up in the morning [48]. It is clear then that having the ability to control light intensity and gate light onset could have negative impacts (when used to interrupt the sleep-wake cycle) and positive impacts (when used to regulate light intake and sleep).

In indigenous hunter - gatherer communities living near the equator, with no access to electric light, sleep onset occurs 2 to 4 hours after sunset and sleep duration on average is 7.7 hours, with wake onset roughly 1 hour prior to sunrise. These communities spend a large proportion of the day outside and as a result receive a large amount of high intensity light (averaging 4000 lux). In periods of darkness, before dawn and after dusk, the only light source is small fires

(less than 5 lux). This 'natural' light profile is very different from that seen in industrialized countries today.

Light intake is now prolonged well into the evening due to universal indoor lighting, television and mobile devices. These light sources are personally activated meaning that the user now has some control in manipulating their circadian clocks. The amount of light received during the day is reduced by an order of magnitude relative to pre-industrialized societies [62, 63] since far more adults now spend the majority of the day working indoors. Individuals with longer intrinsic circadian periods are thought to be more sensitive to the impact of evening artificial light [58].

One of the key contributors to evening light exposure is shift work occurring during the night, which has become commonplace in modern society. Not only does exposure to artificial light at night suppress the pineal hormone melatonin but shift workers undergo regular disruption to their circadian rhythms and sleep deprivation. It has been hypothesized that this can lead to reduced immune response and changes in metabolism [60] which have been linked to obesity, type II diabetes and cardiovascular disease. Epidemiologic studies found that female night shift workers are also at a higher risk of cancer, in particular 41% more likely to have skin cancers and 32% more likely to have breast cancers [64] than women that only worked in the day. Alongside the sleep schedule disruption it is likely that other factors contribute to the wide range of health issues caused by night time shift work. Shift workers are less likely to find time to exercise and eat regular healthy meals which are risk factors for a wide range of diseases.

Wake onset can now be triggered on demand by an alarm clock and is often imposed by social constraints such as work and school start times. Early wake onset during the week leads to an accumulation of 'sleep debt' which is then recovered during free days by sleeping later and longer, closer to an individuals natural circadian wake propensity rhythm. This pattern of accruing sleep debt on working days and recovery on free days is called 'social jet-lag' [65] named because of the similarities in sleeping out of phase with the circadian clock seen when travelling through time zones.

With improvements in aviation it is now common for people to travel by plane across several time zones for either work or holiday. The result can be a desynchrony between environmental cues and the internal clock [66], the internal clock is misaligned with the actual time in the new location, this is known as jet lag. Symptoms related to jet lag can range from daytime sleepiness and night time insomnia to gastrointestinal issue and mild depression [67]. These effects are usually only temporary as the internal clock readjusts a little each day until it becomes entrained with external environmental cues. Eating at appropriate times, being active and getting exposure to light during daylight hours in the new time zone can speed up recovery. Typically a flight across six or more time zones will take the traveller 4-6 days to return to a normal sleep schedule

and not have daytime sleepiness.

1.1.6 Media and mobile applications

In recent years there has been a lot of media attention surrounding the importance of sleep. This has led to an increase in accessible sleep optimisation tools on mobile devices and online. Some of these applications use mathematical models to predict preferable sleep/ wake onset times for people recovering from jet lag, adjusting sleep patterns for shift work and people with sleep disorders. Applications such as Entrain [68] ask users to input data about their sleep/ wake times and light intensity throughout the day before making long distance flights across time zones. The application is then able to give optimal sleep schedules [69], with the aim of fast re-entrainment, by adjusting your light intake and sleep pattern over the period of travel. We will discuss the underlying mathematical models of Entrain in the next section.

Mobile applications like 'Sleep as Android' [70] use sleep actigraphy to track sleep phase and timing. Many of these applications offer other services such as *smart wake up*, which finds the optimal moment in your sleep cycle for your alarm clock to wake you, or *cycle count and percentage of deep sleep*, which gives an indication of how healthy your sleep is and can help identify sleep deprivation issues. The advantage of using sleep actigraphy in the modern age is that most mobile devices have a built-in accelerometer sensor which is very sensitive to movement, therefore sleep tracking can be done personally and at home. Since during deep sleep muscle movements are suppressed the actigraph will output an almost flat sleep graph. During the lighter sleep phases more movement is detected which are displayed as peaks in the sleep graph.

To increase the accuracy when categorising sleep phase 'Sleep as Android' also considers noise intake through the microphone on the device and allows for heart rate detection data to be used from external heart rate sensors. Many fitness trackers now contain a heart rate sensor, some of which will even track sleep-wake cycles for you. Fitbit, one of the current leading fitness tracker brands has dedicated sleep monitoring and is thought to be more accurate than using a mobile phone since it is worn on the wrist and monitors both activity and heart rate simultaneously. Most fitness trackers come with a companion application which allows you to visualise all of your data, set exercise goals, record additional information such as food and water intake and indicate your preferred sleep schedule. Using this information some of these applications will give food intake and bedtime reminders to help you personally achieve your sleep schedule. Again, this gives the user an opportunity to interact with and personalise their sleep-wake patterns.

As well as monitoring and adapting sleep schedules the general population are becoming more aware of the effects of artificial light in the evening. It is known that the blue and green

light emitted from electronic screens can disrupt sleep cycles when used at night [71], delaying the circadian clock and suppressing levels of sleep-promoting melatonin [72]. Applications such as f.lux [73] will change the colour of light omitted from a computer screen throughout the day. The reduction of blue light in the evening emulates sunset in an attempt to reduce the effects of artificial light on sleep-wake cycles.

A better understanding of mathematical models of sleep could allow for more accurate sleep optimization schedules, which in turn could improve many peoples' health.

1.2 Mathematical models of sleep-wake regulation

Mathematical models have been used for decades to help understand sleep-wake cycles and circadian rhythms. The classical models of sleep-wake regulation focus on the desire to sleep after periods of wakefulness, the circadian rhythm driven by the brain's SCN and other cyclic behaviour which occurs in the transitions between REM and NREM sleep (approximately 90 minutes per cycle). These interactions have motivated coupled oscillator models [74, 75] and the reciprocal interaction model for REM sleep cycling [76, 77]. However, the most well known of these classical mathematical models of sleep regulation is the two process model.

The two process model was first described in [78] and extended in [79] and has since provided a theoretical framework and even the language now commonly used to describe sleep-wake regulation. The model proposes that the sleep-wake cycle can be understood in terms of the interaction of two oscillatory processes: a sleep dependent homeostatic process and a sleep independent circadian oscillator. The term homeostasis in sleep refers to the body's internal biochemical system aimed at maintaining physiological sleep need within reasonable bounds. It is modelled on a sleep pressure that increases monotonically during wake and decreases monotonically during sleep. The direct cause of this sleep pressure is not known, but one suggestion is that it is a consequence of adenosine build-up during the day. Switching between the sleep and wake states occurs at threshold values of the sleep pressure, with the transition from wake to sleep occurring at the upper threshold and from sleep to wake at the lower threshold. Both thresholds are modulated by the circadian oscillation, as illustrated in Figure 1.3.

An accepted physiological marker for the homeostatic sleep pressure in the two process model is slow wave activity (SWA) in the electroencephalogram (EEG) during sleep [78–80]. It is possible to approximate the time constants, which determine the growth and decay of the homeostatic sleep pressure, relevant to humans in the two process model [81]. These constants are different for wake and sleep. The model can be used to describe many different types of sleep phenomena. By changing parameters in the model one can: create monophasic (one sleep-wake cycle per day) and polyphasic (multiple cycles per day) sleep patterns and emulate the sleep

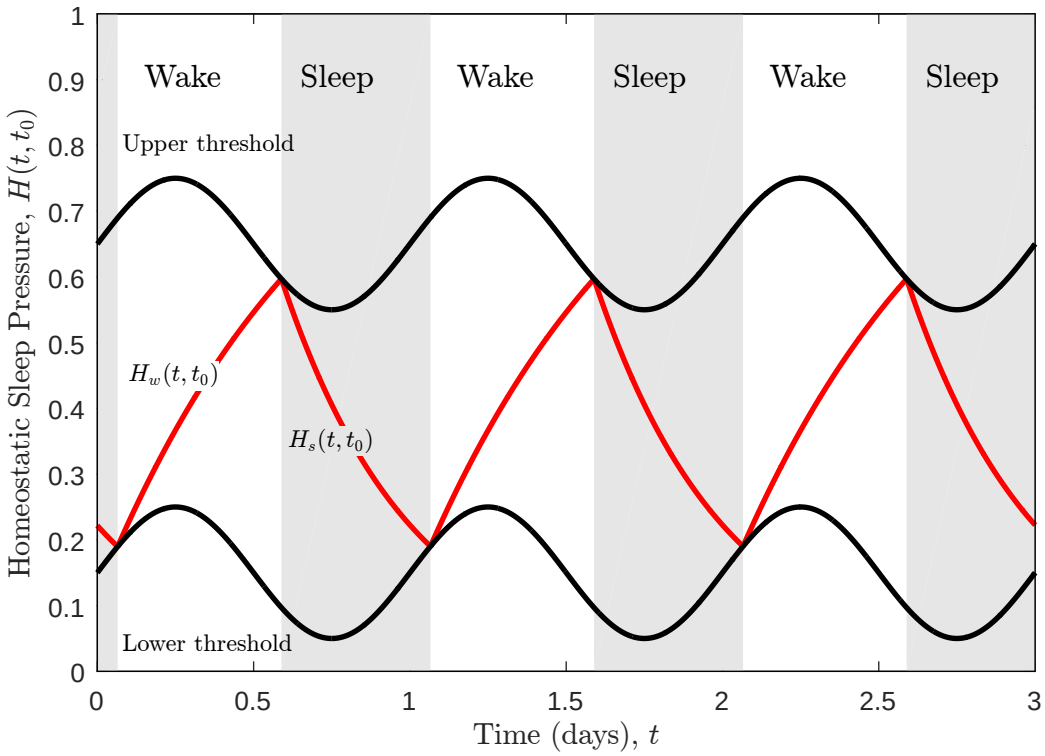

Figure 1.3: A simulation of the two process model showing both the thresholds which include the circadian oscillation (black) and the homeostatic sleep pressure (red). The homeostatic sleep pressure decreases during sleep and increases during wake. Switching between the two states occurs at the intersection between the homeostatic sleep pressure and the thresholds.

cycles of babies.

Other mathematical models are similar to the two process model [82], usually using both the homeostatic and circadian processes alongside some other additional processes. The model of ultradian variation of slow-wave activity [83–85] allows a similar homeostatic process to determine the build-up and saturation levels of SWA during NREM episodes. Other models include a sleep inertia process, becoming a three process model [86, 87], to simulate sleepiness/ alertness.

Although some simulations of the two process model have been carried out there is only a little analysis of the large range of dynamics and behaviour it can show, therefore it can be difficult to understand how the model parameters are linked to the physiology. One of the first models of (REM) sleep regulation grounded in some physiology was the reciprocal interaction model [76] which used interactions between neurons to understand the basis of ultradian cycling between REM and NREM sleep. Due to a greater recent understanding of the neuronal mechanisms that underly sleep-wake regualtion [88], more complex neuronal models have been formulated [89–94]. However, the reciprocal interaction model structure is still an underlying

feature of the REM sleep regulation in many of these more complex models. The Phillips and Robinson (PR) model [90] is based on sleep-wake regulation being a result of the interaction between sleep-promoting and wake-promoting neurons. The PR model considers the mutual inhibition of sleep promoting neurons and wake promoting neurons regulated by homeostatic and circadian processes. Whilst giving basic sleep-wake cycles the PR model is also able to estimate the effects of: sleep deprivation, caffeine, impulsive stimuli and shift work [95]. Also, by changing parameters in the model it is possible to understand the interspecies differences in mammalian sleep [96]. Mutual inhibition models, like the PR model, are increasingly being used to understand many sleep-wake phenomena.

The two process model has been mathematically associated with the PR model [97] enabling some aspects of the two process model to be interpreted more physiologically. It has been shown that there is also a relationship between the two process model and other more general neuronal models [98]. Consequently understanding the dynamics of the two process model is important for two reasons. Firstly, because of the central role of this model in the understanding of sleep-wake regulation and, secondly, in providing a deeper understanding of some of the interesting phenomena that have been observed in neuronal models of sleep-wake regulation.

As stated many mathematical models of sleep have incorporated a circadian oscillator, this oscillator is usually considered to be approximately sinusoidal and of fixed phase. However, an extension of the PR model considers a dynamic circadian oscillator to explain interactions between the sleep-wake state and circadian [99]. One of the interactions sometimes considered is modulation of light by sleep onset times [100] where sleep onset is used to gate incoming light signals [101]. Many studies exploring the effect of light on the human pacemaker have implemented a classic van der Pol type oscillator [102, 74], which contains a cubic nonlinearity, since the pacemaker acts as a limit cycle oscillator [103]. The classic van der Pol type model can be used alongside some process L, which converts a light signal into an effective drive on the circadian oscillator [104]. In fact, the mobile application Entrain uses a circadian clock given by this simple type of cubic model. More complex models employ a higher degree of nonlinearity [105, 106] however, the cubic model has been shown to be as, or more, accurate in predicting the results of human phase response experiments [104].

Throughout this thesis we analyse the dynamics of the two process model and consider some of its applications. Since it has been shown that neuronal models can be related to the two process model [97, 98] a better understanding of its underlying dynamics could give an insight into the behaviour observed in more complex models of sleep-wake regulation.

1.3 One dimensional maps

It has been shown that the two-process model can be represented as a one-dimensional map with discontinuities [107, 108]. A one-dimensional map is a function from an interval in $\mathbb{R}$ into itself and can help give an understanding of the evolution of a variable's dynamics. We are motivated by the transitions between monophasic and polyphasic sleep-wake patterns in the two process model, to understand these patterns individually we construct one dimensional maps. We begin by introducing the notion of a one dimensional map.

Consider $x_{n+1} = f(x_n)$, where x_n denotes the current state of the system, x_{n+1} the next state and f is some function which will be assumed to be differentiable, mapping x_n to x_{n+1}. A fixed point occurs if $x_n = x_{n+1}$. Thus, in a one-dimensional map solving $x_n = f(x_n)$ for x_n gives the fixed points.

There are several ways to understand the stability of these fixed points. For example we may consider a nearby orbit $x_n = x^* + \epsilon_n$ and check whether this orbit is attracted or repelled from x^*. Similarly we could consider the gradient of the map at the fixed point where

- $|f'(x^*)| < 1$, linear stability (local attractor)
- $|f'(x^*)| = 1$, marginal
- $|f'(x^*)| > 1$, unstable (local repeller)
- $|f'(x^*)| = 0$ superstable.

A cobweb diagram is a way to visualise the stability of the fixed points of the map. To do this we would take the graphical representation of the map and begin on the x_n-axis at some initial point x_0. The initial point gets mapped to a new point under the map $x_{n+1} = f(x_n)$ which is found by drawing a vertical line up until we hit the map. We then move horizontally to the $x_n = x_{n+1}$ line and continue to find points in our orbit following this process (going vertically to the map and horizontally to the identity line). Stable fixed points will be attractors in the cobweb plot. In Figure 1.4 we see a typical cobweb diagram of the logistic map, $x_n = rx_n(1 - x_n)$, where we have chosen $r = 3$. The point x^* occurs as the map crosses the identity line, since $|f'(x^*)| < 1$ we know that x^* is a stable fixed point.

The inherent periodicity of the circadian process in the two process model means that its one-dimensional map can be linked to a circle map. Consequently, both classic results for circle maps and well-known results for maps with gaps will be relevant to our discussion.

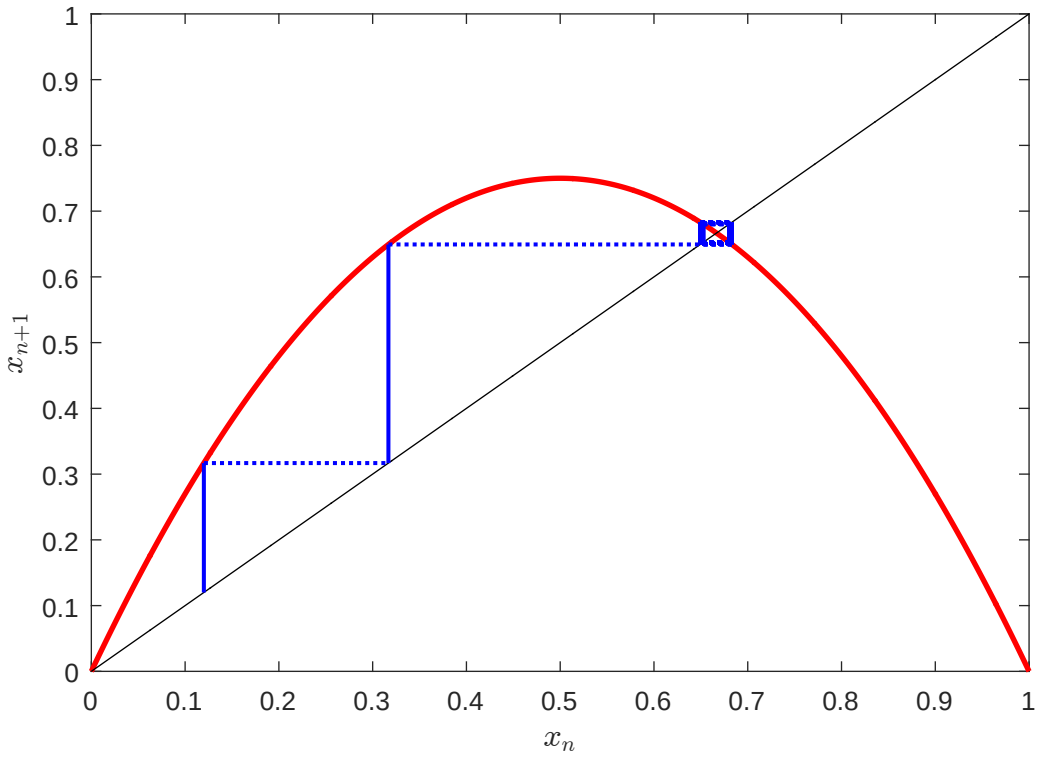

Figure 1.4: A cobweb plot of the logistic map. The diagonal black line is the identity line where $x_n = x_{n+1}$, the red curve is the logistic map and the series of blue lines shows how the cobweb plot converges to a stable periodic solution.

1.3.1 Circle maps and Arnold tongues

A circle map is a function that takes the circumference of a circle and maps it onto itself and behaves differently from maps of $\mathbb{R}$, since the circle is bounded. Such maps occur naturally in the periodic forcing of oscillators and, since the seminal paper by Arnold [109], have played an important role in understanding the behaviour of a variety of physical [110] and biological systems [111]. Here we will introduce some notation, some basic known properties of circle maps and focus in particular on the Arnold map.

Let $f : \mathbb{S}^1 \to \mathbb{S}^1$. The n^{th}-composition of f with itself is

$$f^n(x) = \underbrace{f \circ f \circ \cdots f(x)}_{\text{n - times}}$$

and the sequence $\{x_0, f(x_0), f^2(x_0), \ldots, f^n(x_0), \ldots\}$, or $\{x_n\}_{n=0}^{\infty}$, is called the orbit of x under f.

We define $\pi : \mathbb{R} \mapsto \mathbb{S}^1$ to be the covering map, a map that wraps $\mathbb{R}$ around $\mathbb{S}^1$ which is

continuous, monotone and periodic, with period 1. Then, $F : \mathbb{R} \mapsto \mathbb{R}$ is a lift of f if $\pi \circ F = f \circ \pi$. Note that since the covering map is not unique there are always an infinite number of lifts for a given map $f : \mathbb{S}^1 \mapsto \mathbb{S}^1$. The lift of the map to $\mathbb{R}$ is often used to study the dynamics of a circle map.

An archetypal example of a circle map is the two-parameter family (or standard family), $F_{\omega,\epsilon}$, given by iterating the map

$$F_{\omega,\epsilon}(\theta_n) = \theta_n + 2\pi\omega + \epsilon \sin\theta_n$$

which is the lift of the circle map

$$x_{n+1} = f_{\omega,\epsilon}(x_n) = x_n + \omega - \frac{\epsilon}{2\pi}\sin(2\pi x_n) \mod 1,$$

where ϵ is a constant denoting the strength of non-linearity and ω is some externally applied frequency. Such maps are referred to as Arnold maps.

For values of ϵ less than 1 and certain values of ω, regions of the map exhibit mode locking/ phase locking. In a phase-locked region, θ_n values progress essentially as rational multiples of n where the limiting behaviour is given by the rotation number [112]

$$\rho(F_{\omega,\epsilon}) = \lim_{n\to\infty} \frac{F^n(x_0) - x_0}{n},$$

which is well-defined and independent of x_0 [113]. A rotation number is rational (i.e. $\exists p, q \in \mathbb{N}$ such that $\rho = \frac{p}{q}$) if and only if there is $F^q(x_n) = x_n + p$ for some $x \in \mathbb{R}$. If $\rho(F_{\omega_0,\epsilon}) = \frac{p}{q}$ is rational, $f_{\omega_0,\epsilon}$ has a periodic point of period q and there exists an $x_0 \in \mathbb{R}$ such that

$$F^q_{\omega_0}(x_0) = x_0 + p.$$

On the other hand, if $\rho(F_{\omega,\epsilon})$ is irrational then f has no periodic solutions [114].

It was originally thought that the existence of rotation numbers ρ followed directly from having a circle map which was strictly increasing, continuous and of degree one ($F(x+1) = F(x)+1$). It was later proved that the map only needs to satisfy two conditions [115] to ensure the existence of rotation numbers, that is being non-decreasing [116] and of degree one. Solutions of non-decreasing circle maps can only be either periodic or aperiodic [115, 117].

For each rational number, there is an interval in ω with non-empty interior on which $\rho(F_{\omega,\epsilon}) = \frac{p}{q}$. However, there are also infinitely many values of ω for which $\rho(F_{\omega,\epsilon})$ is irrational [114]. If the map depends smoothly and monotonically on a parameter, then the periodic solutions occur in intervals with a devil's staircase structure dependence on the parameter, a

shape that is generally similar to the Cantor function (i.e. the graph of $\rho(F_{\omega,\epsilon})$ is constant on intervals corresponding to rational numbers, yet everywhere continuous).

Regions in the $\omega - \epsilon$ plane where $\rho(F_{\omega,\epsilon})$ is a fixed rational number form "tongues" which extend from each point $(\epsilon = 0, \omega = \frac{p}{q})$. These regions are known as Arnold tongues and denote the phase-locked regions mentioned earlier. For $\epsilon < 1$, Arnold tongues are non-overlapping and all have non-empty interior. At the boundary of these tongues a fixed point for $f_{\omega,\epsilon}$ is created in a saddle-node bifurcation. This fixed point separates into two fixed points inside the tongue, each fixed point goes around the unit circle until meeting in another saddle-node bifurcation on the other tongue boundary, and then disappearing.

The same sequences of periodic solutions have been repeatedly observed in monotonic maps with gaps of the real line [118], and have been termed period-adding sequences. The observation of period-adding sequences is typically linked with border collision bifurcations where fixed points of the map are created/destroyed by colliding with the gap.

1.3.2 One dimensional maps with gaps

For some parameter regimes the one dimensional map of the two process model has discontinuities. At the discontinuity, border collision bifurcations occur as periodic solutions are created/ annihilated by the edge of the gap in the map. Border collision bifurcation theory has been used to investigate a range of physical systems such as the dynamics of the impact oscillator [119], switching systems [120, 121] and various other piecewise smooth systems [122]. Most notably Jain and Banerjee (2002) [123] give a classification of the border collision bifurcations that occur in linear one dimensional maps on $\mathbb{R}$ with a discontinuity. The maps considered in the context of border collision bifurcation theory are usually linear.

Take a one-dimensional map $f(x, \mu)$ that maps $\mathbb{R}^1$ to itself and depends smoothly on μ. This map can be divided by a point, sometimes called a borderline value, on the real line $x = x_b$ into two regions R_A and R_b which are continuous in (x, μ) in both regions yet discontinuous at x_b [124]. Therefore the map $f(x, \mu)$ is called piecewise continuous. To visualise what happens as a fixed point crosses the point of the discontinuity x_b, a one-dimensional discontinuous map of the form

$$x_{n+1} = \begin{cases} L : ax_n + \mu & \text{if } x_n < x_b = 0, \\ R : bx_n + \mu + l & \text{if } x_n > x_b = 0, \end{cases}$$

can be considered. Here, l denotes the length of the discontinuity, the discontinuity lies at the origin and the state space is divided into two halves: L (left of the discontinuity) and R (right of the discontinuity).

Since the map is piecewise linear there is at most one fixed point either side of the discon-

tinuity. As before fixed points of the map are found by setting $x_n = x_{n+1}$. Therefore the fixed point in L is located at $x_L^* = \frac{\mu}{1-a}$ and that in R is located at $x_R^* = \frac{\mu+l}{1-b}$, a detailed discussion classifying the dynamics for different regions of the parameter space (a, b) is given in [123]. For L to have an intersection with the identity line, μ needs to be less than 0 and for R, $\mu > -l$. Therefore, collisions at the border occur for the fixed point x_L^* at $\mu = 0$ and for x_R^* at $\mu = -l$. Thus, as the parameter μ is varied, we expect two border collision events, one at either edge of the discontinuity.

One of the key aims of this thesis is to understand the bifurcation behaviour of the two process model and understand how transitions between different types of periodic solutions occur. As a parameter is varied in the two process model, its one dimensional map transitions from a continuous monotonic circle map to a monotonic circle map with gaps. We will see that border collisions in maps with gaps can play a similar role to saddle-node bifurcations in continuous circle maps in forming boundaries for existence regions of periodic solutions.

1.4 Overview

The layout of this thesis is as follows. In Chapter 2, *The two process model, its associated map and periodic solutions*, we formally define the two process model and show some of its basic dynamics. We then give the one-dimensional map reduction of the two process model and consider periodic solutions with p sleeps over q days. Finally, we show that for small circadian amplitudes regions of periodic solutions form 'wedges', which approximate the boundaries of Arnold tongues for 1 sleep over q days.

In Chapter 3, *Bifurcations of periodic solutions*, we focus on the bifurcations in the two process model and consider further the boundaries of the Arnold tongues. We first show that there is a parameter regime where the one-dimensional map is a lift of a continuous monotonic circle map and hence the regions of existence of different types of periodic solutions form Arnold tongues bounded by saddle-node bifurcations. We then find the parameter regions for which gaps in the map occur and show that these discontinuities in the map result in border collision bifurcations. Combining these results we explain how border collisions in gap maps can play a similar role to saddle-node bifurcations in continuous circle maps in forming boundaries for existence regions of periodic solutions. We end with a discussion section that summarises the key results from Chapters 2 and 3.

A condensed version of Chapters 2 and 3 has been published in the European Journal of Applied Mathematics (EJAM) [125].

In Chapter 4, *Voles and the two process model*, we derive parameter values for the two process model using spontaneous sleep data from 6 common voles. We then attempt to predict timings of

spontaneous sleep and sleep deprivation using the two process model with its standard circadian oscillator. However, the model predictions for sleep deprivation do not align with observations in the data and from previous experiments. Therefore, we consider a modified version of the two process model which has an additional component in its threshold. We show that this modified version of the model gives a good prediction of sleep deprivation behaviour and explain how the additional component is 'hidden' during parameter fitting.

In Chapter 5, *A modified two process model including an external zeitgeber*, we introduce another modified version of the two process model in which the circadian process incorporates a cubic van der Pol oscillator which is driven by an external light signal. We go on to show that by varying parameters in the model we can explain experimental data on sleep timing and duration across the human lifespan.

In Chapter 6, *Conclusions and future work*, we give a summary of the main findings of this thesis and highlight potential areas of interest for future study.

2

The two process model, its associated map and periodic solutions

In this chapter we introduce the two process model first formulated by Borbély [78,79]. Using a re-parametrized version of the model, we make some physiologically motivated assumptions and discuss the model's complex dynamics. We show that the two process model can be reduced to a one-dimensional map and begin to explore some of the properties of this map. Finally we show how periodic solutions arise in both the model and the associated map and give an analysis of a region in which these solutions exist. A condensed version of this chapter and the next one have been published in the European Journal of Applied Mathematics (EJAM) [125].

2.1 General structure of the model

The two-process model consists of a single circadian pacemaker $C(t)$, which is presumed to be located in the SCN and entrained by the light-dark cycle, and a continuous homeostatic sleep pressure $H(t)$. The homeostatic sleep pressure increases monotonically during wake, which can be viewed as creating a pressure to sleep. During sleep the homeostatic sleep pressure decreases monotonically, reducing this pressure. Therefore the homeostatic process has two forms, one for sleep denoted by $H_s(t)$ and one for wake $H_w(t)$. During sleep $H_s(t)$ decreases until it hits the lower threshold governed by the circadian pacemaker $C(t)$. The homeostat then switches to $H_w(t)$ and increases until hitting the upper threshold and switching back to the sleep state, this sequence is then repeated. The interaction between the homeostatic process and the circadian pacemaker can account for many aspects of sleep regulation. Basic model behaviour is shown in Figure 1.3 showing a monophasic periodic sleep pattern. The frequency of switching between sleep and wake states depends on the growth/ decay of the homeostatic process, the amplitude of the circadian pacemaker and the distance between the circadian thresholds.

In the remainder of this section we will introduce the equations which govern the model's behaviour and re-parametrize to reduce the number of parameters. The re-parametrized model

will become the basis for the remainder of the work on the two process model.

2.1.1 Model equations

We express the behaviour of the homeostatic sleep pressure by two ODE's, one for sleep

$$\chi_s \frac{dH_s}{dt} + H_s = \mu_s, \tag{2.1}$$

and one for wake

$$\chi_w \frac{dH_w}{dt} + H_w = \mu_w. \tag{2.2}$$

Here μ_s and μ_w are the lower and upper asymptotes respectively, these are the values that the homeostatic pressure would reach if no wake-sleep or sleep-wake switch occurred. Switching between wake and sleep occurs when the upper threshold $H^+(t)$ is reached by the homeostatic pressure $H(t)$. The upper threshold is given by

$$H^+(t) = H_0^+ + aC(t), \tag{2.3}$$

where H_0^+ is some mean value and $C(t) = \sin(\omega(t + \phi))$ is a 24 hour periodic circadian process with a as its amplitude. The switch between sleep and wake occurs when $H(t)$ reaches the lower threshold, given by

$$H^-(t) = H_0^- + aC(t). \tag{2.4}$$

Equations (2.1) and (2.2) along with (2.3) and (2.4) govern the value of the homeostatic sleep pressure over time.

Note that we are taking the simplest cases for the upper and lower threshold. More complicated forms of the circadian oscillation, such as

$$\begin{aligned} C(t) =& 0.97 \sin \omega(t - \alpha) + 0.22 \sin 2\omega(t - \alpha) + 0.007 \sin 3\omega(t - \alpha) \\ &+ 0.03 \sin 4\omega(t - \alpha) + 0.001 \sin 5\omega(t - \alpha) \end{aligned}$$

have been used [81] and noise has been added for more realistic simulations of sleep-wake timing [79].

The simple version of the model used here has nine parameters: $\mu_s, \mu_w, a, \chi_s, \chi_w, H_0^+$, H_0^-, ω and ϕ. In the next section we rescale the model to reduce the number of parameters.

2.1.2 Re-parametrization

We begin by re-scaling (2.1) and (2.2), the two ODE's that describe the system. Firstly we shift the homeostat by μ_s and redefine $\tilde{H}_{s,w} = H_{s,w} - \mu_s$, notice here that $\frac{dH_{s,w}}{dt} = \frac{d\tilde{H}_{s,w}}{dt}$. Therefore (2.1) and (2.2) become

$$\chi_s \frac{d\tilde{H}_s}{dt} + \tilde{H}_s = 0, \tag{2.5}$$

and

$$\frac{\chi_w \frac{d\tilde{H}_w}{dt} + \tilde{H}_w}{\mu_w - \mu_s} = 1. \tag{2.6}$$

We define $\hat{H}_{s,w} = \frac{\tilde{H}_{s,w}}{\mu_w - \mu_s}$ to get

$$\chi_s \frac{d\hat{H}_s}{dt} + \hat{H}_s = 0, \tag{2.7}$$

and

$$\chi_w \frac{d\hat{H}_w}{dt} + \hat{H}_w = 1. \tag{2.8}$$

Notice that $\hat{H}^{\pm}(t) = \frac{\tilde{H}^{\pm}(t)}{\mu_w - \mu_s}$ where, $\tilde{H}^{\pm}(t) = \tilde{H}_0^{\pm} + aC(t)$, thus we have

$$\hat{H}^{\pm}(t) = \frac{\tilde{H}_0^{\pm} + aC(t)}{(\mu_w - \mu_s)} = \frac{H_0^{\pm} - \mu_s + aC(t)}{(\mu_w - \mu_s)},$$

and can define $\hat{H}_0^{\pm} = \frac{H_0^{\pm} - \mu_s}{\mu_w - \mu_s}$ and $\hat{a} = \frac{a}{\mu_w - \mu_s}$, giving $\hat{H}^{\pm}(t) = \hat{H}_0^{\pm} + \hat{a}C(t)$.

We wish to solve (2.7) and (2.8) to understand how the homeostatic sleep pressure behaves over time. Note that the general solution to an ODE of the form

$$\frac{dF(t)}{dt} + AF(t) = 0,$$

for some constant A is

$$F(t) = B \exp\left[-\int_{t_0}^{t} A dx\right].$$

Since for (2.7) we have

$$\frac{d\hat{H}_s}{dt} + \frac{\hat{H}_s}{\chi_s} = 0,$$

the solution is

$$\hat{H}_s(t, t_0) = \hat{H}_s(t_0, t_0) e^{\frac{t_0 - t}{\chi_s}}, \quad t \geq t_0.$$

Taking t_0 to be the moment of wake-sleep switching, the initial position $\hat{H}_s(t_0, t_0)$ is where the homeostatic sleep pressure is at the upper threshold, $\hat{H}^+$, since a switch to sleep has just

occurred. Therefore, when $t = t_0$ we have $\hat{H}_s(t_0, t_0) = \hat{H}^+(t_0)$, thus

$$\hat{H}_s(t, t_0) = \hat{H}^+(t_0)e^{\frac{t_0 - t}{\chi_s}}, \quad t \geq t_0. \tag{2.9}$$

Using the same method for (2.8), we have

$$\hat{H}_w(t, t_0) = 1 + (\hat{H}^-(t_0) - 1)e^{\frac{t_0 - t}{\chi_w}}, \quad t \geq t_0, \tag{2.10}$$

where now t_0 is taken to be the moment of sleep-wake switching. Since, $C(t) = \sin(\omega(t + \phi))$ we can re-scale time as $\hat{t} = \frac{\omega(t-\phi)}{2\pi}$ so that oscillations have period one. Therefore we define $t = \frac{2\pi}{\omega}\hat{t} + \phi$ with functions $\hat{H}^{\pm}(\hat{t})$ and $\hat{H}_{s,w}(\hat{t}, \hat{t_0})$. The solution for sleep (2.9) becomes

$$\hat{H}_s(t, t_0) = \hat{H}_s\left(\frac{2\pi}{\omega}\hat{t} + \phi, \frac{2\pi}{\omega}\hat{t_0} + \phi\right) = \hat{H}^+(\hat{t}_0)\exp\left[\frac{\frac{2\pi}{\omega}(\hat{t}_0 - \hat{t})}{\chi_s}\right], \quad t \geq t_0, \tag{2.11}$$

thus we choose $\hat{\chi}_s = \frac{\omega}{2\pi}\chi_s$ as a re-scaling. Following the same method for wake equation (2.10) we choose $\hat{\chi}_w = \frac{\omega}{2\pi}\chi_w$.

By substituting in all of our re-scalings our new model becomes,

$$\hat{H}_s(\hat{t}, \hat{t_0}) = \hat{H}^+(\hat{t}_0)\exp\left[\frac{\hat{t}_0 - \hat{t}}{\hat{\chi}_s}\right], \quad \hat{t} \geq \hat{t}_0,$$

which is a solution of the initial value problem $\hat{\chi}_s\hat{H}_s' = -\hat{H}_s$, $\hat{H}_s(\hat{t}_0) = \hat{H}^+(\hat{t}_0)$ during sleep and

$$\hat{H}_w(\hat{t}, \hat{t_0}) = 1 + (\hat{H}^-(\hat{t}_0) - 1)\exp\left[\frac{\hat{t}_0 - \hat{t}}{\hat{\chi}_w}\right], \quad \hat{t} \geq \hat{t}_0,$$

which is a solution of the initial value problem $\hat{\chi}_w\hat{H}_w' = 1 - \hat{H}_w$, $\hat{H}_w(\hat{t}_0) = \hat{H}^-(\hat{t}_0)$ during wake, where the primes indicate differentiation with respect to $\hat{t}$. These rescaled equations have an upper asymptote of 1 and a lower asymptote of 0.

In summary, the upper and lower thresholds are now $\hat{H}^+(t) = \hat{H}_0^+ + \hat{a}\hat{C}(\hat{t})$ and $\hat{H}^-(t) = \hat{H}_0^- + \hat{a}\hat{C}(\hat{t})$ respectively, where $\hat{C}(\hat{t}) = \sin(2\pi\hat{t})$. The ODE's describing the system are given by

$$\hat{\chi}_s\frac{d\hat{H}_s}{dt} + \hat{H}_s = 0, \quad \hat{H}_s(\hat{t}_0, \hat{t}_0) = \hat{H}^+(\hat{t}_0)$$

during sleep and

$$\hat{\chi}_w\frac{d\hat{H}_w}{dt} + \hat{H}_w = 1, \quad \hat{H}_w(\hat{t}_0, \hat{t}_0) = \hat{H}^-(\hat{t}_0)$$

during wake, where our new parameters are defined by

$$\hat{t} = \frac{\omega}{2\pi}(t-\phi), \qquad \hat{\chi}_s = \frac{\omega\chi_s}{2\pi}, \qquad \hat{\chi}_w = \frac{\omega\chi_w}{2\pi},$$

$$\hat{H}^+(\hat{t}) = \frac{H^+\left(\frac{2\pi}{\omega}\hat{t}+\phi\right)-\mu_s}{\mu_w-\mu_s}, \qquad \hat{H}^-(\hat{t}) = \frac{H^-\left(\frac{2\pi}{\omega}\hat{t}+\phi\right)-\mu_w}{\mu_w-\mu_s},$$

$$\hat{H}_0^{\pm} = \frac{H_0^{\pm}-\mu_s}{\mu_w-\mu_s}, \qquad \hat{a} = \frac{a}{\mu_w-\mu_s}.$$

Upon dropping the hats, we get the model below. Though $\hat{H}_s(t,t_0)$ and $\hat{H}_w(t,t_0)$ depend on the initial time t_0, for the remainder of this thesis we will not write the parameter t_0 if no confusion will arise.

For the remainder of this report we will use this re-parametrized version of the model which has been reduced to five parameters: sleep and wake constants χ_s, χ_w which determine the rate of decay and growth of the homeostatic process; the mean values of the upper and lower thresholds, H_0^+ and H_0^- respectively, and the amplitude of the circadian oscillation, a.

The Two Process Model

The equations for the homeostat are

$$H_s(t) = H^+(t_0)e^{\frac{t_0-t}{\chi_s}}, \quad t \geq t_0, \tag{2.12}$$

during sleep and

$$H_w(t) = 1 + (H^-(t_0)-1)e^{\frac{t_0-t}{\chi_w}}, \quad t \geq t_0, \tag{2.13}$$

during wake.

Switching occurs from wake to sleep at the upper threshold,

$$H^+(t) = H_0^+ + a\sin(2\pi t), \tag{2.14}$$

and from sleep to wake at the lower threshold,

$$H^-(t) = H_0^- + a\sin(2\pi t). \tag{2.15}$$

In Figure 2.1 we plot the periodic solutions of the two process model for some parameter values and label these equations. We see the growth and decay of the homeostatic sleep pressure and how different choices of parameters can yield a variety of sleep patterns. Also, note in Figure 2.1(d) that the model allows for the homeostatic process to pass through the upper threshold during sleep. Similarly the homeostatic process during wake can pass through the

lower threshold.

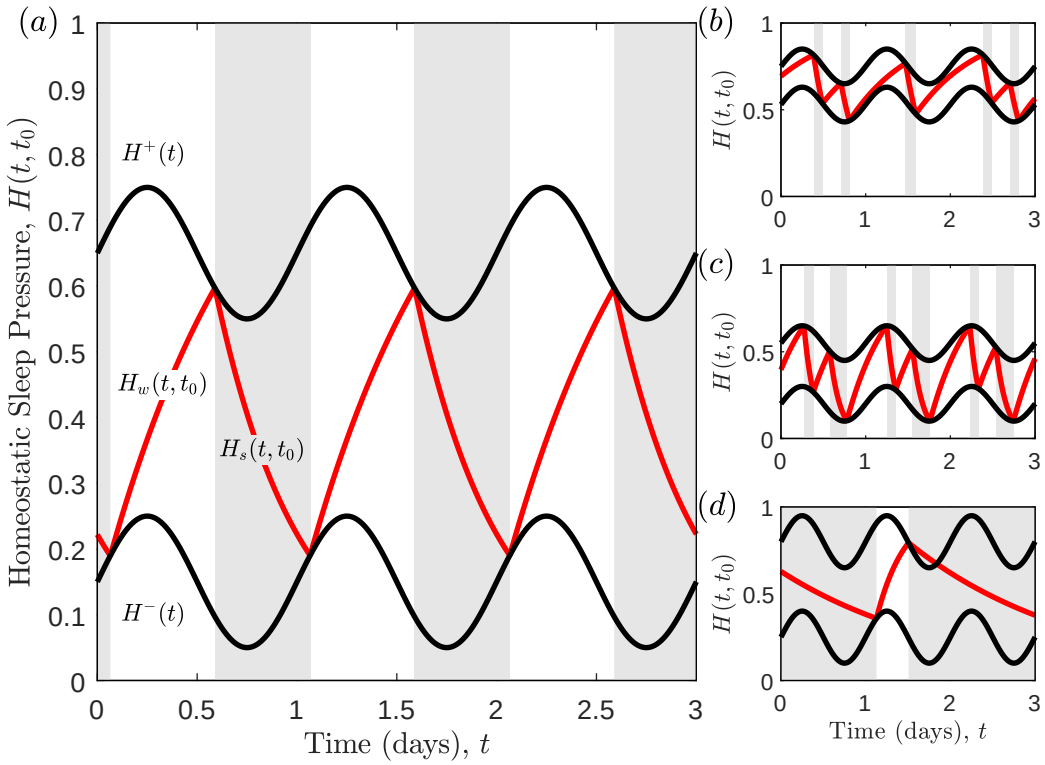

Figure 2.1: The two process model. (a) A one sleep/day periodic sleep-wake cycle, showing the homeostatic sleep pressure (shown in red) increasing during wake until it hits the upper threshold and then decreasing during sleep (shaded regions) until it hits the lower threshold. The thresholds are shown in black. Parameter values: $a = 0.1, H_0^- = 0.15, H_0^+ = 0.65, \chi_s = 0.417, \chi_w = 0.75$. *(b),(c) and (d) show three other possible patterns that occur as parameters are varied. Parameter values: (b)* $a = 0.1, H_0^- = 0.53, H_0^+ = 0.75, \chi_s = 0.25, \chi_w = 0.75$ *giving a sleep-wake cycle that repeats every two days with three sleep episodes; (c)* $a = 0.1, H_0^- = 0.2, H_0^+ = 0.55, \chi_s = 0.124, \chi_w = 0.5$ *giving a sleep-wake cycle that repeats every day with two sleep episodes; (d)* $a = 0.15, H_0^- = 0.25, H_0^+ = 0.8, \chi_s = 2, \chi_w = 0.3$ *giving a sleep-wake cycle that repeats every two days with one sleep episode.*

Next we discuss some restrictions that we impose on possible values of the parameters defined in this section.

2.1.3 Physiologically motivated assumptions

We now consider some basic physiological properties of the sleep-wake cycle and the restrictions this places on the parameter values in the model, namely:

1. Sleep pressure decreases monotonically during sleep, i.e., H_s is monotonically decreasing.

2. Sleep pressure increases monotonically during wake, i.e., H_w is monotonically increasing.

3. For a sleep-wake cycle to exist switching between sleep and wake and vice versa must occur.

These requirements have implications for which values of a, $H_0^{\pm}$ and $\chi_{s,w}$ are biologically relevant. Specifically, for the homeostat to decrease on sleep and increase on wake it is necessary that $\chi_{s,w} > 0$. To further impose this we restrict the lower threshold such that it cannot be above the upper asymptote and the upper threshold cannot be below the lower asymptote, ensuring that the homeostatic sleep pressure sits in the region $(0, 1)$. Therefore, $H_0^- + a < 1$ and $H_0^+ - a > 0$.

Also, switching from sleep to wake occurs if $H_s(t)$ is able to intersect with $H^-(t)$ giving,

$$H_0^- + a > 0, \tag{2.16}$$

and switching from wake to sleep occurs if $H_w(t)$ is able to intersect with $H^+(t)$ giving,

$$H_0^+ - a < 1. \tag{2.17}$$

Also, without loss of generality we consider $a \geq 0$ and restrict $H_0^- < H_0^+$. In Figure 2.2 (a)-(b) we give examples of the cases where the switching conditions (2.16) on H_0^- and (2.17) on H_0^+ are not met. We see that the homeostatic sleep pressure $H_s(t)$ is asymptotic to 0 and $H_w(t)$ is asymptotic to 1, when the thresholds sit on the outside of these regions no switch between sleep and wake can occur, this is not physiologically reasonable and thus we do not consider such cases in for the remainder of this work. Our assumptions allow for the upper and lower thresholds to lie only partially in region which gives switching, as illustrated in Figure 2.2 (c)-(d).

In summary we have the biologically relevant restrictions given below.

Parameter restrictions

$$\chi_s > 0; \qquad \chi_w > 0; \qquad a \geq 0;$$

$$-a < H_0^- < 1 - a; \qquad a < H_0^+ < 1 + a; \qquad H_0^- < H_0^+. \tag{2.18}$$

In the next section we will show that there exists a symmetry in the two process model.

2.1.4 Symmetry in ODE solutions

We now introduce a discrete symmetry that maps solutions of the sleep and wake ODE's onto each other. Consider an initial value problem of the form

$$\chi \frac{dH(t)}{dt} + H(t) = 0, \qquad H(t_0) = S(t_0) = S_0 + a\cos(2\pi t_0)$$

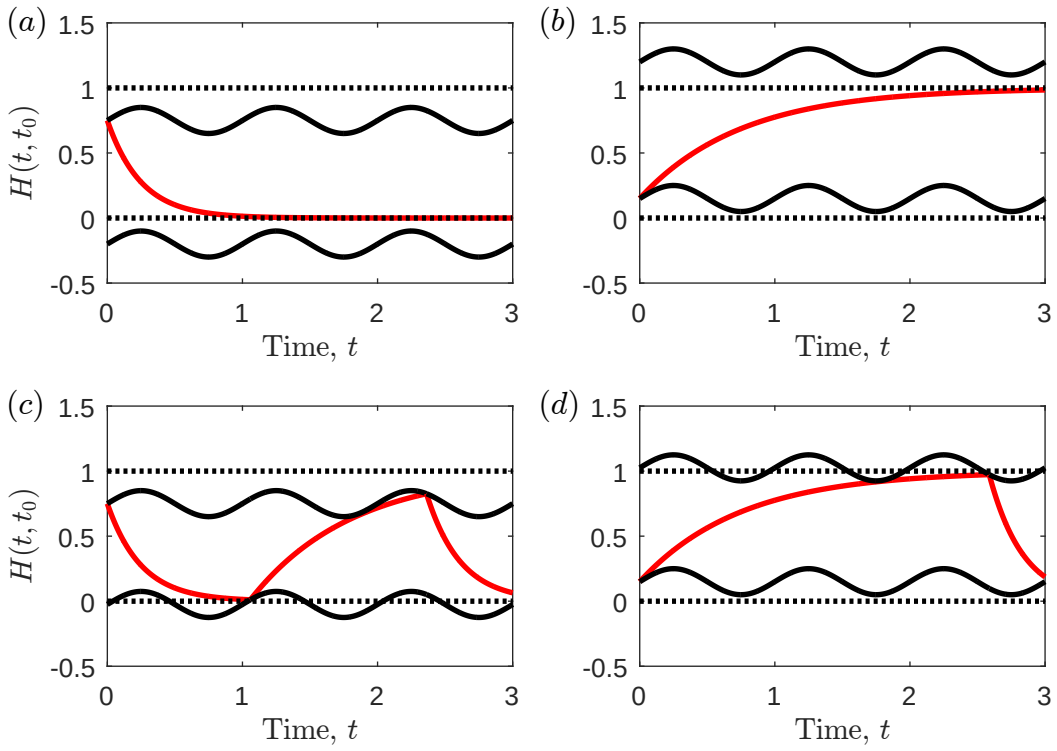

Figure 2.2: (a) The homeostat on sleep has an asymptote of 0*. If* $H_0^- + a \leq 0$ *then no sleep-wake switch can occur. (b) Similarly the homeostatic sleep pressure on wake has an asymptote of* 1 *therefore, no wake-sleep switch occurs if* $H_0^+ > 1 + a$*. Since it is not physiologically reasonable that someone could be awake or asleep forever, we impose strict bounds on* H_0^- *and* H_0^+ *to ensure that switching between wake and sleep can occur. (c)-(d) The threshold values only need to lie partially in* $(0, 1)$ *to ensure switching. These cases may sometimes not be viewed as physiological however, we have not excluded them in our assumptions.*

which has solutions

$$H(t) = S(t_0)e^{\frac{t_0 - t}{\chi}}.$$

To get the sleep initial value problem, we use $S_0 = H_0^+$ and $\chi = \chi_s$, then $H = H_s$. The wake initial value problem can be obtained from this expression too. Write $H(t) = 1 - H_w(t + \frac{1}{2})$, $\chi = \chi_w$, $S_0 = 1 - H_0^-$ then

$$\chi_w \frac{dH_w}{dt} + H_w = 1 \Leftrightarrow -\chi \frac{dH}{dt} + 1 - H = 1 \Leftrightarrow \chi \frac{dH}{dt} + H = 0$$

and

$$H_w(t_0) = H^-(t_0) \Leftrightarrow H(t_0) = 1 - H^- \left(t_0 + \frac{1}{2}\right) = S\left(t_0 + \frac{1}{2}\right),$$

as the ODE is translation invariant.

The symmetry relating solutions from the sleep and wake dynamics is therefore given below.

Symmetry relations

$$(t, H_s; \chi_s, H_0^+, H_0^-, a, t_0) \longmapsto (t + \frac{1}{2}, 1 - H_w; \chi_w, 1 - H_0^-, 1 - H_0^+, a, t_0 + \frac{1}{2}) \tag{2.19}$$

The symmetry given in (2.19) will be used in Section 3.2.2, to relate results involving the homeostatic sleep pressure during sleep to analogous results for the homeostatic sleep pressure during wake.

Now that we have introduced the equations governing the two process model we look at a special case where the amplitude of the circadian oscillation is zero. We will show that this case yields only periodic solutions and find the length of the period.

2.1.5 Special case with zero amplitude circadian oscillator

In this section we look at the case where the circadian oscillator has zero amplitude ($a = 0$) and show that all solutions in this system are as sketched in Figure 2.3 and hence periodic. This periodicity gives a basis for finding regions of periodicity at non-zero amplitudes.

First we consider how setting $a = 0$ affects the thresholds and the parameter constraints. The threshold functions H^+ and H^- become constants given by the mean value of the respective thresholds, H_0^+, H_0^-. The homeostat is now defined by

$$H_s(t) = H_0^+ e^{\frac{t_0 - t}{\chi_s}},$$

on sleep and

$$H_w(t) = 1 + (H_0^- - 1)e^{\frac{t_0 - t}{\chi_w}},$$

on wake. Note that the switching assumptions (2.16), (2.17) become

$$0 < H_0^- < H_0^+ < 1,$$

ensuring that the homeostatic sleep pressure reaches the thresholds.

We begin the homeostatic sleep pressure at $t = t_0$ on the upper threshold on a sleep trajectory $H_s(t_0) = H_0^+$ and let $t = t_s$ be the point the sleep homeostatic sleep pressure meets the lower threshold. Therefore we have

$$H_s(t_s) = H_0^+ e^{\frac{t_0 - t_s}{\chi_s}} = H_0^-,$$

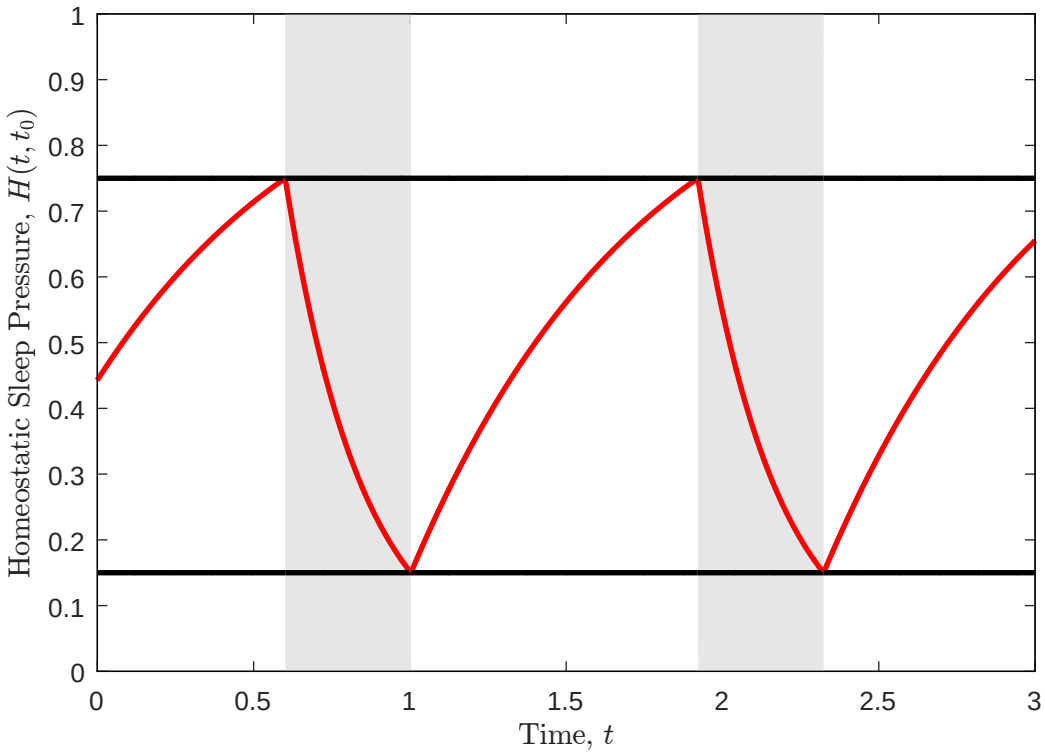

Figure 2.3: When the circadian oscillator has zero amplitude all solutions are periodic. Here we see that the length of wake and sleep (shaded) is the same for every cycle, independent of the starting point.

which can be rearranged to give

$$t_s = t_0 - \chi_s \ln\left(\frac{H_0^-}{H_0^+}\right).$$

Similarly, let $t = t_w$ be the point the wake homeostatic sleep pressure meets the upper threshold where $t = t_s$ is taken to be the initial time value. Here we get

$$H_w(t_w) = 1 + (H_0^- - 1)e^{\frac{t_s - t_w}{\chi_w}} = H_0^+,$$

yielding

$$t_w = t_s - \chi_w \ln\left(\frac{H_0^+ - 1}{H_0^- - 1}\right).$$

At time t_w, the homeostat has returned to the upper threshold at $H_w(t_w)$, which has the same value as $H_s(t_0)$. Therefore we see that any $t_0 \in [0, 1]$ will result in a solution which repeats with

period T_n given by

$$T_n = t_w - t_s + t_s - t_0 = \chi_s \ln\left(\frac{H_0^+}{H_0^-}\right) + \chi_w \ln\left(\frac{H_0^- - 1}{H_0^+ - 1}\right), \tag{2.20}$$

where $\chi_s \log\left(\frac{H_0^+}{H_0^-}\right)$ is the length of a sleep episode and $\chi_w \log\left(\frac{1-H_0^-}{1-H_0^+}\right)$ is the length of a wake episode. Note that such solutions have p sleeps over q days, when

$$T_n = \frac{q}{p},$$

where a 'day' corresponds to a period of the circadian oscillator. We will return to this case in more detail later as it forms a basis for constructing an approximation of periodic solutions when the two process model has a small amplitude circadian oscillation.

Whilst the zero amplitude case is interesting in itself, there exists a much wider range of dynamics for $a > 0$. In the next section we introduce some of the sleep-wake patterns which can be seen by varying parameters in the two process model.

2.1.6 Complex dynamics

It is well known that the two-process model can show a range of different sleep-wake cycles. In humans, the most common sleep-wake pattern in modern society is monophasic, consisting of one sleep and one wake per day. However the model can describe patterns with both fewer or more sleep-wake cycles per day [79]. The patterns of sleep with more than one sleep per day are called polyphasic. In Figure 2.4 we see that by varying only two parameters we can achieve a wide range of sleep behaviour.

The polyphasic patterns which arise in the model have biological significance. For example babies exhibit polyphasic patterns which gradually transition into monophasic sleep over the first few years of development [126]. In Chapter 4 we consider another example, exploring the polyphasic sleep-wake patterns of the common vole using the two process model.

A bifurcation diagram can be created by varying one parameter in the model and observing the sleep-wake pattern after the transient has decayed. The bifurcation diagram given by varying the amplitude, a, is shown in Figure 2.5. For larger values of a we see a monophasic sleep-wake pattern (one sleep-wake episode each day). As we decrease the value of a, transitions from monophasic to polyphasic (multiple sleep-wake episodes per day) occurs.

One of the key aims in this thesis is to gain a better understanding of the bifurcation structures associated with the transitions between monophasic and polyphasic sleep-wake patterns and the role played by the model parameters. It has been shown [107] that the two process model can be linked to a one-dimensional map, which is a useful way to explore the dynamics

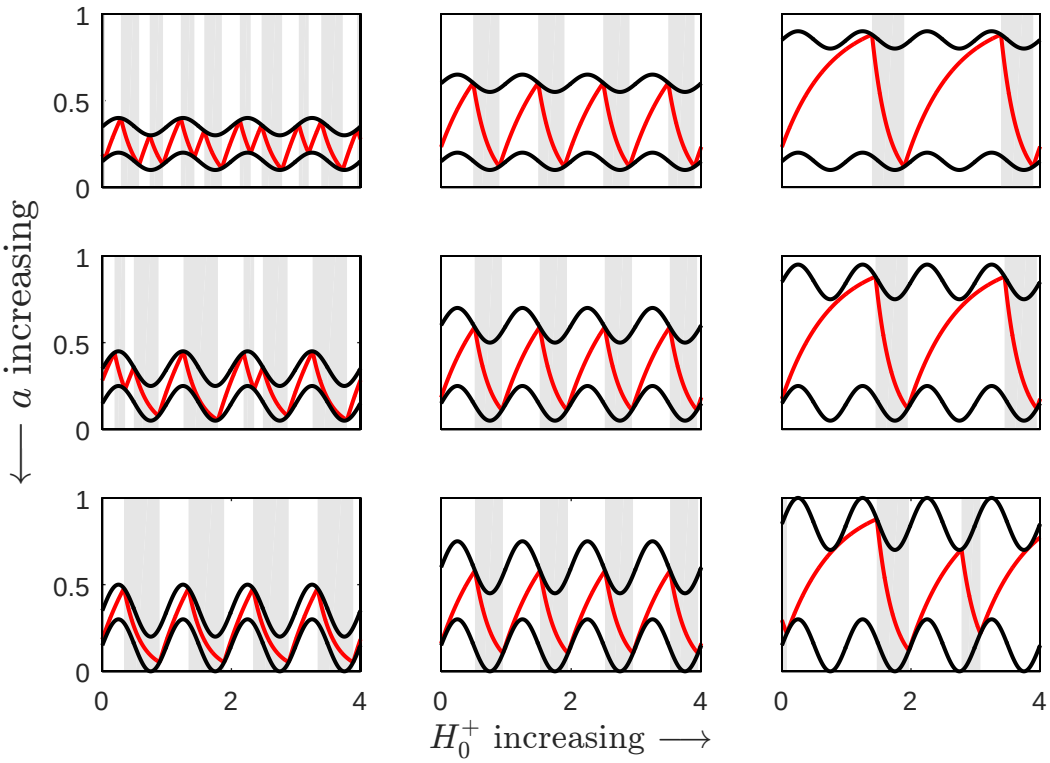

Figure 2.4: Nine sample simulations of the two process model showing the orbit after the transient has decayed for 3 amplitude values (a = 0.05, 0.10, and 0.15) with 3 levels of the upper threshold (H_0^+ = 0.35, 0.60, and 0.85).

of the model. In the remainder of this chapter we will define this one-dimensional map and explore its properties. This leads us to formally define periodicity in the two-process model. We then consider the small amplitude approximation for the specific case of periodic solutions with 1 sleep over any number of days.

2.2 The associated one-dimensional map

In this section we show how the two process model can be represented as a one-dimensional map and explore some of the properties of the map and its fixed points.

2.2.1 The composite map

There are multiple ways in which we can construct a one-dimensional map from the two process model. However, to study periodicity and begin to understand the bifurcation structure associated with the transitions between different periodic sleep-wake patterns it is sufficient to consider the map that takes a point on the upper threshold and maps it into the next point

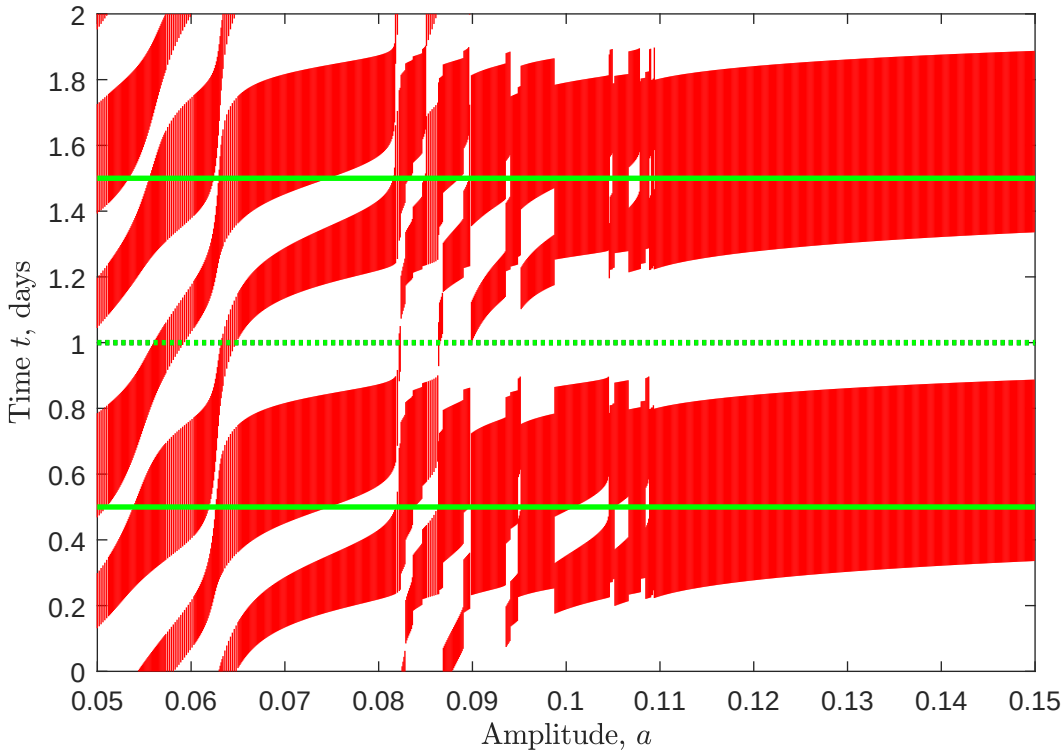

Figure 2.5: A bifurcation diagram showing transitions from the left column of Figure 2.4 by varying the amplitude, a, between 0.05 and 0.15 when $H_0^- = 0.15, H_0^+ = 0.35, \chi_s = 0.25, \chi_w = 0.75$. Sleep is given in red and wake in white. At $a = 0.05$ we have $2-3$ sleeps per day, at $a = 0.1$ we have a very defined 2 sleep on the first day and 1 sleep on the second day and for $a = 0.15$ we have one sleep per day. Time is plotted over two days so that patterns over multiple days can be observed. The bold and dashed green lines indicate the maximum and minimum of the circadian phase respectively.

on the upper threshold (iterating the model through one sleep-wake cycle) This map can be regarded as the composition of two maps. Here we introduce the notion of a 'down' and 'up' map which together form the composite map used for the remainder of this report. To understand dynamical properties such as periodicity we will focus on a map in terms of time.

First we consider the map that goes from the upper threshold to the lower threshold, since the homeostatic sleep pressure decreases during sleep. We define this as the down map $T_d : \mathbb{R} \to \mathbb{R}$ where $T_d(t_0)$ is the first time greater than t_0 such that

$$H_s(T_d(t_0), t_0) = H^-(T_d(t_0)).$$

Similarly we define the up map $T_u : \mathbb{R} \to \mathbb{R}$ as the map that goes from the lower threshold to

the upper threshold, during wake where $T_u(t_0)$ is the first time greater than t_0 such that

$$H_w(T_u(t_0), t_0) = H^+(T_u(t_0)).$$

We can then define the composite map $T_s : \mathbb{R} \to \mathbb{R}$ which maps the upper threshold onto itself via the down and up maps thus,

$$T_s(t_0) = T_u(T_d(t_0)). \tag{2.21}$$

Since we have constructed the circadian process in such a way that the upper and lower thresholds are one-day periodic it follows that all three maps satisfy

$$T_i(t_0 + 1) = T_i(t_0) + 1, \quad i = d, u, s.$$

Typical examples of the three maps, $T_i, i = d, u, s$ are shown in Fig. 2.6. In Fig 2.6(c) the 1-1 line allows us to visualise fixed points of the map, these correspond to periodic solutions of the two process model.

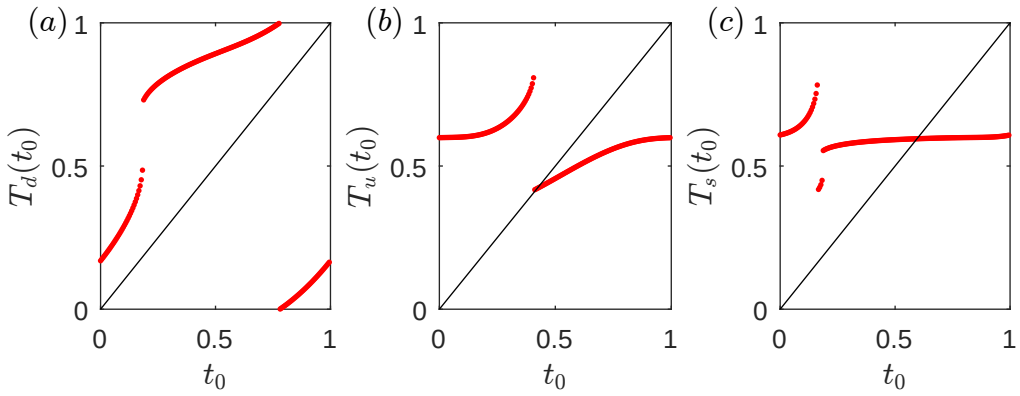

Figure 2.6: Typical examples of T_i mod 1 for $i = d, u, s$. Parameter values: $a = 0.15, H_0^- = 0.25, H_0^+ = 0.75, \chi_s = 0.25, \chi_w = 0.75$. For the remainder of the examples in this chapter and the next we take H_0^+, χ_s, χ_w to be the values given here but a and H_0^- will vary.

For large regions of the parameter plane, including small values of the parameter a, T_s is the degree 1 monotonic circle map on the interval $[0, 1]$ and hence the theory of monotonic circle maps with and without gaps can be applied. Thus the map has a unique rotation number given by

$$\rho(T_s) = \lim_{n\to\infty} \frac{T_s^n(t_0) - t_0}{n}.$$

This rotation number does not depend on the value t_0. If the rotation number is rational, then the map has periodic solutions.

Now that we have defined the composite map we will consider its derivative. We will use the

derivative in Section 3.1.1, when we consider bifurcations of the fixed points.

2.2.2 Derivative of the map

Later we will need the gradient of the composite map which can be found by differentiating (2.21) with respect to t_0, giving

$$T_s'(t_0) = T_u'(T_d(t_0))T_d'(t_0), \tag{2.22}$$

To find expressions for T_d', T_u' we revisit the equations which govern the homeostatic process namely,

$$H_s(t,t_0) = H^+(t_0)e^{\frac{t_0-t}{\chi_s}}, \quad H^+(t) = H_0^+ + a\sin(2\pi t),$$

during sleep and

$$H_w(t,t_0) = 1 + (H^-(t_0)-1)e^{\frac{t_0-t}{\chi_w}}, \quad H^-(t) = H_0^- + a\sin(2\pi t).$$

during wake.

At $t = T_d(t_0)$ the sleep trajectory is on the lower threshold thus we have an equation relating t_0 and $T_d(t_0)$ given by,

$$H_0^- + a\sin(2\pi T_d(t_0)) = \big(H_0^+ + a\sin(2\pi t_0)\big)e^{\frac{t_0-T_d(t_0)}{\chi_s}}. \tag{2.23}$$

Also, at $t = T_u(T_d)$ the wake trajectory is on the upper threshold and have an equation relating T_d and $T_u(T_d)$ given by,

$$H_0^+ + a\sin(2\pi T_u(T_d)) = 1 + \big(H_0^- + a\sin(2\pi T_d - 1)\big)\, e^{\frac{T_d-T_u(T_d)}{\chi_w}}. \tag{2.24}$$

By separating the variables, equation (2.23) becomes

$$\big(H_0^- + a\sin 2\pi T_d(t_0)\big)\, e^{\frac{T_d(t_0)}{\chi_s}} = \big(H_0^+ + a\sin 2\pi t_0\big)\, e^{\frac{t_0}{\chi_s}}, \tag{2.25}$$

and equation (2.24) reads

$$\big(H_0^- - 1 + a\sin 2\pi S_0\big)\, e^{\frac{S_0}{\chi_w}} = \big(H_0^+ - 1 + a\sin 2\pi T_u(S_0)\big)\, e^{\frac{T_u(S_0)}{\chi_w}}, \tag{2.26}$$

where $S_0 = T_d(t_0)$. Both sides of (2.25) and (2.26) are of the form

$$f(H,\tau(S)) = f(H,S) \quad \text{with} \quad f(H,S) = (H + a\sin(2\pi S))e^{\frac{S}{\chi}},$$

with $\tau(S) = T_d(S)$ in (2.25) and $\tau(S) = \tau_u(S)$ in (2.26). This relation can be differentiated with respect to S to give

$$f'(H,\tau(S))\tau'(S) = f'(H,S) \quad \text{with} \quad \frac{\partial}{\partial S}f(H,S) = \left(2\pi a\cos(2\pi S) + \frac{H}{\chi} + \frac{a}{\chi}\sin(2\pi S)\right)e^{\frac{S}{\chi}}. \tag{2.27}$$

When $T_d(t_0)$ is locally well defined, using (2.27) we see that the derivative of (2.25) with repect to t_0 is

$$\left(2\pi a\cos(2\pi T_d(t_0)) + \frac{H_0^-}{\chi_s} + \frac{a}{\chi_s}\sin(2\pi T_d(t_0))\right)e^{\frac{T_d(t_0)}{\chi_s}}\cdot T_d'(t_0) = \left(2\pi a\cos(2\pi t_0) + \frac{H_0^+}{\chi_s} + \frac{a}{\chi_s}\sin(2\pi t_0)\right)e^{\frac{t_0}{\chi_s}}.$$

Therefore the derivative of the down map is

$$T_d'(t_0) = \frac{\left(2\pi a\cos(2\pi t_0) + \frac{H_0^+}{\chi_s} + \frac{a}{\chi_s}\sin(2\pi t_0)\right)e^{\frac{t_0 - T_d(t_0)}{\chi_s}}}{\left(2\pi a\cos(2\pi T_d(t_0)) + \frac{H_0^-}{\chi_s} + \frac{a}{\chi_s}\sin(2\pi T_d(t_0))\right)}. \tag{2.28}$$

We also consider (2.26) and differentiate with respect to S_0 to give,

$$T_u'(S_0) = \frac{\left(2\pi a\cos(2\pi S_0) + \frac{H_0^- - 1}{\chi_w} + \frac{a}{\chi_w}\sin(2\pi S_0)\right)e^{\frac{S_0 - T_u(S_0)}{\chi_w}}}{\left(2\pi a\cos(2\pi T_u(S_0)) + \frac{H_0^+ - 1}{\chi_w} + \frac{a}{\chi_w}\sin(2\pi T_u(S_0))\right)}, \tag{2.29}$$

the derivative of the up map.

In the next section we give conditions for the existence of periodic solutions with p sleeps over q days.

2.3 Periodic solutions

We showed in Section 2.1.5 that if $a = 0$, all solutions are periodic with fixed period, dependent on the parameters. If $a \neq 0$ this is not true any more. In this section, we characterise (p, q) periodic orbits with p sleeps in q days and find regions of existence for $(1, q)$ solutions with small a.

2.3.1 Definition of a (p, q)-periodic solution

First we define a periodic solution in the two process model with p sleeps in q days. We say that t_0 generates a (p, q)-periodic orbit if

$$T_s^p(t_0) = t_0 + q; \quad (T_s^j(t_0) - t_0) \notin \mathbb{N} \quad \text{for} \quad j = 1, \ldots, p-1.$$

Note that for the parameter regions we will consider only periodic orbits where p and q are coprime occur, however, for higher circadian amplitudes this is not always necessarily the case. By definition the time $T_s^j(t_0)$ is the j^{th} return to the upper threshold after some initial sleep onset at t_0 (or the $(j+1)^{st}$ sleep onset time). Sometimes when introducing general conditions we will use the notation $t_0 = T_s^0(t_0)$. Since the homeostatic sleep pressure runs forward in time we have $t_0 = T_s^0(t_0) < T_d(t_0) < T_u(T_d(t_0)) = T_s(t_0)$ and the inequality $T_s^0(t_0) < T_s(t_0) < T_s(T_s(t_0)) = T_s^2(t_0) < \cdots < T_s^j(t_0)$, must be satisfied. Note that if T_s has a (p, q) periodic orbit, the greatest common divisor of p and q will be 1 and the theory of monotonic circle maps gives that function T_s has the rotation number $\rho(T_s) = \frac{q}{p}$.

The (p, q) periodic orbit generated by t_0 satisfies

$$H_s(t_0) = H_s(T_s^p(t_0)), \quad t_0 + q = T_s^p(t_0).$$

Hence the homeostatic sleep pressure returns to its initial values on the upper and lower thresholds after p sleeps and q days. Using the continuity of $H(t)$ for all switches in a (p, q) orbit, we get at the lower threshold

$$H_s(T_d(T_s^j(t_0)), T_s^j(t_0)) = H_w(T_d(T_s^j(t_0)), T_d(T_s^j(t_0))) = H^-(T_d(T_s^j(t_0))), \quad j = 0, \ldots, p-1,$$

and at the upper threshold

$$H_s(T_s^j(t_0), T_s^j(t_0)) = H_w(T_s^j(t_0), T_d(T_s^{j-1}(t_0))) = H^+(T_s^j(t_0)), \quad j = 1, \ldots, p-1.$$

Therefore if a point t_0 is the generator of a (p, q) orbit then the $2p$ conditions below are satisfied.

Necessary conditions for a (p, q) periodic orbit

$$H_s(T_d(T_s^j(t_0)), T_s^j(t_0)) = H^-(T_d(T_s^j(t_0))), \quad j = 0, \ldots, p-1 \tag{2.30a}$$

$$H_w(T_s^j(t_0), T_d(T_s^{j-1}(t_0))) = H^+(T_s^j(t_0)), \quad j = 1, \ldots, p-1 \tag{2.30b}$$

$$H_w(t_0 + q, T_d(T_s^{p-1}(t_0))) = H^+(t_0 + q) = H^+(t_0). \tag{2.30c}$$

The condition (2.30c) denotes the final return from the lower threshold to the upper threshold at time $t_0 + q$. Note that when $p = 1$ we only need to consider conditions (2.30a) and (2.30c) since $\{1, \dots, p-1\}$, as in (2.30b), becomes the empty set.

In the next section we focus on analysing the case where $p = 1$ with small amplitude circadian oscillator and approximate the H_0^- values for which periodic solutions exist. In Chapter 3 we will expand on this analysis and consider behaviour in the (H_0^-, a) parameter plane.

2.3.2 Analysis for $(1, q)$ periodic solutions

In this section we look at the existence of periodic solutions consisting of exactly one sleep-wake cycle, with length q days. This is a special case of the conditions found in the previous section.

In the particular case where $p = 1$ equations (2.30a) becomes

$$H^+(t_0)e^{\frac{t_0 - T_d(t_0)}{\chi_s}} = H^-(T_d(t_0)) = H_0^- + a\sin(2\pi T_d(t_0)), \tag{2.31}$$

giving continuity on the lower threshold, and (2.30c) becomes

$$H^+(t_0) = 1 + \left(H^+(t_0)e^{\frac{t_0 - T_d(t_0)}{\chi_s}} - 1\right) e^{\frac{T_d(t_0) - t_0 - q}{\chi_w}}, \tag{2.32}$$

giving both periodicity and continuity on the upper threshold.

Thus (2.31) and (2.32) are two equations for two unknowns t_0 and $T_d(t_0)$. These equations can be rewritten to make analysis easier by defining the length of the sleep episode as

$$\tau := T_d(t_0) - t_0 \in (0, q). \tag{2.33}$$

Substituting this into both (2.31) and (2.32) gives

$$H^+(t_0)e^{-\frac{\tau}{\chi_s}} = H_0^- + a\sin(2\pi(\tau + t_0)), \tag{2.34}$$

and

$$H^+(t_0) = 1 + \left(H^+(t_0)e^{-\frac{\tau}{\chi_s}} - 1\right) e^{\frac{\tau - q}{\chi_w}}, \tag{2.35}$$

respectively. Now we have two equations for two unknowns t_0, τ. In the next steps we will analyse these equations.

We begin by defining

$$\alpha(\tau) = \frac{1 - e^{\frac{\tau - q}{\chi_w}}}{1 - e^{-\frac{\tau}{\chi_s}} e^{\frac{\tau - q}{\chi_w}}}. \tag{2.36}$$

Since the derivative $\alpha'(\tau)$ will appear throughout this section we determine it here:

$$\alpha'(\tau) = \frac{\left(\frac{1}{\chi_w} - \frac{1}{\chi_s}\right)\left(1 - e^{\frac{\tau-q}{\chi_w}}\right) e^{\frac{\tau-q}{\chi_w} - \frac{\tau}{\chi_s}} - \frac{1}{\chi_w} e^{\frac{\tau-q}{\chi_w}} \left(1 - e^{\frac{\tau-q}{\chi_w} - \frac{\tau}{\chi_s}}\right)}{\left(1 - e^{\frac{\tau-q}{\chi_w} - \frac{\tau}{\chi_s}}\right)^2}. \tag{2.37}$$

Rearranging (2.35) gives

$$H^+(t_0) = \alpha(\tau), \tag{2.38}$$

a relation between t_0 and τ. In Appendix A.1. we show that $\alpha(\tau)$ is a monotonically decreasing function for $\tau \in [0, q]$ with $\alpha(0) = 1$ and $\alpha(q) = 0$. In other words, α is a bijection between $[0, q]$ and $[0, 1]$.

Using (2.38), given some initial time t_0 where $H(t_0)$ is on the upper threshold we can find the corresponding length of sleep. This implicitly defines a function $\tau(t_0)$ for values of t_0 such that $H_0^+ + a\sin(t_0) \leq 1$. We will use this relation throughout the analysis that follows.

Taking (2.34) we also introduce the function

$$\beta(\tau, t_0) = H^+(t_0)e^{-\frac{\tau}{\chi_s}} - a\sin(2\pi(t_0 + \tau)). \tag{2.39}$$

We can rewrite the conditions (2.30) for the existence of a $(1, q)$ periodic orbit as finding the pair $(t_0, \tau) \in (0, q) \times (0, q)$ such that the conditions below hold.

Necessary conditions for a $(1, q)$ periodic orbit

$$H^+(t_0) = \alpha(\tau) \quad \text{where} \quad \alpha(\tau) = \frac{1 - e^{\frac{\tau-q}{\chi_w}}}{1 - e^{-\frac{\tau}{\chi_s}} e^{\frac{\tau-q}{\chi_w}}}, \tag{2.40}$$

and

$$H_0^- = \beta(\tau, t_0) \quad \text{where} \quad \beta(\tau, t_0) = H^+(t_0)e^{-\frac{\tau}{\chi_s}} - a\sin(2\pi(t_0 + \tau)). \tag{2.41}$$

As indicated before $\alpha(\tau)$ is well defined for $\tau \in (0, q)$ and (2.40) gives an implicit relation between τ and t_0, depicted in Figure 2.7. Since $\alpha(\tau)$ is monotonically decreasing choosing a sleep length τ gives one fixed value of $\alpha(\tau)$, valid if and only if $\alpha(\tau) \in [H_0^+ - a, H_0^+ + a]$. Since $H^+(t_0)$ is a sine wave with amplitude, a, using the condition (2.40) gives two corresponding t_0 values (or one) which satisfy $\alpha(\tau) = H_0^+ \pm a\sin(2\pi t_0)$. Similarly, taking some initial t_0 it is possible to find the corresponding length of sleep τ.

In the next section we will use conditions (2.40) and (2.41) to find a small amplitude approximation of the H_0^+ values for which a periodic solution exists. We will also revisit these conditions in the next chapter to find numerically the wedge shaped regions of existence for $(1, q)$-periodic solutions.

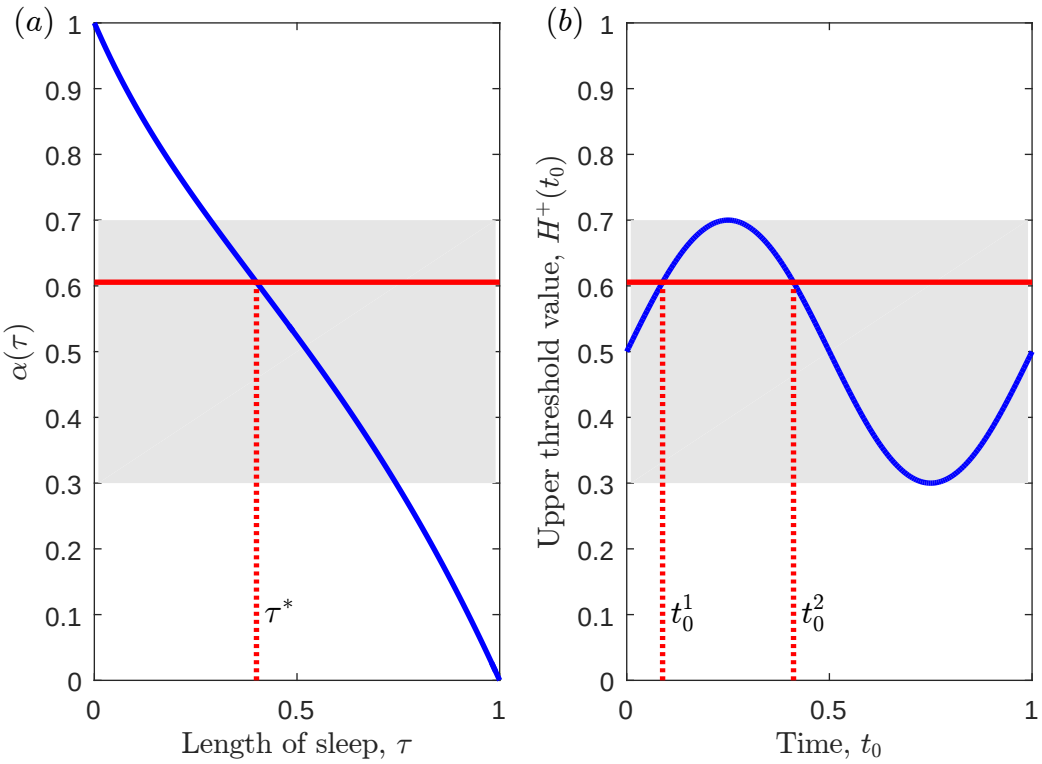

Figure 2.7: (a) The blue curve shows $\alpha(\tau)$ monotonically decreasing. The dotted red line shows the value of some sleep length τ^* such that $\alpha(\tau) \in [H_0^+ - a, H_0^+ + a]$. The relevant region of $\alpha(\tau)$ is shaded and given by the minimum and maximum values of $H^+(t_0)$. The horizontal red line is the constant $\alpha(\tau^*)$. (b) Looking at the intersections of $\alpha(\tau^*)$ with $H^+(t_0)$ (the blue curve) gives the two corresponding t_0 values. Parameter values used here are: $a = 0.2, H_0^- = 0.25, H_0^+ = 0.5, \chi_s = 0.25, \chi_w = 0.75$.

2.3.3 Small circadian amplitude approximation for $(1, q)$ periodic solutions

We have shown that by defining the length of the sleep episode as $\tau := T_d(t_0) - t_0 \in (0, q)$ and introducing the functions $\alpha(\tau)$ and $\beta(\tau, t_0)$ we can rewrite the conditions (2.30) for the existence of a $(1, q)$ periodic orbit as finding the pair $(t_0, \tau) \in (0, q) \times (0, q)$ such that (2.40) and (2.41) are satisfied. In this section we find $(1, q)$-periodic solutions for $a = 0$ and expand this case to give an approximation for solutions for a small.

We begin by considering the case where $a = 0$, the case examined in Section 2.1.5. First we define $\tau_0 = \tau(t_0)$ to be the length of sleep which yields a $(1, q)$-periodic solution for zero amplitude, given implicitly by (2.40). At $a = 0$, $H^+(t) = H_0^+$ and the unique length of sleep that leads to a one day periodic solution is given by $\alpha(\tau_0) = H_0^+$. Substituting this and $a = 0$ into (2.41) gives

$$H_0^- = H_0^+ e^{-\frac{\tau_0}{\chi_s}} \tag{2.42}$$

or equivalently

$$\chi_s \log\left(\frac{H_0^+}{H_0^-}\right) = \tau_0 \tag{2.43}$$

which is the length of sleep found in Section 2.1.5. Since the thresholds are non-oscillatory for $a = 0$, any $t_0 \in (0, q)$ will generate a $(1, q)$-periodic solution.

Next we show that the length of wake can be found using equations (2.42) and (2.40). We then show that together the lengths of sleep and wake are equivalent to $T_n = q$ where T_n is given by (2.20). First, equation (2.42) gives that $e^{\frac{-\tau_0}{\chi_s}} = \frac{H_0^-}{H_0^+}$ which can be substituted into (2.40) to give

$$H_0^+ = \frac{1 - e^{\frac{\tau_0 - q}{\chi_w}}}{1 - \frac{H_0^-}{H_0^+} e^{\frac{\tau_0 - q}{\chi_w}}}.$$

Rearranging this leads to

$$\chi_w \log\left(\frac{1 - H_0^-}{1 - H_0^+}\right) = q - \tau_0,$$

which is the length of wake found in Section 2.1.5. Therefore the period of the periodic solution satisfies

$$T = q = q - \tau_0 + \tau_0 = \chi_s \log\left(\frac{H_0^+}{H_0^-}\right) + \chi_w \log\left(\frac{1 - H_0^-}{1 - H_0^+}\right) = \tau_0 + q - \tau_0 = T_n.$$

We now fix χ_s, χ_w and H_0^+ and show that when a is small, there is an interval of H_0^- values close to $H_0^+ e^{-\frac{\tau_0}{\chi_s}}$ for which $(1, q)$-periodic solutions exist. We will show that for each $t_0 \in [0, 1]$ it is possible to find a periodic solution for an appropriate value of H_0^-. The function $\tau(t_0)$ can be expanded as $\tau(t_0) = \tau_0 + a\tau_1(t_0) + \mathcal{O}(a^2)$. By considering $\alpha(\tau(t_0)) = H^+(t_0)$ it follows immediately that

$$\tau_1 = \frac{\sin(2\pi t_0)}{\alpha'(\tau_0)}.$$

Therefore the $\tau(t_0)$ expansion is given by

$$\tau(t_0) = \tau_0 + \frac{a \sin(2\pi t_0)}{\alpha'(\tau_0)} + \mathcal{O}(a^2),$$

Now (2.41) gives the range of H_0^- values for which $(1, q)$ periodic orbits exist, parametrized by t_0:

$$H_0^- = \beta(\tau(t_0), t_0) = \left[H_0^+ + a \sin(2\pi t_0)\right] e^{-\frac{\tau(t_0)}{\chi_s}} - a \sin(2\pi(t_0 + \tau(t_0))).$$

Using the $\tau(t_0)$ expansion we get

$$e^{-\frac{\tau(t_0)}{\chi_s}} = e^{-\frac{\tau_0}{\chi_s}} \left(1 - \frac{a\tau_1}{\chi_s}\right) + \mathcal{O}(a^2) = e^{-\frac{\tau_0}{\chi_s}} \left(1 - \frac{a \sin(2\pi t_0)}{\chi_s \alpha'(\tau_0)}\right) + \mathcal{O}(a^2),$$

and

$$\sin(2\pi t_0 + \tau) = \sin(2\pi t_0 + \tau_0) + \mathcal{O}(a).$$

Making these substitutions gives

$$\begin{aligned} H_0^- &= \left[H_0^+ + a\sin(2\pi t_0)\right]\left(e^{-\frac{\tau_0}{\chi_s}}\left(1 - \frac{a\sin(2\pi t_0)}{\chi_s \alpha'(\tau_0)}\right)\right) - a\sin(2\pi(\tau_0 + t_0)) + \mathcal{O}(a^2) \\ &= H_0^+ e^{-\frac{\tau_0}{\chi_s}} + a\left(e^{-\frac{\tau_0}{\chi_s}}\sin(2\pi t_0)\left(1 - \frac{H_0^+}{\chi_s \alpha'(\tau_0)}\right) - \sin(2\pi(\tau_0 + t_0))\right) + \mathcal{O}(a^2). \end{aligned}$$

For a small we write

$$H_0^-(a, t_0) = H_0^+ e^{-\frac{\tau_0}{\chi_s}} + aH_{0_1}^-(t_0) + \mathcal{O}(a^2), \tag{2.44}$$

therefore

$$H_{0_1}^-(t_0) = e^{-\frac{\tau_0}{\chi_s}}\sin(2\pi t_0)\left(1 - \frac{H_0^+}{\chi_s \alpha'(\tau_0)}\right) - \sin(2\pi(\tau_0 + t_0)). \tag{2.45}$$

Using the double angle formula $\sin(A + B) = \sin A \cos B + \cos A \sin B$, (2.45) becomes

$$\begin{aligned} H_{0_1}^- &= e^{-\frac{\tau_0}{\chi_s}}\sin(2\pi t_0)\left(1 - \frac{H_0^+}{\chi_s \alpha\prime(\tau_0)}\right) - \sin(2\pi t_0)\cos(2\pi\tau_0) - \cos(2\pi t_0)\sin(2\pi\tau_0) \\ &= \sin(2\pi t_0)\left(e^{-\frac{\tau_0}{\chi_s}}\left(1 - \frac{H_0^+}{\chi_s \alpha\prime(\tau_0)}\right) - \cos(2\pi\tau_0)\right) - \cos(2\pi t_0)\sin(2\pi\tau_0). \end{aligned}$$

So we may write $H_{0_1} = \rho\sin(2\pi(t_0 + \theta))$ where θ and ρ satisfy

$$\rho\cos(\theta) = \left(e^{-\frac{\tau_0}{\chi_s}}\left(1 - \frac{H_0^+}{\chi_s \alpha'(\tau_0)}\right) - \cos(2\pi\tau_0)\right) \quad \text{and} \quad \rho\sin(\theta) = \sin(2\pi\tau_0),$$

implying

$$\rho = \left[\sin^2(2\pi\tau_0) + \left(e^{-\frac{\tau_0}{\chi_s}}\left(1 - \frac{H_0^+}{\chi_s \alpha'(\tau_0)}\right) - \cos(2\pi\tau_0)\right)^2\right]^{\frac{1}{2}}.$$

This shows that for a small, two $(1, q)$ periodic orbits exist in a wedge with $H_0^- \in [H_0^+ e^{-\frac{\tau_0}{\chi_s}} - a\rho, H_0^+ e^{-\frac{\tau_0}{\chi_s}} + a\rho] + \mathcal{O}(a^2)$, as illustrated in Figure 2.8.

At the edges of the wedge some mechanism must be creating and destroying periodic solutions. In the next Chapter we will explore how, for small amplitudes, saddle-node bifurcations give rise to Arnold tongues, which are approximated by the wedges found in this section. We then consider the higher amplitudes and explore how gaps in the one-dimensional map, giving rise to border collisions, are created by tangencies in the model. Finally we sketch out a picture of the bifurcation set to show how the saddle-node bifurcations and border collisions create windows with (p, q)- periodic solutions.

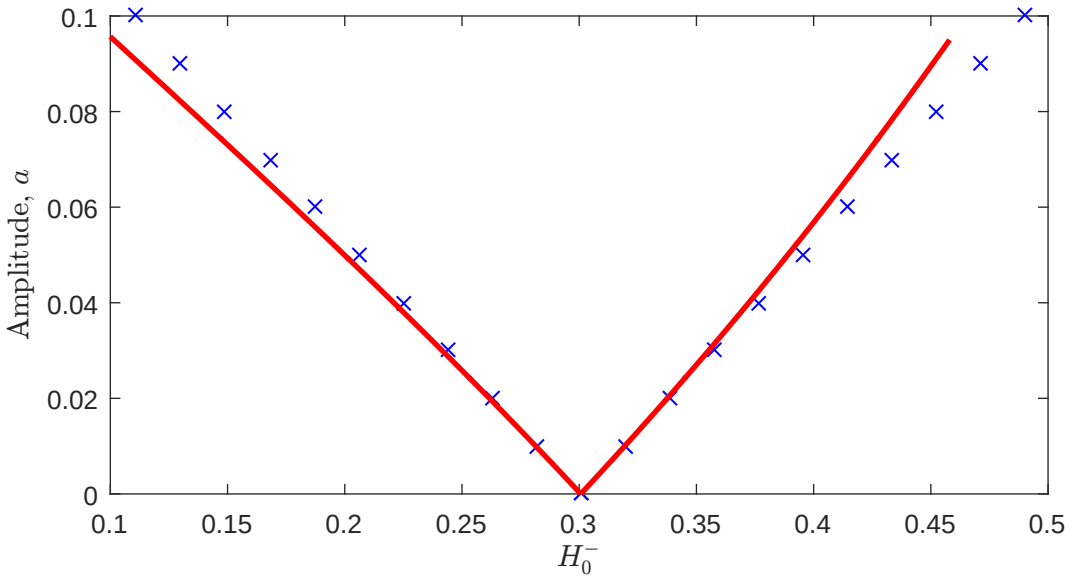

Figure 2.8: A comparison of the numerical computation (solid line) of the Arnold tongues for $(p, q) = (1, 1)$ *and the analytical expression for small* a *given in equation (2.44) (crosses).*

3

Bifurcations of periodic solutions

We have shown that for small circadian amplitudes regions of $(1, q)$ periodic solutions exist. Considering the one dimensional map close to the parameter values approximated in Section 2.3.3, suggests that these regions of periodic solutions are bounded by saddle-node bifurcations. This is illustrated in Figure 3.1, where we vary H_0^- close to the boundary of one of these regions. Figure 3.1 gives a sequence of maps where a transition from no fixed points to a pair of solutions occurs, one of these solutions is stable and the other is unstable. The map T_s depends smoothly on the circadian amplitude, a, hence perturbation theory gives for small a that T_s is monotonic in t_0 and is conjugate to the degree 1 monotonic, continuous Arnold circle map. Therefore, regions of (p, q)-periodic orbits of the map form tongue-like regions [109] for small amplitude, a, in a two dimensional parameter plane consisting of a and one of the four parameters χ_s, χ_w, H_0^+ and H_0^-. Varying any of these four parameters will give changes in the length of the sleep-wake orbit T_n at $a = 0$.

In the remainder of this chapter we consider the bifurcation behaviour of the periodic solutions as a function of a and H_0^-. Since T_n is a monotonic function of χ_s, χ_w, H_0^+ and H_0^- we expect the results to be qualitatively similar if any of the first three had been selected instead of H_0^-.

3.1 Saddle node bifurcations

In this section we give a numerical method for finding the boundary of (p, q)-tongues as generated by saddle-node bifurcations.

3.1.1 Calculation of general (p, q) tongues

In section 2.3.3 we found analytically an approximation for the region of existence of periodic solutions for $p = 1$ and small a. Now we will extend this and find numerically the regions

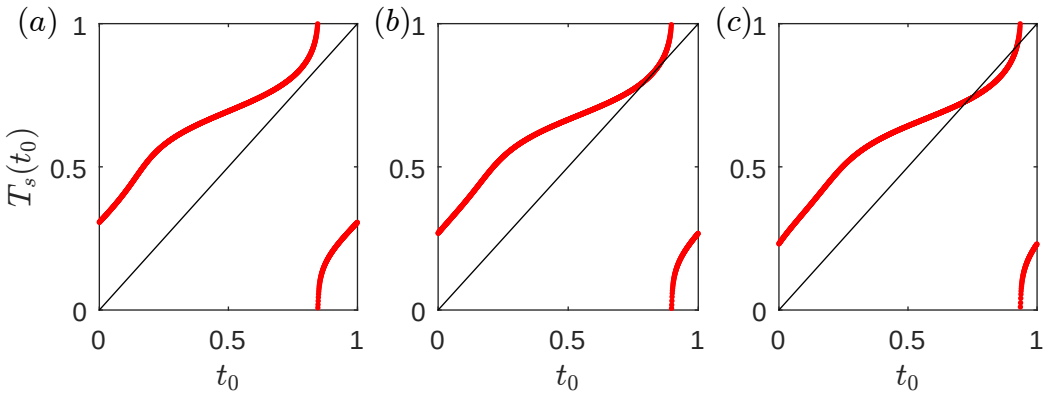

Figure 3.1: The creation of a pair of $(p, q) = (1, 1)$ solutions via a saddle-node bifurcation for $a = 0.05$ and H_0^- varying. (a) No fixed points, $H_0^- = 0.177$; (b) at the saddle-node bifurcation, $H_0^- = 0.197$; (c) two fixed points, $H_0^- = 0.217$. Note that for these parameter values, the primary effect of H_0^- is to shift the position of the map rather than change its gradient.

where periodic solutions exist in the (a, H_0^-) parameter set. If a is small the boundary of the region of existence will be formed by saddle-node bifurcations. In order to compute the saddle-node boundary of the tongue for any (p, q)-periodic orbit we consider two conditions. Firstly, a condition for periodicity such that after q days the model has returned to its initial conditions. Therefore for fixed a we wish to find the values of (t_0, H_0^-) such that

$$T_s^p(t_0) = t_0 + q. \tag{3.1}$$

As well as this, we use the condition that the one dimensional map at a saddle-node bifurcation has gradient 1. Therefore,

$$\begin{aligned}(T_s^p)'(t_0) &= \prod_{j=0}^{p-1} T_u'(T_d(T_s^j(t_0)))\, T_d'(T_s^j(t_0)) \\ &= T_u'(T_d(T_s^{p-1}(t_0)))T_d'(T_s^{p-1}(t_0))T_u'(T_d(T_s^{p-2}(t_0)))T_d'(T_s^{p-2}(t_0))\ldots T_u'(T_d(t_0))T_d'(t_0) \\ &= 1,\end{aligned} \tag{3.2}$$

where χ_s, χ_w, H_0^+ and a are fixed and $T_d'(t_0)$ and $T_u'(T_d)$ are defined in (2.28) and (2.29) respectively.

As we want to use a continuation approach, to numerically find the boundary of the tongues we first must find a starting solution. To do this we take the fixed parameters, an initial guess for H_0^- and t_0 and use the nonlinear system solver, *fsolve*, in Matlab on equations (3.1) and (3.2). From this we find the value for H_0^- at which a saddle-node bifurcation occurs. We then follow the path of H_0^- values by iterating over small steps in the amplitude, a, where we use the

previous value of H_0^- as an initial guess.

In Figure 2.8 we compared the analytical expression (2.44) with the numerical solution for the $(1,1)$-periodic tongue. For small amplitudes the analytical expression gives an accurate approximation to the numerical solution but as a increases the approximation and the numerical solution diverge. This is to be expected since we took an approximation for small amplitude. For (p,q)-periodic tongues note that there are p values of $t_0 \in (0,1]$ which lead to the same solution, as illustrated for $(p,q) = (2,1)$ in Figure 3.2. Here we have plotted the second iterate of the map i.e., t_0 against $T_s^2(t_0)$ at a saddle-node. Observe that there are two points where the map is tangent to the 1-1 line. Both of these periodic solutions belong to the same periodic orbit where applying T_s to one leads to the other, and hence correspond to the same saddle-node bifurcation.

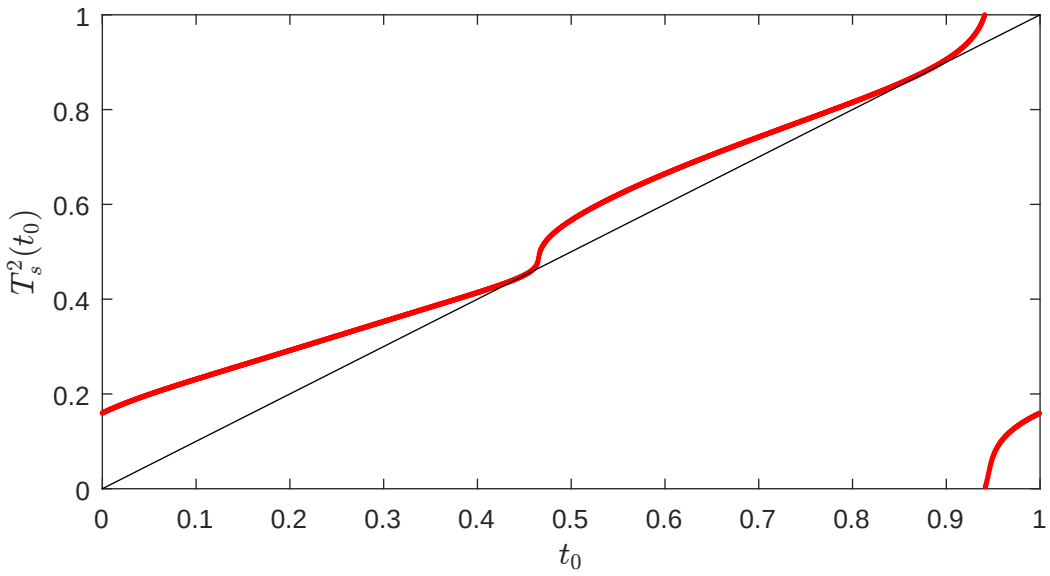

Figure 3.2: The second iterate of the map of the two process model for $a = 0.05$ and $H_0^- = 0.55$ where a saddle-node bifurcation for the $(2,1)$ periodic solutions occurs.

In Figure 3.3 the saddle-node bifurcation curves are plotted for several different (p,q) periodic orbits. The (red) dashed lines mark the restrictions (2.18) imposed on the parameters such that they are biologically sensible. The solid (red) lines mark the saddle-node bifurcations. Note that the right-hand boundary of each tongue comes to an end, at this point the saddle-node bifurcations cease to exist. In the sections that follow we will give an explanation for this and complete the bifurcation set for higher amplitudes. As is known for circle maps [109], a tongue exists for each pair of values (p,q), $\gcd(p,q) = 1$, although only a few of the largest tongues are plotted in Fig. 3.3(a).

To visualise the change in sleep-wake patterns which correspond to the sequence of bifurca-

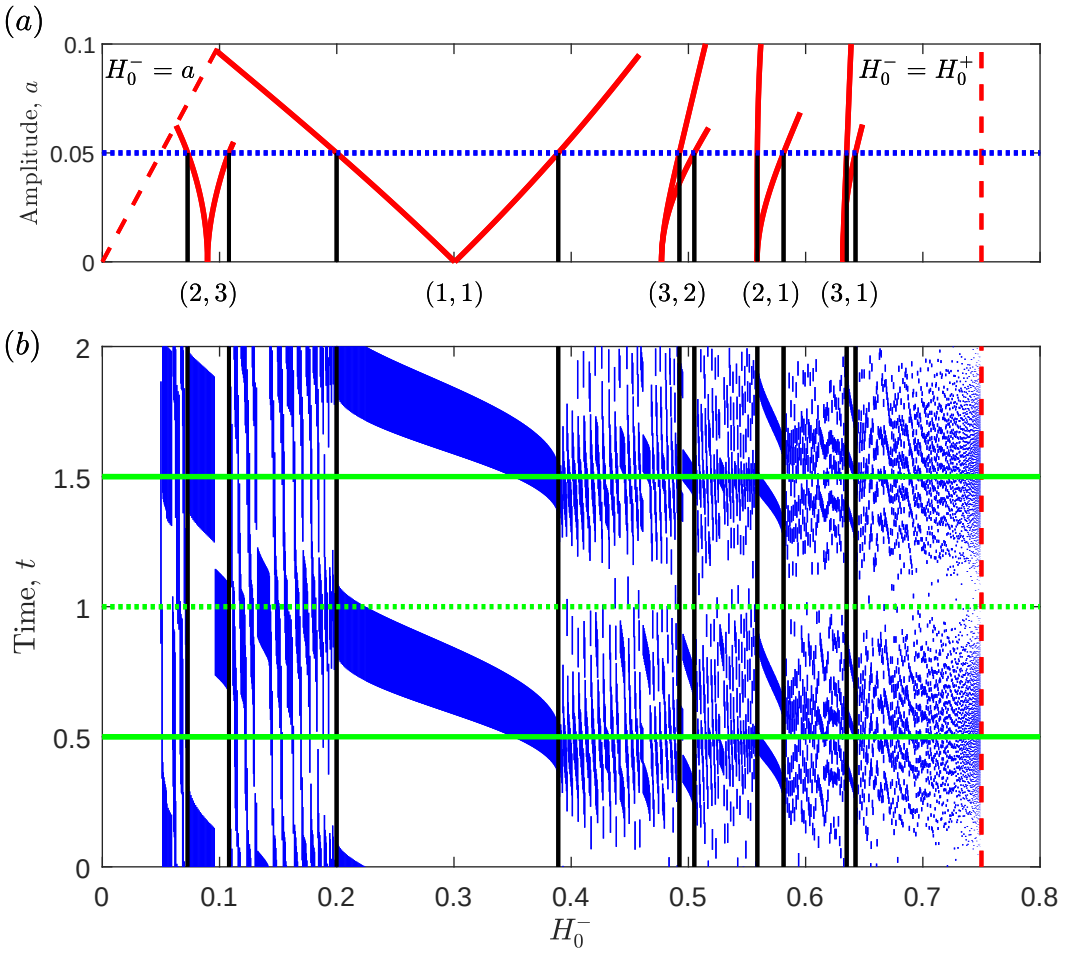

Figure 3.3: (a) Bifurcation curves in the (H_0^-, a)-plane showing the largest few tongues. (b) Bifurcation diagram for $a = 0.05$. Black lines on panel (a) and on panel (b) have been drawn to help identify the boundaries of the Arnold tongues at $a = 0.05$. The bold and dashed green lines indicate the maximum and minimum of the circadian phase respectively.

tions, a bifurcation diagram is shown in Figure 3.3(b). Here we take a slice of the bifurcation set for fixed amplitude $a = 0.05$ and plot the sleep-wake cycles for successive values of H_0^-. For each H_0^- value, the two process model has been iterated sufficiently long (100 days) that transients have decayed then the final 2 days are plotted. The vertical axis shows time over two days with the blue regions representing times for which sleep occurs. Vertical black lines have been drawn to help guide the eye to the regions of existence of the $(2, 3), (1, 1), (3, 2), (2, 1)$ and $(3, 1)$ solutions. The apparent discontinuities in the band in the $(2, 3)$ and the start of the $(3, 2)$ tongues represent the fact that for each $(2, 3)$ (or $(3, 2)$) periodic solution, there are two (or three) values on the upper threshold that can act as its starting point. The discontinuity is due to the numerical solution undergoing a phase shift between these starting points.

We have shown that the boundaries of Arnold tongues occur at saddle-node bifurcations where there is a transition from 0 to 1 (at the boundary) to 2 (p, q)-periodic solutions or vice versa. However, in Figure 3.3(a) the boundary of each tongue comes to an end on the right hand side for larger amplitudes. For the small amplitude case investigated so far the one dimensional map is continuous and saddle-node bifurcations are the only mechanism in which periodic solutions are created and destroyed. In the next section we show that for larger amplitudes the map becomes discontinuous and we continue to explore how the transitions between (p, q) periodic orbits occur for larger amplitudes a. For discontinuous maps, both saddle-node bifurcations and border collisions can create/ annihilate periodic solutions.

3.2 Gaps in the map

In this section we consider the way that discontinuities in the one dimensional map occur and discuss the regions of the parameter plane for which the map has discontinuities.

Gaps in the map of the two process model can arise when either the homeostatic sleep pressure during sleep, $H_s(t, t_0)$, becomes tangential to the lower threshold, $H^-(t)$, or the homeostatic sleep pressure on wake, $H_w(t, t_0)$, becomes tangential to the upper threshold, $H^+(t)$ [97]. The case where the wake homeostatic sleep pressure is tangential to the upper threshold in the two process model is illustrated in Figure 3.4(a). Here we see that two sleep-wake trajectories with only slightly different initial conditions can give rise to a large change in the length of a sleep-wake orbit. When considering the associated map, as in Figure 3.4(b), we see that a discontinuity occurs at the initial time which leads to a tangency, t_0^u. Tangencies in the two process model explain the results of the Åkerstedt experiment (1981) [127] which was discussed in the original two process model formulation [78]. In this sleep deprivation experiment, sleep duration first decreased below its regular level and then increased well beyond the baseline, as the length of sleep deprivation was increased incrementally by 4 hour intervals. The existence of gaps such as this can lead to border collisions, where a fixed point of the map collides with the gap.

First we will investigate tangencies in the model analytically, then use this analysis to numerically find border collisions and in turn complete the bifurcation set from Section 3.1.1 for higher amplitudes, a.

3.2.1 Tangencies on the lower threshold

We aim to find the regions of the parameter space in which tangencies occur between the homeostat and thresholds and to understand the relationship between these tangencies in the model and gaps in the map. We will first consider the case where the homeostat during sleep,

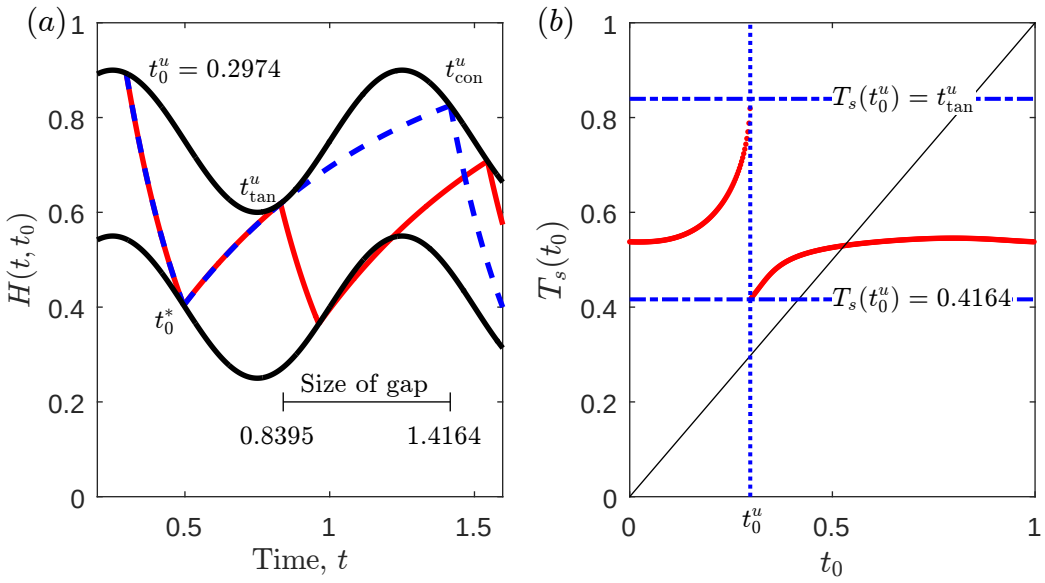

Figure 3.4: A small perturbation in the start time t_0 can lead to large changes in the value of $T_s(t_0)$ if a tangency occurs between the homeostatic sleep pressure on sleep $H_s(t)$ and the lower threshold, or the homeostatic sleep pressure on wake $H_w(t)$ and the upper threshold. (a) Two possible trajectories with initial time t_0^u are shown. The bold red line shows the homeostatic sleep pressure switching at the tangency point $H^+(t_{\text{tan}}^u)$ and dashed blue line shows the homeostatic sleep pressure missing the tangency and continuing on a wake trajectory; (b) The corresponding map shows the gap in $T_s(t_0)$ occurring at t_0^u. Here we use $a = 0.15$ and $H_0^- = 0.4$.

$H_s(t, t_0)$, becomes tangential to the lower threshold, $H^-(t)$.

We denote the time a tangency occurs on the lower threshold by $t_{\text{tan}}^l \equiv T_d(t_0^l)$, where t_0^l is an initial time which leads to the tangency. The necessary and sufficient conditions for the tangency to occur are that the trajectory of the homeostat is at the lower threshold at t_{tan}^l:

$$H^+(t_0^l)e^{\frac{t_0^l - t_{\text{tan}}^l}{\chi_s}} = H_0^- + a\sin(2\pi t_{\text{tan}}^l), \tag{3.3}$$

and that the gradients of the lower threshold and trajectory of the homeostat match at t_{tan}^l giving

$$-\frac{H^+(t_0^l)}{\chi_s}e^{\frac{t_0^l - t_{\text{tan}}^l}{\chi_s}} = 2\pi a\cos(2\pi t_{\text{tan}}^l). \tag{3.4}$$

The last relation is found by differentiating (3.3). By construction we know that the left hand side of (3.4) is always negative in the two process model, since $H^+(t)$ and $\chi_s > 0$. Therefore to have a tangency on the lower bound we need the gradient of the lower threshold to also be negative, thus

$$2\pi a\cos(2\pi t_{\text{tan}}^l) < 0,$$

which implies that $t_{\text{tan}}^l \in \left(\frac{1}{4}, \frac{3}{4}\right)$. Furthermore, for the tangency to be related to the first inter-

section between the homeostat and the threshold, the homeostat has to approach the threshold at the tangency from above.

For the remainder of this section we build towards a proof of the theorem stated below.

Theorem 3.1. *For $-a < H_0^- \leq \min(a\gamma_s\chi_s, 1-a)$, there is exactly one tangency in $[0,1]$ that hits the lower threshold from above. This tangency is at*

$$t^l_{\tan} = \frac{\arccos\left(-\frac{H_0^-}{a\chi_s\gamma_s}\right) + \arccos\left(\frac{2\pi}{\gamma_s}\right)}{2\pi} \quad \in \left(\frac{1}{4}, \frac{3}{4}\right), \tag{3.5}$$

where

$$\gamma_s = \sqrt{4\pi^2 + \frac{1}{\chi_s^2}}.$$

The proof is given through a series of lemmas. First we explore equations (3.3) and (3.4) to find relations which $t^l_{\tan}$ must satisfy.

Lemma 3.2. *There exists a tangency, given by $t^l_{\tan}$, and the time of the tangency satisfies*

$$\cos(2\pi t^l_{\tan} + B) = -\frac{H_0^-}{a\chi_s\gamma_s}, \tag{3.6}$$

where

$$B = 2\pi - \arccos\left(\frac{2\pi}{\gamma_s}\right) \in \left(\frac{3\pi}{2}, 2\pi\right).$$

Proof. We begin by rearranging (3.4) and equating with (3.3) to obtain

$$2\pi\cos 2\pi t^l_{\tan} + \frac{\sin 2\pi t^l_{\tan}}{\chi_s} = -\frac{H_0^-}{a\chi_s}. \tag{3.7}$$

We may rewrite the left hand side of (3.7) using the double angle formula $\cos(A+B) = \cos A\cos B - \sin A\sin B$ where $A = 2\pi t^l_{\tan}$. By comparing coefficients and using the equality in (3.7) we see that

$$\gamma_s\cos B = 2\pi, \qquad \gamma_s\sin B = -\frac{1}{\chi_s}. \tag{3.8}$$

Thus (3.7) can be written as

$$\cos(2\pi t^l_{\tan} + B) = -\frac{H_0^-}{a\chi_s\gamma_s}.$$

As $\gamma_s > 0$ and $\chi_s > 0$, from (3.8) we have

$$\cos B > 0 \quad \text{and} \quad \sin B < 0,$$

which implies that $B \in \left(\frac{3\pi}{2}, 2\pi\right)$.

□

Solutions $t^l_{\tan}$ to the tangency time equation (3.6) only exist if

$$-1 \leq -\frac{H_0^-}{a\chi_s\gamma_s} \leq 1.$$

The restrictions to biologically plausible parameter values ensures that the right-hand inequality is always satisfied as $H_0^- > -a > -a\chi_s\gamma_s$. The left-hand inequality gives a necessary condition on the circadian amplitude for the existence of gaps in the down map $T_d(t_0)$, namely

$$H_0^- \leq a\chi_s\gamma_s. \tag{3.9}$$

The region given by this condition and the biological constraints is illustrated as the shaded region in Fig. 3.5.

For $H_0^- = a\chi_s\gamma_s$ there exists only one $t^l_{\tan}$ such that (3.6) is satisfied being

$$t^l_{\tan} = \frac{\arccos(-1) + \arccos\left(\frac{2\pi}{\gamma_s}\right)}{2\pi} = \frac{1}{2} + \frac{\arccos\left(\frac{2\pi}{\gamma_s}\right)}{2\pi}.$$

For $H_0^- < a\chi_s\gamma_s$, (3.6) has two possible solutions. These two solutions correspond to tangencies that would occur as a result of $H_s(t, t_0)$ approaching the lower threshold from above and from below. An example of this is shown in Figure 3.6, it is obvious that only the tangency which hits from above is relevant in the two process model since the other occurs after the homeostatic sleep pressure has passed through the lower threshold which the model does not allow for.

From the definition of the down map $T_d(t_0)$ it follows that all $t \in (t_0, T_d(t_0))$ have to satisfy $H_s(t, t_0) \geq H^-(t)$. Therefore a tangency point $t^l_{\tan}$ from the region shown in Figure 3.5 is only relevant to gaps in the map if the trajectory of $H_s(t, t_0)$ approaches the lower threshold from above. In the following lemma we consider the local behaviour of $H_s(t, t_0)$ near the tangency point which will allow us to determine the relevant $t^l_{\tan}$.

Lemma 3.3. *Let $t^l_{\tan}$ be a tangency. Then, $t^l_{\tan}$ is a tangency such that the homeostatic sleep pressure during sleep approaches the lower threshold from above if and only if it satisfies*

$$H_s''(t^l_{\tan}) + 4\pi^2 a \sin(t^l_{\tan}) > 0. \tag{3.10}$$

This tangency is related to a gap in the map in the sense that it creates a discontinuity in the return times of the composite map $T_s(t^l_0)$.

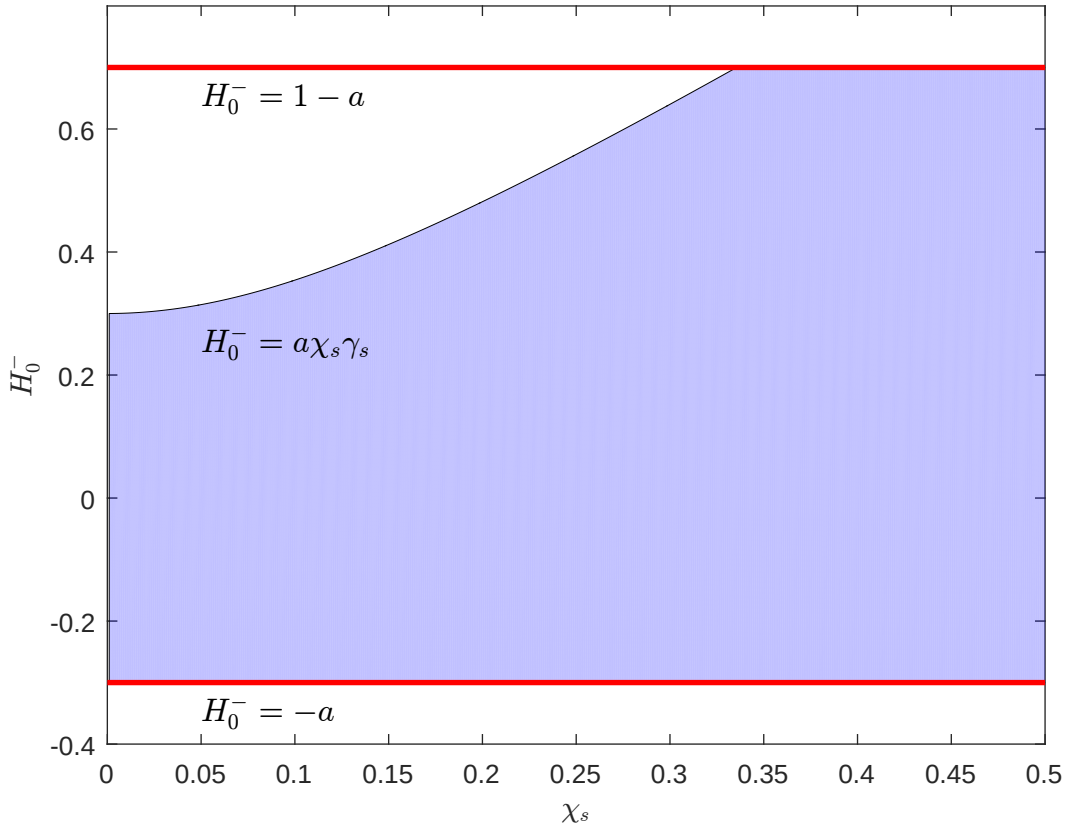

Figure 3.5: The shaded region denotes the parameter space in which tangencies can occur on the lower threshold but gives no indication of what values $t^l_{\tan}$ can take. The red lines are given by the restrictions imposed on H_0^- in Chapter 2. In this case we have set $a = 0.3$.

Proof. We know that the lower threshold is given by

$$H^-(t) = H_0^- + a\sin(2\pi t),$$

and the homeostatic sleep pressure on sleep by

$$H_s(t) = \left(H_0^+ + a\sin(2\pi t_0)\right) e^{\frac{t_0 - t}{\chi_s}}.$$

So at the point of tangency we have

$$H_s(t^l_{\tan}) = H_0^- + a\sin(2\pi t^l_{\tan}),$$

$$H_s'(t^l_{\tan}) = 2\pi a\cos(2\pi t^l_{\tan}). \tag{3.11}$$

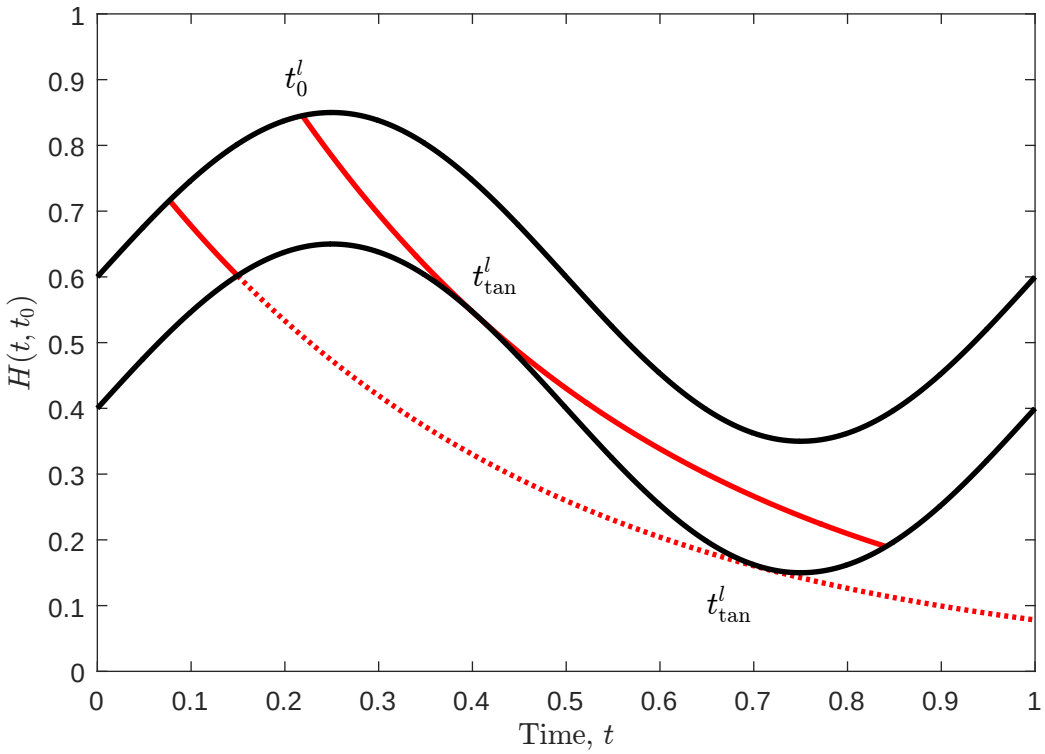

Figure 3.6: We see two potential tangencies between the homeostat on a sleep trajectory and the lower threshold. However, we are only interested in the tangency which approaches the lower threshold from above, this trajectory begins on the upper threshold at t_0^l. The dashed red line shows the trajectory which approaches the tangency from below. Since switching from sleep to wake occurs when the homeostat on sleep intersects the lower threshold, this tangency is not possible in the two process model.

The homeostat must be above the lower circadian threshold when on a sleep trajectory so,

$$H_s(t) \geq H_0^- + a\sin(2\pi t_{\tan}^l) = H^-(t), \qquad \text{for} \qquad t \in [t_0, t_{\tan}^l].$$

We now Taylor expand,

$$\begin{aligned} H_s(t) - H^-(t) &= H(t_{\tan}^l) + H'(t_{\tan}^l)(t - t_{\tan}^l) + \frac{H''(t_{\tan}^l)(t - t_{\tan}^l)^2}{2} \\ &\quad - \left(H_0^- + a\sin(2\pi t_{\tan}^l) + 2\pi a\cos(2\pi t_{\tan}^l)(t - t_{\tan}^l) - 4\pi^2 \frac{a\sin(2\pi t_{\tan}^l)(t - t_{\tan}^l)^2}{2} \right) + \mathcal{O}\left((t - t_{\tan}^l)^3\right) \\ &= \frac{H''(t_{\tan}^l)(t - t_{\tan}^l)^2}{2} + 4\pi^2 \frac{a\sin(2\pi t_{\tan}^l)(t - t_{\tan}^l)^2}{2} + \mathcal{O}((t - t_{\tan}^l)^3) \\ &= \frac{H''(t_{\tan}^l) + 4\pi^2 a\sin(2\pi t_{\tan}^l)}{2}(t - t_{\tan}^l)^2 + \mathcal{O}((t - t_{\tan}^l)^3). \end{aligned}$$

Therefore, $H_s(t) - H^-(t) \geq 0$ for t near $t^l_{\tan}$ if and only if

$$H''(t^l_{\tan}) + 4\pi^2 a \sin(2\pi t^l_{\tan}) > 0$$

and equations (3.3) and (3.4) hold.

□

Next we wish to analyse the inequality (3.10) and visualise what this means for possible tangency times $t^l_{\tan}$.

Lemma 3.4. *If a tangency $t^l_{\tan}$ exists then (3.10) holds if and only if the inequality*

$$0 < 2\pi t^l_{\tan} + B < \pi$$

is satisfied.

Proof. The result of lemma 3.3 gives (3.10),

$$H''_s(t^l_{\tan}) + 4\pi^2 a \sin(2\pi t^l_{\tan}) > 0.$$

From the definition of $H_s(t^l_{\tan})$ and (3.11) we also know

$$\begin{aligned} H'_s(t^l_{\tan}) &= 2\pi a \cos(2\pi t^l_{\tan}), \\ H''_s(t^l_{\tan}) &= -\frac{1}{\chi_s} H'(t^l_{\tan}). \end{aligned}$$

Therefore we have

$$H''_s(t^l_{\tan}) = -\frac{2\pi}{\chi_s} a \cos(2\pi t^l_{\tan}),$$

which can be substituted into (3.10) to give

$$f(t^l_{\tan}) := -\frac{2\pi}{\chi_s} a \cos(2\pi t^l_{\tan}) + 4\pi^2 a \sin(2\pi t^l_{\tan}) > 0. \tag{3.12}$$

We wish to find the values of τ^* for which $f(\tau^*) = 0$. We first rearrange $f(\tau^*) = 0$ to give

$$\tan(2\pi\tau^*) = \frac{1}{2\pi\chi_s}. \tag{3.13}$$

Since

$$\cos B = \frac{2\pi}{\gamma_s}, \qquad \sin B = -\frac{1}{\chi_s \gamma_s}, \tag{3.14}$$

we have,

$$\tan B = \frac{\sin B}{\cos B} = -\frac{1}{\gamma_s \chi_s}\frac{\gamma_s}{2\pi} = -\frac{1}{2\pi\chi_s}. \tag{3.15}$$

Comparing (3.13) and (3.15) yields the solutions

$$2\pi\tau^* = -B + k\pi.$$

Since

$$-B = -2\pi + \arccos\left(\frac{2\pi}{\gamma_s}\right) \in \left(0, \frac{\pi}{2}\right) \qquad \text{and} \qquad -B + \pi \in \left(\pi, \frac{3\pi}{2}\right),$$

we need only check $t^l_{\tan} = 0$ to find out when $f(t^l_{\tan})$ is positive or negative. At $t^l_{\tan} = 0$ we have

$$f(0) = -\frac{a2\pi}{\chi_s} < 0.$$

Thus we know that $f(t^l_{\tan}) > 0$ if and only if

$$-B < 2\pi t^l_{\tan} < \pi - B,$$

or equivalently

$$0 < 2\pi t^l_{\tan} + B < \pi.$$

□

Taking the restrictions $-a < H_0^- < 1 - a$ along with lemma 3.4 allows us to plot the region in which first hit tangencies exist, see Figure 3.7. We see that for all values of χ_s the tangency at $H_0^- = -a$ is at $t^l_{\tan} = \frac{1}{4}$. This is shown analytically in Appendix B.1.

We can now use Lemmas 3.2 to 3.4 to prove Theorem 3.1.

Proof of Theorem 3.1: Using the arccos to rewrite (3.6) gives two solutions

$$2\pi t^l_{\tan} + B = \arccos\left(-\frac{H_0^-}{a\gamma_s\chi_s}\right) \in (0, \pi), \tag{3.16}$$

and

$$2\pi t^l_{\tan} + B = 2\pi - \arccos\left(-\frac{H_0^-}{a\gamma_s\chi_s}\right) \in (\pi, 2\pi). \tag{3.17}$$

From lemmas 3.3 and 3.4 we know that (3.16) gives the tangency that hits the lower circadian threshold from above, since it satisfies the inequality $0 \leq 2\pi t^l_{\tan} + B < \pi$. We can disregard (3.17) since it does not satisfy the inequality. Therefore by substituting

$$B = 2\pi - \arccos\left(\frac{2\pi}{\gamma_s}\right) \qquad \in \left(\frac{3\pi}{2}, 2\pi\right),$$

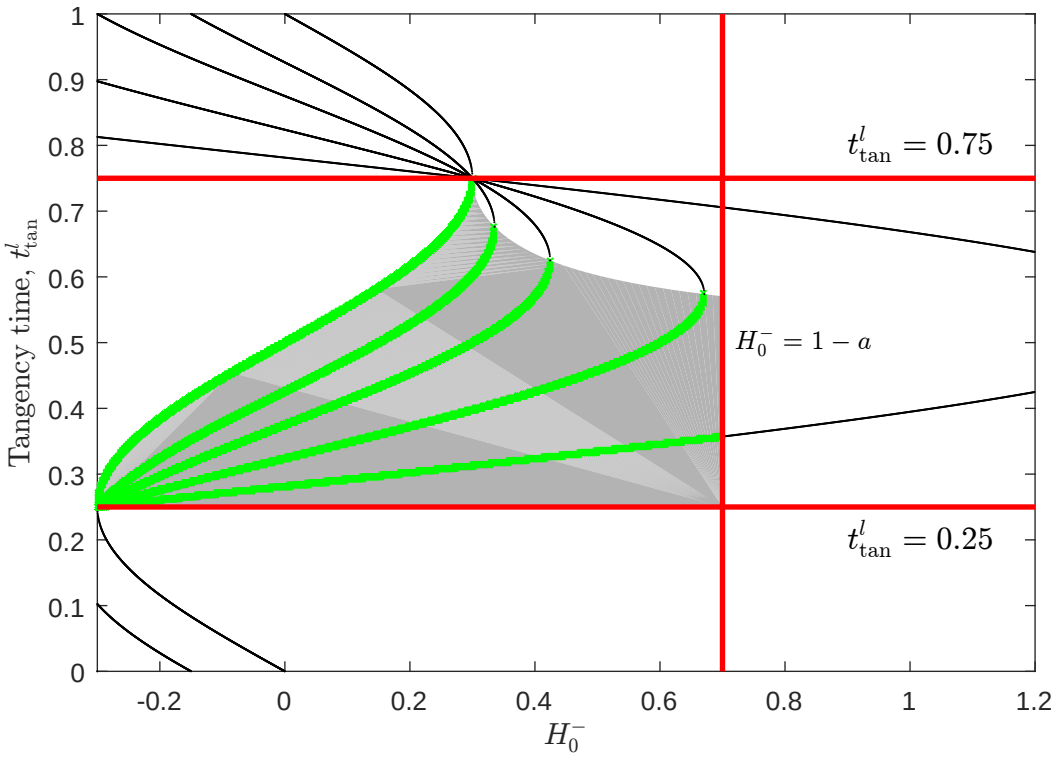

Figure 3.7: For any χ_s, there is always a first hit tangency if $H_0^- \in [-a, \min(a\chi_s\gamma_s, 1-a)]$. Here $a = 0.3$ and each curve represents the relation (3.6) between $t^l_{\tan}$ and H_0^- where $\chi_s = 10^{-9}, 0.5, 1, 2, 5$ from left to right. The grey region indicates where $t^l_{\tan}$ values satisfy Lemma 3.4, i.e., they are a first hit tangency. The green curves shows how the grey region fills up as $\chi_s \to \infty$, bounded by $t^l_{\tan} = 0.25$ from below, $\chi_s = 0$ from the left, $H_0^- = a\chi_s\gamma_s$ from above and $H_0^- = 1 - a$ from the right.

into (3.16) we get

$$2\pi t^l_{\tan} + 2\pi - \arccos\left(\frac{2\pi}{\gamma_s}\right) = \arccos\left(-\frac{H_0^-}{a\gamma_s\chi_s}\right) \in (0, \pi)\,. \tag{3.18}$$

By rearranging (3.18) and then shifting $t^l_{\tan}$ by 1 we have

$$t^l_{\tan} = \frac{\arccos\left(-\frac{H_0^-}{a\chi_s\gamma_s}\right) + \arccos\left(\frac{2\pi}{\gamma_s}\right)}{2\pi} \quad \in \left(\frac{1}{4}, \frac{3}{4}\right),$$

for $-a < H_0^- \leq a\gamma_s\chi_s$, thus finishing the proof of Theorem 3.1. □

We will now use the symmetry of the two process model to find the points at which the wake homeostatic sleep pressure is tangent to the upper threshold.

3.2.2 Using symmetry to find tangencies on the upper threshold

It is possible to find tangency points, $t^u_{\tan}$, where the wake homeostatic sleep pressure is tangent to the upper threshold following the same method as in Section 3.2.1. However, there exists a symmetry as given in (2.19), such that

$$(t, H_s; \chi_s, H_0^+, H_0^-, a, t_0) \longmapsto (t + \frac{1}{2}, 1 - H_w; \chi_w, 1 - H_0^-, 1 - H_0^+, a, t_0 + \frac{1}{2}),$$

maps results for the sleep homeostatic sleep pressure and the lower threshold onto results for the wake homeostatic sleep pressure and the upper threshold. Therefore we can map any of results for Section 3.2.1 directly to results for tangencies between wake homeostatic sleep pressure and the upper threshold. We are interested in two things in particular, the existence region of tangencies in the parameter space and the times at which a tangency occurs.

For tangencies between sleep homeostatic sleep pressure and the lower threshold, the existence region in parameter space is given by

$$-a < H_0^- \leq \min(a\gamma_s\chi_s, 1 - a).$$

Making the substitutions given by the symmetry, the region for which there is a tangency between the wake homeostatic sleep pressure and the upper threshold is given by

$$-a < 1 - H_0^+ \leq \min(a\gamma_w\chi_w, 1 - a)$$

thus,

$$\max(1 - a\gamma_w\chi_w, a) \leq H_0^+ < 1 + a,$$

where

$$\gamma_s \longmapsto \gamma_w = \sqrt{4\pi^2 + \frac{1}{\chi_w^2}}.$$

To find the tangency time on the upper threshold we use the symmetry on $t^l_{\tan}$ given in (3.5) to give

$$t^l_{\tan} \longmapsto t^u_{\tan} + \frac{1}{2} = \frac{\arccos\left(\frac{2\pi}{\gamma_w}\right) + \arccos\left(-\frac{1-H_0^+}{a\gamma_w\chi_w}\right)}{2\pi}.$$

Using $\arccos(-x) = \pi - \arccos(x)$, this can be rearranged to give the tangency time on the upper threshold

$$t^u_{\tan} = \frac{\arccos\left(\frac{2\pi}{\gamma_w}\right) - \arccos\left(\frac{1-H_0^+}{a\gamma_w\chi_w}\right)}{2\pi} \quad \in \left[0, \frac{1}{4}\right] \cup \left[\frac{3}{4}, 1\right].$$

In summary, the results in the section lead us to a theorem for tangencies which occur on the upper threshold.

Theorem 3.5. *For* $\max(1-a\gamma_w\chi_w, a) \leq H_0^+ < 1+a$*, there is exactly one tangency that hits the upper threshold from below. This tangency is at*

$$t^u_{\tan} = \frac{\arccos\left(\frac{2\pi}{\gamma_w}\right) - \arccos\left(\frac{1-H_0^+}{a\gamma_w\chi_w}\right)}{2\pi} \quad \in \left[0, \frac{1}{4}\right] \cup \left[\frac{3}{4}, 1\right], \tag{3.19}$$

where

$$\gamma_w = \sqrt{4\pi^2 + \frac{1}{\chi_w^2}}.$$

Now that we have found where tangencies occur in the two process model we want to relate the tangencies to discontinuities in the one-dimensional map. In the next section we discuss when $t^l_{\tan}$ and $t^u_{\tan}$ are relevant to gaps in the map and find the size of the gap.

3.2.3 Discontinuities in the one dimensional map

The one dimensional map is constructed by plotting t_0 against $T_s(t_0)$, where t_0 denotes a sleep onset time occurring on the upper threshold, $H^+(t_0)$. First we consider how tangencies on the lower threshold relate to the one dimensional map.

Since $T_s(t_0) = T_u(T_d(t_0))$ a discontinuity in T_d will generically also give a discontinuity in T_s. Note that the tangency time $t^l_{\tan}$ does not directly give the time of this discontinuity in the composite map. To find where the discontinuity caused by a tangency on the lower threshold occurs we need to find the initial time t^l_0 which leads to $t^l_{\tan}$. By rearranging the tangency condition (3.4) we find

$$t^l_0 = t^l_{\tan} + \chi_s \ln\left(-\frac{2\pi\chi_s a\cos(2\pi t^l_{\tan})}{H^+(t^l_0)}\right).$$

By separating the variables $t^l_0, t^l_{\tan}$ and substituting $H^+(t^l_0) = H_0^+ + a\sin(2\pi t^l_0)$ we arrive at

$$\left(H_0^+ + a\sin(2\pi t^l_0)\right)\exp\left(\frac{t^l_0}{\chi_s}\right) = -2\pi\chi_s a\cos(2\pi t^l_{\tan})\exp\left(\frac{t^l_{\tan}}{\chi_s}\right). \tag{3.20}$$

This implicit relation between t^l_0 and $t^l_{\tan}$ is visualised in Figure 3.8. Since we know the tangency time $t^l_{\tan}$ from equation (3.5) we need only solve (3.20) for times $t^l_0 < t^l_{\tan}$.

It is also possible to find the size of the gap in the down map $T_d(t_0)$ by continuing the homeostatic sleep pressure on sleep H_s through the tangency point, $H^-(t^l_{\tan})$, until the next hit on the lower threshold, as in Figure 3.9. The difference between the tangency time $t^l_{\tan}$ and this

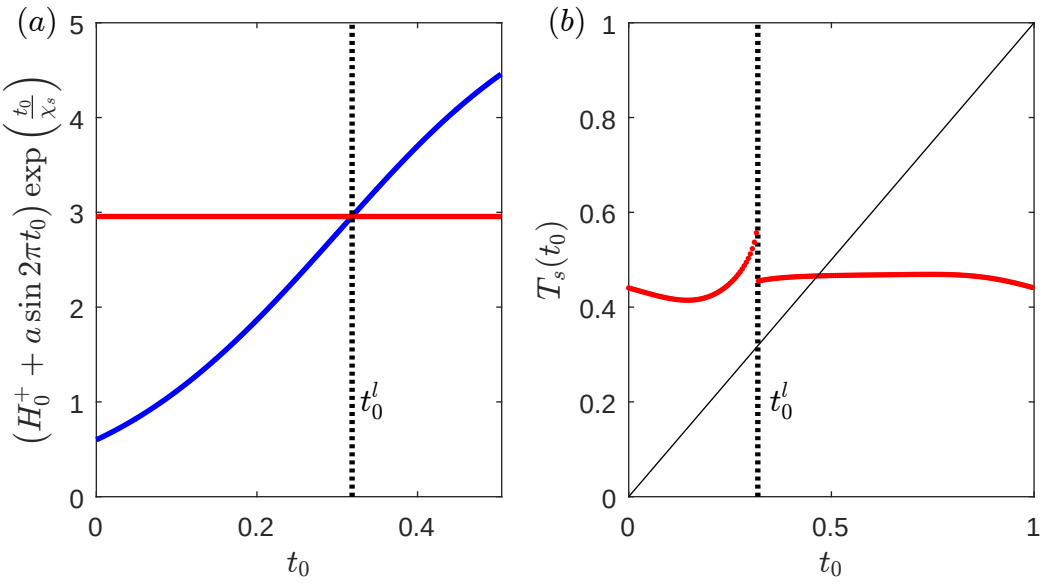

Figure 3.8: (a) A graphical representation of (3.20) where substituting t^l_{tan} into the right hand side gives the constant red line and the blue curve is given by the left hand side. The intersection point gives t^l_0 which we can then relate to the one-dimensional map. (b) The discontinuity in the one-dimensional map occurs at the initial time, t^l_0 (denoted by the red line), which leads to a tangency on the lower threshold and hence a discontinuity in T_d and T_s. The parameters used are: $a = 0.25, H_0^- = 0.4, H_0^+ = 0.6, \chi_s = \frac{1}{4}, \chi_w = \frac{3}{4}$.

second hit gives the size of the gap in T_d. The second hit is the first $t^l_{\text{con}} > t^l_{\text{tan}}$ which satisfies

$$H^-(t^l_{\text{tan}})e^{\frac{t^l_{\text{tan}}-t^l_{\text{con}}}{\chi_s}} = H_0^- + a\sin(2\pi t^l_{\text{con}}). \tag{3.21}$$

By rearranging (3.21) we get

$$H^-(t^l_{\text{tan}})e^{\frac{t^l_{\text{tan}}}{\chi_s}} = H^-(t^l_{\text{con}})e^{\frac{t^l_{\text{con}}}{\chi_s}}, \quad t^l_{\text{con}} > t^l_{\text{tan}}. \tag{3.22}$$

Since $T_s = T_u \circ T_d$, the size of the gap in T_s is $T_u(t^l_{\text{con}}) - T_u(t^l_{\text{tan}})$.

The lower threshold tangency creates a region of unattainable lower threshold values. When no tangency occurs on the lower threshold then $T_d(t_0)$ is continuous and the range of T_d is $D = [0, 1]$. However, when a tangency on the lower threshold exists the created discontinuity means that $t_0 \in [0, 1]$ maps to

$$T_d(t_0) \in D = \begin{cases} [0, t^l_{\text{tan}}] \cup [t^l_{\text{con}}, 1] & \text{if} \quad t^l_{\text{tan}} < t^l_{\text{con}} \mod 1 \\ [t^l_{\text{con}} \mod 1, t^l_{\text{tan}}] & \text{if} \quad t^l_{\text{tan}} > t^l_{\text{con}} \mod 1 \end{cases}.$$

The $t^l_{\text{tan}} < t^l_{\text{con}}$ case is plotted in Figure 3.9. Since we are interested in the composite map,

$T_s = T_u \circ T_d$, we only consider initial times $T_d \in D$ as starting values for the up map $T_u(T_d)$. Therefore tangencies of the upper threshold can be missed in both $T_u(T_d)$ and the composite map $T_s(t_0)$ if $T_d(t_0^u) \notin D$, where t_0^u is the initial time on the upper threshold such that $T_u(T_d(t_0^u))$ leads to a tangency on the upper threshold.

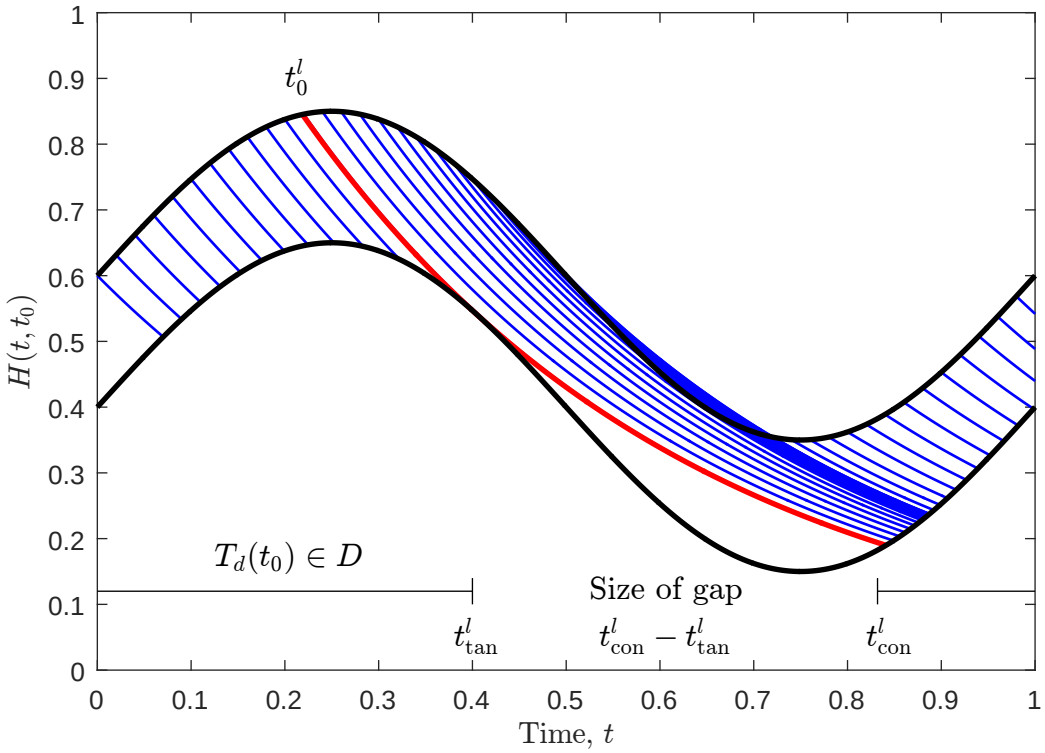

Figure 3.9: Each blue line represents a sleep trajectory which start at evenly spread t_0 values on the upper threshold. The red line is the sleep trajectory which passes through the tangency point. We see that the tangency creates a gap in the map $T_d(t_0)$.

Tangencies on the upper threshold occur at time $T_s(t_0^u) = t_{\text{tan}}^u$ and therefore are always seen in the composite map, T_s. Note that a tangency on the upper threshold relates to the map if and only if $T_d(t_0^u) \in D$. To find the initial time t_0^u we trace back through $T_u(T_d)$ to a time t_0^*, the wake onset time lying on the lower threshold which leads to a tangency. We then consider $T_d(t_0^u)$ to find the initial time t_0^u which leads to the gap in the composite map. In Figure 3.10 we give a graphical representation of this process and show where values $t_0^u, t_0^*, t_{\text{tan}}^u$ lie in the model.

We will now compute t_0^u to find where the discontinuity caused by a tangency on the upper threshold occurs. Similarly to the lower threshold we begin by rearranging the tangency condition (3.19) to find

$$t_0^* = t_{\text{tan}}^u + \chi_w \ln\left(\frac{2\pi\chi_w a \cos(2\pi t_{\text{tan}}^u)}{1 - H^-(t_0^*)}\right).$$

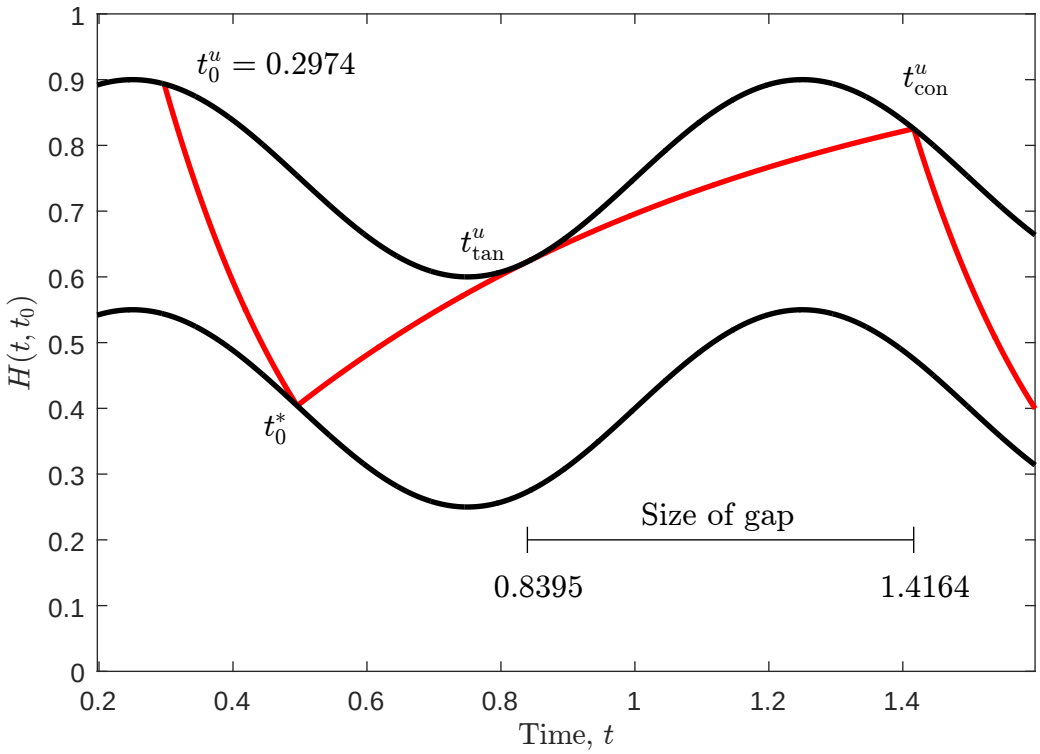

Figure 3.10: A plot of the two process model passing through a tangency point on the upper threshold. We see that the initial time t_0^u leads to both t_{tan}^u and t_{con}^u, in the context of the composite map, $T_s(t_0)$, the value of t_0^u gives the position of the gap on the x-axis and t_{tan}^u and t_{con}^u give the end points of the gap on the y-axis. Note that wake trajectories in the composite map $T_s(t_0)$ will only start at values $T_d(t_0) \in D$ therefore, if $T_d(t_0^u) = t_0^* \notin D$ then an upper threshold tangency is not seen in the composite map.

By separating the variables t_0^*, t_{tan}^u and substituting $H^-(t_0^*) = H_0^- + \sin(2\pi t_0^*)$ we arrive at

$$\left(1 - H_0^- - \sin(2\pi t_0^*)\right) \exp\left(\frac{t_0^*}{\chi_w}\right) = 2\pi\chi_w a \cos(2\pi t_{\text{tan}}^u) \exp\left(\frac{t_{\text{tan}}^u}{\chi_w}\right). \tag{3.23}$$

Since we know the tangency time t_{tan}^u from equation (3.19), we can solve (3.23) to find the initial time t_0^* which sits on the lower threshold and leads to a tangency on the upper threshold. To find the time t_0^u which leads to a discontinuity in the composite map we use the equation for the homeostatic sleep pressure on sleep (2.12) and numerically solve the implicit equation

$$H^-(t_0^*) e^{\frac{t_0^*}{\chi_s}} = H^+(t_0^u) e^{\frac{t_0^u}{\chi_s}}.$$

Using the same method as for the lower threshold, by continuing the homeostatic sleep pressure on wake through the tangency point, t_{tan}^u, until the next hit on the upper threshold t_{con}^u, one finds that the size of the gap in the up map T_u is given by $t_{\text{con}}^u - t_{\text{tan}}^u$. If t_0^* is in the

range of T_d, then this is also the size of the gap in T_s, otherwise T_s has no gap. In Fig. 3.4 we show the relationship between the two process model and the size of the gap, illustrating that the size of the gap is the same in T_u as in T_s.

In the maps displayed in Figures 2.6, 3.4 and 3.8, the derivative of the map to the left of the gap in the down, up, and sleep map appears to be infinite. We consider the derivative of the sleep map T_s with respect to t_0, given in equation (2.22), to check the gradient of the map at the discontinuity.

In section 2.2.2 we showed that when $T_d(t_0)$ and $T_u(T_d(t_0))$ are locally well defined the derivative of the down map is

$$T_d'(t_0) = \frac{\left(2\pi a\cos(2\pi t_0) + \frac{H_0^+}{\chi_s} + \frac{a}{\chi_s}\sin(2\pi t_0)\right) e^{\frac{t_0 - T_d(t_0)}{\chi_s}}}{\left(2\pi a\cos(2\pi T_d(t_0)) + \frac{H_0^-}{\chi_s} + \frac{a}{\chi_s}\sin(2\pi T_d(t_0))\right)},$$

as in (2.28) and the derivative of the up map is

$$T_u'(T_d) = \frac{\left(2\pi a\cos(2\pi T_d) + \frac{H_0^- - 1}{\chi_w} + \frac{a}{\chi_w}\sin(2\pi T_d)\right) e^{\frac{T_d(t_0) - T_u(T_d)}{\chi_w}}}{\left(2\pi a\cos(2\pi T_u(T_d)) + \frac{H_0^+ - 1}{\chi_w} + \frac{a}{\chi_w}\sin(2\pi T_u(T_d))\right)},$$

as in (2.29).

First we consider discontinuities corresponding to tangencies between the homeostatic sleep pressure on sleep and the lower threshold. By multiplying both sides of the tangency condition (3.3) by $-\frac{1}{\chi_s}$ and combining with condition (3.4) gives that a tangency point t^l_{tan} satisfies

$$2\pi a\cos(2\pi t^l_{\text{tan}}) + \frac{H_0^-}{\chi_s} + \frac{a}{\chi_s}\sin(2\pi t^l_{\text{tan}}) = 0,$$

which is the denominator of the derivative of the down map (2.28). Therefore if t^l_0 is such that $T_d(t^l_0) = t^l_{\text{tan}}$ then (2.28) is not differentiable at t^l_0 and it can be seen that $T_d'(t_0) \to \infty$ as t_0 approaches t^l_0 from the left. As t_0 approaches t^l_0 from the right, $T_d(t_0)$ approaches t^l_{con} which is not equal t^l_{tan} and the derivative is finite. Similarly, for discontinuities corresponding to tangencies between the homeostatic sleep pressure on wake and the upper threshold, if t^u_0 is such that $T_u(T_d(t^u_0)) = t^u_{\text{tan}}$, then $T_u'(T_d(t^u_0))) \to \infty$ as t_0 approaches t^u_0 from the left and is finite if t_0 approaches t^u_0 from the right.

The presence of gaps in the map can alter the transient behaviour, but more significantly gives an alternative mechanism for the creation/annihilation of fixed points of the map and thus periodic solutions in the two process model, via border collisions. In the next section we give a description of how we numerically find these border collisions with the aim of extending our

understanding of the bifurcation set, illustrated in Figure 3.3, to larger amplitudes.

3.3 Border collisions

At a border collision, a fixed point of the map (or its iterate) coincides with the endpoint of a gap. As parameters are varied in the model, this gives a mechanism for the creation/annihilation of periodic solutions, as seen in Figure 3.11.

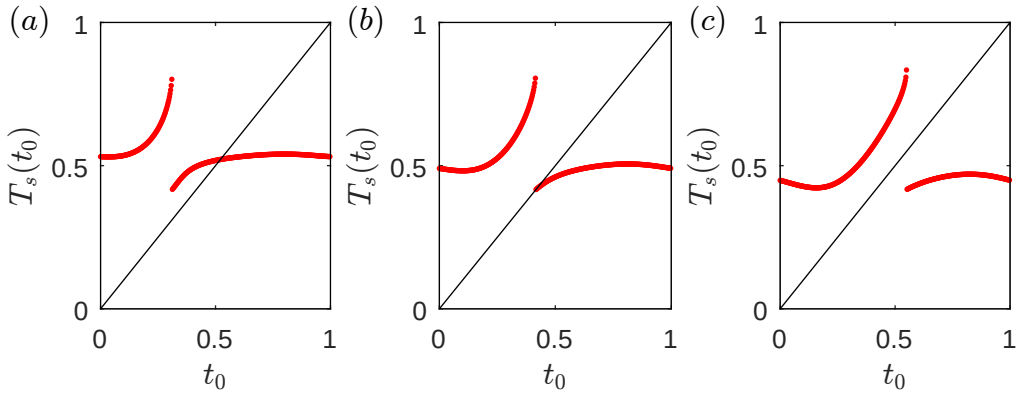

Figure 3.11: The destruction of a stable $(p, q) = (1, 1)$ periodic solution via a border collision for $a = 0.15, H_0^+ = 0.75, \chi_s = 0.25; \chi_s = 0.75$ and H_0^- varying. (a) One stable fixed point, $H_0^- = 0.5052$; (b) at the border collision, $H_0^- = 0.5151$; (c) no fixed points, $H_0^- = 0.5251$. Note that for these parameter values, the primary effect of H_0^- is to shift the position of the map rather than change its gradient.

Two types of border collision are possible within the two process model. Firstly, where a fixed point of the map coincides with the side of the gap where the derivative of the map is infinite, resulting in the creation/annihilation of an unstable fixed point. This corresponds to a periodic sleep-wake cycle occurring in the two process model where the homeostatic sleep pressure switches at a tangency point, $t_{\text{tan}}^{u,l}$. In what follows these will be referred to as Type I border collisions.

Secondly, where a fixed point of the map coincides with the side of the gap where the derivative is finite, resulting in the creation/destruction of either a stable or an unstable fixed point. This corresponds to a periodic sleep-wake cycle occurring in the two process model where the homeostatic sleep pressure 'ignores' the tangency point and switches at the first continuation point, $t_{\text{con}}^{u,l}$. These will be referred to as Type II border collisions. Both types of border collision are illustrated in Fig. 3.12.

Clearly, since gaps result from tangencies with either the lower threshold or upper threshold, four cases should be considered namely, Type I and II border collisions for the lower threshold and Type I and II border collisions for the upper threshold. In the next two subsections we focus on methods for computing border collisions with gaps due to tangencies occurring on the

upper threshold. Similar ideas can be used to find those due to the lower threshold.

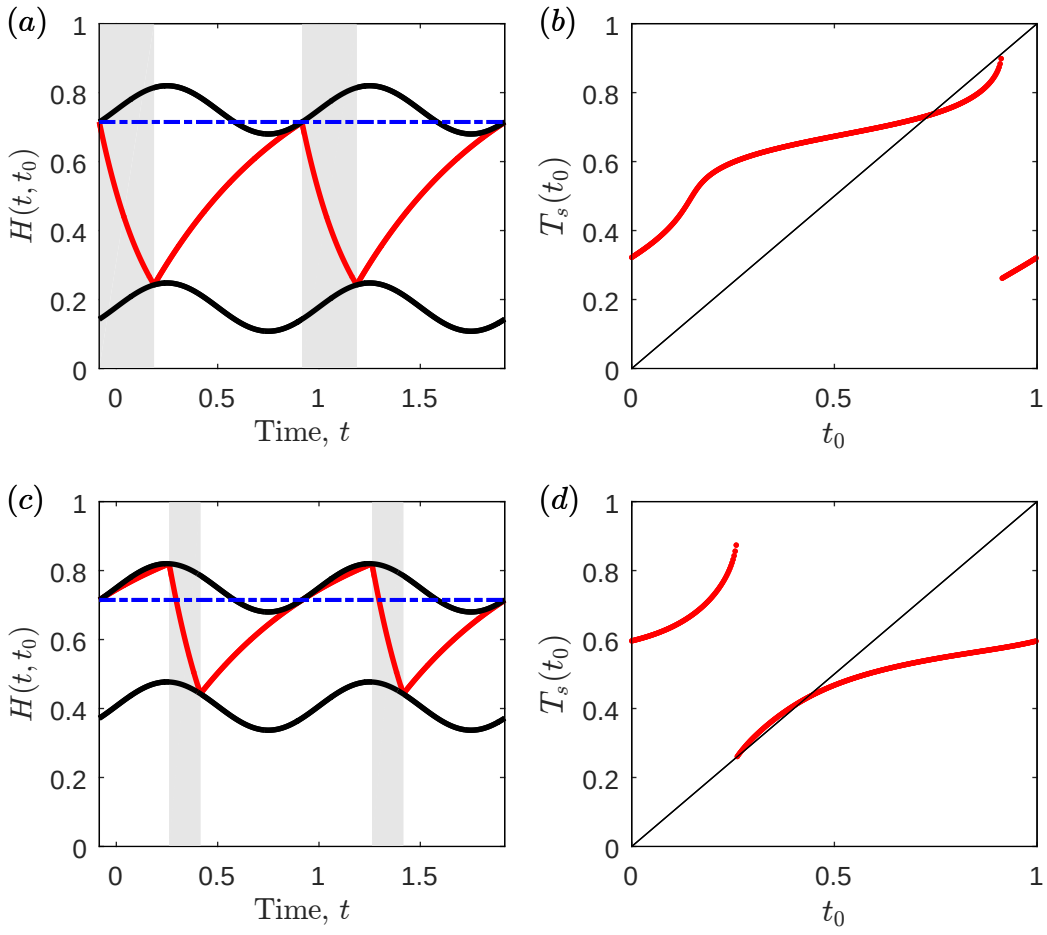

Figure 3.12: Type I and Type II border collisions of a $(1,1)$ periodic solution are shown for $a = 0.07$. The dashed blue lines in (a) and (c) represent the value, $H^+(t^u_{\text{tan}})$. (a) A sleep-wake cycle for a Type I border collision, switching from wake to sleep occurs at the time t^u_{tan} on the upper threshold; (b) The corresponding one-dimensional map shows the infinite derivative at the Type I border collision; (c) A sleep-wake cycle for a Type II border collision where the homeostatic sleep pressure on wake misses the upper threshold at $H^+(t^u_{\text{tan}})$, switching at a later time (see Section 3.2.3); (d) The one-dimensional map for the Type II border collision. In (a,b) we have $H_0^- = 0.178$ and for (c,d) $H_0^- = 0.4071$.

3.3.1 Type I

The necessary conditions for a Type I (p, q) border collision for the upper threshold are that it occurs at a fixed point of T_s^q (satisfying $T_s^q(t_0) = t_0 + p$) and the homeostatic sleep pressure on wake switches from wake-sleep at a tangency point. To find Type I border collisions of (p, q) periodic solutions, we fix all parameters except for H_0^-. We use the explicit expression from equation (3.19) to find the tangency time t^u_{tan}. We then take an initial guess for the parameter

H_0^- and use a nonlinear solver to iterate on this parameter to find the value of H_0^- such that the p^{th} forward iteration of the two process model starting on the upper threshold at $t = t^u_{\text{tan}}$ leads to a return of the homeostatic sleep pressure to $H^+(t^u_{\text{tan}})$ at time $t = t^u_{\text{tan}} + q$. Therefore H_0^- satisfies

$$H^+(t^u_{\text{tan}}) = 1 + (H_0^- + a\sin(2\pi T_d(T_s^{p-1}(t^u_{\text{tan}}))) - 1)e^{\frac{T_d(T_s^{p-1}(t^u_{\text{tan}}))-(t^u_{\text{tan}}+q)}{\chi_w}}.$$

Although this looks like an explicit equation for H_0^- note that both maps T_d and T_u depend on H_0^-.

In Figure 3.12 (a) a typical example of a sleep-wake cycle with Type I behaviour is shown and Figure 3.12(b) shows the associated one dimensional map, clearly showing the infinite derivative at the border collision.

3.3.2 Type II

The necessary conditions for a Type II border collision are that it occurs at a fixed point and the homeostat passes through the continuation of a tangency point. Again, to be specific we consider the case of a gap in the map that has arisen as a result of a tangency with the upper threshold and consider H_0^- as the bifurcation parameter for a type II border collision of a (p, q) periodic solution. As before, equation (3.19) gives the tangency time t^u_{tan}. We next determine the time point at the other side of the gap t^u_{con}, as described in Section 3.2.3. The forward iteration starts at this point and H_0^- is tuned such that the p^{th} forward iteration of the two process model starting on the upper threshold at $t = t^u_{\text{con}}$ leads to a return of the homeostatic sleep pressure to $H^+(t^u_{\text{con}}$ at time $t = t^u_{\text{con}} + q$. Thus H_0^- satisfies

$$H^+(t^u_{\text{con}}) = (1 + (H_0^- + a\sin(2\pi T_d(T_s^{p+1}(t^u_{\text{con}}))) - 1)e^{\frac{T_d(T_s^{p+1}(t^u_{\text{con}}))-(t^u_{\text{con}}+q)}{\chi_w}}.$$

In Figure 3.12(c) we show how t^u_{con} is found by continuing the homeostatic sleep pressure on a wake trajectory from the tangency t^u_{tan} and the resulting periodic solution for the tuned H_0^- value. The associated map in Figure 3.12(d) shows that the fixed point now coincides with the other side of the gap.

Computing type I and type II border collisions for the lower threshold is possible using the methods discussed in this section. The conditions for a Type I (p, q) border collision for the lower threshold are that it occurs at a fixed point of T_s^q (satisfying $T_s^q(t_0) = t_0 + p$) and the homeostatic sleep pressure on sleep switches from sleep-wake at a tangency point. A Type II border collision for the lower threshold must also occur at fixed point and the homeostatic sleep pressure passes through the continuation of a tangency on the lower threshold. In the next

section we extend the bifurcation set to include boundaries due to border collisions.

3.4 Bifurcation set

We have shown that gaps in the map occur at larger amplitudes and give rise to another type of bifurcation, allowing for creation and annihilation of periodic solutions via border collisions. In this section we illustrate how gaps in the map extend the saddle-node bifurcation diagram given in Figure 3.3 and discuss the impact this has on periodic solutions in each region.

In Figure 3.13 we plot the curves related to the two types of border collisions and the saddle-node bifurcations in the (H_0^-, a) parameter plane.

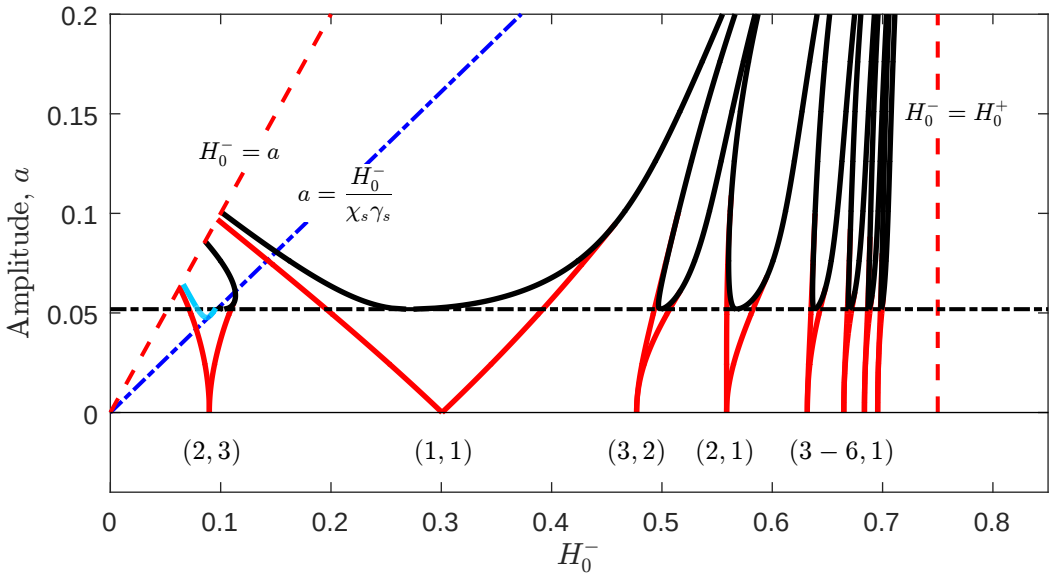

Figure 3.13: Bifurcation curves in the (H_0^-, a)-plane. Tangencies on the upper threshold occur above the dot-dashed black line corresponding to $a = \frac{1-H_0^+}{\chi_w \gamma_w}$. Tangencies on the lower threshold occur above the dot-dashed blue line corresponding to $a = \frac{H_0^-}{\chi_s \gamma_s}$. As in Fig. 3.3, the saddle-node bifurcations are shown as solid red lines. Border collisions emerge from the lines demarking the onset of tangencies, forming u-shaped regions. These are shown in black for those occurring as a result of tangency with the upper threshold and in light blue for those resulting from tangency with the lower threshold. Type I border collisions occur to the left of each u-shaped region and Type II border collisions occur to the right. The bifurcations are bounded by the biological constraints on the parameters (dashed red).

From the analysis in section 3.2, it follows that for $a < \frac{H_0^-}{\chi_s \gamma_s}$ and $a < \frac{1-H_0^+}{\chi_w \gamma_w}$, there are no tangencies in the two process model and consequently no gaps in the one-dimensional map. In this region, the one-dimensional map is the lift of a continuous circle map and regions of (p, q) periodic solutions form Arnold tongues bordered by saddle-node bifurcations, where within each tongue there is a pair of periodic solutions, one stable and one unstable.

Gaps can occur in the map T_s for $a \geq \frac{H_0^-}{\chi_s \gamma_s}$ or $a \geq \frac{1-H_0^+}{\chi_w \gamma_w}$ as a result of tangencies on the

lower and upper thresholds respectively. For some regions, the presence of gaps has no impact on the number and stability of fixed points of the map, although their presence can alter the transient dynamical behaviour. However, as can be seen in Figure 3.13, the gaps lead to border collisions that define roughly u-shaped regions 'in' each tongue. The left-hand side of these u-shaped regions are linked to Type I border collisions and appear to asymptote to the saddle-node bifurcation line. Note that these two types of bifurcations cannot coincide because at the saddle-node bifurcation the gradient of the map is one, whereas at the Type I border collision the gradient of the map is infinite.

The right-hand side of the black u-shaped region is linked to Type II border collisions. The saddle-node bifurcation and the Type II border collision meet at a point where the gradient of the map at the Type II border collision is 1, leaving only the border collision. This explains how the right saddle-node curves in Figure 3.3 terminate since the border collision curve now creates the boundary of the tongue.

For the (H_0^+, χ_s, χ_w) parameter choice shown in Figure 3.13, the Arnold saddle-node tongues with rotation number $\frac{q}{p} < 1$ end in the region with $\frac{1-H_0^+}{\chi_w\gamma_w} < a < \frac{H_0^-}{\chi_s\gamma_s}$. In this region, the up map T_u has a gap, but the down map T_d does not have a gap. Thus the relevant border collisions for these tongues are those due to a tangency with the upper threshold. The right endpoint of the $(1,1)$ tongue is in this region as well, hence here the border collision is due to a tangency with the upper threshold. The left endpoint of the $(1,1)$ tongue is in the region with $a > \max\left(\frac{H_0^-}{\chi_s\gamma_s}, \frac{1-H_0^+}{\chi_w\gamma_w}\right)$, hence both border collisions due to a tangency with the upper threshold and due to a tangency with the lower threshold could play a role. However, for the parameter values used we have not found any numerical evidence for border collisions due to the lower thresholds in the $(1,1)$ tongue.

The Arnold tongues with rotation number $\frac{q}{p} > 1$ lie partially in regions where border collisions with both the upper and lower thresholds potentially are important. In Figure 3.14 we enlarge the (2,3) tongue and see that the curve for the type II border collision with the lower threshold intersects with the curve for the type I border border collision with the upper threshold. At this point in parameter space, the endpoint of the gap due to the lower threshold, t^l_{con}, coincides with the start point of the gap due to the upper threshold, t^u_{tan}. Hence the endpoint of the gap due to the lower threshold "jumps" to t^u_{con}, the numerical solver struggles to find a solution at this point hence the small gap between upper and lower border collisions in the figure. As illustrated by the plot, at the intersection of the two curves, the border collisions disappear. This is a result of both gaps in the map meeting and "eating" the trajectories between them which leads to the 1-1 line passing through the gap and one periodic solution being lost.

To further illustrate the changes in each region we plot the one-dimensional maps for various (H_0^-, a) pairs inside and outside the $(1,1)$ tongue, this allows us to visualise the changes in the

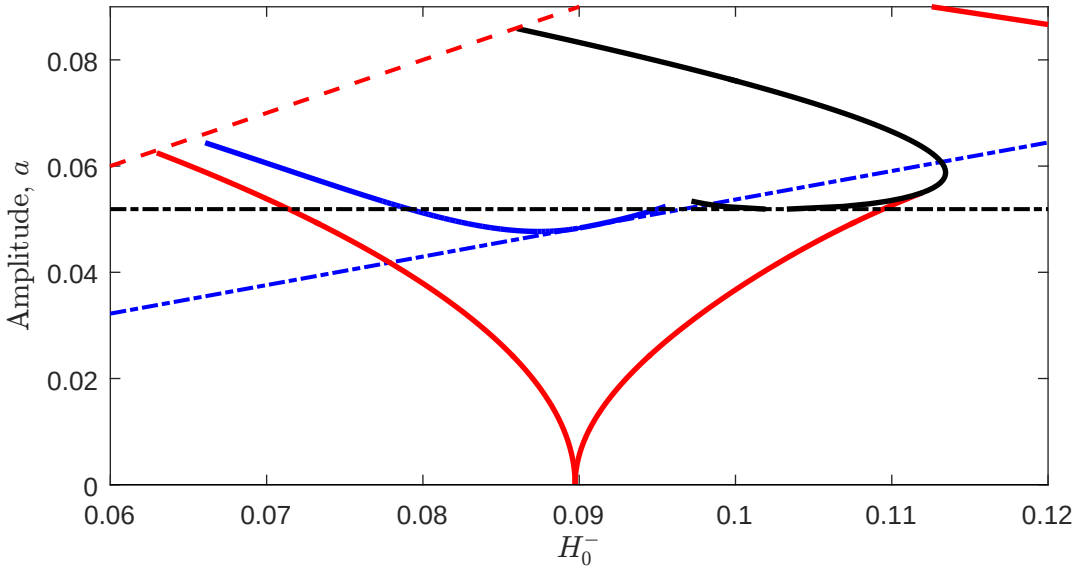

Figure 3.14: An enlarged plot of the $(2,3)$ *tongue. Note that the upper and lower threshold border collisions approach each other and probably intersect. The boundaries disappear close to their intersection since the numerical solver struggles to find a solution close to the intersection point.*

one-dimensional map when crossing the bifurcation curves associated with gaps in the map. In Figure 3.15 we enlarge the tongue and label regions in and outside of the bifurcation boundaries.

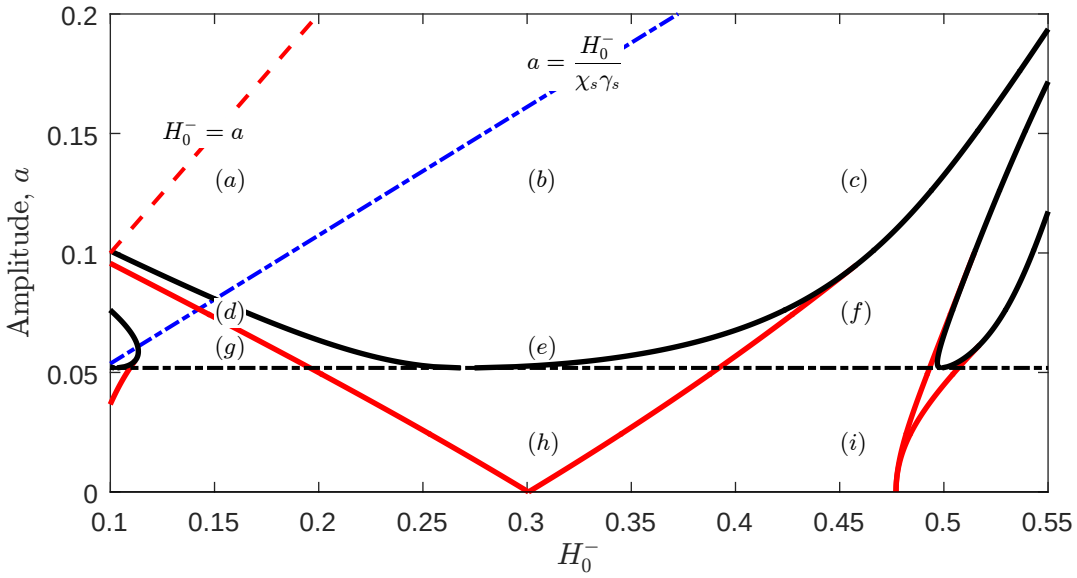

Figure 3.15: A enlarged plot of the $(1,1)$ *tongue labelled at the parameter values denoting the corresponding one dimensional maps. The parameter values labelled are as follows, (a)* $H_0^- = 0.15, a = 0.13$ *(b)* $H_0^- = 0.3, a = 0.13$ *(c)* $H_0^- = 0.45, a = 0.13$ *(d)* $H_0^- = 0.15, a = 0.075$ *(e)* $H_0^- = 0.3, a = 0.06$ *(f)* $H_0^- = 0.45, a = 0.075$ *(g)* $H_0^- = 0.15, a = 0.06$ *(h)* $H_0^- = 0.3, a = 0.02$ *(i)* $H_0^- = 0.45, a = 0.02$.

Typical one-dimensional maps in these regions are then plotted in Figure 3.16. Below we give a description of the behaviour in those regions:

(a) In this region both tangencies of the lower and upper threshold occur, leading to 2 gaps in the one-dimensional map. There is one stable periodic solution since we are inside the border collision boundaries.

(b) In going from region (a) to region (b), we have crossed the line at which tangencies with the lower threshold occur. This is demonstrated by the fact that there is now only one gap which is related to a tangency on the upper threshold, the one stable periodic solution persists as no border collisions curves are crossed.

(c) We are close to the border collision boundary where the $1-1$ line meets the gap in the map. This region is qualitatively the same as in (b).

(d) Here we are in the region where a tangency occurs at the upper threshold, but not the lower threshold, and between the saddle-node and border collision boundaries. Going from region (a) to region (d), we have crossed the border collision boundary and are no longer in the region where tangencies with the lower threshold lie. Therefore we have gained an unstable periodic solution and lost one gap.

(e) We are inside the border collision region but close to the boundary. Therefore we see one stable periodic solution and the $1-1$ line close to the edge of the gap. This region is qualitatively similar to (b) and (c).

(f) No $(1,1)$ periodic solutions exist here since we are outside of the tongue however, we are close to both the saddle-node bifurcation and border collision.

(g) No $(1,1)$ periodic solution exist in this region as in going from region (d) to region (g) we have crossed the saddle-node boundary and have therefore lost both periodic solutions.

(h) We are inside the tongue but in a region where no tangencies exist as in going from (e) to (h) the tangency line has been crossed. At this amplitude only saddle-node bifurcations can create or destroy periodic solutions. Since we are inside the tongue two periodic solutions exist, one stable and one unstable. The one-dimensional map here is the lift of a continuous circle map.

(i) No $(1,1)$ periodic solutions or tangencies exist in this region. The one-dimensional map here is the lift of a continuous circle map.

Note that we have chosen to focus on the one-dimensional maps associated with the $(1,1)$ tongue since this gives the simplest visualisation. However, we expect the behaviour of the

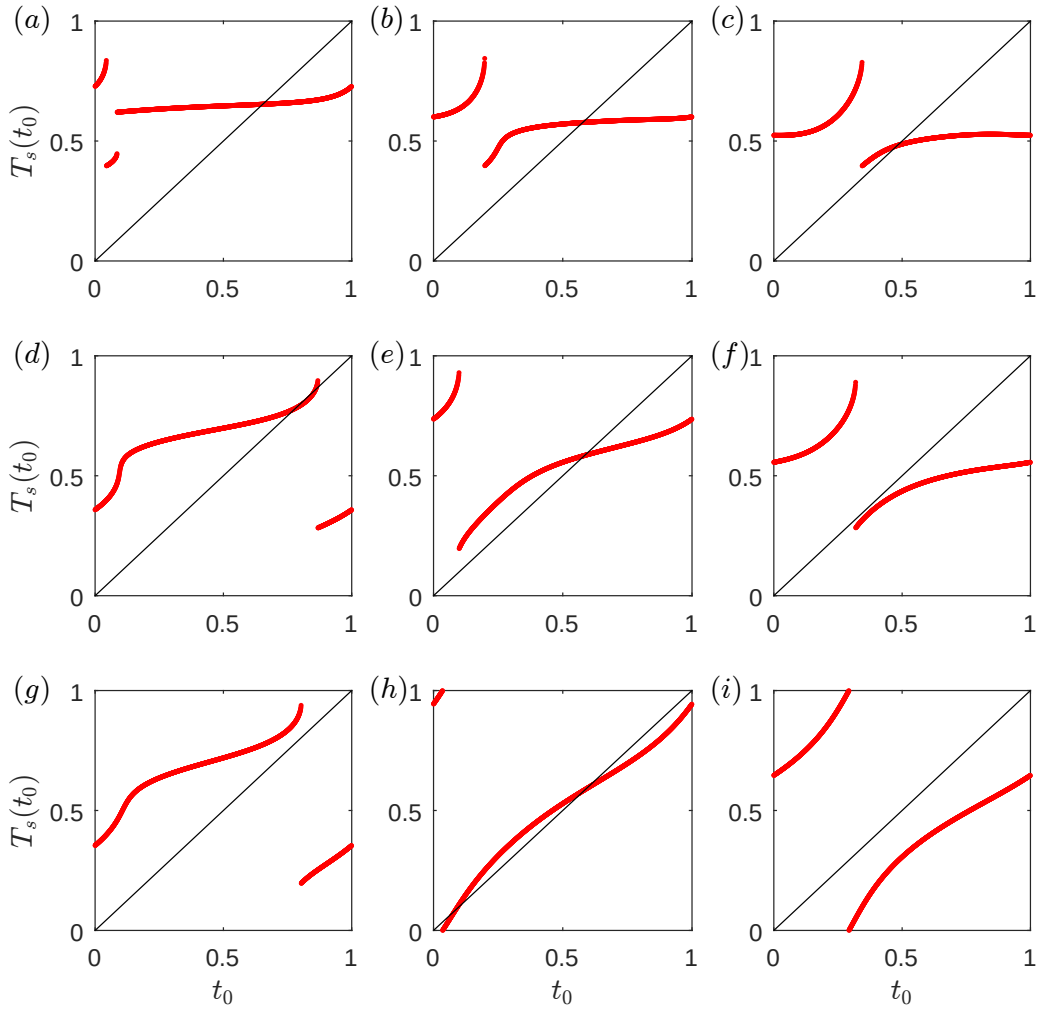

Figure 3.16: One dimensional maps for different regions of the $(1,1)$*-periodic Arnold tongue. Parameter values as in Figure 3.15.*

iterated one-dimensional maps to be similar for the other (p,q) periodic tongues. For example refer back to Figure 3.2, where the second iterate of the two process model gives a saddle-node bifurcation of two $(2,1)$ periodic solutions.

3.5 Discussion

In the previous two chapters the focus has been on introducing the two process model and understanding its dynamical structure and in doing this, giving a novel description of the dynamical transitions between continuous and discontinuous maps. The resulting structures are mathematically interesting and have the potential to highlight the strengths and weaknesses of

the two process model as a quantitative model of sleep/wake regulation.

In Chapter 2 we introduced the two process model for sleep-wake regulation and showed that it has complex dynamics which can describe a wide range of sleep patterns. We then reduced the two process model to a one dimensional map and characterized (p, q) periodic solutions. In Chapter 3, we have shown that the two process model is an interesting, potentially non-smooth dynamical system which brings together results from continuous monotonic circle maps and maps with gaps. For small amplitudes a we found that the one-dimensional map is the lift of a continuous circle map and regions of (p, q) periodic solutions form Arnold tongues bordered by saddle-node bifurcations. For higher amplitudes, tangencies between the homeostatic sleep pressure and the circadian thresholds lead to gaps in the map. Through analysis of these bifurcation mechanisms we plot the resulting bifurcation set in which both the saddle-node bifurcations and border collisions create/ annihilate fixed points of the map.

We have shown that fixed points in the map correspond to periodic solutions in the full dynamical system and represent different (periodic) patterns of sleep/wake. We see that at low circadian amplitudes, varying the bifurcation parameter H_0^- leads to a sequence of periodic solutions arising through saddle-node bifurcations, as is known to happen in continuous monotonic circle maps. For fixed a and varying H_0^-, the rotation number associated with the map has a devil's staircase structure and the intervals with constant rotation number are bounded by saddle-node bifurcations. At larger amplitudes, varying the same parameter leads to the same devil's staircase sequence for the rotation number, but now both border collisions and saddle-node bifurcations are important for the creation/destruction of periodic orbits.

Within the black u-shaped regions (border collision boundaries) of the bifurcation set, in Figure 3.13, there is only one periodic solution. For the parameter values we have explored in detail, the map is monotonic and has a unique rotation number $\frac{q}{p}$ corresponding with the (p,q) periodic orbits. The type I border collision creates/ annihilates an unstable periodic solution (due to its infinite derivative), hence the remaining solution is stable. However, we note that our choice of $H_0^+ = 0.75$ restricts the value of a to less than 0.25. For other parameter regimes, the maps T_d, T_u and $T_s = T_u \circ T_d$ are not monotonic. We will briefly discuss how the one-dimensional map becomes non-monotonic below.

Just as a gap is created in the down map T_d when there is a tangency between the homeostatic sleep pressure during sleep and the lower threshold H^-, it has a turning point (and hence is non-monotonic) when there is a tangency between the homeostatic sleep pressure during sleep and the upper threshold H^+, as in Figure 3.17(a). We see that this leads to multiple t_0 values occurring on the same sleep trajectory and hence also leads to non-monotonicity in the composite map, as in Figure 3.17(b). Similarly a turning point occurs in T_u when there is a tangency between the homeostatic sleep pressure during wake and the lower threshold. At the turning points in T_d

and T_u both maps are no longer injective, since multiple initial values of t_0 lead to the same end point and this gives the non-monotonicity. The composite map, T_s, also becomes non-monotonic if it is not injective. If T_u is non-injective then T_s is also non-injective however, if non-injectivity in T_d occurs outside of the image of T_u, then it is possible for T_s to still be injective.

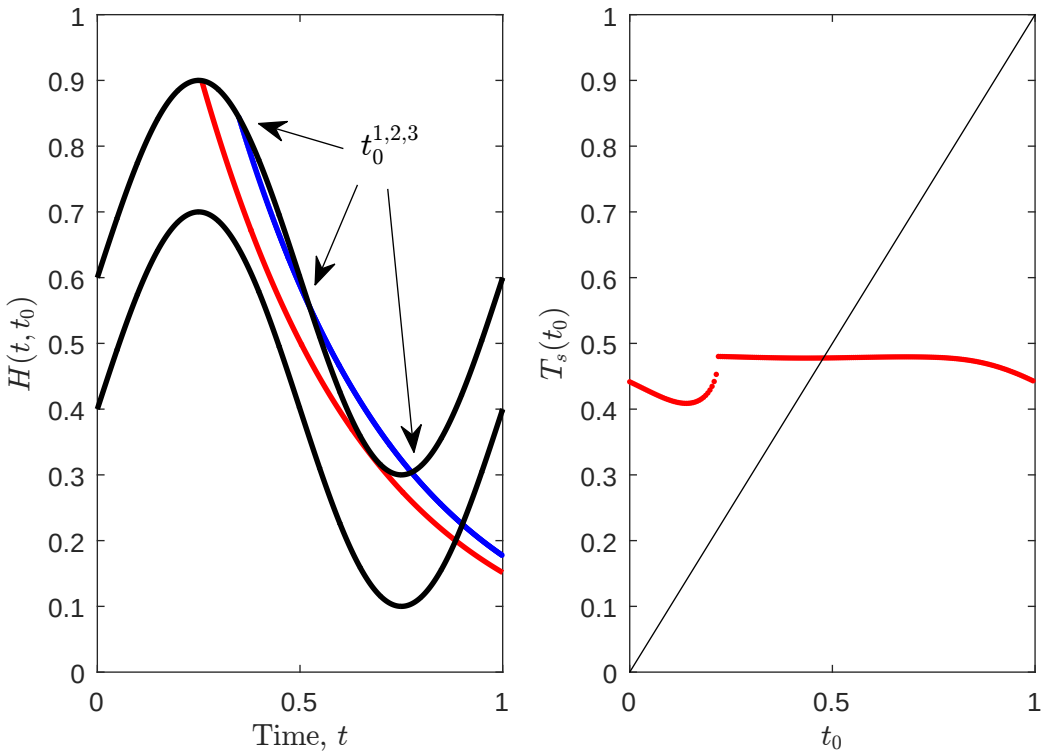

Figure 3.17: (a) The red line shows the trajectory on which there is a tangency between the homeostatic sleep pressure during sleep and the upper threshold. The blue line shows that multiple initial times, t_0, can lie on the same trajectory. This only occurs for trajectories with initial times between the initial time leading to a tangency and the time of the tangency itself. (b) The non-monotonic composite map associated with the sleep-wake dynamics in (a). The parameters used here are: $\chi_s = 10/24, \chi_w = 18/24, a = 0.3, H_0^- = 0.4, H_0^+ = 0.6$.

As the upper threshold and the lower threshold are identical apart from in their mean value, the symmetry relations (2.19) can be used to derive the criteria for non-monotonicity of the down, up, and sleep maps. So for the down map, we get from (3.9) with the mean value H_0^- replaced by the mean value H_0^+, that the down map T_d is non-monotonic if

$$a > \frac{H_0^+}{\chi_s \gamma_s}.$$

Similarly, for the up map with the mean value H_0^+ replaced by the mean value H_0^-, the down

map T_u is non-monotonic if

$$a > \frac{1 - H_0^-}{\chi_w \gamma_w}.$$

Thus the sleep map $T_s = T_d(T_u)$ is non-monotonic if

$$a > \min\left(\frac{H_0^+}{\chi_s \gamma_s}, \frac{1 - H_0^-}{\chi_w \gamma_w}\right).$$

To visualise this condition we plot an additional (green) line onto the bifurcation set, in Figure 3.18, to show the region of parameter space where the one dimensional map is non-monotonic.

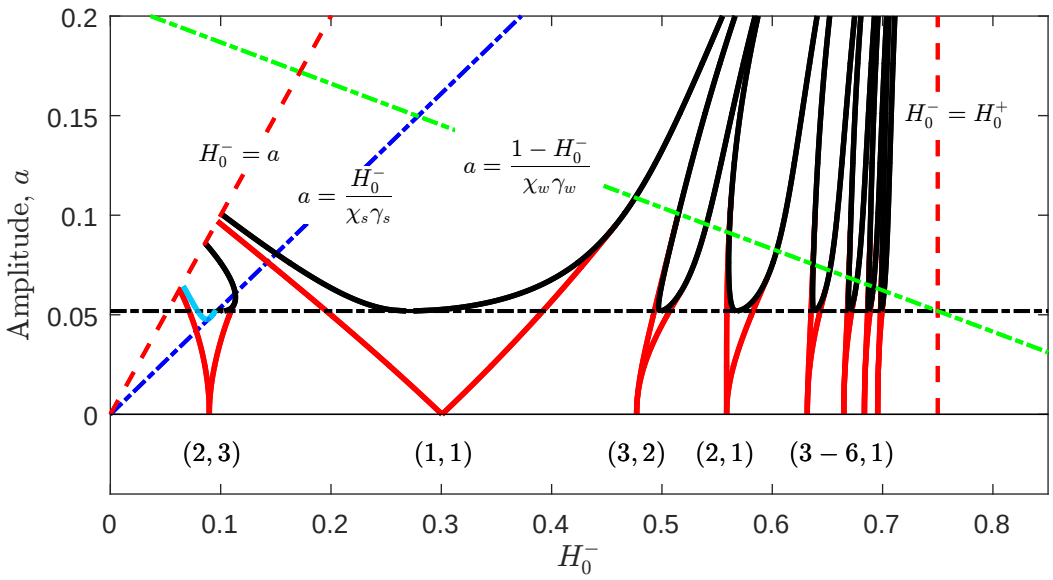

Figure 3.18: Here we see the bifurcation set with the addition of a dot-dashed green line. For the region above the dot-dashed green line the corresponding one-dimensional maps are non-monotonic.

This non-monotonicity has the potential to lead to more complex dynamics, including period-doubling and chaos, as was shown for continuous but non-monotonic maps of the circle by [128].

Finally, we note that although there is an extensive literature on maps, previous studies have either focussed on maps with gaps or maps with no gaps. Here we have considered the transition between the two, showing how border collision can take over from saddle-node bifurcations to form boundaries of Arnold tongues and highlighting a link between the devil's staircase structure of periodic solutions seen in both cases.

4

The common vole and the two process model

In this chapter we examine to what extent the two process model can explain the sleep-wake patterns of the common vole, *Microtus Arvalis*.

First we will introduce the biological data and derive the parameters for the two process model from the electroencephalogram (EEG) and sleep timing data. Next we explain how the two process model predicts spontaneous (under everyday conditions) sleep-wake cycles. Then we show that the two process model is not sufficient to predict the length of recovery sleep after sleep deprivation. Finally we propose an alteration to the two process model involving an additional ultradian oscillation. This modified model describes both spontaneous sleep-wake cycles and the response to sleep deprivation.

The purpose of this chapter is to use mathematical modelling to understand the mechanisms which govern the sleep cycles of the common vole. Some of the questions we will be considering in this chapter are:

- Can the two process model or an extension explain the spontaneous sleep-wake cycle?
- Is the two-process model a good predictor of recovery sleep after sleep deprivation?
- What physiological meaning can we derive from the results?

In the first instance, we examine to what extent observed sleep phenomena can be explained using the two-process model. In order to use the two process model to simulate spontaneous sleep-wake cycles and predict the effects of sleep deprivation we first find suitable parameter estimates for the two-process model, namely: χ_s, χ_w the strength of growth/decay in the homeostatic process; a, the amplitude of the upper and lower circadian thresholds; H_0^-, H_0^+ the mean value of the lower and upper thresholds respectively; ϕ, the phase of circadian oscillation.

The biological data that we use in this chapter are sleep timings and the EEG response during spontaneous and sleep deprivation conditions for six voles [129], each caged without

running wheels. Alongside this we also consider a larger data set of sleep/wake timings during spontaneous and deprivation conditions from a previous study [130]. In the next section we will lay out the basics of the experiment that generated the biological data, such as: housing for the voles, light scheduling and the sleep deprivation protocol. After this we describe the methodology used to monitor the voles and take EEG readings in the experiment. This is followed by an explanation of how these EEG readings are scored into wake, NREM sleep and REM sleep categories and the assumptions made to define sleep and wake bouts.

4.1 Biological data

In the experiment [129] the voles were individually housed in sound reduced, lightproof cabinets and were provided with non-restricted access to food and water. The voles were entrained to a 12 hour light-dark (LD) cycle (alternating periods of 12 hours light and dark) with a light intensity at the bottom of the housing of $750mW/m^2$ (220 lux) during the light period. Note that usually the common vole is more active during the dark and is more inactive and has a higher proportion of sleep during the light. All experimental procedures received a favourable opinion by the University of Surrey Animal Ethics Committee and were carried out under a U.K. Home Office License and in accordance with the Declaration of Helsinki.

Data recording begins with a day of spontaneous sleep episodes under 12 hours of light followed by 12 hours of dark. After this period each vole is sleep deprived for 6 hours by gentle handling, then spontaneous conditions are observed for another 42 hours as the voles undergo recovery sleep and return to their spontaneous sleep-wake cycles. Overall, EEG data has been collected for a total of 3 days for each of the six voles.

A similar experiment was performed on the common vole in 1991 [130]. It showed the effects of lengthening the period of wake on the subsequent sleep length (i.e. the effects of sleep deprivation on subsequent sleep length). During the sleep deprivation period of this experiment the voles were also food deprived. The experiment's results are displayed in Figure 4.1. Both wake and subsequent sleep length are given proportional to the average sleep-wake period length, $\tau\prime$, of the individual vole. We see a decreasing trend where the length of subsequent sleep is reduced as sleep deprivation is extended. The gradient of the decreasing trend is around -1 and is such that each sleep-wake pair has a length which is roughly a multiple of $\tau\prime$. As the length of subsequent sleep approaches 0 there is a jump from a short sleep to a long sleep at each $\tau\prime$ period. This was used by the authors in [130] to suggest the presence of an ultradian rhythm in the mechanisms that drive sleep-wake timing in *Microtus Arvalis*.

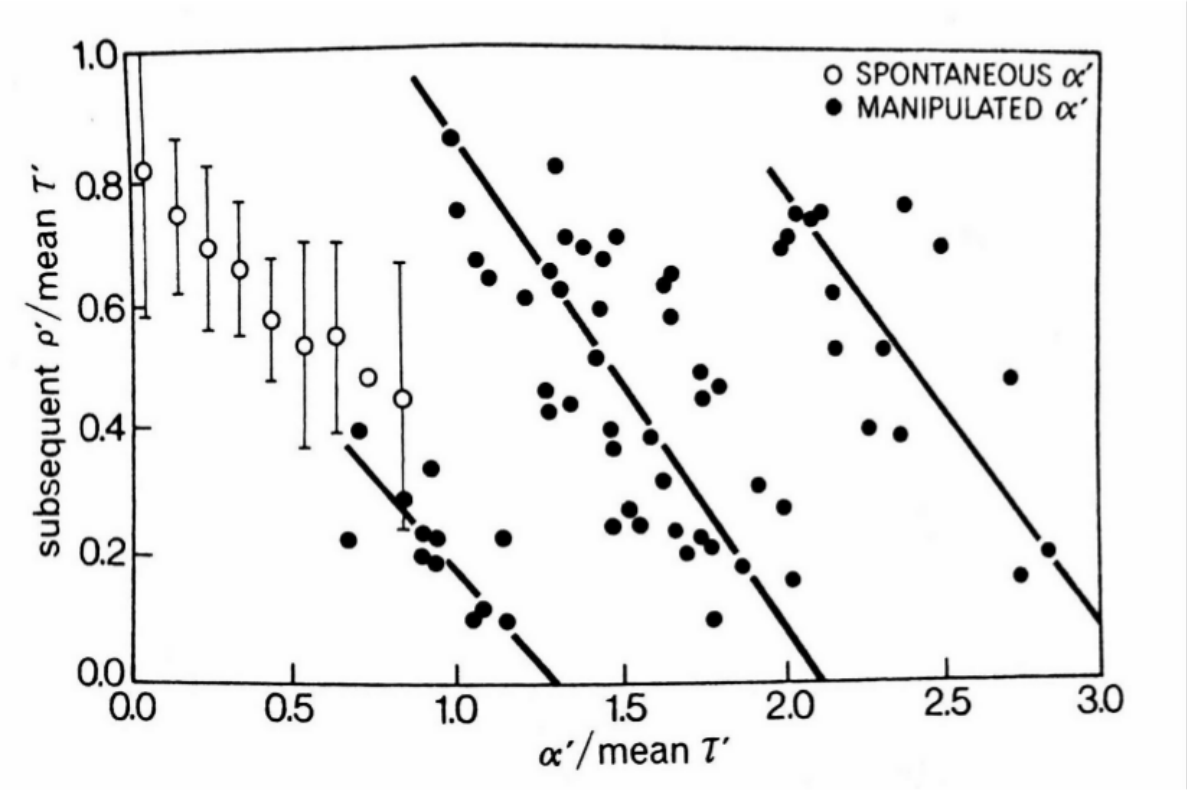

Figure 4.1: The effect of lengthening wake, $\alpha\prime$, on subsequent sleep, $\rho\prime$, from [130]. The quantities $\alpha\prime$ and $\rho\prime$ are expressed as a proportion of mean sleep-wake period length $\tau\prime$. Note that $\tau\prime$ varies across individual voles. Spontaneous sleep is denoted by the open circles (means ± SD) and for sleep deprivation (filled circles). The black lines indicate lines of best fit through the sleep deprivation data.

4.1.1 Electroencephalogram (EEG) data

In this section we introduce the method of EEG data collection for *Microtus Arvalis* and describe the techniques used to score raw EEG data into sleep-wake categories.

For *Microtus Arvalis* EEG data was recorded using the method described in [131]. Each vole is fitted with two stainless-steel EEG electrodes (length of screw shaft, 2.4 mm; outer diameter of screw thread, 1.19 mm). These are placed over the right frontal and parietal cortices under anesthesia and connected, by medical-grade stainless steel wires (cased in silicone), to a telemetry transmitter which is positioned beneath the skin along the left dorsal flank of the vole. In addition to this two stainless-steel Electromyography (EMG) leads are inserted and sutured in place in the neck muscle about 5 mm apart to record the electrical activity produced by the skeletal muscles. After surgery the voles have a recovery period of 7 days before any recording begins.

The EEG and EMG signals were modulated with a high-pass (3 dB, 0.5 Hz) and a low-pass, anti-aliasing (50 Hz) analog filter. The telemetric EEG and EMG data were transmitted at 455 kHz to an RPC-1 receiver (Data Science International) and sampled at 256 Hz (recording one measurement at every $\frac{1}{256}$ seconds) across a 12 hour light-dark cycle. Sleep is scored in 4 second epochs, which gives 1024 data points in each epoch. Sleep scoring is supported by a computer programme called Sleep Sign; both the EEG/ EMG measurements are put into the program for analysis. For EMG, any muscle movement will give a wave-like pattern and no movement gives a flat line recording, this gives an indication as to whether the vole is active and probably awake, or not. For EEG, Sleep Sign performs Fourier analysis on each epoch and a histogram is produced showing the existing frequencies in each epoch. It is important to note that sleep scoring is done manually by a trained biologist. The scorer will visually inspect both EEG and EMG data and score each epoch as either wake, NREM sleep or REM sleep.

Although the EEG data is scored into NREM sleep, REM sleep and wake it is important to define what is meant by a sleep or wake period. The scored data contains many brief awakenings which could be considered to occur during a sleep period. In the next section we use the scored data to define the minimum length a consolidated episode of wakefulness must have to be, to be classified as "wake" for the two process model.

4.1.2 Finding sleep - wake onset times from scored EEG data

From the scored EEG data we need to find onset times for sleep and wake in the two process model. To do this we focus on periods of wakefulness since voles have consolidated wake periods, whereas during periods of sleep we may see brief awakenings. We begin by allowing NREM and REM sleep to both be labeled as sleep such that we have only two categories, sleep and wake, for simulations of the model. Therefore, the homeostatic sleep process of the two process model decays during both NREM and REM sleep. We then define the initial epoch scored as sleep or wake to be an onset time, however we need to make a rational decision on how long a vole is must be awake to consider it a wake period.

We begin by considering the frequency distribution of wake lengths across all voles. To do this we sum the consecutive epochs scored as wake to find the length of each wake bout. In Figure 4.2a we plot the frequencies of these wake lengths, in 5 minute bins. Notice that there is a high frequency of wake periods with small length (< 15 minutes), therefore we choose to define a period of wake as having a length greater than 20 minutes. The frequency distribution of wake lengths over 20 minutes is shown more clearly in Figure 4.2b. For the remainder of this work we disregard any wake length of less than 20 minutes when classifying wake periods. These shorter wake bouts are defined as brief awakenings during a sleep period.

Taking a minimum wake length of 20 minutes yields sleep-wake cycles as shown in Figure 4.3.

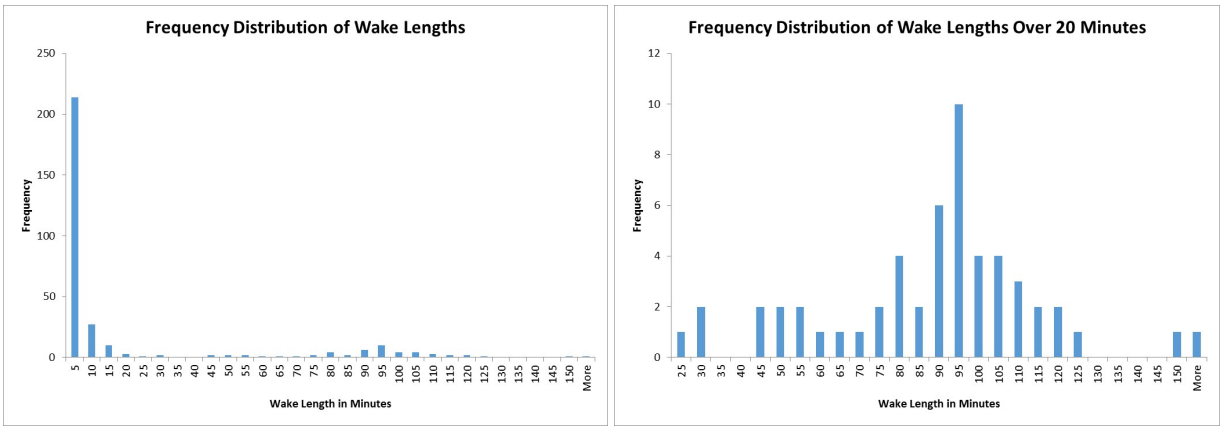

(a) *(b)*

Figure 4.2: We find the length of every wake period across all voles and plot the frequency distribution of these wake lengths. (a) The frequency distribution of all wake lengths including brief awakenings. (b) The frequency distribution of wake lengths greater than 20 *minutes gives a more even distribution.*

Each sleep-wake interval begins at sleep onset and we see that brief awakenings occur during the period defined as 'sleep'. To the right of each sleep-wake interval we see that period defined as 'wake' is consolidated (the vole remains in the wake state for 20 minutes or more) compared with the switches between brief awakening, NREM sleep and REM sleep seen during the sleep period. Whilst it is necessary to have a definition of what a wake interval is, it should not affect the results in this chapter if any wake length cut off between $20 - 40$ minutes is chosen. We will explore this later when looking at the sensitivity of the results to choices made in the analysis.

Next we use EEG data during wake and NREM sleep to determine the strength of growth and decay of the homeostatic process in the two process model and determine the other parameters in the model.

4.2 Finding two process model parameters

In this section we will derive values for χ_s and χ_w from EEG power data and then use these parameters alongside the found sleep-wake onset times to give estimates for the remaining parameters.

4.2.1 Using EEG data to find χ_s, χ_w

First we use the EEG data of the voles to find parameters χ_s, χ_w which govern the strength of decay in the homeostatic process in sleep and strength of growth during wake. It is well established that the global decline in EEG slow-wave activity (SWA) is a biomarker for the decay in homeostatic sleep pressure. During the sleep EEG, SWA is measured by the EEG

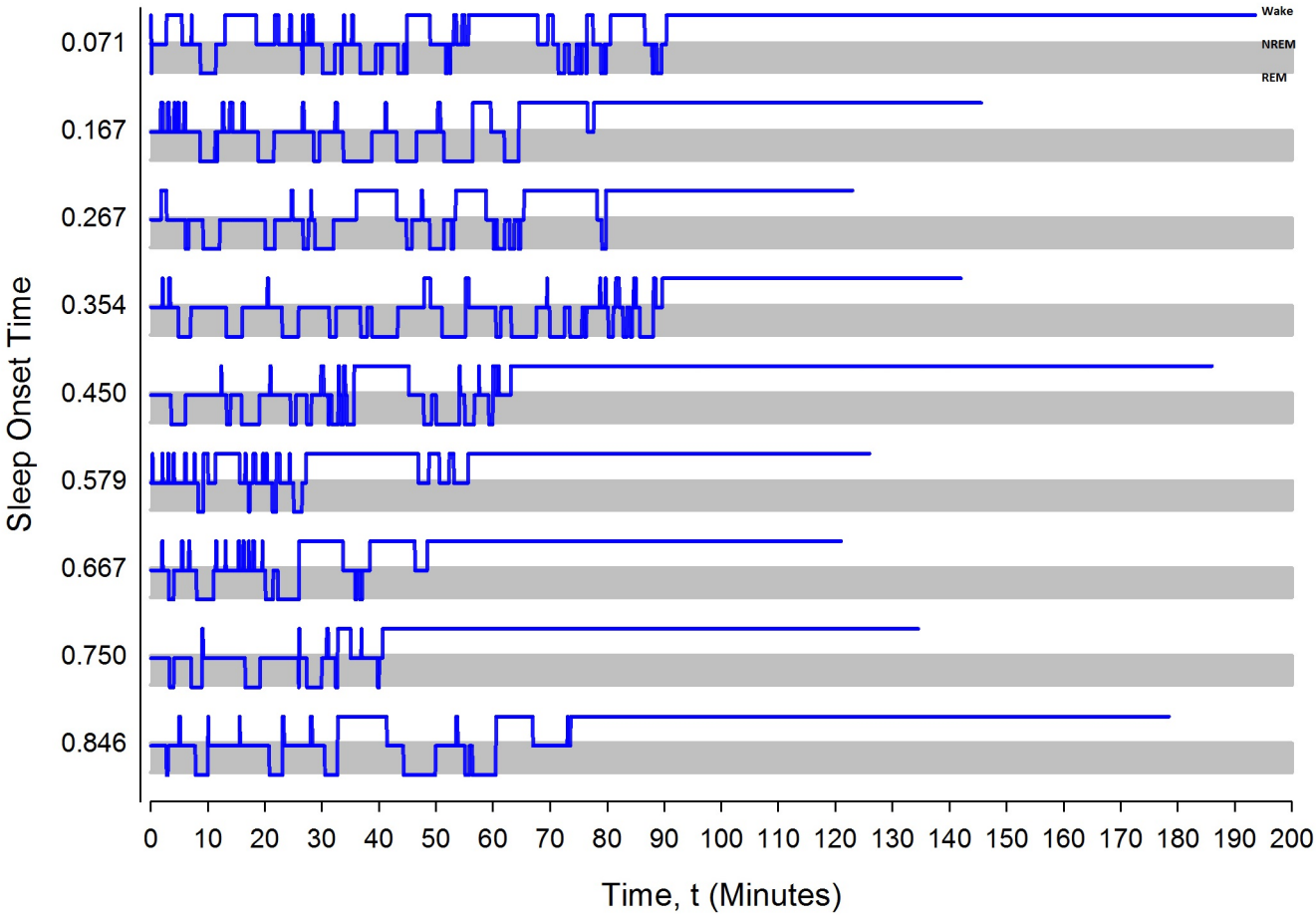

Figure 4.3: Sleep-wake intervals for Vole 1 using a 20 minute minimum wake length to categorise wake, NREM sleep and REM sleep. Each sleep-wake interval begins with sleep onset (the initial time on the vertical axis is given in days) and ends with a period of wakefulness, of length greater than 20 minutes.

power in the delta band (1-4 Hz range) during NREM sleep [100, 132, 133]. Hence a value of χ_s can be found by observing the decay of SWA in the delta band [134].

In humans a value for χ_w can be found by observing the rise of SWA after sleep deprivation. An alternate method for finding a wake time constant χ_w is to derive it from EEG power in the theta band (5-9 HZ range). For the common vole, this will turn out to be a suitable method.

To derive the time constant χ_s we begin by taking the sum of the EEG power across the delta band in NREM sleep for each epoch (once every 4 seconds). We then segment the full day into non-overlapping 5 minute periods and take a mean value of the delta activity in NREM sleep for each of these periods. Note that given the sleep/wake clarification in Section 4.1.2 an NREM epoch can only occur in a sleep interval and only epochs scored as wake can occur in both sleep and wake intervals (due to the brief awakenings which occur during sleep). Also, if no

NREM sleep is present in a 5 minute period then that period has mean value zero. We use the same method for χ_w using theta activity during wakefulness. Since we are looking for parameters which describe the strength of exponential growth/decay we have taken the natural log and then fitted a regression line where the slope gives the parameter approximations. Figures 4.4 and 4.5 show the global decline in delta activity during NREM sleep and increase in theta activity during wakefulness respectively for each individual vole. Note that theta activity is not always increasing. This may be due to the influence of circadian components and could perhaps be avoided by considering only longer sleep periods, for example during sleep deprivation. However, we will show that even if the the value of growth/ decay of the homeostatic process is significantly different the result of this chapter remain the same.

Note that here we are only interested in negative gradients during NREM sleep (since χ_s governs homeostatic decay) and positive gradients in wake (since χ_w governs homeostatic growth). Taking the mean of the gradients which satisfy this criteria across all sleep-wake periods for an individual vole gives the parameter estimates for χ_s, χ_w shown in Table 4.1.

Vole	**1**	**2**	**3**	**4**	**5**	**6**	Mean	SD
χ_s values	0.5067	0.5986	0.4961	0.5280	0.2255	0.4706	0.4475	0.1116
χ_w values	0.5448	1.1525	0.4154	0.3945	1.2160	0.1895	0.6521	0.4276

Table 4.1: Values of both χ_s and χ_w are shown for each of the six voles alongside the mean and standard deviation.

We see that the value of χ_s is relatively consistent (apart from Vole 5) however, χ_w has a large standard deviation which could be due to the method used to find χ_w from growth in the theta band. Later we explore how the choice of parameters χ_s, χ_w effects the final results in this chapter.

In the next section we use the parameter values for χ_s, χ_w and the sleep-wake onset times from the data to find estimates for the remaining parameters in the two process model.

4.2.2 Sleep-wake fitting for remaining parameters

Now we have determined parameter values for χ_s and χ_w, we focus on estimating the remaining four two process model parameters, a, ϕ, H_0^-, H_0^+. We suppose that a sleep-wake cycle is

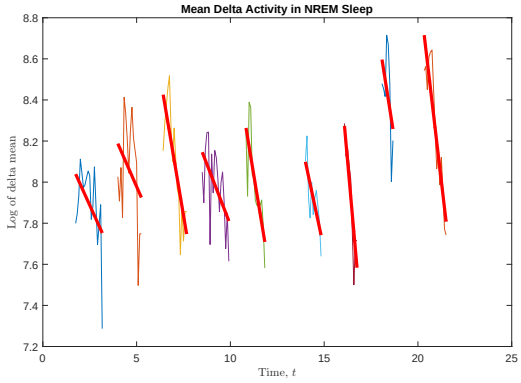

(a) Vole 1

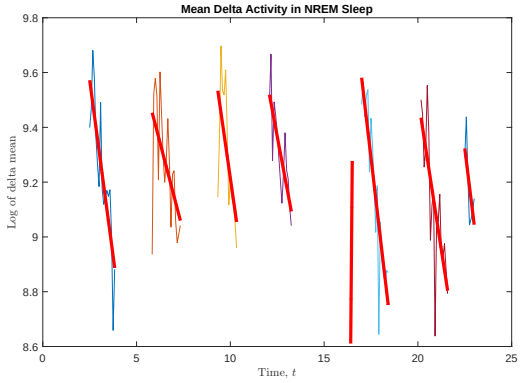

(b) Vole 2

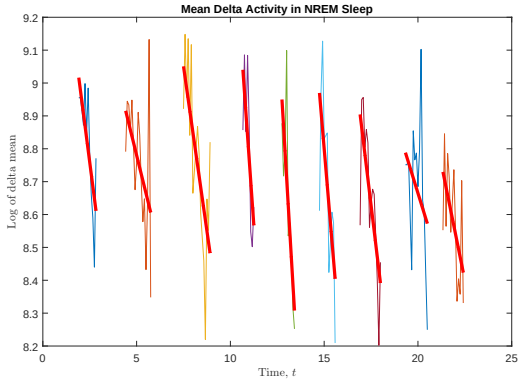

(c) Vole 3

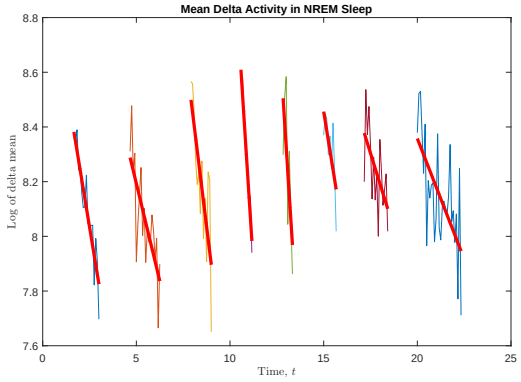

(d) Vole 4

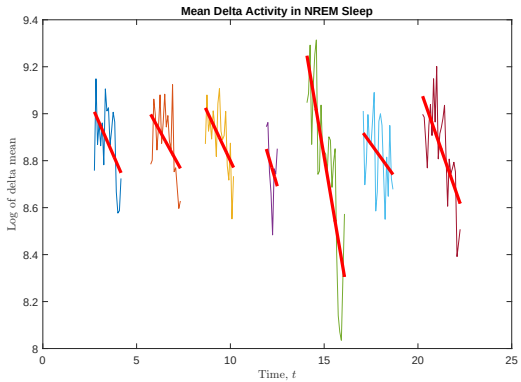

(e) Vole 5

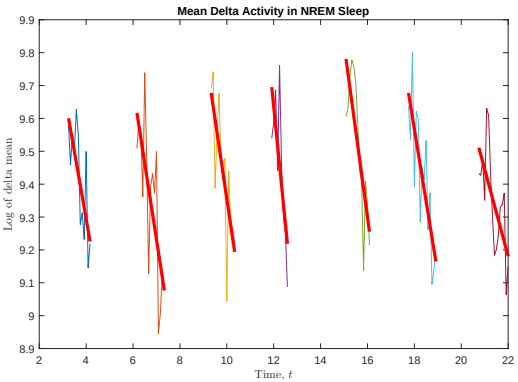

(f) Vole 6

Figure 4.4: Decay in the mean delta activity during NREM sleep only. Each point represents the mean value of delta activity during 5 *minute time intervals across the spontaneous day (i.e. the first day of data) for all* 6 *voles. Successive data points are joined by straight lines to guide the eye. We take a line of best fit across each sleep period and observe the mean gradient of decay for each vole to find a value for* χ_s.

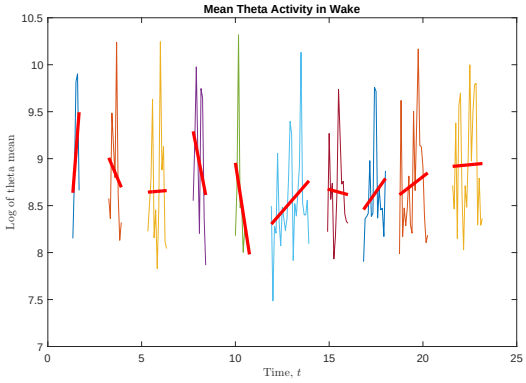

(a) Vole 1

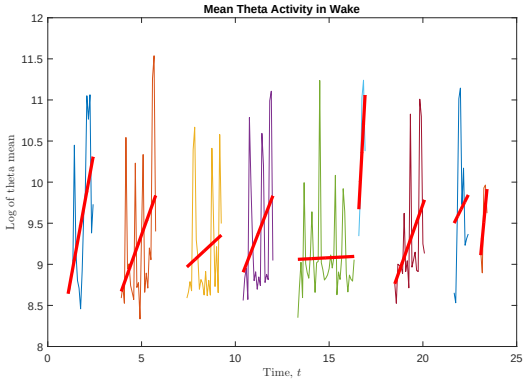

(b) Vole 2

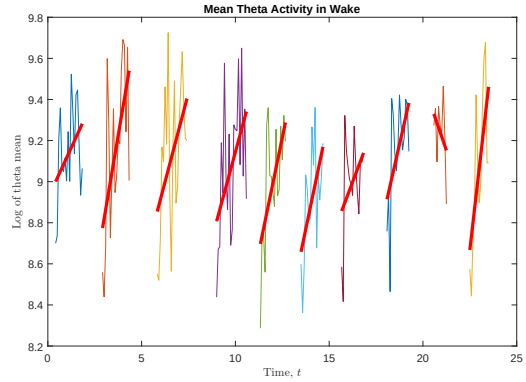

(c) Vole 3

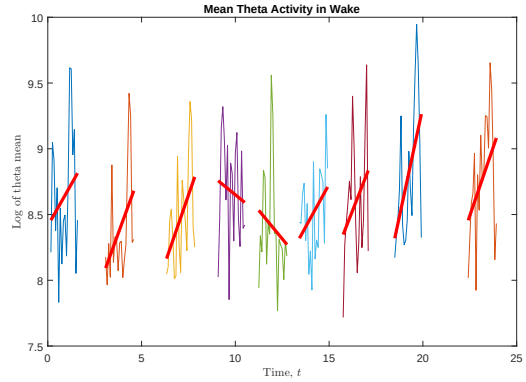

(d) Vole 4

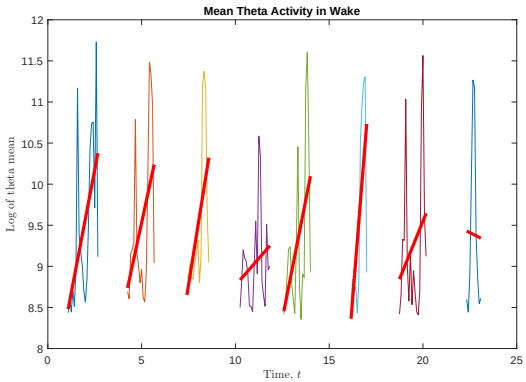

(e) Vole 5

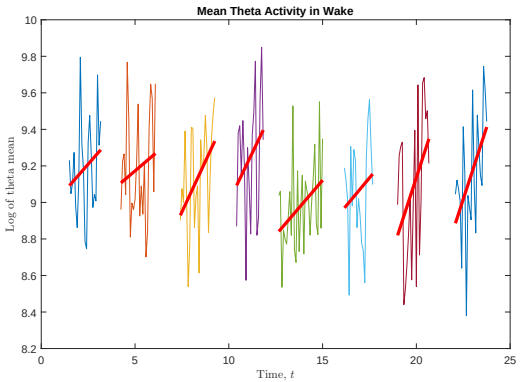

(f) Vole 6

Figure 4.5: Growth in the mean theta activity during wake only. Each point represents the mean value of theta activity during 5 minute time intervals across a the spontaneous day for all 6 voles. We take a line of best fit across each wake period and observe the mean gradient of growth for each vole to find a value for χ_w. Here we only take an average of the positive values since we need a positive value to represent growth in the homeostatic sleep pressure. The robustness of the results to parameter values are discussed later in Section 4.6.

described by the two process model. Hence there is a homeostatic sleep pressure which satisfies

$$\begin{aligned} H(t) &= H(t_s^n)e^{\frac{t_s^n - t}{\chi_s}} && \text{for} \quad t \in [t_s^n, t_w^n], && \text{(sleep)} \\ H(t) &= 1 + (H(t_w^n) - 1)e^{\frac{t_w^n - t}{\chi_w}} && \text{for} \quad t \in [t_w^n, t_s^{n+1}] && \text{(wake)}, \end{aligned} \tag{4.1}$$

where $H_s(t_w^n) = H_w(t_w^n)$ and $H_w(t_s^{n+1}) = H_s(t_s^{n+1})$. Note that switching occurs at (the yet unknown) thresholds at the sleep/wake onset times t_s^n, t_w^n derived from the data as described in Section 4.1.2.

The dynamics of the two process model allows us to find the switching values for $H(t_s^n)$ and $H(t_w^n)$ by simulation of the dynamics. If the data can be described by the two process model then the switching values $H(t_s^n)$ and $H(t_w^n)$ should lie on the upper and lower thresholds respectively. We start the homeostatic sleep pressure on a sleep trajectory at $H(t_s^1) \in (0,1)$. Next we continue the homeostatic sleep pressure as described in (4.1) with the daily repeated sleep-wake onset times. Any starting value $H_s(t_w^1)$ will converge to a periodic solution, as depicted in Figure 4.6. Indeed, if after one day, $H_s(t_w^1+1) > H_s(t_w^1)$, then all homeostat values in the next day are above those in day one. By construction $H_s(t_w^n)$ is bounded above by 1 thus the iteration has to converge to a periodic orbit. A similar argument holds for the case $H(t_w^1+1) < H(t_w^1)$ since $H_w(t_s^n)$ is bounded below by 0. The model has converged to a periodic solution once $H_{s,w}(t) = H_{s,w}(t+1)$, as depicted in Figure 4.7. The periodic solutions for each vole are plotted in Figure 4.8.

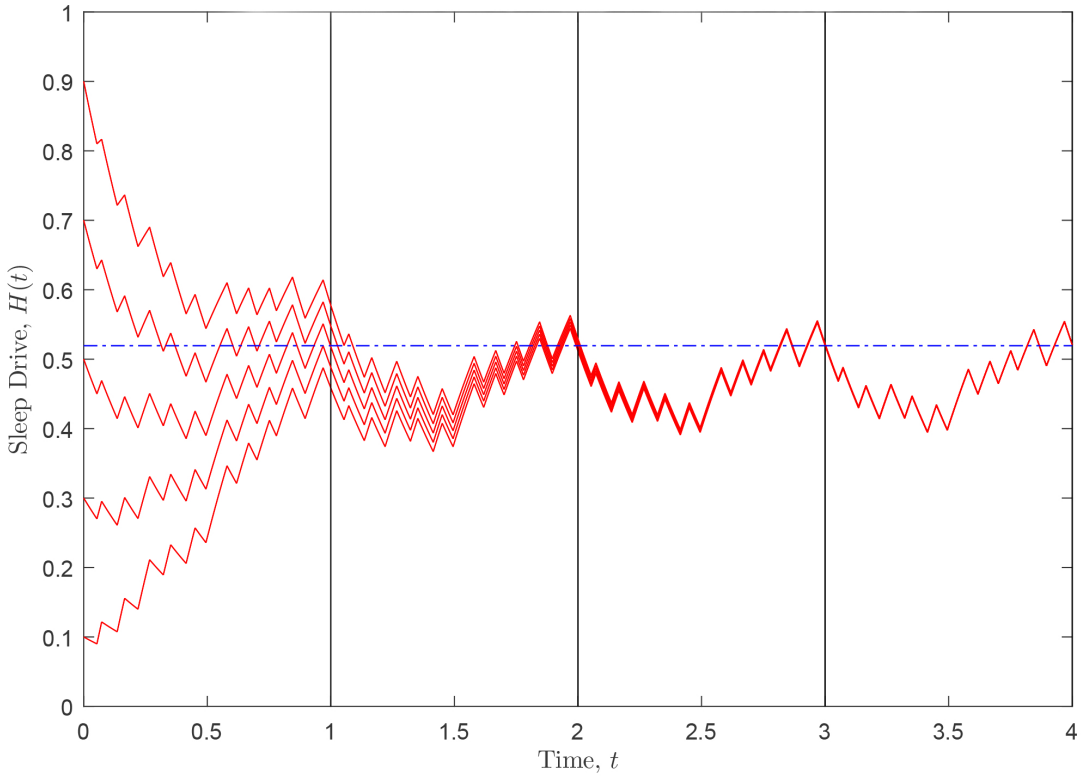

Figure 4.6: Using the χ_s, χ_w values and sleep-wake onset times for Vole 1 we begin the homeostatic process (red) at various values namely, $0.1, 0.3, 0.5, 0.7, 0.9$. Notice that any starting value $H(t)$ converges towards a periodic solution, where $H(t) = H(t+1)$. The dashed blue line shows the converged homeostat value at $t = 0 \mod 1$. Note that the homeostatic processes above cannot cross since they are governed by the same constants of growth/ decay.

We now have values for $H(t_s^n), H(t_w^n)$, i.e. the homeostatic sleep pressure values at the

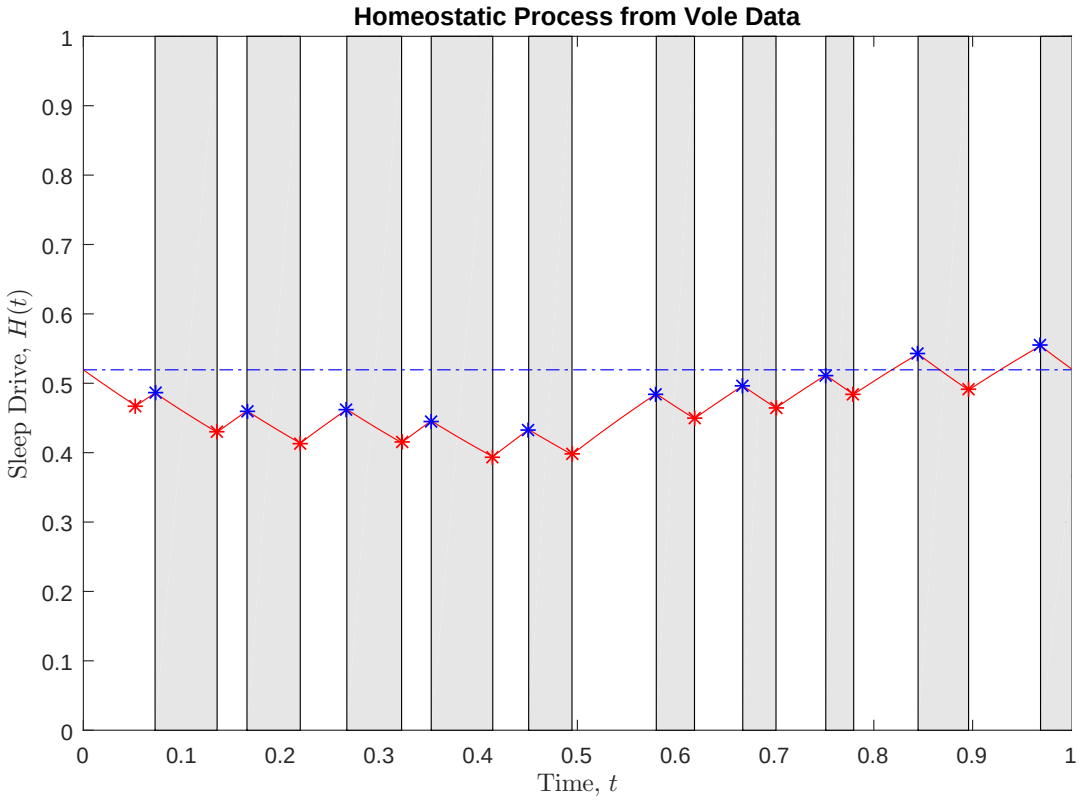

Figure 4.7: Model convergence occurs when $H(t) = H(t+1)$, this is represented by the dashed blue line which shows that the homeostat values at times $t = 0$ and $t = 1$ are equal. The red line denotes the homeostatic process with the shaded regions indicating sleep and the blank regions wake. The switching points t_w^n, t_s^n are given by the red and blue stars respectively.

sleep-wake switching times. We therefore simultaneously fit a sinusoid to the upper and lower homeostatic sleep pressure values by choosing H_0^-, H_0^+, a_1 and a_2 such that the function

$$\sum_n \left((H(t_w^n) - f_{lower}(t_w^n))^2 + (H(t_s^n) - f_{upper}(t_s^n))^2 \right)$$

is minimized. Here

$$f_{lower}(t_w^n) = H_0^- + a_1 \cos(2\pi t_w^n) + a_2 \sin(2\pi t_w^n)$$

and

$$f_{upper}(t_s^n) = H_0^+ + a_1 \cos(2\pi t_s^n) + a_2 \sin(2\pi t_s^n),$$

where we have used $a \sin(2\pi t + \phi) = a_1 \cos(2\pi t) + a_2 \sin(2\pi t)$.

The best fit for each vole is shown in Figure 4.9 thus, we have found estimates for all 6 parameters in the two process model for each vole. The values H_0^-, H_0^+ are given by the mean

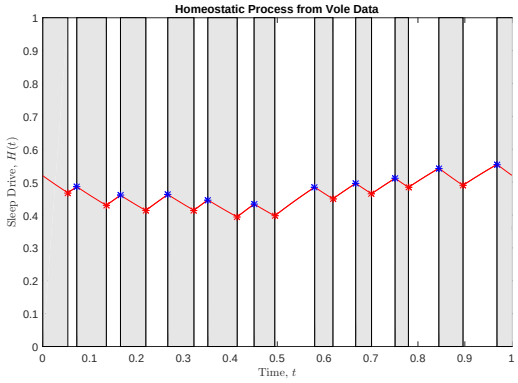

(a) Vole 1

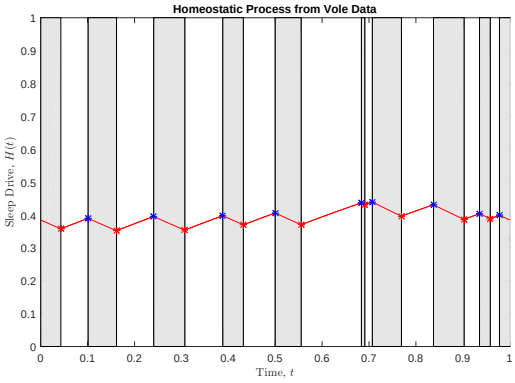

(b) Vole 2

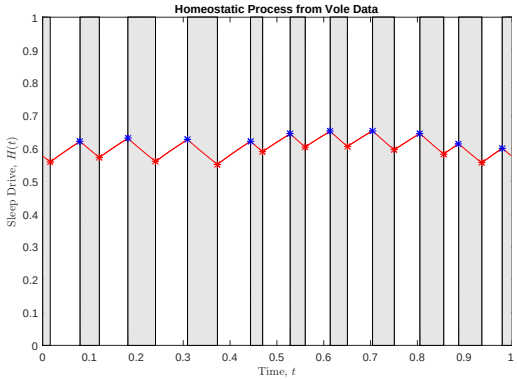

(c) Vole 3

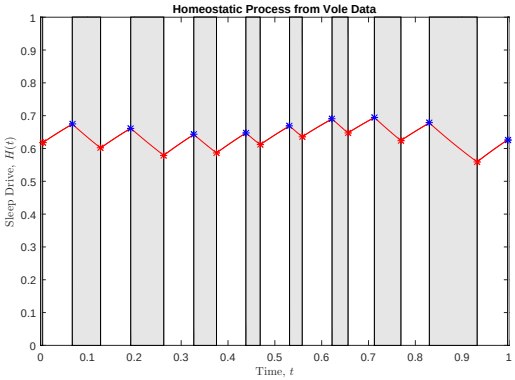

(d) Vole 4

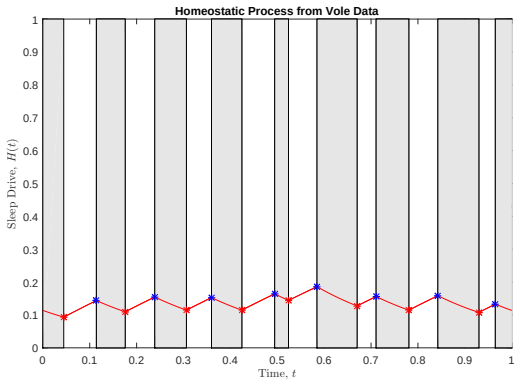

(e) Vole 5

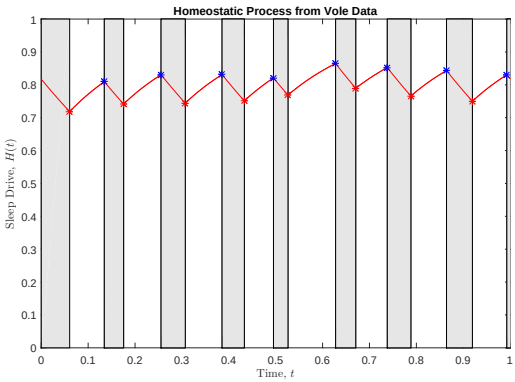

(f) Vole 6

Figure 4.8: Simulations of the homeostatic process using the values χ_s, χ_w and sleep/ wake onset times from the vole data. The values for the upper and lower circadian thresholds vary strongly across the voles but we note that the amplitude of circadian oscillation is small for all sampled voles.

values of the lower and upper threshold fits respectively and since both thresholds are fitted simultaneously each threshold has the same amplitude $a = \sqrt{a_1^2 + a_2^2}$ as required.

Since there is only a small variation in switching values, $H(t_s^n), H(t_w^n)$, we observe a small

Vole	**1**	**2**	**3**	**4**	**5**	**6**	Mean	SD
χ_s values	0.5067	0.5986	0.4961	0.5280	0.2255	0.4706	0.4709	0.1278
χ_w values	0.5448	1.1525	0.4154	0.3945	1.2160	0.1895	0.6521	0.4276
a, amplitude	0.0489	0.0273	0.0197	0.0219	0.0168	0.0215	0.0260	0.0117
H_0^+, upper threshold	0.4886	0.4087	0.6304	0.6640	0.1553	0.8350	0.5303	0.2357
H_0^-, lower threshold	0.4437	0.3775	0.5774	0.6066	0.1154	0.7539	0.4791	0.2215
ϕ, phase	0.6223	0.4701	0.3769	0.4287	0.3088	0.4115	0.4364	0.1060

Table 4.2: All 6 parameter estimates for the six voles alongside mean and standard deviation.

resulting amplitude. Thus it is important to check whether fitting sinusoidal thresholds gives a better fit than a less complicated model with no circadian amplitude ($a = 0$). Here and throughout this chapter we will perform an F-test, using the method in Appendix C.1., to find p-values to test whether or not a model with more parameters produces a significantly better fit. When fitting sinusoidal thresholds to all voles, as in Figure 4.9, we see that fitting a sinusoid does give a significantly better fit than a model with no circadian amplitude with p-values $2.8638 \times 10^{-7}, 5.1578 \times 10^{-4}, 0.0031, 0.0262, 0.0016, 0.0014$ for voles one to six respectively. A summary of the parameter values found is shown in Table 4.2.

We observe that χ_s has relatively small standard deviation suggesting that the mean could give a good estimate for all voles. However, the remaining parameters show much larger variations. The variation in H_0^+ and H_0^- is probably due to the variations in χ_w as smaller values of χ_w give faster growth of the homeostat during wake and therefore a periodic solution has higher upper and lower threshold values. The small amplitude found across all voles is due to small variation in the values found for $H(t_s^n)$ and $H(t_w^n)$.

We will now use these parameters in the two process model and make comparisons between various markers such as: proportion of sleep, number of sleep episodes and behaviour under spontaneous (non-deprivation) conditions.

4.3 Comparison of the two process model with spontaneous data

In the previous section we found estimates for the parameters of the two process model for each vole, given in Table 4.2. In this section we will use these parameters to make comparisons between the data and simulations made by the two process model during spontaneous sleep. We

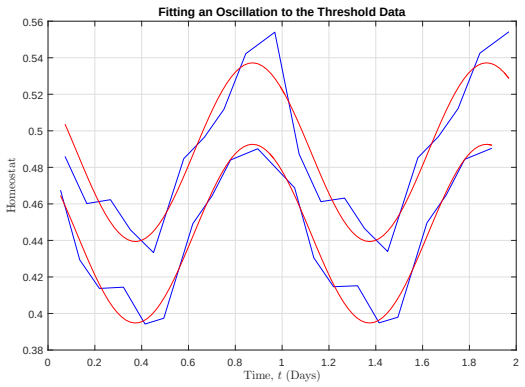

(a) Vole 1

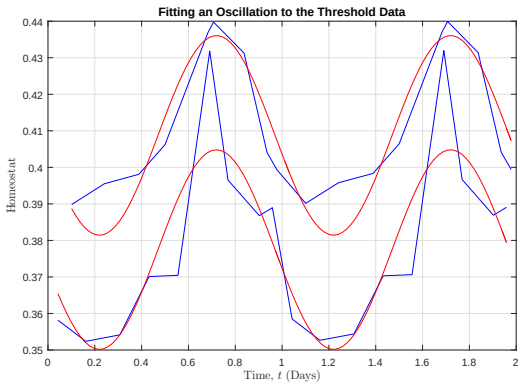

(b) Vole 2

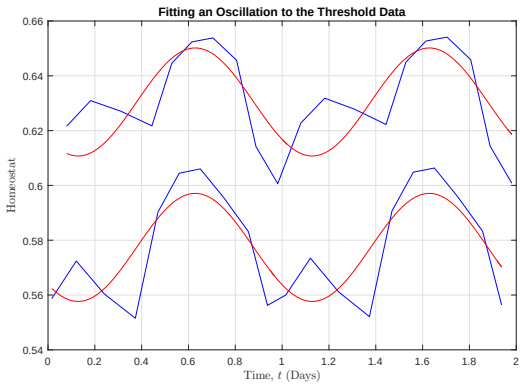

(c) Vole 3

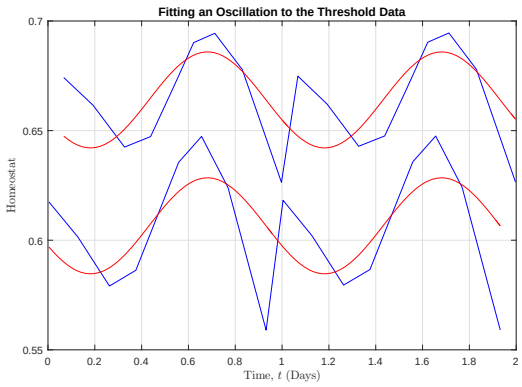

(d) Vole 4

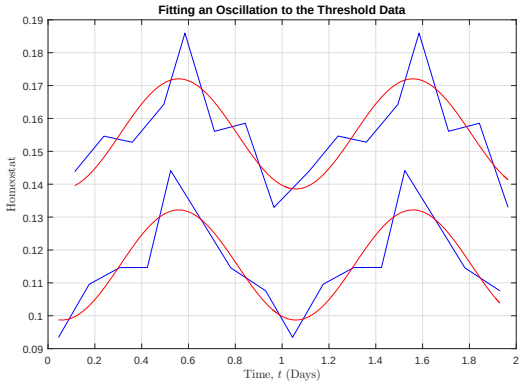

(e) Vole 5

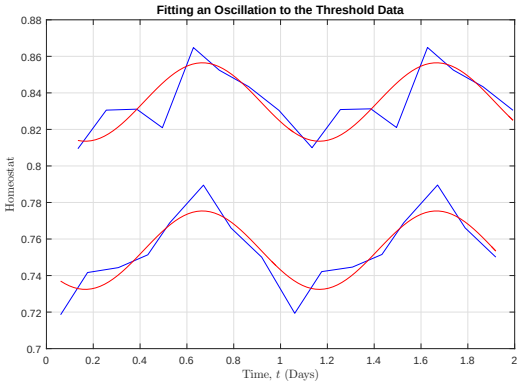

(f) Vole 6

Figure 4.9: Simultaneously fitting a sinusoid (red) to the upper and lower threshold points (blue) determined by the simulation in Figure 4.8. This allows us to find the mean values H_0^-, H_0^+ and an amplitude a.

begin by running the two process model to test its accuracy in predicting sleep/wake patterns for the voles by comparing the proportion of sleep throughout the day and the number of sleep-wake episodes between model and data. Furthermore we will use the mean of each parameter value

and consider the same observations to see if this gives a good representation of an 'average' vole. Finally we go on to explore what the two process model with parameters fitted to the spontaneous data predicts about the length of the recovery sleep after sleep deprivation.

Firstly, we simulate spontaneous sleep-wake cycles for each vole, shown in Figure 4.10. This allows us to compare the proportion of sleep during light and dark periods and also the number of sleep episodes across the day. These two comparisons are shown in Table 4.3 and Table 4.4.

In Table 4.3 we compare the proportion of sleep given by the two process model, after transients have decayed, against the sleep-wake onset times from the data. The values given show the percentage of sleep during light (not-shaded) and dark (shaded). The values given by the model and the data are not in total agreement however we see that the mean across all voles is a good estimate of average sleep proportions for a vole. The two process model also predicts the larger sleep proportions of voles 1 (during light) and 5 (during light and dark) in comparison to the other voles. The large inter-individual differences in sleep proportion suggest the need for individual parameter sets and not just the use of average parameter values across all voles.

Vole Sleep (%)	1	2	3	4	5	6	Mean	SD
Model	59.4	46.81	40.64	43.55	50.36	40.21	46.83	7.26
Actual	66.31	42.6	41.06	42.66	48.72	41.1	47.08	9.84
Model	41.51	41.67	45.23	41.84	58.29	37.01	44.26	7.35
Actual	36.58	46.81	46.64	44.32	60.28	36.3	45.16	8.79

Table 4.3: Proportion of sleep during light (not shaded) and dark (shaded).

To further investigate the link between sleep onset times and the corresponding lengths of sleep, we have plotted those quantities against each other in Figure 4.11. We find that the length of sleep across the day varies, with the longest sleeps occurring at light onset (i.e. the start of the day) and the shortest at lights out (after 12 hours). This is consistent with the fact that we found a non-zero amplitude for the circadian oscillation in the two process model for all six voles. Having even a small circadian amplitude creates slight variations in sleep length as different sleep onset times are considered.

Another comparison that can be made is the predicted number of sleep episodes across the day in comparison with the data. In Table 4.4 we count the number of sleep episodes the model predicts and compare this with those seen in the data. We find that for all the voles the model accurately predicts the number of sleeps during the one day period of recorded spontaneous sleep.

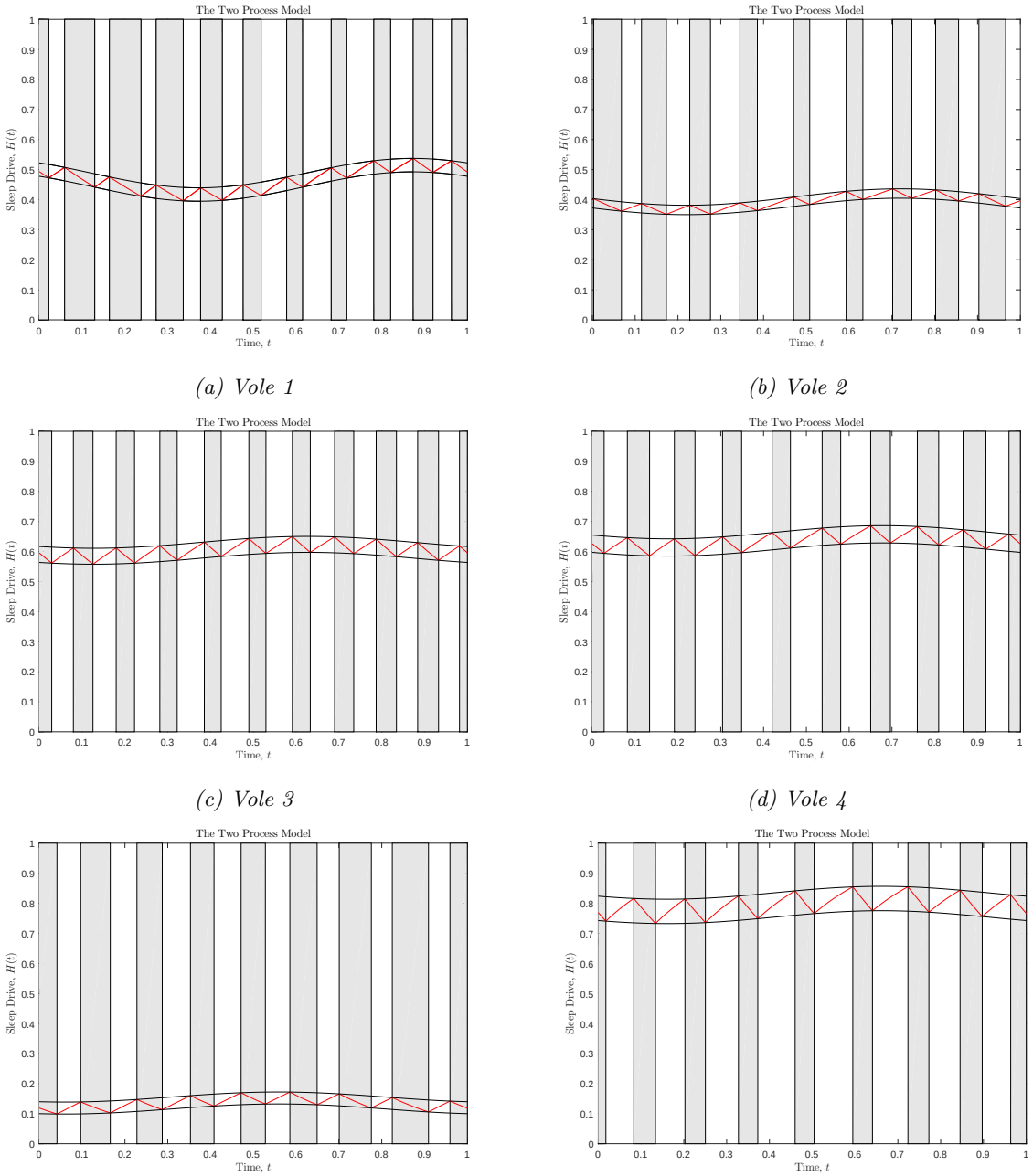

(a) Vole 1

(b) Vole 2

(c) Vole 3

(d) Vole 4

(e) Vole 5

(f) Vole 6

Figure 4.10: Running the two process model using all 6 *parameters found from the EEG data and sleep/ wake onset times. Depicted are the sleep/ wake timings, where sleep indicated by the shaded areas, and sleep distribution across the day.*

However, it is important to note that we are only trying to predict one day of observations, if the observations were over a longer period it may be more difficult to predict any variations in the number of sleeps per day.

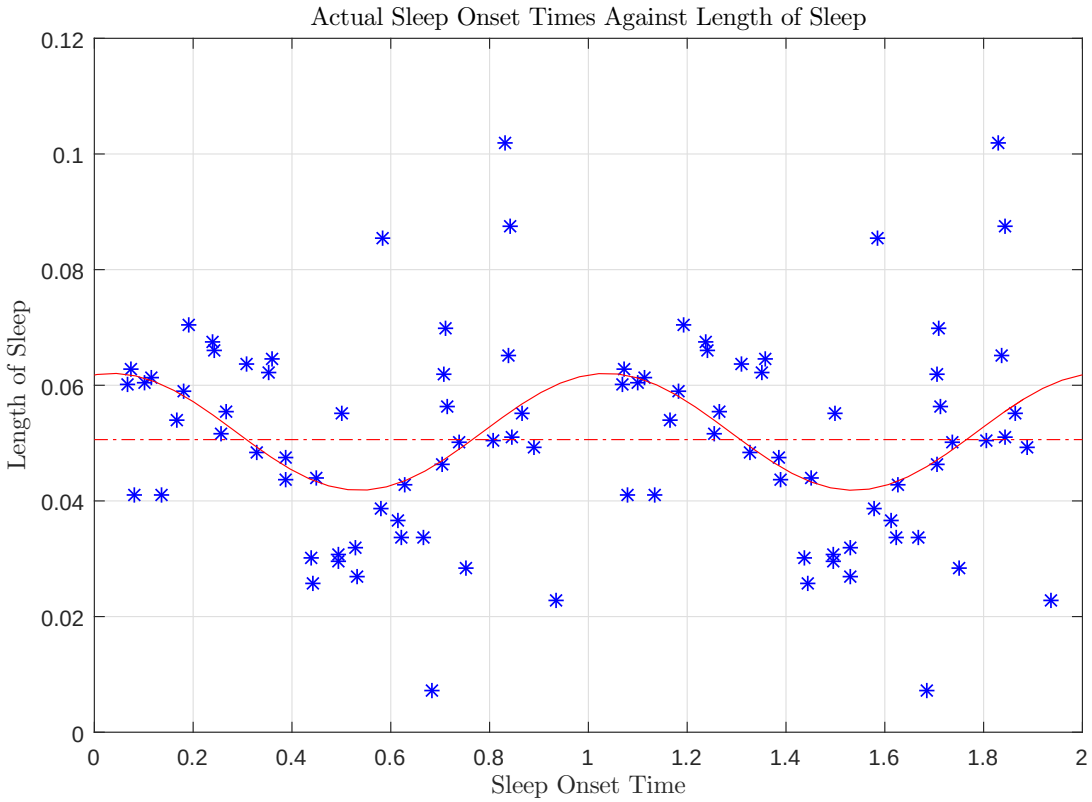

Figure 4.11: Sleep onset times plotted against the corresponding lengths of sleep are given by the blue dots. The dashed red line shows a one parameter fit which can be compared to the solid red three parameter fit (circadian). The figure is double plotted to show the circadian behaviour. We find that the circadian oscillation gives a better fit with a p value of 0.0301.

Vole	1	2	3	4	5	6
Model	10	9	10	9	8	8
Actual	10	9	10	9	8	8

Table 4.4: Number of sleep-wake episodes across one day.

It is interesting to consider the mean values of all 6 parameters in the two process model, given in Table 4.5, to determine whether these mean parameter values can give results which coincide with the average sleep proportions and sleep episodes. However, we expect that running the two process model with the parameters in Table 4.5 would not be sufficient to explain the behaviour of all voles individually.

As before we run the two process model, now using the mean paramater values. The com-

	χ_s	χ_w	a	H_0^+	H_0^-	ϕ
Mean Vole	0.4709	0.6521	0.0260	0.5303	0.4791	0.4364

Table 4.5: Mean parameter values across all six voles.

parison between the average vole behaviour in the data against the models results during spontaneous sleep is given in Table 4.6 and the sleep-wake cycle is shown in Figure 4.12.

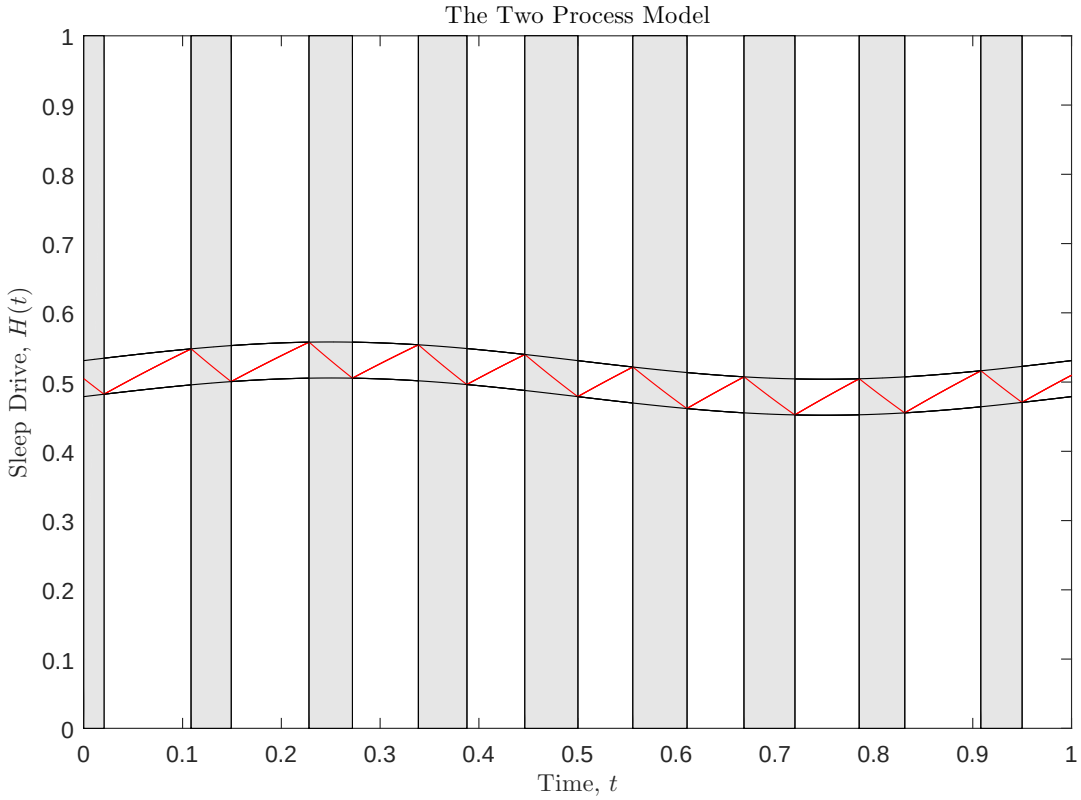

Figure 4.12: A run of the two process model using mean parameter values $\chi_s = 0.4475$, $\chi_w = 0.6521$, $a = 0.0269$, $H_0^+ = 0.5310$, $H_0^- = 0.4790$.

Notice that with the mean parameters the two process model is a good predictor of the number of sleep episodes across the day however, the proportion of sleep in the light and dark phase is predicted to be much shorter than observed in the data. As well as this, when compared with Table 4.3 we see that these values are not representative of all voles, since the number and proportion of sleep varies significantly. This gives a strong argument for treating each vole individually when considering the relationship between parameters.

Vole	Sleep (Light)	Sleep (Dark)	Number of Sleeps
Average Vole	41.4086	38.6848	9
Mean (Actual)	47.08	45.16	9

Table 4.6: Proportion of sleep during the light and dark alongside the number of sleep episodes for the 'average' vole against the mean values from Table 4.3.

Finally, since we have a day of spontaneous data for six voles we have enough data points to check whether the voles are behaving in the same way as in Figure 4.1, from Gerkema [130]. By using the sleep-wake onset timings of the voles we find the lengths of sleep and wake, which we use to plot the length of wake $\alpha\prime$ against the length of subsequent sleep $\rho\prime$ proportional to the length of the average sleep-wake period length $\tau\prime$ of each individual vole. The value $\tau\prime$ is found by taking the length of each sleep-wake period, beginning with wake, across the day of spontaneous sleep and dividing by the number of sleeps across this day. This value varies across all voles as seen in Table 4.7. In Figure 4.13 we plot these values and show that a linear two parameter fit with a similar negative gradient as seen in Figure 4.1 (given by the open circles) is a significantly better fit than a one parameter fit of just a constant. Therefore the voles exhibit similar behaviour under spontaneous conditions as seen in the study [130].

Vole	1	2	3	4	5	6
$\tau\prime$	0.0970	0.1111	0.1011	0.1113	0.1236	0.1222

Table 4.7: Value of $\tau\prime$ given in days for each individual vole based on the 1 day of spontaneous experimental data.

We can simulate all possible wake lengths against corresponding length of sleep using the two process model by starting the model on all possible positions on the lower threshold. Figure 4.14 shows the possible values given for the parameters of vole 1 alongside the values found in the data. Note that the model predicts values which sit amongst the values seen in the data and we also observe a declining trend as seen in [130].

In the next section we will extend this work by looking at how the two process model predicts sleep deprivation and we discuss whether the model we are using is sufficient when trying to understand this aspect of the common voles' sleep-wake cycles.

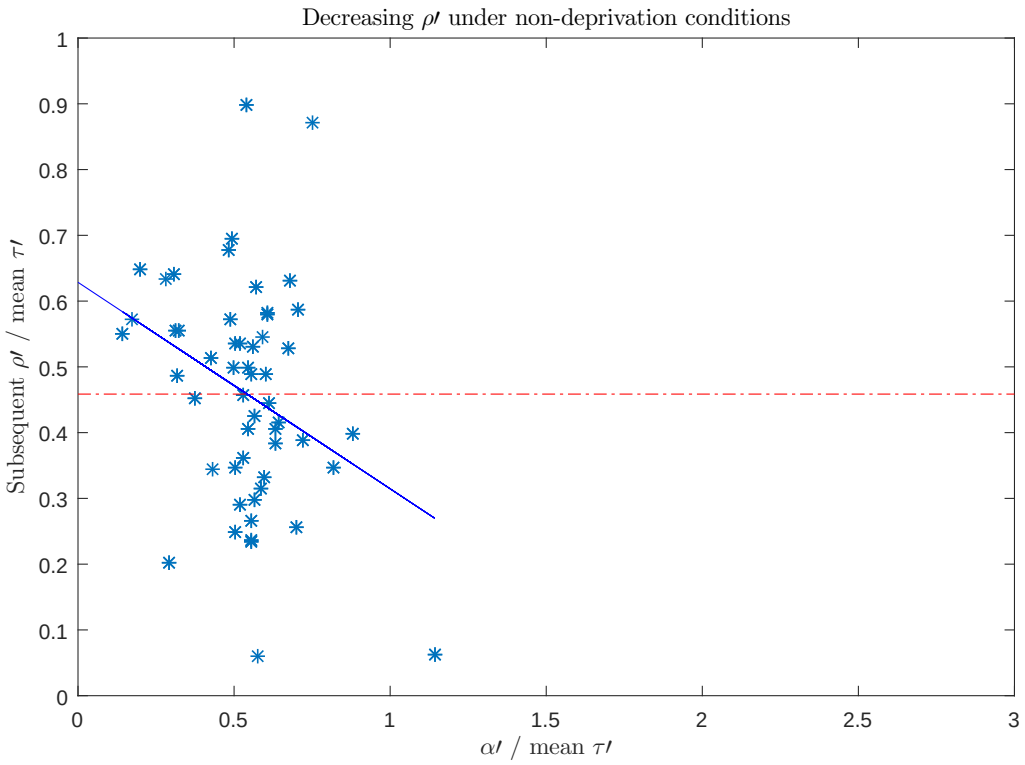

Figure 4.13: For all voles the relative length of wake from the vole data, denoted by $\frac{\alpha\prime}{\tau\prime}$, plotted against the relative length of the subsequent sleep, given by $\frac{\rho\prime}{\tau\prime}$, where $\tau\prime$ is the average sleep-wake length for an individual vole, plotted in blue. The dashed red line shows a one parameter fit which can be compared to the solid blue line, a two parameter fit. We find that the decreasing fit gives a better fit with a p value of 0.0007.

4.4 Modelling sleep deprivation

In this section we use the two process model with parameters as derived in the previous section to predict effects of sleep deprivation on the common vole. We consider how the two process model predicts recovery sleep after the deprivation period and compare this to the values from the data. We will then discuss whether the standard two process model gives a good prediction for the length of sleep after sleep deprivation in the common vole.

Sleep deprivation is the condition of having prolonged wake which delays the natural sleep onset time. Sleep deprivation is often used in laboratory studies of human and animal sleep. Study in this area has proliferated since there is now strong evidence that links poor or mistimed sleep in mammals to many health conditions such as obesity, diabetes, heart disease as well as increased mortality.

The protocol in this experiment was to sleep deprive each vole for 6 hours, after a day of spontaneous sleep data recording, using gentle handling when a vole seems to be falling

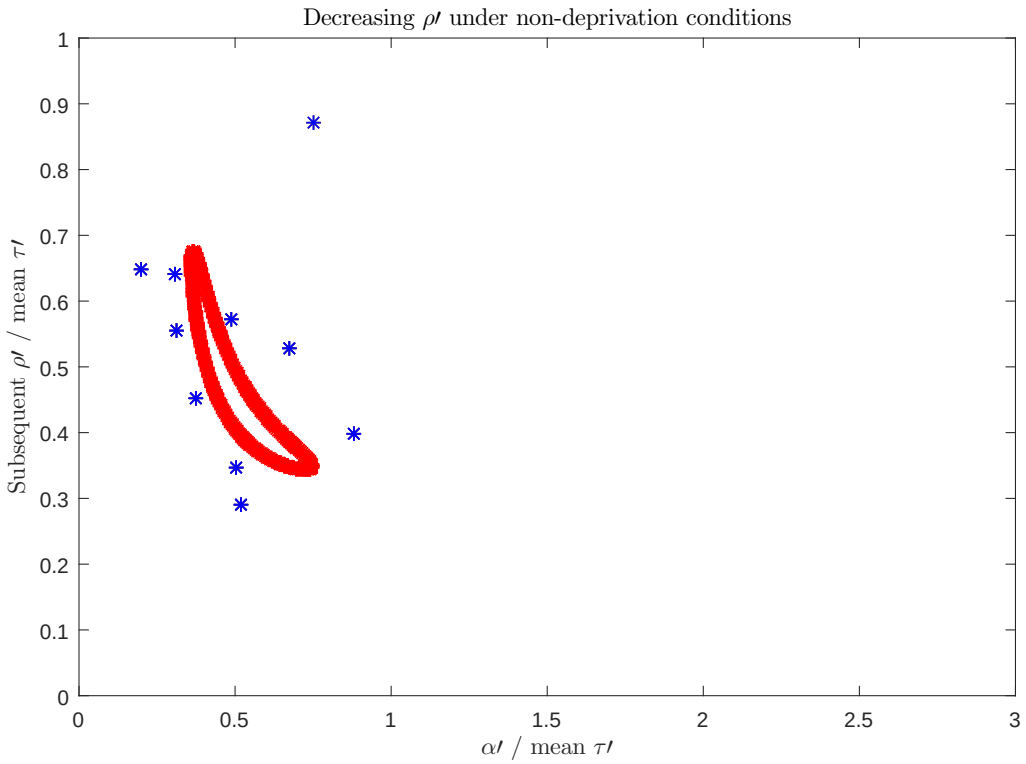

Figure 4.14: The red points represent the two process predictions for the relative wake length against subsequent relative sleep length for one set of parameters. We find these points by running the two process model for vole 1 *from all possible wake onset times for one sleep-wake pair and plotting the corresponding lengths. The blue points are those from the data for vole* 1*, as in Figure 4.13.*

asleep [129]. For each vole, sleep deprivation begins at light onset and after six hours the voles are given the opportunity to sleep freely. Observation continues for another 42 hours as the voles recover from the sleep deprivation and settle back into a spontaneous sleep routine.

We now simulate sleep deprivation using the two process model and discuss whether it is a satisfactory model for predicting sleep-wake onset times and other sleep phenomena associated with sleep deprivation.

4.4.1 Two process model predictions of sleep deprivation

A standard way to simulate sleep deprivation in the two process model is to allow the upper threshold to be passed through during the deprivation period, this mimics the ability to remain awake, overriding the impulse to sleep. We run the two process model, starting on wake at the first wake onset time given by the data, for the first day of spontaneous sleep. This is followed by 6 hours of sleep deprivation, at the time representing light onset, where the homeostatic sleep pressure is allowed to pass through the upper threshold. At the end of the 6 hours of

sleep deprivation the model falls asleep immediately (since the homeostat is above the threshold value) and we record the recovery sleep timings. In Figure 4.15 we display the behaviour of each vole using the individual parameter estimations in the two process model of Section 4.3.

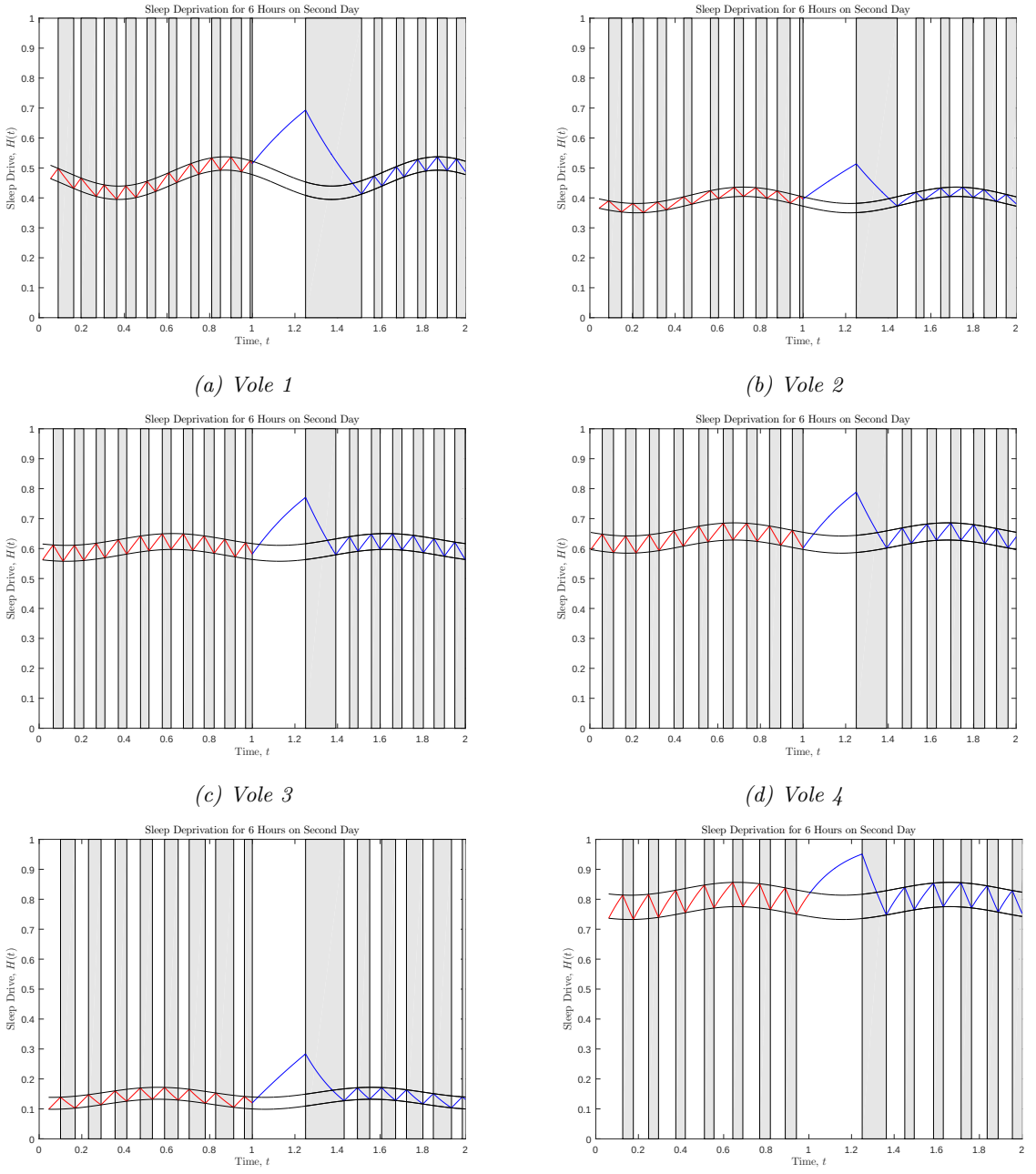

(a) Vole 1 *(b) Vole 2*

(c) Vole 3 *(d) Vole 4*

(e) Vole 5 *(f) Vole 6*

Figure 4.15: We run the two-process model for all six voles using the 6 parameter estimates from the initial wake time given by the data. After the initial 24 hours (red) the voles are then sleep deprived for 6 hours and then allowed to recover and sleep as normal (blue).

Vole	1	2	3	4	5	6
Sleep Deprivation	1.5147	1.442	1.3981	1.3980	1.4321	1.3644
No Dep 1	1.266	1.258	1.309	1.325	1.290	1.293
No Dep 2	1.362	1.366	1.412	1.438	1.411	1.418
No Dep 3	1.453	1.486	1.516	1.555	1.531	1.552
No Dep 4	1.544	1.612	1.620	1.671	1.652	1.688
No Dep 5	1.643	1.728	1.722	1.785	1.779	1.817

Table 4.8: Predicted wake onset times in the two process model after sleep deprivation (shaded) and the first 5 *wake onset times that would be seen if no deprivation had occurred.*

By allowing the model to run without deprivation we can compare wake onset times between spontaneous sleep and after the 6 hour deprivation period, as in Table 4.8. We see that for all of the voles the expected time of wake onset after deprivation occurs multiple sleep-wake periods later than the wake onset times predicted for the no deprivation case, which occur after the period of deprivation. The two process model predicts that there will be one long recovery sleep after deprivation which is much longer than a normal sleep-wake period length. However, it is shown in Figure 4.1 that this is not necessarily the case. Gerkema [130] suggests that the relationship between sleep and wake, during spontaneous and sleep deprivation conditions, in the common vole is governed by the vole's average sleep-wake period length, $\tau\prime$. Thus, after any amount of wake the subsequent sleep will only last for the remaining portion of the current $\tau\prime$ period.

To further understand how sleep duration changes when one lengthens wake in the two process model we repeatedly run a single sleep-wake cycle and extend the length of wake and observe the subsequent sleep length. Figure 4.16(a) shows these sleep-wake cycles for a fixed wake onset time and a variety of wake lengths. By allowing deprivation to begin in this way from the prediction of spontaneous sleep length after wake given in Figure 4.14, we see that there is a region of possible subsequent sleep lengths after deprivation predicted by the model, as displayed in Figure 4.16(c).

Note that all of the voles have a set of parameters with small amplitude and a small gap between the upper and lower thresholds, this in turn leads to the homeostatic sleep pressure passing through and remaining above the upper threshold quite quickly, during sleep deprivation.

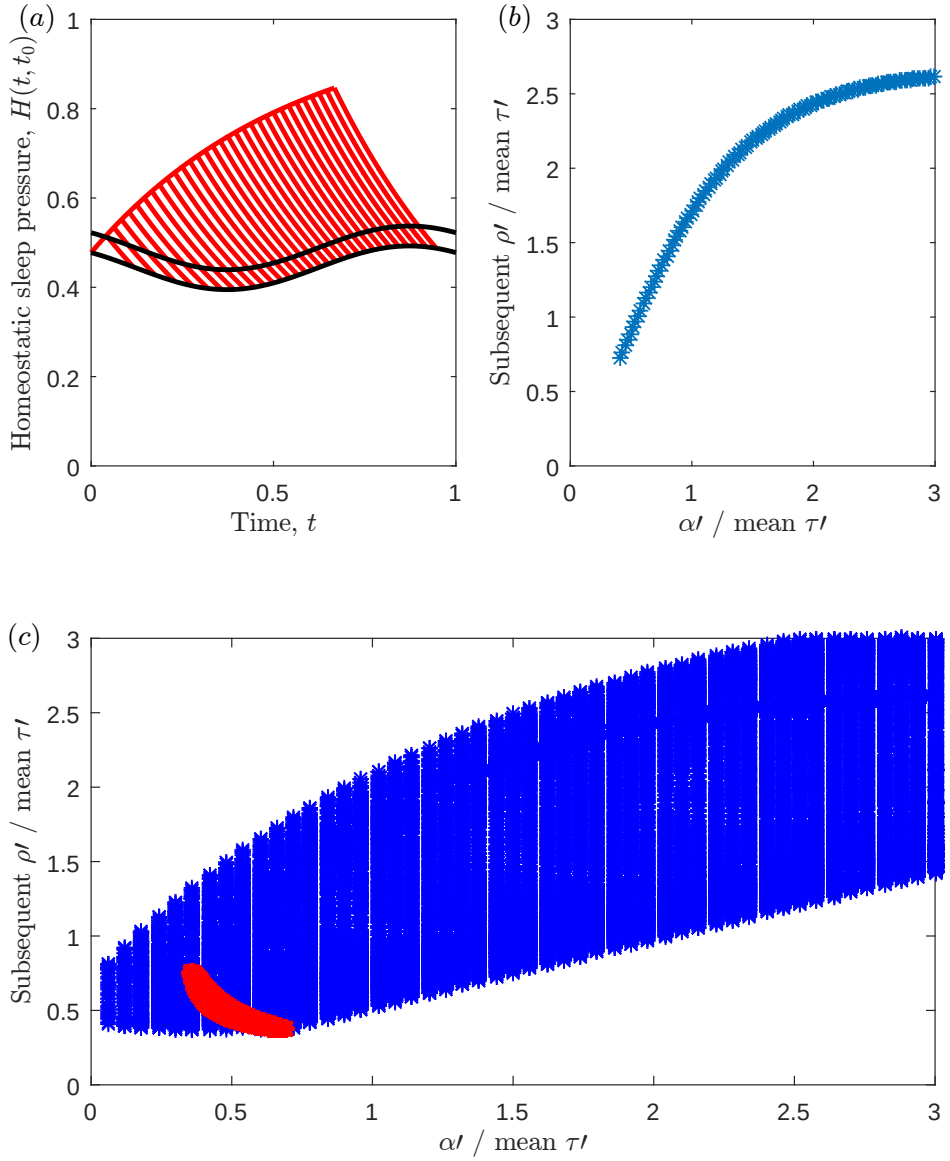

Figure 4.16: (a) Using the parameter values of Vole 1 we run the homeostat (red) of the two process model multiple times, extending the length of wake on each iteration to simulate the effect of sleep deprivation in the model. Each sleep-wake episode begins at time $t = 0$ on a wake trajectory (b) We plot the length of wake against the length of corresponding sleep, proportional to the $\tau\prime$ period. Note that the two process model predicts an increase in the length of subsequent sleep as the length of wake increases. (c) The blue region here represents the area that the two process model predictions would cover by fixing $a, H_0^-, \phi, \chi_s, \chi_w$ and varying the length of sleep deprivation from all values of the homeostatic sleep pressure on the spontaneous sleep-wake cycle. The red curve shows the points given in non-deprivation conditions in Figure 4.14.

As the length of wake increases we see that there is a sharp rise in recovery sleep length, shown in Figure 4.16(b). Therefore the two process model alone does not give the prediction of decreasing subsequent sleep with a sharp increase at τ-multiple periods.

The results seen here do not correspond to those in [130] and by looking at the sleep deprivation sleep-wake onset times from the data we find that various phenomena were not predicted by the two process model in its current form. We see in this experiment that the voles do not have a long recovery sleep as predicted by the two process model and also the voles do not fall asleep instantly as we have assumed.

In the next section we explore an extension of the two process model which reproduces the behaviour given in Figure 4.1 [130] and discuss how this extension is consistent with the parameter fitting carried out in Section 4.2.2 for the standard two process model.

4.5 The hidden rhythm

We begin by considering what kind of adaptation to the two process model would yield results similar to Figure 4.1. The experimental data in [130] explores the length of wake and subsequent sleep proportional to the the average sleep-wake period length, τ, of each individual vole. It is shown that as the length of sleep deprivation is increased there is a decrease in subsequent sleep from roughly τ to 0 until the length sleep deprivation approaches roughly a multiple of τ and the length of subsequent sleep approaches 0. At the point where the length of sleep deprivation extends into the next τ-period there is a jump in the length of subsequent sleep, back to τ. In essence the length of subsequent sleep 'completes' the next τ-period such that the sleep-wake period is a multiple of τ.

In Figure 4.17 we overlay spontaneous and sleep deprivation data from the voles onto Figure 4.1. From observation it is clear that all six voles lie are in line with the data seen in [130]. If the prediction made by the two process model was correct we would expect the points denoting sleep deprivation to sit much higher on the vertical-axis, a subsequent sleep of around 3-4 $\tau\prime$ periods in length.

The fact that the length of subsequent sleep decreases across each $\tau\prime$ period and makes a sudden jump at the end of each period suggests that the two process model has to be modified such that the homeostatic process passes through the lower threshold multiple times during long periods of deprivation. As the homeostatic sleep process on wake approaches the lower threshold from above, the length of subsequent sleep decreases however, once the homeostatic sleep process passes through the lower threshold there will be a discontinuity in subsequent sleep length.

To achieve this we add an ultradian oscillation on top of the circadian threshold. The period of this oscillation is given by $\tau\prime$ as we expect the ultradian rhythm to regulate sleep timings and

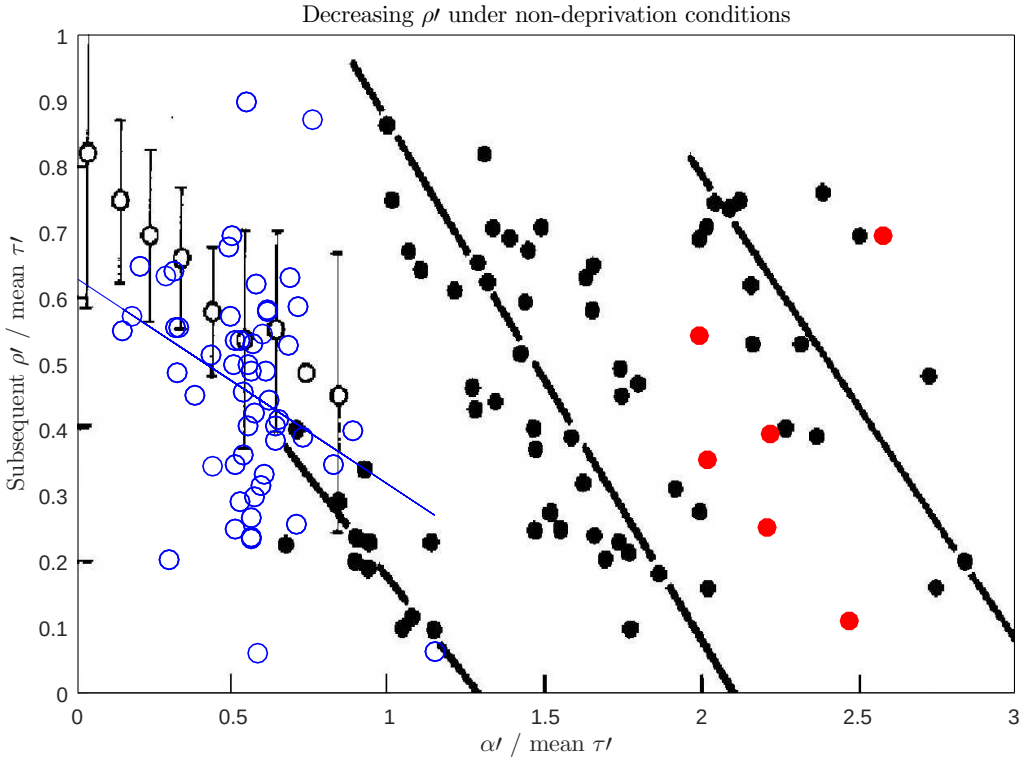

Figure 4.17: We overlay the data from the experiment in [129] over Figure 4.1. The open blue circles represent the spontaneous sleep-wake lengths and the six filled red circles show the manipulated (sleep deprivation) values for all six voles. Note that if the two process model prediction were correct then the red circles would have a y-value greater than 1.

a jump from short to long subsequent sleep to occur after each wake length which is a multiple of $\tau\prime$. Since the period of such an oscillation is less than one day it is called an ultradian oscillator. We now denote the upper and lower thresholds by

$$H^+(t) = H_0^+ + a\sin(2\pi(t-\phi)) + a^u \sin\left(\frac{1}{\tau\prime}2\pi t\right)$$

and

$$H^-(t) = H_0^- + a\sin(2\pi(t-\phi)) + a^u \sin\left(\frac{1}{\tau\prime}2\pi t\right)$$

respectively, where a^u is the amplitude of the ultradian oscillator. In Figure 4.18 we observe a 6 hour deprivation period for one of the voles with the thresholds being an ultradian oscillation, the size of the ultradian amplitude is set to be large enough such that there are multiple crossing points between the homeostat and the upper threshold. We see that having an additional oscillation can explain the phenomenon of prolonged wake after long periods of deprivation. This is caused by the homeostatic process being below the upper threshold at the end of the

deprivation period and therefore the homeostat continues on a wake trajectory until it hits the upper threshold and switches to a sleep trajectory.

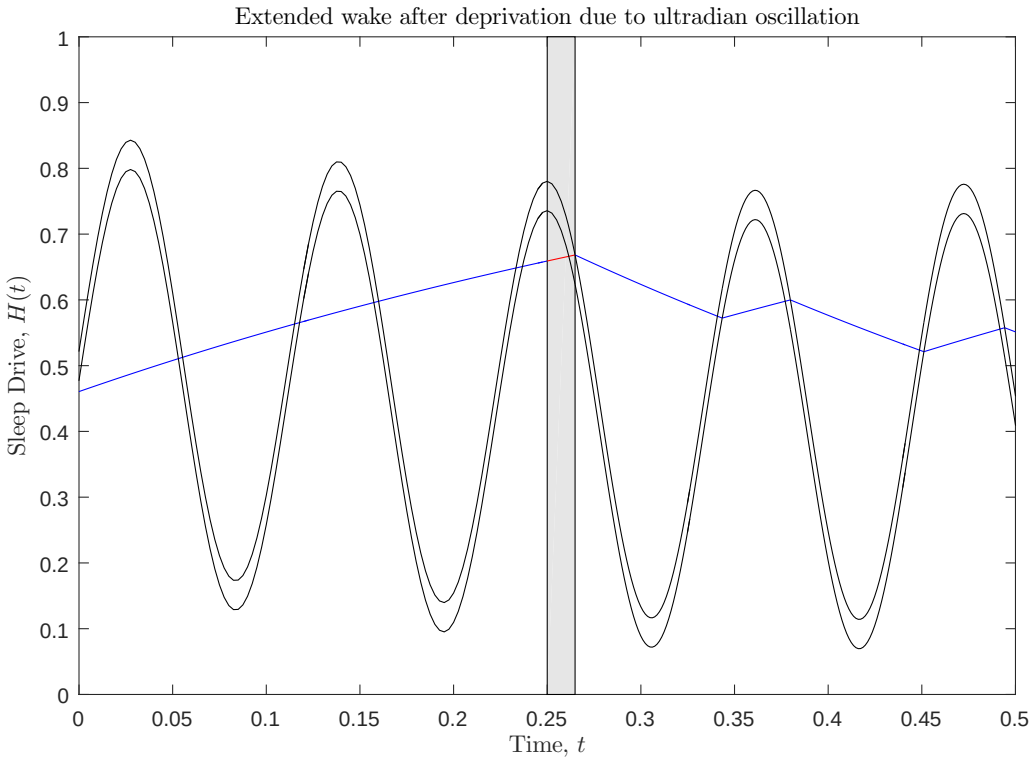

Figure 4.18: We introduce a large amplitude ultradian oscillation to the two process model. Here we deprive a subject for 6 *hours and see that after deprivation the subject remains awake (shaded region) since the homeostat is below the upper threshold.*

We now wish to explore sleep deprivation predictions made by the modified two process model, with parameters $\chi_s, \chi_w, H_0^-, H_0^+, \phi, a$ and a^u. Using the same method as before we repeatedly run a single sleep-wake cycle and extend the length of wake and observe the subsequent sleep length. Figure 4.19 shows sleep-wake cycles for a fixed wake onset time and a variety of wake lengths. We see that the homeostat passes through the upper and lower thresholds multiple times during the deprivation period and can see that this affects the length of subsequent wake. As the homeostat approaches the lower threshold whilst on a wake trajectory (during sleep deprivation) the length of subsequent sleep decreases towards 0. However, once the homeostatic sleep pressure has passed through the upper threshold from above it must stay on a wake trajectory until it is again above the upper threshold. This causes a period of wake lengths which are not attainable since a vole will remain awake when the homeostatic sleep pressure is below the upper threshold. As well as this the length of subsequent sleep jumps up, this is due to the homeostatic process on sleep becoming further from hitting the lower threshold from

above at the end of the extended wake period.

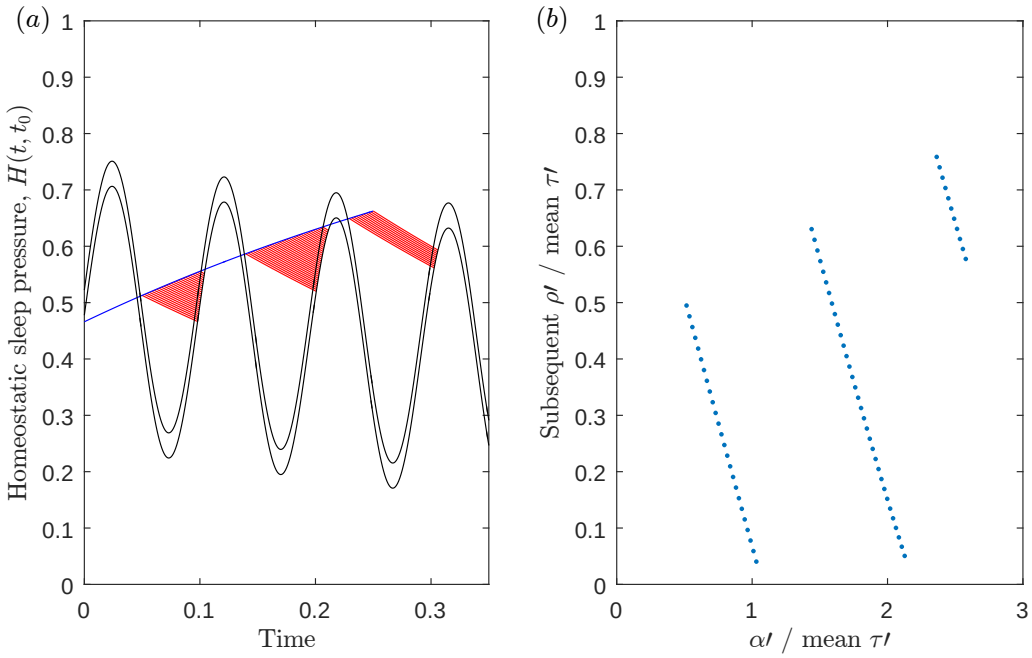

Figure 4.19: (a) The two process model for Vole 1 with a large ultradian amplitude in addition to the original parameters. The ultradian oscillation has period $\tau = 0.0970$ given by the average sleep-wake period length in Vole 1's spontaneous data. Note that there is a large increase in sleep length when the homeostatic sleep pressure on wake (increasing blue line) passes through the lower threshold. (b) Wake length plotted against the following sleep length where both are proportional to the spontaneous τ period length. Here we see similar behaviour as in Figure 4.1 where the amount of recovery sleep depends on the proportion of the current sleep-wake period occupied by wake.

We want to check how well the prediction of the modified two process model on the relation between $\frac{\alpha'}{\tau'}$ and $\frac{\rho'}{\tau'}$ correlates with the results of the experiments in [130]. Since the value of $\tau\prime$ for each vole is often not a divisor of a 1 day period we expect the ultradian rhythm to shift over multiple days. If this is the case then a vole could be deprived at any point during its shifting ultradian phase. To simulate this we perform the method used in Figure 4.19(a) across multiple days. In figure 4.20 we show that the shift in ultradian phase across multiple days leads the regions between subsequent sleep lengths in Figure 4.19(b) to fill up.

Although Figure 4.19(b) displays the behaviour seen in [130] it is important to consider that the onset of sleep deprivation could have occurred at any ultradian phase for the voles. Since $\tau\prime$ is not taken as a divisor of 1 day the ultradian rhythm is shifting across multiple days. Figure 4.20 shows that if this is the case we do not get the distinct decreasing bands of subsequent sleep after deprivation with jumps, as in [130].

From experiments it is observed that when entrained to a light dark cycle the common vole shows very good sleep timing regulation, it appears that there is a circadian signal timed

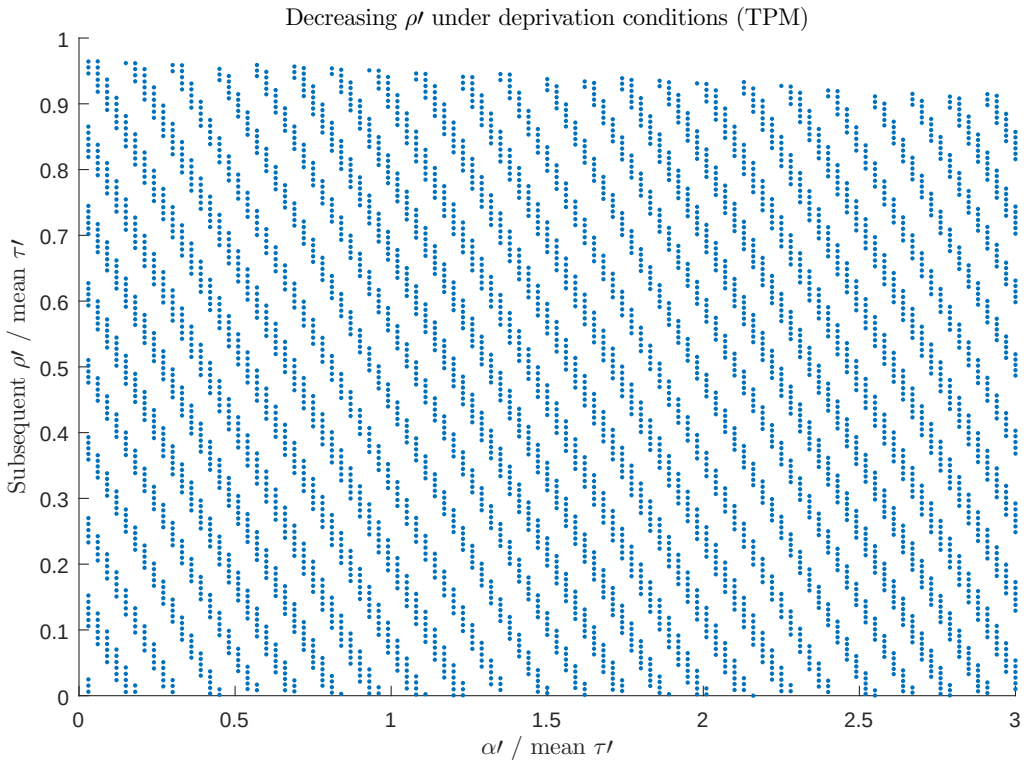

Figure 4.20: Length of subsequent sleep after sleep deprivation relative to τ' period for vole 1 simulated over multiple days using the method in Figure 4.19. Since the values found for τ' are not divisors of 1 day the ultradian oscillations do not occur at the same time each day for the voles. Therefore the ultradian 'shifts' slightly each day and the whole region begins to fill, no longer giving the same behaviour as in Figure 4.1.

around light onset that achieves this entrainment [135]. This characteristic means that once a vole is entrained, as in this experiment, it exhibits similar sleep-wake onset times each day [129]. Unfortunately, due to the lack of spontaneous data this periodicity in sleep-wake timing is not evident in the data. However, it motivates us to make the assumption that each vole has an integer number of sleeps per day, so that the average sleep-wake period length is a divisor of one day therefore

$$\tau\prime = \frac{1}{\text{No. of sleep-wake episodes}}.$$

Making this change yields the reviewed $\tau\prime$ values given in Table 4.9. By using these values in the new model we know that taking the same wake onset time on any day yields the same result. This is due to the circadian and ultradian components being entrained to a one day rhythm.

In Figure 4.21 we display subsequent sleep length after deprivation for all six voles using the reviewed τ' values given in Table 4.9. Using the same method as in Figure 4.20 we consider deprivation onset times at all possible points along the spontaneous sleep-wake cycle. We also

Vole	1	2	3	4	5	6
Original $\tau\prime$	0.0970	0.1111	0.1011	0.1113	0.1236	0.1222
Reviewed $\tau\prime$	$\frac{1}{10}$	$\frac{1}{9}$	$\frac{1}{10}$	$\frac{1}{9}$	$\frac{1}{8}$	$\frac{1}{8}$

Table 4.9: Both the original (from table 4.7) and the reviewed $\tau\prime$ values given for each individual vole. The reviewed values are calculated using the number of sleep-wake episodes seen in the spontaneous data, given in Table 4.4.

consider values between $\tau' \pm 10\%$ for each vole, this is to simulate any daily variations that may occur in ultradian phase, we will discuss this in more detail later. We see that the model with revised $\tau\prime$ values displays a piecewise decreasing relation between $\frac{\alpha'}{\tau'}$ and $\frac{\rho'}{\tau'}$ and jumps at the integer points, as seen in [130]. The model exhibits decreasing bands of subsequent sleep as the length of wake increases, when the length of wake exceeds each $\tau\prime$ period there is a jump up to a long subsequent sleep of roughly one $\tau\prime$ period in length. Therefore we see that two similar lengths of sleep deprivation could yield almost no recovery sleep in the first sleep after deprivation or a large recovery sleep when sleep deprivation ends, as the homeostatic sleep pressure is close to the upper threshold.

We have shown that by adapting the two process model such that the upper and lower threshold contain an additional, ultradian, oscillator both the spontaneous and sleep deprivation data of experiments [129] and [130] can be explained. However, many of the assumptions that we have made could potentially change the results displayed here. One main assumptions used in this Chapter is that the length of a period of wakefulness needs to be a minimum of 20 minutes to be classified as a wake episode. By changing this assumption we could vary the number of defined sleep-wake episodes each vole has per day.

To derive the parameters χ_s and χ_w, which determine the strength of the growth and decay of the homeostatic sleep pressure, from the sleep EEG we considered the decay of delta power during NREM sleep and the growth of theta power during wake respectively. We use a method which is similar in approach to [134] however, it is important to note that other possible methods could have been used to derive these parameters [136]. A change in the method used could lead to differences in the values found for χ_s and χ_w and potentially the results of this chapter. Therefore, in the next section we consider how different values for the parameters would affect the model behaviour during both spontaneous and sleep deprivation conditions.

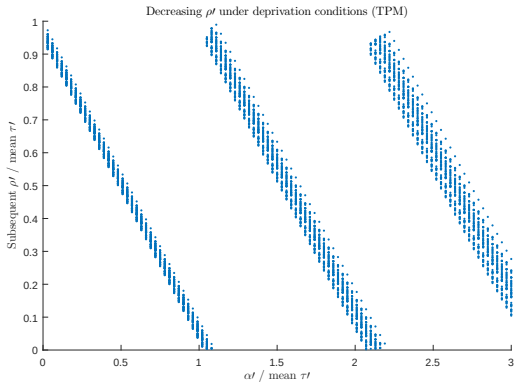

(a) Vole 1

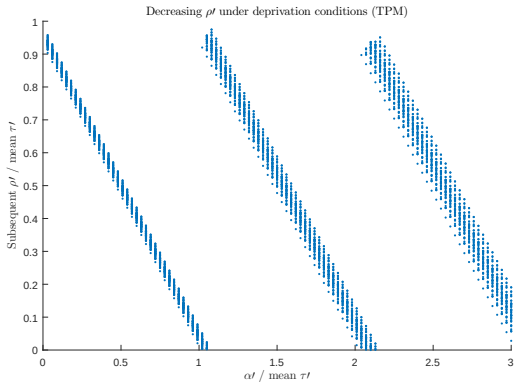

(b) Vole 2

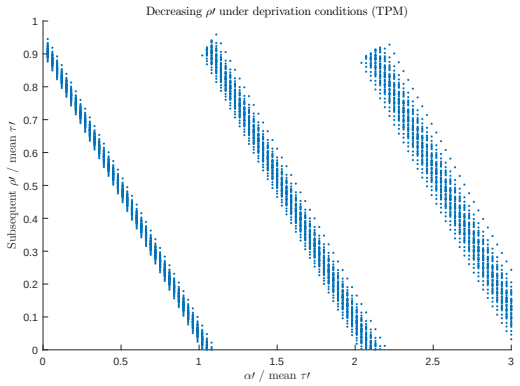

(c) Vole 3

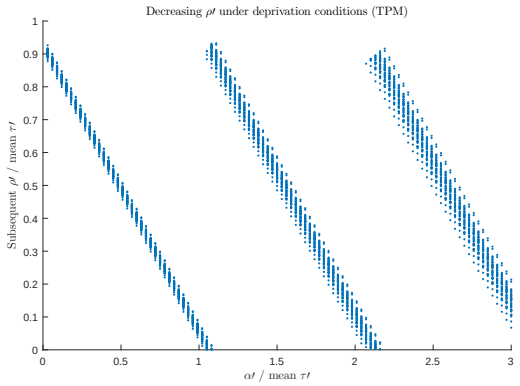

(d) Vole 4

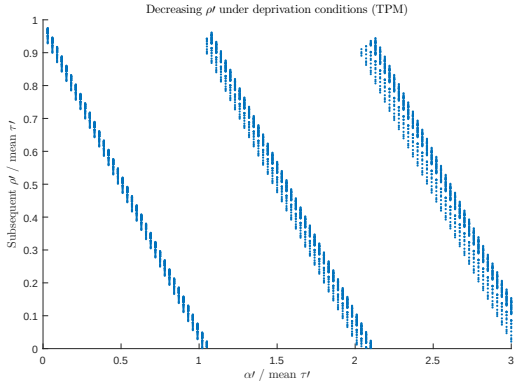

(e) Vole 5

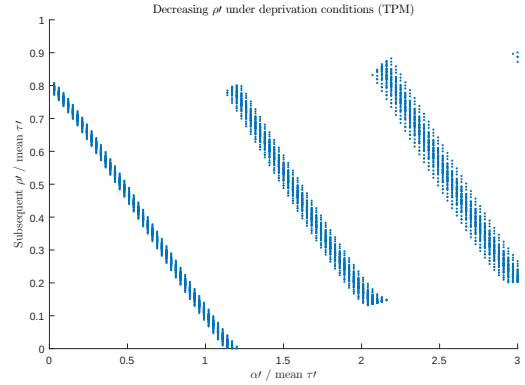

(f) Vole 6

Figure 4.21: Plots for each vole showing the how the modified two process model predicts length of subsequent sleep after deprivation. We see a decreasing $\rho\prime$ which jumps up to a sleep length of $\tau\prime$ after the vole has been awake for any multiple of $\tau\prime$ periods.

4.6 Parameter sensitivity

We will now investigate the sensitivity of the conclusions to the assumptions made while carrying out the analysis. We consider the effects of selecting different minimum wake lengths and varying

$\chi_{s,w}$ values on the results in this Chapter.

4.6.1 Minimum wake length

In Section 4.1.2 we observed that the longer periods of wake were uninterrupted however, there is a high frequency of brief awakenings during sleep. We decide that such brief awakenings can be ignored as they are just small interruptions in, otherwise consolidated, sleep. Therefore we made an assumption about the length of time that a vole must be awake for it to be considered a wake period. We chose to take a minimum wake length of 20 minutes since this removed the high frequency of brief awakenings. We were then able to find sleep-wake onset times from the data since anything that is not a wake period is consider sleep.

We will now explore how selecting different minimum wake lengths changes the main results seen during sleep deprivation.

Results given a 40 *minute minimum wake length*

Here we increase the minimum wake length to 40 minutes in vole 1. In doing this we reduce the number of sleep-wake episodes from 10 to 9 and after fitting we find a different set of parameters. A comparison between found parameters is shown in Table 4.10.

	χ_s	χ_w	a	H_0^+	H_0^-	ϕ	No. of Sleeps	$\tau\prime$
20 minutes	0.5067	0.5448	0.0489	0.4886	0.4437	0.6223	10	$\frac{1}{10}$
40 minutes	0.5448	0.1406	0.0793	0.8014	0.7274	0.5570	9	$\frac{1}{9}$

Table 4.10: Found parameter and $\tau\prime$ values given minimum wake lengths of 20 *and* 40 *minutes.*

Notice that there are large changes in many of the parameters when a different number of sleep-wake periods is found. In particular we see that the value of χ_w (found by observing the growth of EEG power in theta activity during wakefulness) changes drastically, becoming less than a third of the size whereas the value of χ_s is relatively unchanged, this means that the strength of growth has increased proportional to decay. In turn this drives the homeostatic sleep pressure towards the upper asymptote during fitting, as seen in Figure 4.22.

Since the homeostatic sleep pressure is forced to converge closer to the upper asymptote the values of H_0^- and H_0^+ are both increased. In Figure 4.23 we plot the two process model after fitting the upper and lower threshold parameters to the homeostatic sleep pressure values at the sleep/wake onset times. Note that there is an obvious increase in the mean upper and lower

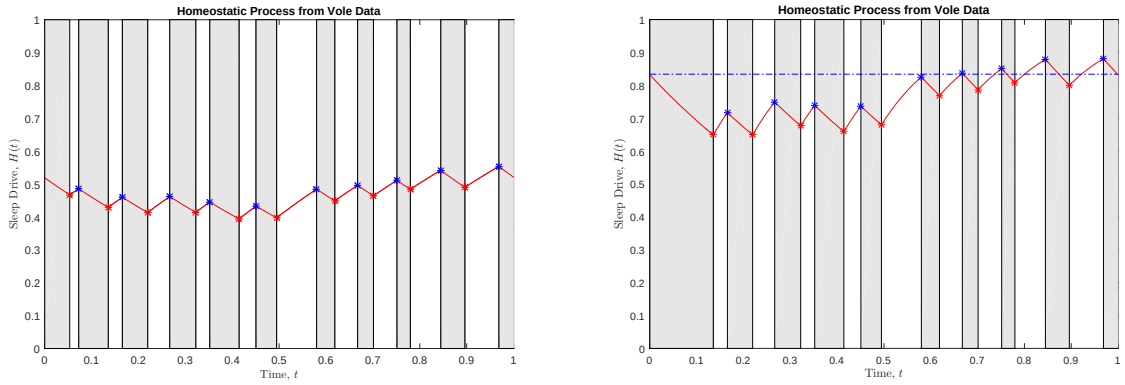

(a) *(b)*

Figure 4.22: Allowing the two process model to converge to a one-day periodic solution using sleep/wake onset times from the data and the χ_s, χ_w found from the EEG recordings. (a) A wake period is assumed to be more than 20 minutes in length giving 10 sleep periods. (b) Assuming that a wake period is at least 40 minutes in length we see the number of sleeps decreases to 9, this in turn changes the derived values of χ_s and χ_w and gives a homeostatic sleep process which converges much higher.

threshold values and also the amplitude, a. Whilst, in this case, most parameters exhibit large changes when the minimum wake length is increased, we still see a conservation of the main properties of the proportion of sleep across light and dark in the simulations of spontaneous sleep-wake patterns. Both simulations predict that more sleep will occur during the light period, this is due to the relatively small change in the circadian phase, ϕ. In both simulations we observe that the peak of the thresholds sits during the dark period which means that the upper threshold increases alongside the wake homeostat during the dark period, increasing the length of the wake period.

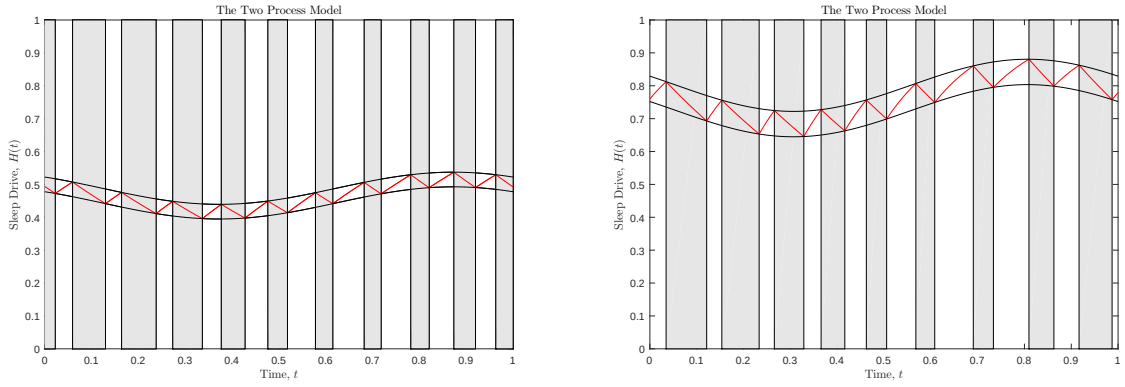

(a) *(b)*

Figure 4.23: We see an increase in the amplitude and threshold mean values, a, H_0^- and H_0^+, when fitting the thresholds ot the data assuming (a) a minimum wake length of 20 minutes and (b) a minimum wake length of 40 minutes.

We now consider whether increasing the minimum wake length, and therefore reducing the number of sleep-wake episodes, has any effect on the final results with respect to the decay of subsequent sleep after sleep deprivation until the end of a τ' period. By adding a large ultradian rhythm, as before, we aim to reproduce the decreasing trend of subsequent sleep after sleep deprivation with jumps between 0 and $\tau\prime$ at each wake length $\tau\prime$. Note that since we enforce $\tau\prime$ to be a divisor of 1 day the original value $\tau\prime = \frac{1}{10}$ (ten sleep-wake episodes) increases to $\tau\prime = \frac{1}{9}$ (nine sleep-wake episodes). In Figure 4.24 the results for both 20 and 40 minute minimum wake lengths are displayed, we see that despite the reduced number of sleep-wake periods and large changes in many of the estimated parameters the modified two process model predicts that the length of subsequent sleep after deprivation will complete the current τ' period.

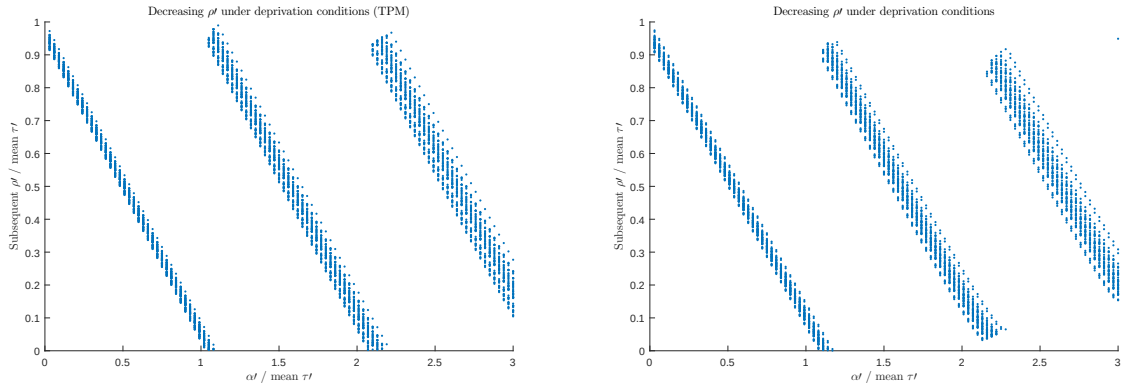

(a) *(b)*

Figure 4.24: Predicted lengths of subsequent sleep after deprivation. Both (a) and (b) display similar dynamics where subsequent sleep, ρ', decreases towards 0 until the wake length α' reaches the end of a τ' period. The length of subsequent sleep then jumps up to a length τ' and begins decreasing towards 0 again (with roughly gradient -1).

We will now briefly explore the effects of variation in the choice of parameters for the homeostatic growth and decay parameters χ_s, χ_w.

4.6.2 Varying the sleep strength parameter, χ_s

We wish to see how changes in the estimated values of χ_s and χ_w affect the predictions from the modified two process model. Do the values of χ_s, χ_w really have any major influence on the final result? To test this we take two different values for χ_s for vole 1. We take $\chi_s^* = \frac{1}{3}\chi_s, 3\chi_s$, fit the remaining parameters and then run simulations with the modified two process model using a large ultradian amplitude.

In the first case with $\chi_s^* = \frac{1}{3}\chi_s$ we see that the strength of the sleep homeostatic decay is increased and therefore the homeostatic process converges closer to the lower asymptote, as shown in Figure 4.25a. However, we see again that the length of subsequent sleep decays until

the length of sleep-wake reaches the end of a τ' period and then jumps back up to a length of roughly τ', this is plotted in Figure 4.25b.

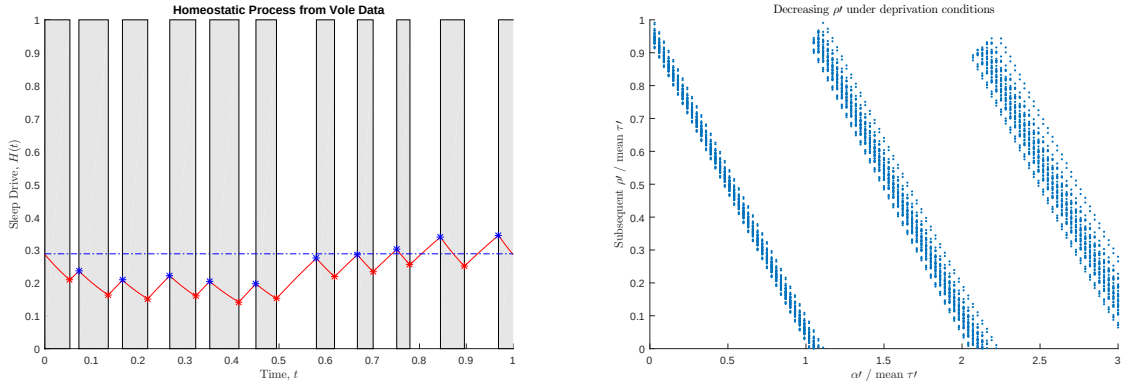

(a) *(b)*

Figure 4.25: Taking $\chi_s^* = \frac{1}{3}\chi_s$ we again allow the two process model to converge using sleep/ wake onset times (therefore maintaining the number of sleeps) in (a). The homeostatic sleep pressure now converges much lower however the length of subsequent sleep after deprivation still exhibits the same 'decrease then jump' phenomena in (b).

We see in Figure 4.26b that the model exhibits similar behaviour when $\chi_s^* = 3\chi_s$. In this case the strength of the homeostatic sleep pressure on sleep has decreased meaning that the homeostatic sleep pressure on wake has a higher proportional power, this pushes the homeostatic sleep pressure towards the upper threshold (as in the example examining different minimum wake lengths).

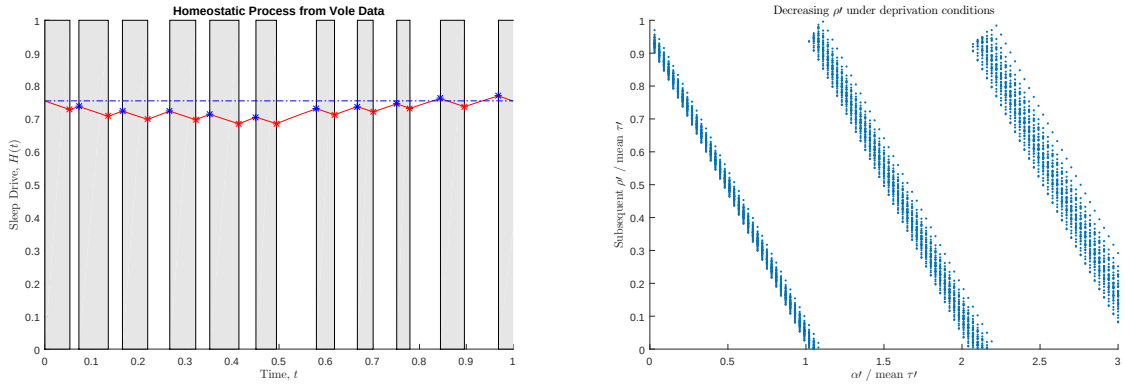

(a) *(b)*

Figure 4.26: Taking $\chi_s^* = 3\chi_s$ we again allow the two process model to converge using sleep/ wake onset times (therefore maintaining the number of sleeps) in (a). The homeostatic sleep pressure now converges higher than before however the length of subsequent sleep after deprivation still exhibits the same 'decrease then jump' phenomena in (b).

After this analysis, we conclude that by significantly varying parameter values in the model

the main result is still observed. Namely, the prediction that $\frac{\rho'}{\tau'}$ decreases with $\frac{\alpha'}{\tau'}$ increasing, until α' is a multiple of τ' and then ρ' jumps up back to τ'. Additional simulations have shown that this is the same when varying any of the parameter values.

In the next section we will explore the bifurcation set relevant for the common vole and discuss the implications on $(p, 1)$ periodic solutions.

4.7 Arnold tongues for the common vole

In Chapter 3 we showed how periodic solutions are created at the boundaries of Arnold tongue saddle-node bifurcations and how border collision bifurcations, which arise when the one-dimensional map of the two process model has gaps, extend and supplement these tongues. In this section we will consider the bifurcation set of the two process model without any modifications, using the parameters of the 'average' vole given in Table 4.5, namely:

$$\chi_s = 0.4709, \chi_w = 0.6521, a = 0.0260, H_0^+ = 0.5303, H_0^- = 0.4791.$$

Note that the circadian amplitude a is very small and the threshold values, H_0^- and H_0^+, are close together. This is a consistent feature of all six voles. We will vary a and H_0^- and focus on the region of the bifurcation set with the relevant number of sleeps $(7 - 10)$ per day and small circadian amplitude.

With the average vole parameters, tangencies between the homeostatic sleep pressure and the upper threshold exist when the amplitude satisfies

$$a \geq \frac{1 - H_0^+}{\chi_w \gamma_w} = 0.114,$$

and for tangencies between the homeostatic sleep pressure and the lower threshold

$$a \geq \frac{H_0^-}{\chi_s \gamma_s} = \frac{H_0^-}{3.1232} \geq 0.145,$$

for the value of H_0^- considered. Since the amplitude, a, is small for all voles tangencies in the two process model are not relevant when considering their sleep-wake dynamics. In other words, we are in a region of the bifurcation set where the map is a lift of a monotonic circle map and only saddle-node bifurcations will be important for our discussion.

The boundaries of the Arnold tongues are loci of saddle-node bifurcations which we compute in the same way as described in Chapter 3, by locating a periodic point at a saddle-node bifurcation and following it along the bifurcation curves by varying one parameter and solving for the other. The Arnold tongues corresponding to the average vole parameters are plotted

in Figure 4.27. Finding suitable start points and continuing along the curves for these tongues proved more difficult than the tongues computed in Figure 3.13 which had lower values of p. Since the tongues are so narrow in this region the parameter values on the two saddle-node boundaries are close together for each tongue and the solution can jump between the two boundaries, making careful continuation necessary.

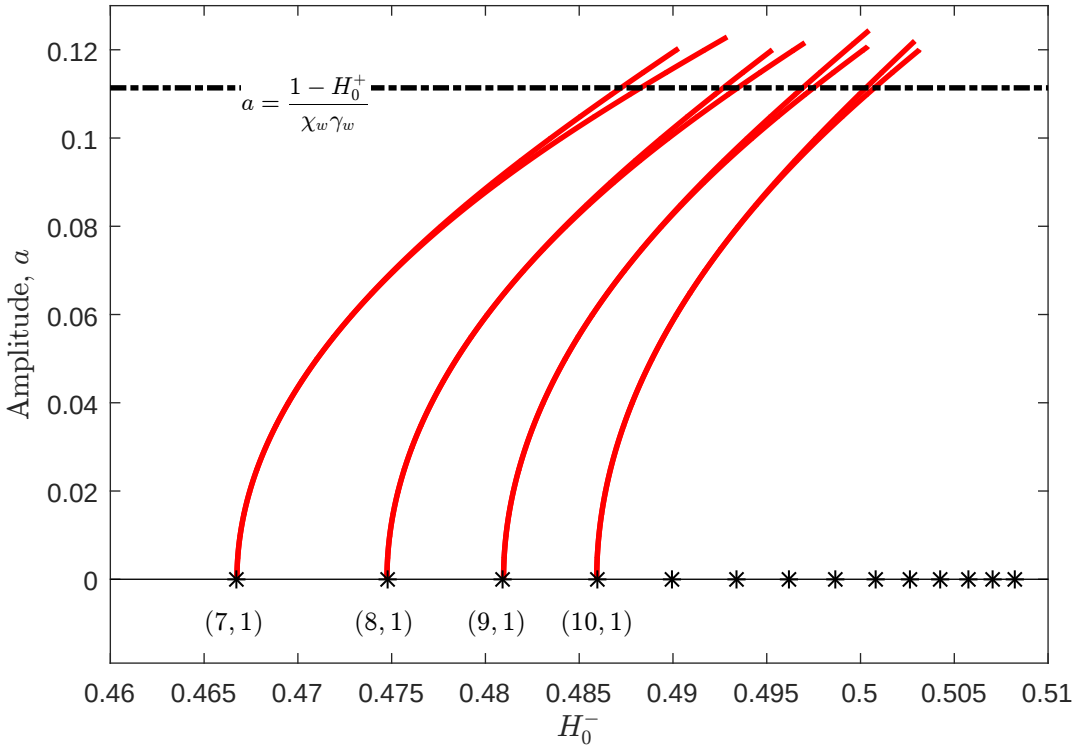

Figure 4.27: Bifurcation set for the average vole parameters ($\chi_s = 0.4709, \chi_w = 0.6521, H_0^+ = 0.5303$). Arnold tongues for periodic regions of 7 to 10 sleeps per day are denoted by the red curves. Above the black dashed line is the region for existence of tangencies. The black stars at $a = 0$ denote the starting points of the 4 tongues given and the next 10 tongues, $(11 - 20, 1)$. It is clear that these points become closer together as they are bounded by the upper threshold.

It is known that the tongues generically open at a finite angle [137] however, this angle decreases as number of sleeps per day p or the number of iterations of the map q increases. The black stars in Figure 4.27 show the H_0^- values corresponding to the the decreasing natural period T_n for periods $(7 - 20, 1)$ at $a = 0$. The H_0^- values are found by solving

$$H_0^- = H_0^+ \exp(\frac{-\tau_0}{\chi_s}),$$

and the value of τ_0 is found using a modified form of (2.40),

$$H^+(t_0) = \alpha(\tau_0) \quad \text{where} \quad \alpha(\tau_0) = \frac{1 - e^{\frac{\tau_0 - \frac{q}{p}}{\chi_w}}}{1 - e^{-\frac{\tau_0}{\chi_s}} e^{\frac{\tau_0 - \frac{q}{p}}{\chi_w}}},$$

which accommodates for multiple sleeps, p, over q days. At $a = 0$ the tongues begin to 'bunch' together for higher period orbits, where we see a decreasing sequence of rotation numbers ($\frac{1}{7}, \frac{1}{8} \ldots, \frac{1}{20}$ are plotted) bounded above by the upper threshold H_0^+. Therefore there is less space for each tongue as the rotation number is decreased and they become increasingly narrow towards the threshold.

Since the tongues are narrow any small perturbation in parameters could lead a vole to be outside of the Arnold tongue saddle-node boundary, and therefore away from the (p, q) periodic orbit. By taking $\tau' = \frac{1}{p}$ we have assumed that each of the voles has a 1 day periodic solution with p sleeps. I.e. the pair (a, H_0^-) lies within it's respective tongue. One justification for this is that (similar to the observations made in other animals with circadian behaviour) in voles, light-dark cycles are a major cue for the synchronization of the SCN [138, 139]. In the experiment considered here all of the voles were entrained to a 12 hour light-dark cycle with fixed light intensity during the light period. We expect that any variation away from the periodic orbit throughout the day will be 'corrected' at light onset. Variations in light intake and light/ dark onset times in the wild could see the voles transitioning between periodic and quasi-periodic sleep-wake cycles.

Light-dark cycles play clearly a role in the regulation of sleep in many animals. For example, it synchronizes the SCN and affects sleep timing in humans that undergo shift work or experience jet lag. In the next chapter we will introduce another modified version of the two process model which includes a dynamic stimulus processor that incorporates light stimuli into the representation of the circadian oscillator. First however, we discuss some of the results in this chapter and their implications.

4.8 Discussion

In this chapter we explored whether the two process model, with the standard circadian rhythm, is sufficient to explain spontaneous sleep and sleep deprivation observations seen in *Microtus Arvailis*, the common vole. We have found that the standard circadian oscillator alone is capable of explaining spontaneous sleep but not the results seen in sleep deprivation. By adding a large ultradian oscillation which occurs at regular intervals across the day, corresponding to the amount of sleep-wake periods seen in spontaneous conditions, we were able to predict that there can be a shorter recovery sleep after a longer period of deprivation or even stay awake when

allowed to sleep. We have also shown that the observed patterns are intrinsic to the model and is not sensitive to parameter fitting which is a testament to the strength of the ultradian rhythm in sleep regulation.

For most mammals it is known that the suprachiasmatic nucleus (SCN) and peripheral oscillators found in many of the body's cells form a circadian timing system which results in daily rhythms. In [139] the expression of circadian clock genes in the SCN and liver of the common vole is examined and it is found that both circadian and ultradian components in feeding and activity rhythms affect the amplitude of circadian liver gene expression. This could explain why the addition of an ultradian oscillator helps to obtain the results seen in sleep deprivation experiments.

It is well known that the two process model can explain both monophasic and polyphasic sleep [79]. After fitting the two process model parameters to sleep/wake onset times and EEG power data we were able to obtain polyphasic sleep-wake patterns which are similar to experimental data. Since we fitted the model to sleep/wake timings it is perhaps unsurprising that the model gives a good estimate for sleep-wake proportions and distribution across the day and correctly predicts average sleep-wake onset times for an entrained vole. However, model predictions for sleep deprivation do not align with observations from the experiments in [130]. By plotting the experimental data from [129] over the data seen in [130] we are convinced that we have consistency between data sets and that some other underlying mechanism is driving both sleep and wake onset after sleep deprivation.

Since ultradian components are observed in activity rhythms and sleep, we considered a modified version of the two process model a threshold that has both circadian and ultradian components. With the assumption of locking to 24 hours and a large ultradian amplitude we are able to reproduce the results seen in [130] through simulation of the model.

One of the main questions that we considered is: Why is an ultradian oscillation not found when fitting the upper and lower threshold in the standard two process model in Section 4.2.2? An obvious restriction is a lack of data points when fitting the thresholds since we only have around 10 data points of sleep/wake onset for each vole. However, even when fitting to this small data set we found that the two process model gave a good prediction for many of the phenomena seen in spontaneous sleep. During fitting we found that the upper and lower thresholds sat close together and that the amplitude, a, was relatively small for all voles.

In Figure 4.28 we see that, the addition of a large amplitude ultradian oscillation to the thresholds, would lead to the same results when fitting to sleep-wake onset times during spontaneous sleep i.e. a small circadian oscillation and a small gap between thresholds. By desynchronizing the circadian and ultradian components through sleep deprivation we were able to see that the ultradian component is the driver for sleep wake onset times and the circadian

oscillation gives the changes in sleep duration across the day. In spontaneous conditions the ultradian rhythm is 'hidden' due to the locking of ultradian and circadian oscillators to a 1 day period.

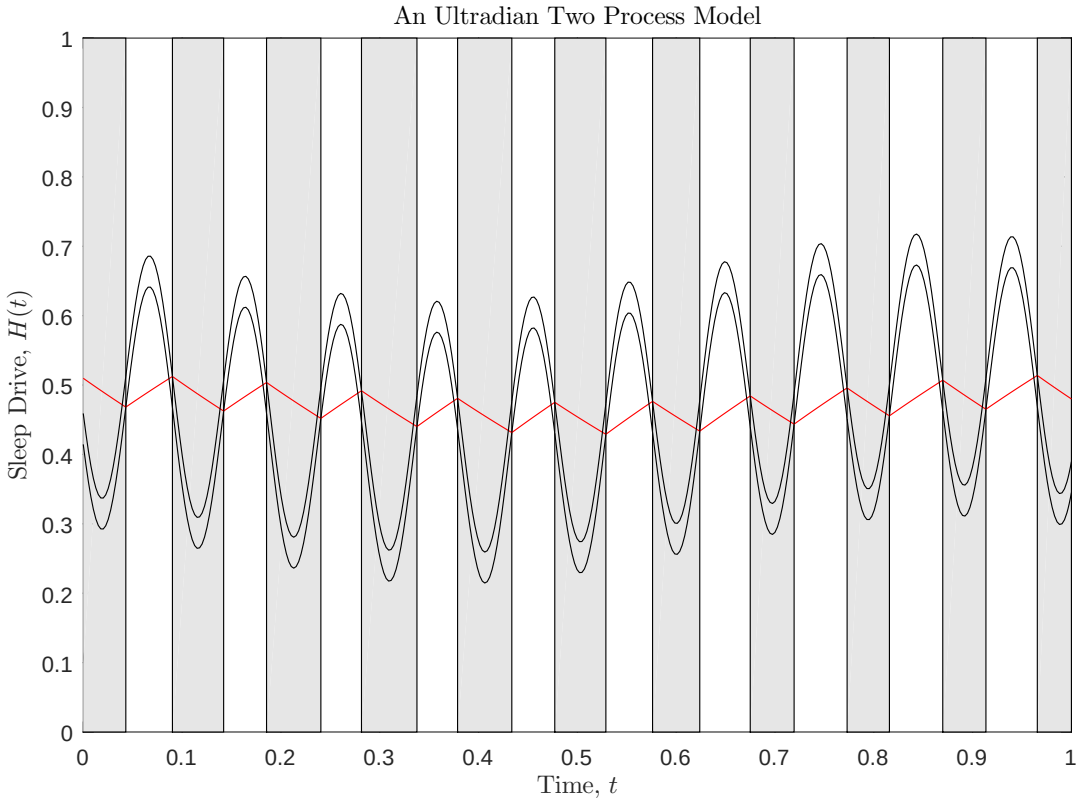

Figure 4.28: A run of the modified two process model explains how an ultradian rhythm may not be obvious when observing spontaneous sleep. The homeostatic process (red) cannot reach the extreme regions formed by the ultradian oscillation since the homeostat does not grow/ decay as quickly. Therefore the homeostat remains at the centre of the ultradian oscillation, this gives only a small variation in homeostat values $H(t)$. The values of $H(t)$ at these sleep-wake onset times govern the fitting of the threshold parameters a, H_0^+ and H_0^-.

This motivates the analysis given in Section 4.7, where the ultradian rhythm is not included. The ultradian rhythm is not considered here since when fitting to the spontaneous sleep-wake cycle, given by the modified two process model, the ultradian rhythm is again hidden. The polyphasic sleep-wake cycles of the common vole appears as one of the $(p, 1)$ periodic solutions in the two process model with $p \in (7, 10)$, allowing us to link results in this chapter to the general bifurcation analysis of Chapter 3.

5

A modified two process model including an external zeitgeber

As we saw in Chapter 4 it is unlikely that the two process model parameters for the common vole would lie and remain inside one of the very narrow tongues. More generally, a weakness of the two process model is that it does not account for individual differences in the intrinsic period of the circadian pacemaker. In humans the intrinsic period is estimated to average 24 hours and 9 minutes ± 12 (SD) minutes and is entrained by external zeitgebers to 24 hours. A zeitgeber (time giver) is an environmental agent or event which acts as a cue in the regulation of an organisms circadian rhythms. An important zeitgeber in mammals is the light-dark cycle, in which light passes through a photoreceptive and phototransductive pathway to influence components of the circadian clock.

In this chapter we first discuss a modified version of the two process model in which the circadian process has a natural period of oscillation but a forcing term derived from the light-dark cycle entrains it to 24 hours. The circadian phase is therefore determined by light input which in turn helps determine sleep timing. We then use this model to explain experimental data on changes in mid-sleep on free days (MSF) and sleep duration across the human lifespan with the aim of showing that the results of [140], which uses a more complex neuronal model to explain the same experimental data, can be replicated using the simpler modified two process model introduced here.

5.1 Background

In [58] it was shown that a modified version of the Phillips-Chen-Robinson (PCR) model [99], which incorporates sleep homeostasis, circadian rhythmicity and also the effects of light, provides a framework to understand the effects of different light profiles on sleep timing. The PCR model is a combination of two earlier models: the Phillips-Robinson (PR) model, describing the switch between sleep/wake states as a result of a drive containing the homeostatic and circadian

components; and the Forger-Jewett-Kronauer (FJK) model [104], describing the entrainment of the circadian rhythmicity by light.

The modified PCR model can show changes in sleep duration and timing across the lifespan for modern industrialized societies and make predictions on what could be observed for pre-industrialized societies. These societies experience vastly different light environments yet the model quantitatively matches the observed data, suggesting that it is a suitable model for simulating the interaction of light with circadian rhythmicity and sleep/wake timing.

More complex neuronal models, in particular the PR model, can be reduced to the two process model [97]. We introduce a modified two process model which incorporates the FJK model as a drive for the circadian process. We then attempt to find parameter values which replicate the changes in MSF and sleep duration across human lifespan, given in [54] and [56] respectively.

5.2 A light inclusive model of the circadian pacemaker

We first introduce the extension of Kronauer's original model [141] of the effect of light on the human circadian pacemaker, the FJK model [104]. In the FJK model the human circadian system is modelled using the classic van der Pol oscillator that generates self-sustaining oscillations. The effect of light on circadian period is included following the method outlined in [105], to model Aschoff's rule, which states that under constant light conditions the period of activity becomes shorter in nocturnal organisms and longer in diurnal organisms. The van der Pol oscillator is driven by a dynamic stimulus model (process L) which represents the biochemical process of converting a light signal into a drive on the circadian pacemaker [106]. A circadian stimulus modulator [142] is also included within the pacemaker, to modulate the effective sensitivity of the van der Pol oscillator to the drive from process L.

Following [106] the cubic van der Pol type oscillator we use is given by

$$\frac{dX}{dt} = \frac{\pi}{12}\left(Y + B\right), \tag{5.1}$$

$$\frac{dY}{dt} = \frac{\pi}{12}\left(\mu_l\left(Y - \frac{4}{3}Y^3\right) - X\left[\left(\frac{24}{0.99669\tau_c}\right)^2 + kB\right]\right), \tag{5.2}$$

where X represents core body temperature and Y is a phenomenological auxiliary variable. Note that τ_c determines the period of the oscillator in constant darkness and μ_l relates to the rate of amplitude growth/ decay after the oscillator is perturbed from the limit cycle. Aschoff's rule is taken account of in the kBX term of (5.2), which gives a direct effect of light on the circadian period.

Next, we introduce the drive due to light from process L and its circadian sensitivity mod-

ulation.

5.2.1 Process L

Process L models the fact that the circadian pacemaker is driven by light interacting with photoreceptors in the eye. This results in a signal to the 'master' pacemaker located in the SCN. We define n as

$$\frac{dn}{dt} = \gamma\left(\alpha(I)(1-n) - \beta n\right), \tag{5.3}$$

the phototransduction pathway through which light from process L drives the circadian system.

As in [106] we define the forward rate constant, α, to depend on I (the light stimulus) such that

$$\alpha(I) = \begin{cases} a_0\left[\frac{I(t)}{I_0}\right]^p, & \text{during wake,} \\ 0, & \text{during sleep.} \end{cases}$$

which has the property that as $I \to 0, \alpha \to 0$. Note that during sleep $I(t) = 0$, this is used to model the gating of light by the eye. We assume that the regeneration rate constant, β, is independent of I. Finally, the circadian modulation of the oscillator's sensitivity to light is given by the output drive,

$$B = G\alpha(I)(1-n)(1-0.4X)(1-0.4Y).$$

Maximum sensitivity is located close to the middle of a typical sleep episode and minimum sensitivity shortly after midday. In late evening, towards conventional sleep onset, this modulation enhances photic response to light. This corresponds to the delay region of the human phase response curve and agrees with experimental data which describes light response during the evening [143].

Since the homeostatic sleep pressure from the two process model has no direct effect on the van der Pol oscillator given here it seems reasonable to use parameter values given in the literature. Therefore, the following parameter values are used in process L to drive the circadian system [99, 58].

Circadian parameters

$$\mu_l = 0.23, \quad \tau_c = 24.2, \quad k = 0.55, \quad \gamma = 60,$$
$$\beta = 0.013, \quad G = 33.75, \quad \alpha_0 = 0.16, \quad I_0 = 9500\,\text{lux}, \quad p = 0.5. \tag{5.4}$$

5.2.2 Modified two process model

To modify the two process model such that it includes the circadian response to light we need to choose an appropriate light stimulus, $I(t)$, incorporate the van der Pol type oscillator described in (5.2) and (5.1) into the circadian process $C(t)$ and find suitable parameter values for the homeostatic sleep pressure and thresholds.

First, we consider the light stimulus, motivated by real world light profiles [62,144], given by

$$I(t) = l_2 + \frac{(l_1 - l_2)}{2}\left(\tanh(c(t - s_1)) - \tanh(c(t - s_2))\right), \tag{5.5}$$

where l_1 denotes the level of light during core day light hours and l_2 the level of light at other times. A switch from l_2 to l_1 occurs at time $t = s_1$ and from l_1 to l_2 at $t = s_2$ with c denoting the speed of the switch between states. The parameters chosen for the simulations in this chapter are given below.

Light parameters

$$c = 0.6, \quad s_1 = 8\text{h}, \quad s_2 = 17\text{h}, \quad l_1 = 700 \text{ lux}, \quad l_2 = 40 \text{ lux} \tag{5.6}$$

Parameter values for s_1 and s_2 are chosen to give a daylight duration of approximately 12 hours centered on roughly midday seen at the equinoxes. To account for daylight saving time both parameters values are shifted up by 30 minutes as in [58]. The value of c, which denotes the steepness of the change between l_1 and l_2, is fixed despite variations across the year. However, it has been chosen such that it relates to average measured light profiles for summer [62]. The light profile $I(t)$ with $l_1 = 700$ and $l_2 = 40$ is give in Figure 5.1(a). During sleep, light is gated by the eye and $I(t) = 0$, at wake onset there is an instant switch in the model to the light profile given in (5.5). The gating of light by the eye does have implications on the van der Pol oscillator namely, it gives a mechanism for sleep/wake timing to turn the forcing of process L off and on.

To incorporate the van der Pol oscillator into the circadian process of the two process model the sinusoidal modulation of the upper and lower thresholds is replaced by a function $\tilde{C}(t)$ that is related to the output of the van der Pol oscillator and models the circadian wake propensity rhythm. Comparison with the PCR model [99] suggests that,

$$\tilde{C}(t) = \frac{1}{2}(1 + X),$$

could be considered. However, to reproduce typical observed sleep duration and timings using realistic light profiles $I(t)$, as in [58], a phase shift is added to give,

$$\tilde{C}(t) = \frac{1}{2}(1 + 0.8X - 0.47Y).$$

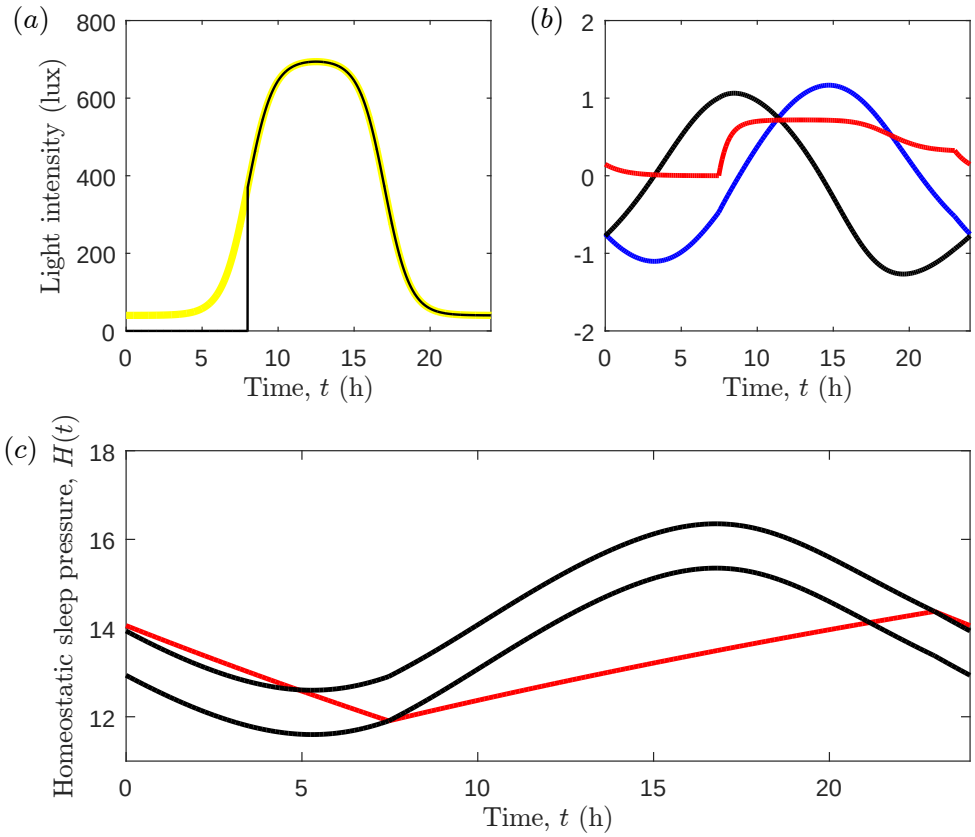

Figure 5.1: (a) The light profile $I(t)$ (yellow) using parameter values as in (5.6). The black line shows a light profile gated by the eyelids. (b) Solutions to equations (5.1) (blue), (5.2) (black) and (5.3) (red) (c) A typical simulation of the modified two process model using all given parameters with $a = 3.37, \mu = 20.37$.

Therefore the upper and lower thresholds of the two process model are now given by

$$H^+(t) = H_0^+ + a\tilde{C}(t) \quad \text{and} \quad H^-(t) = H_0^- + a\tilde{C}(t)$$

respectively. We also express the behaviour of the homeostatic sleep pressure by two ODE's, namely

$$\frac{dH_s}{dt} = \frac{-H_s}{\chi_s}, \tag{5.7}$$

during sleep and

$$\frac{dH_w}{dt} = \frac{-H_w + \mu}{\chi_w}, \tag{5.8}$$

during wake, as in equations (2.1) and (2.2). Note that μ denotes the value of the upper asymptote of the homeostatic sleep pressure on wake. The complete modified two process model is then as given below.

Modified two process model

The equations for the homeostatic sleep pressure during sleep is

$$H_s(t) = H^+(t_0)e^{\frac{t_0-t}{\chi_s}}, \quad t \geq t_0, \tag{5.9}$$

and during wake

$$H_w(t) = \mu + (H^-(t_0) - \mu)e^{\frac{t_0-t}{\chi_w}}, \quad t \geq t_0. \tag{5.10}$$

Switching occurs from wake to sleep at the upper threshold,

$$H^+(t) = H_0^+ + a\tilde{C}(t), \tag{5.11}$$

and from sleep to wake at the lower threshold,

$$H^-(t) = H_0^- + a\tilde{C}(t). \tag{5.12}$$

The modified circadian process is given by

$$\tilde{C}(t) = \frac{1}{2}(1 + 0.8X - 0.47Y), \tag{5.13}$$

where X and Y are the equations for the van der Pol oscillator given by

$$\frac{dX}{dt} = \frac{\pi}{12}(Y + B) \tag{5.14}$$

and

$$\frac{dY}{dt} = \frac{\pi}{12}\left(\mu_l\left(Y - \frac{4}{3}Y^3\right) - X\left[\left(\frac{24}{0.99669\tau_c}\right)^2 + kB\right]\right), \tag{5.15}$$

with a circadian modulation of the oscillator's sensitivity to light given by,

$$B = G\alpha(I)(1-n)(1-0.4X)(1-0.4Y). \tag{5.16}$$

The phototransduction pathway through which light from process L drives the circadian system is given by

$$\frac{dn}{dt} = \gamma\left(\alpha(I)(1-n) - \beta n\right), \tag{5.17}$$

with forward rate constant

$$\alpha(I) = \begin{cases} a_0\left[\frac{I(t)}{I_0}\right]^p, & \text{during wake,} \\ 0, & \text{during sleep,} \end{cases} \tag{5.18}$$

and light stimulus

$$I(t) = l_2 + \frac{(l_1 - l_2)}{2}\left(\tanh(c(t - s_1)) - \tanh(c(t - s_2))\right). \tag{5.19}$$

Again, since the during sleep the eyelid is acting as a gate for light this allows sleep timing to feed back on the influence of light on the circadian pacemaker. During sleep, the external signal from light input is zero and during wake this signal is given by $I(t)$ and is dependent on clock time, as shown by the black line in Figure 5.1(a).

Motivated by the comparison between the two process model [97] and the parameter values commonly used in the PR model [90] to predict human sleep patterns, we take:

Two process model parameters

$$\chi_s = \chi_w = 45, \quad H_0^- = 14.5, \quad H_0^+ = 15.5 \tag{5.20}$$

Hence the new model consists of equations (5.9)-(5.19) along with the parameters in (5.4), (5.6) and (5.20) and values for a and μ. We take these parameter values since we know that the PR model can be reduced to the two process model. By translating the parameters from the PCR model to this modified two process model we hope to illustrate that the two models have a comparable dynamical structure and produce similar results.

The solutions of the van der Pol ODE's and the modified two process model, with all aforementioned parameter values, are given in Figure 5.1(b) and (c) respectively. We will use the resulting sleep-wake cycles of this model to find parameters which match sleep durations and timings across lifespan. For the simulations in the remainder of this chapter we allow the amplitude a and the value of the upper asymptote μ to vary. These parameters are equivalent to the parameters ν_{vc} and μ which are varied in [140].

5.3 Mid-sleep on free days (MSF) and sleep duration data

For the remainder of this chapter we investigate how the modified two process model can predict changes in sleep timing and duration using data on both MSF and sleep duration across lifespan. We consider ages 11 through to 63 using MSF timings given in [54] and sleep duration lengths given in [56].

The midpoint of sleep on free days is deemed to be of particular importance as it is used as a reference point to describe preferred sleep timing. Also, as discussed in the Introduction 1.1.1 sleep duration and mis-timed sleep have been linked to a variety of health issues.

A simple questionnaire (Munich ChronoType Questionnaire, MCTQ [145]) was used to collect the data presented in both studies and stored in a database which has continued to grow. The MSF data published in 2004 included entries from roughly 25000 individuals about their sleep habits on both work and free days. By 2013, when the sleep duration data was published, the database had expanded to 150000 individuals from all over the world. The data for MSF and

sleep duration, from age 11 to 63, are reproduced in Figure 5.2. These data show a monotonic decrease in sleep duration and an 'n'-shaped curve for MSF values, peaking at around age 20.

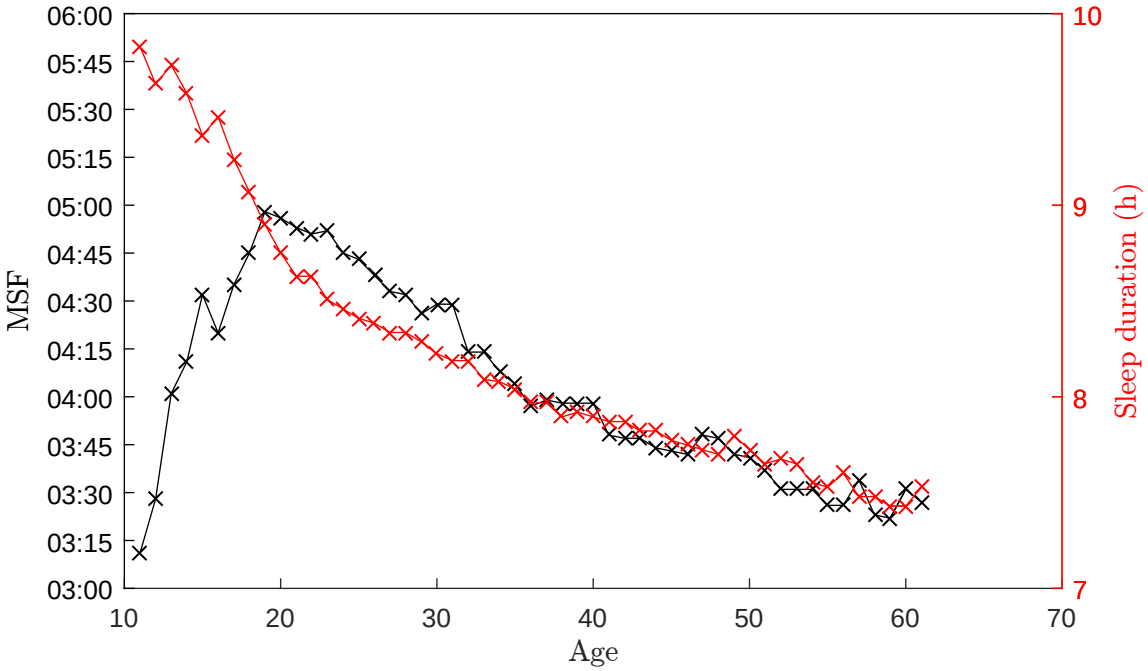

Figure 5.2: Data for mid-sleep on free days (MSF) given in [54] is plotted in black and sleep duration given [56] is plotted in red. The crosses represent each data point and the connecting lines are there to help guide the eye.

In the next section we discuss how the same changes in MSF and sleep duration across the lifespan from Figure 5.2 can be obtained, using the modified two process model, if the parameters a and μ are reduced with age.

5.4 Results

We begin by running simulations of the model to find sleep-wake cycles with sleep duration and MSF as a function of μ and a. In figure 5.3 the contour plots for sleep duration and MSF as a function of μ and a are plotted. We see that sleep duration is only slightly impacted by varying the circadian amplitude since the contours in Figure 5.3(a) are close to vertical. However, the diagonal contours in Figure 5.3(b) show that as μ increases, MSF monotonically decreases, and as a increases, MSF monotonically increases.

The data shown in Figure 5.2 gives a sleep duration and MSF that corresponds to each age. The contour plots in Figure 5.3 suggest that there exists a unique (μ, a) pair for each MSF and

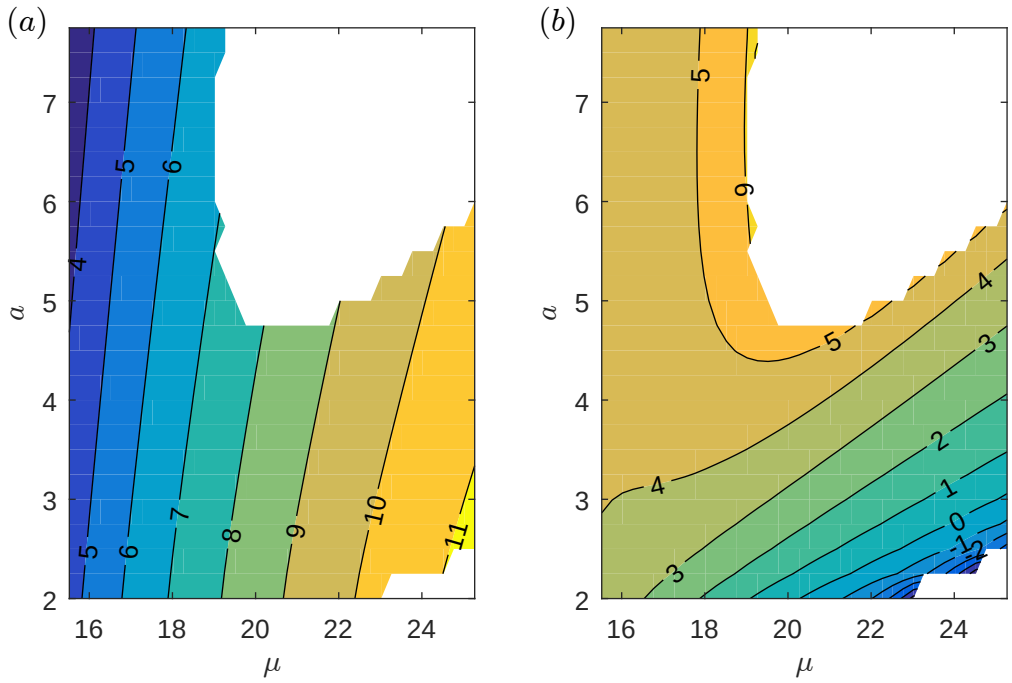

Figure 5.3: Running a simulation of the model results in a sleep-wake cycle with a sleep duration and MSF that is dependent on the values of μ and a. (a) A contour plot for sleep duration as a function of μ and a. (b) A contour plot of MSF as a function of μ and a.

sleep duration across the lifespan. To find the (μ, a) values we optimize

$$f_1 = \frac{MSF - MSF_e}{MSF_e} \quad \text{and} \quad f_2 = \frac{SD - SD_e}{SD_e},$$

where MSF and SD denote the models' simulated sleep mid-sleep on free days and sleep duration respectively, and subscript e represents the experimental data set.

The grid of points used to construct the contour plots forms a surrogate model which we use instead of repeatedly running simulations of the model to reduce computation time. By interpolating over the surrogate model we find corresponding values of (μ, a) that result in the same sleep duration lengths and MSF, giving a direct relationship between μ and a.

The resulting parameter values found using this process are given in Figure 5.4. Note that the circadian amplitude a is roughly constant across adolescence before decaying linearly throughout adulthood. The upper asymptote of the homeostatic sleep pressure on wake μ decreases exponentially. The largest differences in the behaviour of the parameter values across the lifespan occurs during adolescence, with a faster decrease in μ and very little change in a.

We then run the model with the parameter values given in Figure 5.4 to check that sleep duration and MSF timings correlate with the data set. The slight errors seen are due to the use

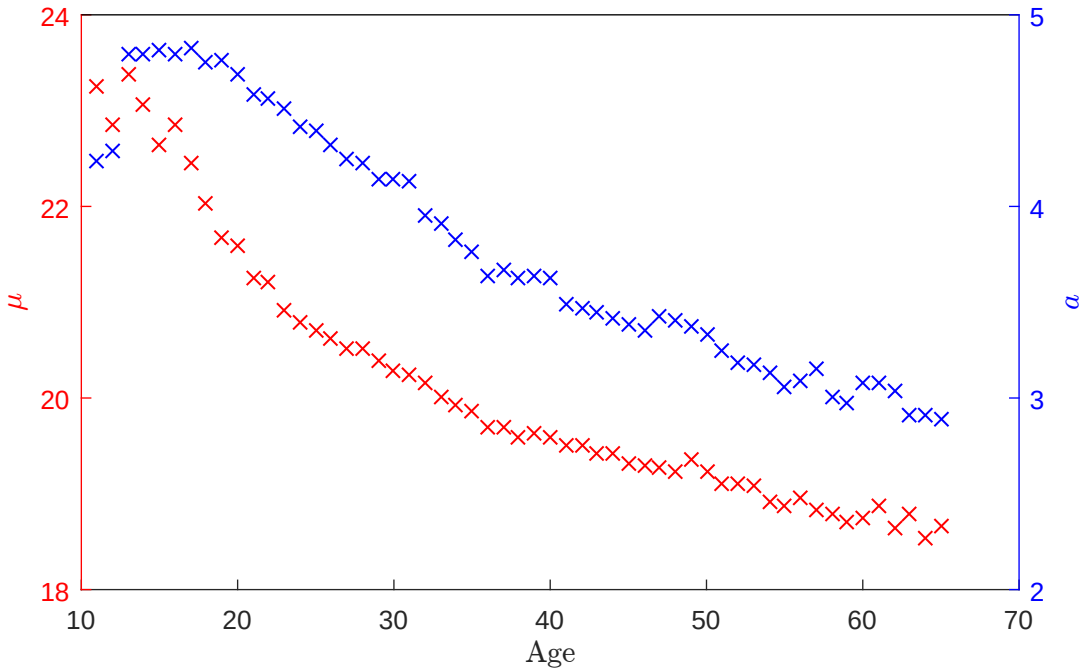

Figure 5.4: The models' parameter values μ (red) and a (blue) which correspond to the age-related changes in sleep duration and MSF using interpolation over the gird of points used to plot Figure 5.3. Note that both μ and a reduce with age.

of the surrogate model where we interpolate over the grid of points used to plot the contours. In Figure 5.5 both the simulated values and the data for each age is plotted. The high correlation is expected since we have used the data set to derive the parameters however, suggests that the modified two process model can be used to explain the observed changes in sleep relative to age. In particular the changes during adolescence which lead to reduced sleep duration and a later timing of sleep. After adolescence we still see progressively earlier sleep timing whilst sleep duration continues to decrease.

Finally, we have shown that for each age, data for MSF and sleep duration can be used to find a unique point (μ, a) which when used in model simulation yields very similar MSF and sleep duration. In Figure 5.6 we bring together the work of this section by plotting the direct relationship between μ, a and age given in Figure 5.4 over the contour plot in Figure 5.3.

5.5 Discussion

In this chapter we have given a modified version of the two process model which includes the effect of light on the human circadian pacemaker. A cubic van der Pol oscillator given in [106] is driven by a process L which converts a light signal into a drive for the circadian pacemaker. Using biologically relevant parameters for humans we showed that both data on MSF timings [54] and

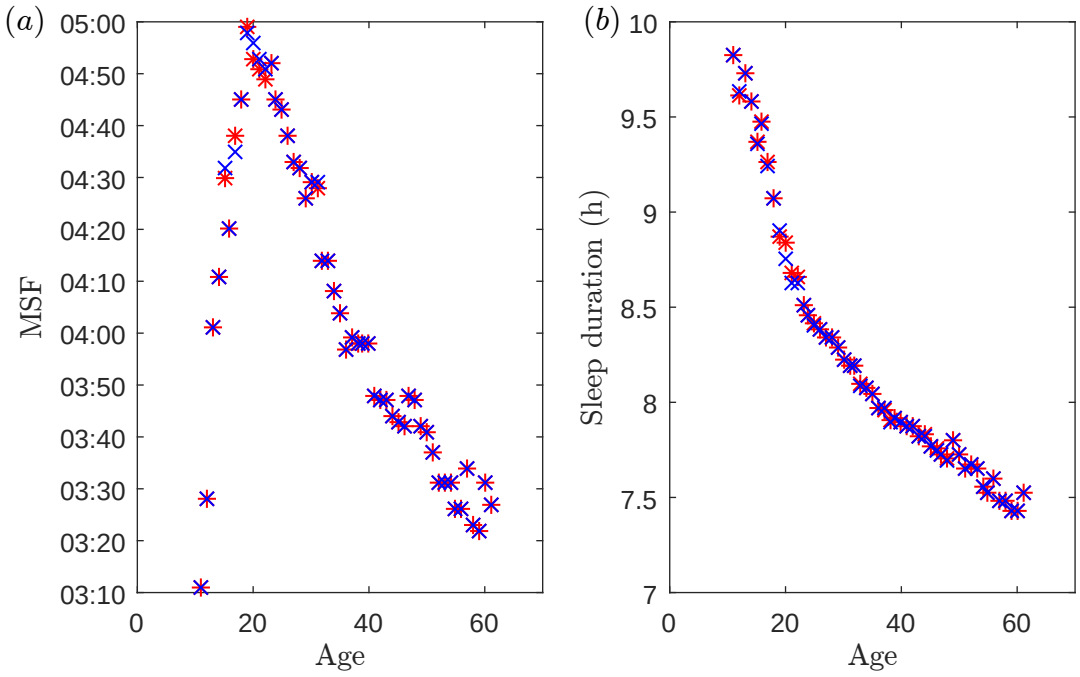

Figure 5.5: (a) Sleep duration, (b) MSF. Visually we can see very good agreement between the model predictions (red stars) and the data (blue crosses).

sleep duration lengths [56] across the lifespan could be recreated by varying only two parameters in the model.

The data in [54] was collected with the aim of understanding differences in chronotype in humans. As with most diurnal animals, human rest-activity patterns are endogenously controlled by biological clocks with a circadian period. When there are no environmental time cues present the circadian clock free runs, usually with a period of about 1 day. Usually the circadian clock is entrained to the 24 hour light dark cycle [146] however, some individuals' clocks entrain very late ('owls') and others very early ('larks'), with the majority lying in between. Normal variation in chronotype is considered to be be sleep-wake cycles ranging from 2 hours either side of average. The chronotype depends on genetic [147] and environmental factors [145] but also varies with age [148–150].

The discussion around the data published in [56] focused more on the changes in sleep duration in the modern world and the possible implications on an individuals health. Comparisons between the length of sleep on work days and work free days across lifespan showed that an individual would sleep for significantly less on work days than work free days throughout their lifespan, with the greatest difference occurring during the teenage years. This means that the majority of the school and work population experience under sleeping on work days and over-sleeping on work free days, leading to 'social jet lag' where the individual switches between their

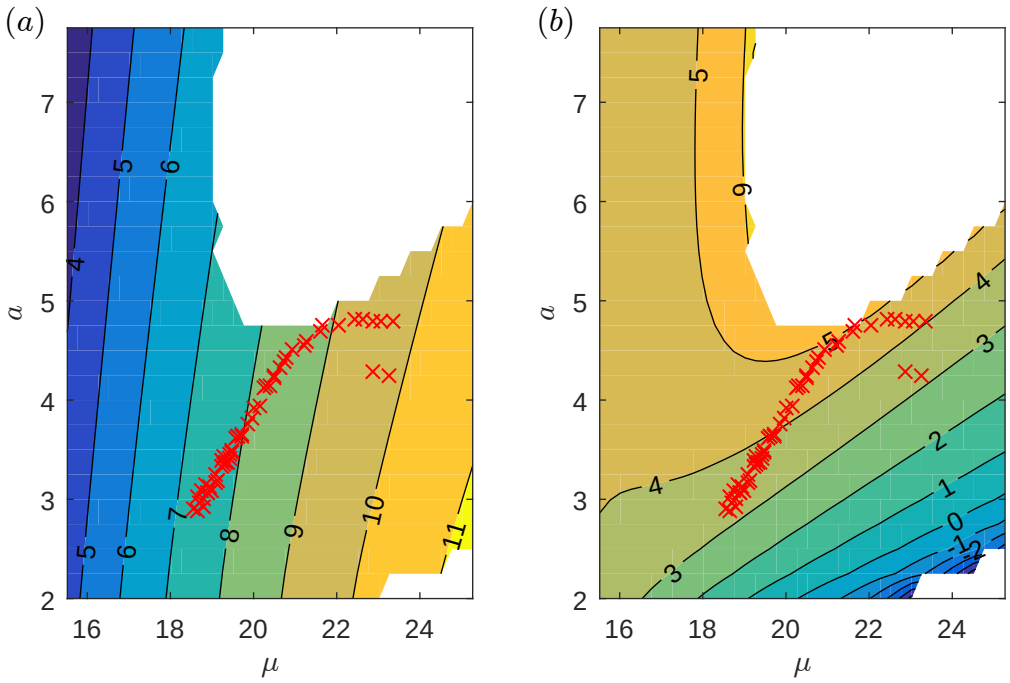

Figure 5.6: The values of μ, a across the lifespan from Figure 5.4 are plotted over the contours from Figure 5.3. Each red cross represent a (μ, a) pair with the right most points corresponding to adolescence moving into adulthood to the left, as the values of μ and a decrease.

work 'time zone' and the sleep-wake schedule determined by their biological clock.

Simulations of the modified two process model show that typical changes in sleep timing and duration, from adolescence to old age, can be explained by reducing both the amplitude of the circadian rhythm, a, and the asymptote of the homeostatic sleep pressure on wake, μ, simultaneously. The results found are qualitatively similar to those seen in [140] which explores the same data set using the Philips-Robinson model [90]. This means that the modified two process model could be used in place of more complex neuronal models to yield similar results and also potentially gives physiological meaning to some of its parameter values. In particular, the upper asymptote μ could be linked to neural activity dependent build-up of homeostatic sleep pressure during wake.

In the white regions of Figures 5.3 and 5.6, light alone is insufficient to entrain the model to a 24 hour period. At the edges of the shaded contour region a saddle-node bifurcation occurs due to a transition from entrained to non-entrained simulations. Note that the largest changes in MSF and sleep duration occur during adolescence, which are modelled using the parameter values denoted by the rightmost crosses in Figure 5.6. During the largest quantitative changes in the data the model parameters approach the saddle-node bifurcation, in this region the circadian phase is most sensitive to slight changes in the light profile.

6 Conclusions and future work

The main achievements of the work in this thesis have been the mathematical analyses of the two process model of sleep regulation and the use of modified versions of the model to help explain experimental data. Here we summarise these main findings in addition to highlighting potential areas of interest for future work.

6.1 The dynamics and bifurcations of the two process model

The two process model includes two fundamental process that are believed to regulate the sleep-wake cycle, a circadian and a homeostatic process. Partly due to its graphical simplicity the two process model has been widely used within the sleep and circadian science community to help understand a variety sleep-wake cycle behaviour, design experiments and interpret data [151,82]. The dynamics and numerical results found in more complicated models of sleep can be explicitly related to the two process model [97]. Therefore, understanding the dynamics of the two process model is very important within the context of sleep regulation.

6.1.1 Results

In Chapters 2 and 3 we showed that the two process model can be understood as a nonsmooth dynamical system, revealing that results from continuous monotonic circle maps and maps with gaps are relevant, resulting in a bifurcation set in which both saddle-node and border collision bifurcations create/ annihilate fixed points of the one dimensional map. We then showed how border collisions can take over from saddle-node bifurcations in forming the boundaries of Arnold tongues and highlighted the devil's staircase structure of periodic solutions. Although there is an extensive literature on maps, previous studies have either focussed on maps with gaps or maps with no gaps. This is the first example of which we are aware where the transition between the two is considered.

First, in Chapter 2, we introduced the two process model as an interaction between an oscillating circadian process, $C(t)$, and a homeostatic sleep pressure, $H(t)$. We began by rescaling to reduce the parameters in the original model and introduced some inequalities which restrict the parameters to biologically relevant regions. In particular, the inequalities introduced ensure that switching occurs in the model and therefore there is never the potential for infinite periods of sleep or wake. The special case where the circadian oscillator has zero amplitude ($a = 0$) is then discussed as it displays simple periodic behaviour. We show that when $a = 0$ any initial time $t_0 \in [0, 1]$ results in a solutions which repeats with period T_n given by

$$T_n = \chi_s \log\left(\frac{H_0^+}{H_0^-}\right) + \chi_w \log\left(\frac{1 - H_0^-}{1 - H_0^+}\right),$$

where $\chi_s \log\left(\frac{H_0^+}{H_0^-}\right)$ is the length of a sleep episode and $\chi_w \log\left(\frac{1-H_0^-}{1-H_0^+}\right)$ is the length of a wake episode. Such solutions have p sleeps over q days, when

$$T_n = \frac{q}{p}.$$

To help understand the transitions between (p, q) periodic solutions we reduced the two process model to a one dimensional sleep map, $T_s : \mathbb{R} \mapsto \mathbb{R}$, which maps the upper threshold onto itself. The fixed points in the map correspond to periodic solutions in the full dynamical system and represent different (periodic) patterns of sleep/wake. For the parameter regions considered in this thesis this map is the degree 1 lift of a monotonic circle map on the interval $[0, 1]$.Non-monotonicity in the map could potentially lead to more complex dynamics, including period-doubling and chaos, as has been shown for continuous but non-invertible maps of the circle [128].

In Chapter 3 we showed that at low circadian amplitudes, varying the bifurcation parameter H_0^- leads to a sequence of periodic solutions arising through saddle-node bifurcations, as is known to happen in continuous monotonic circle maps. For fixed a and varying H_0^-, the rotation number has a devil's staircase structure and Arnold tongues with constant rotation number are bounded by saddle-node bifurcations.

At larger amplitudes, varying the same parameter leads to the same devil's staircase sequence for the rotation number but now both border collisions and saddle-node bifurcations are important for the creation/annihilation of periodic orbits. We showed that the border collisions, which take over from saddle-node bifurcations as the boundaries of the (p, q)-periodic Arnold tongues, are a consequence of tangencies between the homeostatic sleep pressure and the circadian thresholds in the model. There is exactly one tangency where the homeostatic sleep

pressure during wake hits the lower threshold from above which occurs at time

$$t^l_{\tan} = \frac{\arccos\left(-\frac{H_0^-}{a\chi_s\gamma_s}\right) + \arccos\left(\frac{2\pi}{\gamma_s}\right)}{2\pi} \quad \in \left(\frac{1}{4}, \frac{3}{4}\right),$$

where $\gamma_s = \sqrt{4\pi^2 + \frac{1}{\chi_s^2}}$. A tangency from below between the homeostatic sleep pressure during sleep and the upper threshold also occurs at time

$$t^u_{\tan} = \frac{\arccos\left(\frac{2\pi}{\gamma_w}\right) - \arccos\left(\frac{1-H_0^+}{a\gamma_w\chi_w}\right)}{2\pi} \quad \in \left[0, \frac{1}{4}\right] \cup \left[\frac{3}{4}, 1\right],$$

where $\gamma_w = \sqrt{4\pi^2 + \frac{1}{\chi_w^2}}$.

At a tangency point the homeostatic sleep pressure can be viewed as having 2 potentially paths which it can follow. It can either continue on its trajectory through the tangency point or a switch between sleep/wake can occur. Therefore, to find the Arnold tongue boundaries we considered (p, q) periodic solutions which begin and end at a tangency point. This led to two types of border collision (Type I from Section 3.3.1 and Type II from Section 3.3.2) where when solving for a periodic solution numerically the homeostatic sleep pressure begins on either sleep or wake. By fixing all parameter values except from H_0^- we were able to find the corresponding H_0^- value which led to a periodic solution which we then tracked this solution by taking small steps in a to find the border collision boundary in the (H_0^-, a) parameter plane. The resulting bifurcation set which includes the biologically relevant parameter assumptions, saddle-node bifurcations and border collisions is displayed in Figure 3.13.

Finally, when considering the one dimensional map at a Type I border collision we found that the map has an infinite derivative as t_0 approaches t_0^l or t_0^u from the left in the down and up maps respectively. We note that the t-interval region in which the gradient of the one-dimensional map increases rapidly towards infinity can be very small, so in a numerical simulation study it is easy to miss that the gradient becomes infinite. Much of the literature on maps with gaps [118] focusses on piecewise linear maps where the derivative is necessarily finite on both sides, although infinite derivatives at a gap do arise naturally in many applications [152].

6.1.2 Consequences

The two process model displays complex dynamics and the different patterns of sleep that arise in the model have biological relevance. The most common pattern of human sleep corresponds to one sleep per day, $(p, q) = (1, 1)$, however other sleep-wake patterns do occur. Some cultures take a siesta [153], the practice of napping in the afternoon, and in some historical societies people would have two sleeps at night, with only a short wake period between the two [154].

This suggests that relatively small sociological or physiological changes could result in a different sleep pattern.

We have considered a variety of (p, q) periodic orbits both monophasic (one sleep per day) and polyphasic (many sleeps per day). For humans the polyphasic patterns which arise in the model have biological significance since there is a gradual transition from polyphasic to monophasic sleep during the first few years of development [155]. These changes could be explained by gradually varying physiological parameters [97], a phenomenon displayed in the bifurcation diagram plotted in Figure 3.3. A gradual change in the bifurcation parameter results in a transition corresponding to a decreasing number of sleep episodes per day or similarly, a gradual increase in the natural period T_n. We have scaled time so that the circadian period is one, so a lengthened circadian period in the original system is equivalent to increasing T_n as occurs by decreasing H_0^- or increasing H_0^+, χ_s or χ_w.

Transitions between the different kinds of periodic solutions are also relevant in experimental studies showing internal desynchrony. In adult humans, the intrinsic circadian period is entrained to the 24 hour day by external factors including light, eating patterns and exercise. Temporal isolation experiments have shown that by removing these external cues a circadian rhythm persists but is slightly longer than 24 hours [2]. Properties of the circadian clock including inter-individual variability in intrinsic period contribute to differences in the patterns of sleep/wake observed during temporal isolation. The sleep/wake patterns of participants would either: alter to remain in synchrony with the adjusted circadian period, but with an altered phase relationship because of the change in period; desynchronise; switch to a rhythm of one sleep every two days, a so-call circabidian rhythm [10]. In the two process model a switch to a circabidian rhythm corresponds to a transition from the $(p, q) = (1, 1)$ tongue to the $(1, 2)$ tongue. This structure gives the theoretical underpinning for the results of the numerical study carried out in [156] to investigate internal desynchrony and bicircabidian rhythms in a neuronal model.

The polyphasic patterns used to describe different patterns of mammalian sleep [96] and the original two process model results [79] can be explained using the Arnold tongue framework highlighted in Chapter 3. Although in [79] the circadian oscillator also includes a small amplitude higher harmonic term, $\sin 6\pi t$, we would not expect the qualitative Arnold tongue/ border collision structure to change. The main features of monotonicity with a transition to maps with gaps is preserved as the higher order terms are a small perturbation.

6.2 Applications of the two process model

By the end of Chapter 3 we have a good understanding of the dynamics of the two process model, the effects of varying different parameter values and the underlying mechanisms which

give transitions between (p, q) periodic solutions. With this background we went on to consider two applications using modified versions of the two process model. First, we described both sleep-wake patterns of the common vole and then changes in sleep timing through the human lifespan using a light driven circadian pacemaker.

6.2.1 The common vole and the two process model

In Chapter 4 we used the two process model, with only the standard circadian rhythm, to explain spontaneous sleep and sleep deprivation seen in experimental data on *Microtus Arvailis*, the common vole. We began by fitting parameter values a, χ_s, χ_w, H_0^+ and H_0^- for the two process model to EEG and sleep timing data from [129]. First we used the EEG data to derive χ_s and χ_w the growth/ decay rate constants of the homeostatic sleep pressure by considering the decay of delta power during NREM sleep, similar to the approach in [134], and the growth of theta power during wake respectively. It is important to note here that there other methods of deriving the growth and decay rate constants. For example, in [136] a different model of sleep-wake regulation is considered in which the initial values of the equivalent constants for a homeostatic process S are derived from [134] and then optimized, by minimizing the squared error between simulated and empirical SWA during NREM episodes with length greater than 1 minute. The model in [136] is based on equations from an elaborated version of the two process model [84] however, an additional step is added to check the stability of the optimized solution.

To fit the remaining parameters we iterated the homeostatic sleep pressure forward in time using sleep/ wake onset times from the data and the fitted values of χ_s, χ_w until transients had decayed and a 'forced' periodic solution remained. Note that this method relied on choosing a minimum length of wakefulness which would constitute a wake period in the two process model.

After fitting the parameters of the two process model to the data we showed that the model is sufficient to explain the key features of spontaneous sleep, but does not give the results seen in sleep deprivation. We wished to explain the phenomena in [130] where the length of subsequent sleep, ρ' decreases as the length of sleep deprivation, α', increased until the end of a natural sleep-wake period length, τ', and then jumped to a recovery sleep of roughly length τ'. To model this behaviour we added a large amplitude ultradian oscillator which occurred at regular intervals across the day, corresponding to the amount of sleep-wake periods seen in spontaneous conditions.

Due to its large amplitude the ultradian oscillator created threshold 'walls' which the homeostatic sleep pressure on wake (due to sleep deprivation) approached and then passed through. Therefore, if sleep deprivation ended close before one of these threshold walls the length of subsequent sleep would be very short whereas, if sleep deprivation ended just after the homeostatic sleep pressure on wake had passed through the threshold then the length of subsequent sleep

would be much longer. This creates the jump in recovery sleep observed in the data. Note that if sleep deprivation ends beneath the upper threshold then the vole remains awake until the homeostatic sleep pressure hits the upper threshold and switches to a sleep trajectory. This explains the fact that in the data from [129] the voles do not necessarily fall asleep immediately after the end of deprivation.

In Section 4.6 we discussed the sensitivity of the conclusions to the assumptions and parameter fitting used to carry out the analysis and found that variations in parameter values and wake length do not change the fundamental predictions of the two process model. Namely, that $\frac{\rho'}{\tau'}$ decreases with $\frac{\alpha'}{\tau'}$ increasing, until α' is a multiple of τ' and then ρ' jumps up back to τ'.

The temporal isolation/ free run experiments [3] which we have already discussed revealed, through desynchronising entrained rhythms, that it would take a minimum of two oscillators to describe the results seen in humans. In the case of the common vole, desynchrony through sleep deprivation has led us to understand that some additional ultradian component is necessary to explain the experimental results. The large amplitude ultradian oscillator is hidden in the model during spontaneous sleep since the homeostatic sleep pressure always switches before reaching the extreme values of threshold enforced by the ultradian oscillator. The underlying ultradian rhythmicity of the common vole is a key feature of their rest/ activity patterns highlighted by Gerkema [130] and our results are inline with this hypothesis.

Finally, we related the work of this chapter to the previous work on the two process model bifurcation set. The sleep-wake patterns of the common vole appear as $(p, 1)$ periodic solutions in the two process model with $p \in (7, 10)$. In Section 4.7 we linked the results of this chapter to the general bifurcation analysis of Chapter 3. Finally, we plotted the Arnold tongues relevant to the mean parameter values found for the voles. Since the circadian amplitude is small for all of the voles we find that tangencies in the model, and therefore discontinuities in map, do not occur. Therefore, in the parameter regions explored in this chapter the Arnold tongues are formed of saddle-node boundaries and border collisions do not play a role.

The tongues for the voles are very narrow such that any small perturbation in parameters could result in the voles moving away from their $(p, 1)$ periodic orbit. Despite some daily variations in sleep timing the number of sleeps per day for an individual vole usually stays the same [129]. It is possible that even if the physiological parameters lie outside of a $(p, 1)$ periodic tongue it would be difficult to spot just by observing the number of sleep episodes per day since the vole will exhibit behaviour close to this period. However, experimental data suggest that there is a circadian signal timed around light onset which enforces entrainment to the light-dark cycle [135] potentially 'correcting' any daily variations away from the $(p, 1)$-periodic solution. With the standard two process model alone this can not be simulated.

6.2.2 A modified two process model including an external zeitgeber

In Chapter 5 we included a dynamic stimulus processor that incorporates light stimuli into the representation of the circadian oscillator in a modified version of the two process model. A cubic van der Pol oscillator given in [106] is driven by a process L which converts a light signal into a drive for the circadian pacemaker. This is motivated by the observation that in many animals with circadian behaviour, light dark-cycles are a major cue for the synchronization of the SCN and affect sleep timing in humans, especially those that undergo shift work or experience jet lag. Using biologically relevant parameters for humans we show that changes in sleep timing and duration across the lifespan can be explained using the modified two process model by simultaneously decreasing the amplitude of the circadian rhythm, a, and the asymptote of the homeostatic sleep pressure on wake, μ. A similar study using a more complex neuronal model on the same data sets is given in [140]. The key result of the work in this chapter is highlighting that the modified two process model can be used in place of these more complex models to achieve the same results.

After parameter fitting we plot the simulated sleep duration and MSF for each (μ, a) pair, corresponding to an age, over the contour plots given in Figure 5.3. We noted that the largest physiological changes occur close to the white region in the contour. In the white regions of Figures 5.3 and 5.6, the light profile is not able to entrain the modified two process model to a 24 hour period, a similar phenomenon is seen in [58]. The edges of these regions mark a transition through a saddle-node bifurcation boundary between entrained and non-entrained states. Close to this boundary the circadian phase is most sensitive to slight changes in the light profile and therefore the parameter values leading to the biggest changes in sleep duration and MSF, which occur during adolescence, lie close to this boundary.

The light profiles we considered are consistent with [140] and motivated by real world light profiles [62, 144] however, these profiles will vary drastically for each individual depending on many factors such as work schedule, amount of travel and chronotype. Since at the boundary the circadian phase has increased sensitivity to light the results here imply that teenagers have the highest risk of being unable to synchronize to the 24 hour day. With the presence of artificial light we are now able to self-select our own light dark cycle and it is often only social constraints which keep us entrained to the 24 hour day.

There are many changes in human sleep throughout the lifespan. For the first few years from birth sleep is polyphasic and gradually transitions to a monophasic sleep pattern. These transitions can be explained using the bifurcation analysis of the two process model in Chapter 3. In adolescence there is a delay in sleep timing and a reduction in slow wave sleep which is followed by further reductions in slow wave sleep and a slow decrease to earlier sleep timing

during healthy ageing. Although these changes in sleep structure and timing are well established the biological mechanisms which underpin these changes are still being explored. However, it is a common view that changes in the circadian pacemaker lead to the observed changes in sleep timing. The modified two process model given in Chapter 5 can be used in place of more complex neuronal models to give an insight into how changes in sleep occur from adolescence onwards, by varying parameters of the circadian pacemaker. This also allows for parameters of the two process model to be related to parameters in the neuronal models, potentially gaining some physiological meaning.

In summary, we have given an in-depth analysis of the two process model of sleep-wake regulation which can be used to understand the dynamics of more complex mathematical models of sleep. We have also given two interesting applications, using modified versions of the two process model to explain observations seen in experimental data. The use of mathematical models in sleep science has allowed for further understanding of the underlying physiology, sleep phenomena and experimental data. The work in this thesis builds on the rich history of the seminal two process model of sleep regulation [79, 78, 82, 157, 158] as a tool for understanding a variety of different sleep phenomena, successfully simulating sleep timing and sleep intensity across a diverse range of experimental protocols [159].

6.3 Future Work

In the results presented in this thesis, we focused on monotonic maps. However, we have discussed the mechanism for the development of non-monotonicity [160]. The consequences of non-monotonicity for a simplified example containing the key features of the two process model have been examined in [161]. It would be of interest to extend the work of Chapter 3 to examine non-monotonicity in the two process model since it has the potential to lead to more complex dynamics, including period-doubling and chaos. Although we expect the results to be qualitatively the same as in [161] the addition of a second oscillating threshold would lead to an even more interesting discontinuity structure in the map for parameter regions, where both tangencies between the homeostatic sleep pressure and the upper and the homeostatic sleep pressure and the lower threshold are relevant.

In Figure 3.14 we showed that there is a point in the bifurcation diagram where a border collision on the upper threshold collides with a border collision on the lower threshold, which lies in the $(3, 2)$ Arnold tongue. Computation close to the interaction of these border collisions becomes difficult due to both border collision having infinite derivatives. Understanding this complex interaction analytically would be useful as regions where both tangencies on the upper and lower threshold will be more prominent for other parameter regimes.

The experimental data explored in Chapter 4 only contains one day of spontaneous sleep-wake cycles. It would be of interest to consider biological data for spontaneous sleep over a longer time period to check the consistency of sleep-wake onset times each day. This could help give insight into where each vole sits in the Arnold tongue description given in Section 4.7. By checking whether sleep timing shifts over multiple days or is 'corrected' at light onset we could better understand the rigidity of the $(p, 1)$ periodicity for each vole.

The work in Chapter 5 sets out to explore the same experimental data and reproduce the same results as in [140]. We showed that the modified two process model including an external zeitgeber can explain changes in sleep timing and duration by varying parameters in the model, much in the same way as the PCR model [99]. It would be interesting to explore this further and determine whether the PCR model can be reduced to the modified two process model similar to the reduction of the PR model to the two process model given in [97].

A deeper investigation into the effects of different light-dark cycles could help understand the effects of jet lag, shift work and artificial light/ blue light from devices in industrialized societies on sleep-wake patterns. To do this the spectral composition of the light input would need to incorporate the effects of blue light leading to changes in the phase response curve of process L. Work in this area could lead to better sleep scheduling and potentially reduce the health risks associated with desynchrony and mis-timed sleep.

Appendices

A

The two process model, its associated map and periodic solutions

A.1. Monotonicity of $\alpha(\tau)$

In the following lemma we will show that $\alpha(\tau)$ is monotonically decreasing.

Lemma A.1. *The function* $\alpha(\tau) = \frac{1-e^{\frac{\tau-q}{\chi_w}}}{1-e^{-\frac{\tau}{\chi_s}}e^{\frac{\tau-q}{\chi_w}}}$ *is monotonically decreasing from* $\alpha(0) = 1$ *to* $\alpha(1) = 0$.

Proof. At the boundaries of $\alpha(\tau)$ we have $\alpha(0) = 1$ and $\alpha(1) = 0$. For $\alpha(\tau)$ to be monotonically decreasing we need show that $\alpha'(\tau) < 0$. Recall

$$\alpha'(\tau) = \frac{\left(\frac{1}{\chi_w} - \frac{1}{\chi_s}\right)\left(1 - e^{\frac{\tau-q}{\chi_w}}\right)e^{\frac{\tau-q}{\chi_w}-\frac{\tau}{\chi_s}} - \frac{1}{\chi_w}e^{\frac{\tau-q}{\chi_w}}\left(1 - e^{\frac{\tau-q}{\chi_w}-\frac{\tau}{\chi_s}}\right)}{\left(1 - e^{\frac{\tau-q}{\chi_w}-\frac{\tau}{\chi_s}}\right)^2}.$$

Since $\tau \in (0, q)$ we know that

$$\left(1 - e^{\frac{\tau-q}{\chi_w}-\frac{\tau}{\chi_s}}\right)^2 > 0,$$

therefore we need only show that

$$\left(\frac{1}{\chi_w} - \frac{1}{\chi_s}\right)\left(1 - e^{\frac{\tau-q}{\chi_w}}\right)e^{\frac{\tau-q}{\chi_w}-\frac{\tau}{\chi_s}} - \frac{1}{\chi_w}e^{\frac{\tau-q}{\chi_w}}\left(1 - e^{\frac{\tau-q}{\chi_w}-\frac{\tau}{\chi_s}}\right) < 0,$$

Dividing by $e^{\frac{\tau-q}{\chi_w}}$ reduces this to

$$\left(\frac{1}{\chi_w} - \frac{1}{\chi_s}\right)e^{-\frac{\tau}{\chi_s}} - \frac{1}{\chi_w}e^{\frac{\tau-q}{\chi_w}-\frac{\tau}{\chi_s}} + \frac{1}{\chi_s}e^{\frac{\tau-q}{\chi_w}-\frac{\tau}{\chi_s}} - \frac{1}{\chi_w} + \frac{1}{\chi_w}e^{\frac{\tau-q}{\chi_w}-\frac{\tau}{\chi_s}} < 0,$$

which can be rewritten as

$$\left(\frac{1}{\chi_w} - \frac{1}{\chi_s}\right)e^{-\frac{\tau}{\chi_s}} + \frac{1}{\chi_s}e^{\frac{\tau-q}{\chi_w}-\frac{\tau}{\chi_s}} - \frac{1}{\chi_w} < 0.$$

Dividing by $e^{-\frac{\tau}{\chi_s}}$ and rearranging gives

$$\left(\frac{1}{\chi_w} - \frac{1}{\chi_w e^{-\frac{\tau}{\chi_s}}}\right) + \left(\frac{e^{\frac{\tau-q}{\chi_w}}}{\chi_s} - \frac{1}{\chi_s}\right) < 0.$$

Since $e^{\frac{\tau-q}{\chi_w}}, e^{-\frac{\tau}{\chi_s}} \in (0,1)$ we know

$$\frac{1}{\chi_w} < \frac{1}{\chi_w e^{-\frac{\tau}{\chi_s}}},$$

and

$$\frac{e^{\frac{\tau-q}{\chi_w}}}{\chi_s} < \frac{1}{\chi_s}.$$

Therefore we have $\alpha'(\tau) < 0$ and we know that $\alpha(\tau)$ is monotonically decreasing from 1 to 0. □

B

Bifurcations of periodic solutions

B.1. The edge of the tangency existence region

Lemma B.1. *For all $\chi_s > 0$, when $H_0^- = -a$, the homeostatic sleep pressure on sleep is tangent to the lower threshold at $t^l_{\tan} = \frac{1}{4}$.*

Proof. Lemma 3.2 gives

$$\cos(2\pi t^l_{\tan} + B) = -\frac{H_0^-}{a\gamma_s\chi_s},$$

so for $H_0^- = -a$ we have

$$\cos(2\pi t^l_{\tan} + B) = \frac{1}{\gamma_s\chi_s}.$$

From (3.14) we know $\frac{1}{\gamma_s\chi_s} = -\sin B$ which we extend to

$$\frac{1}{\gamma_s\chi_s} = -\sin B = \sin(-B) = \cos\left(-B - \frac{\pi}{2}\right) = \cos\left(B + \frac{\pi}{2}\right).$$

Therefore we have

$$\cos(2\pi t^l_{\tan} + B) = \cos\left(B + \frac{\pi}{2}\right).$$

As $t^l_{\tan} \in [\frac{1}{4}, \frac{3}{4})$, this implies

$$2\pi t^l_{\tan} = \frac{\pi}{2}$$

which gives us $t^l_{\tan} = \frac{1}{4}$. □

C

Voles and the two process model

C.1. F-Test

Throughout Chapter 4 we perform F-tests to check the significance of more complicated models against basic models. Since we will be nesting models by increasing the number of parameters, in an attempt to get a better fit to various data, we use the nested F-test given below.

For a model 1 that is nested in model 2 the test would return an F-value given by

$$F = \left(\frac{RSS_1 - RSS_2}{RSS2} \right) \frac{n - p_2}{p_2 - p_1},$$

where n is the number of data points, p_1, p_2 are the number of parameters in each model and RSS_1, RSS_2 are the residual sum of squares for models 1 and 2 respectively. The residuals for a model $y = f(t)$ are given by $\sum (y_i - f(t_i))^2$ where y_i represents a data point and $f(t_i)$ is the predicted value given by the model. We know $RSS_2 \leq RSS_1$ since a more complicated model will necessarily give a better fit to the data.

This test is to ensure that a more complicated model (a model with more parameters) is significantly better than a simpler model. To check significance we need to translate a found F-value into a p-value where:

- If $p > 0.05$ then the more complicated model (model 2) is not significantly better than the simpler model (model 1). Therefore it is not worth using additional parameters.
- If $p < 0.05$ then the more complicated model (model 2) is significantly better than the simpler model (model 1). Thus, the more complicated model gives a closer fit to the data and should be chosen over the simpler model.

To calculate p-values from F-values a cumulative probability density function for F is used,

namely

$$\begin{aligned} p &= 1 - fcdf(F, p_2 - p_1, n - p_2) \\ &= 1 - \int_0^F \frac{\Gamma\left[\frac{(p_2-p_1)+(n-p_2)}{2}\right]}{\Gamma\left(\frac{p_2-p_1}{2}\right)\Gamma\left(\frac{n-p_2}{2}\right)} \left(\frac{p_2-p_1}{n-p_2}\right)^{\frac{p_2-p_1}{2}} \frac{t^{\frac{p_2-p_1-2}{2}}}{\left[1+\left(\frac{p_2-p_1}{n-p_2}\right)t\right]^{\frac{n-p_1}{2}}} dt. \end{aligned}$$

An example of this is to determine whether a model with circadian oscillation fits the data better than a model with no circadian component.

References

[1] N. Kleitman, *Sleep and wakefulness,* University of Chicago Press, 1963.

[2] J. Aschoff, *Circadian rhythms in man,* Science **148** (1965) 1427.

[3] J. Aschoff, U. Gerecke, and R. Wever, *Desynchronization of human circadian rhythms,* Jpn. J. Physiol. **17** (1967) 450.

[4] R. Wever, *The circadian multi-oscillator system of man,* Int. J. Chronobiol. **3** (1975) 19.

[5] T. Roenneberg, T. Kuehnle, M. Juda, T. Kantermann, K. Allebrandt, M. Gordijn, and M. Merrow, *Epidemiology of the human circadian clock,* Sleep Med. Rev. **11** (2007) 429.

[6] F. Turek and P. Zee, *Regulation of sleep and circadian rhythms,* Marcel Dekker, 1999.

[7] D.-J. Dijk and D. Edgar, *Circadian and homeostatic control of wakefulness and sleep,* Lung Biol. Health Dis. **133** (1999) 111.

[8] C. Czeisler, *Human circadian physiology: Internal organization of temperature, sleep-wake and neuroendocrine rhythms monitored in an environment free of time cues,* Ph. D. Thesis Stanford University **1** (1979).

[9] C. Czeisler, E. Weitzman, M. Moore-Ede, J. Zimmerman, and R. Knauer, *Human sleep: its duration and organization depend on its circadian phase,* Science **210** (1980) 1264.

[10] R. Wever, *The circadian system of man: results of experiments under temporal isolation,* Springer Science & Business Media, 2013.

[11] P. Zlomanczuk and W. Schwartz, *Cellular and Molecular Mechanisms of Circadian Rhythms in Mammals,* Lung Biol. Health Dis. **133** (1999) 309.

[12] E. V. Cauter and K. Spiegel, *Circadian and Sleep Control of Hormonal Secretions,* Lung Biol. Health Dis. **133** (1999) 397.

[13] A. Zager, M. Andersen, F. Ruiz, I. Antunes, and S. Tufik, *Effects of acute and chronic sleep loss on immune modulation of rats,* Am. J. Physiol-Reg. I. **293** (2007) 504.

[14] K. Gümüstekin, B. Seven, N. Karabulut, Ö. Aktas, N. Gürsan, S. Aslan, M. Keles, E. Varoglu, and S. Dane, *Effects of sleep deprivation, nicotine, and selenium on wound healing in rats,* Int. J. Neurosci. **114** (2004) 1433.

[15] R. Brown, R. Basheer, J. McKenna, R. Strecker, and R. McCarley, *Control of sleep and wakefulness,* Physiol. Rev. **92** (2012) 1087.

[16] C. Portas, M. Thakkar, D. Rainnie, R. Greene, and R. McCarley, *Role of adenosine in behavioral state modulation: a microdialysis study in the freely moving cat,* Neuroscience **79** (1997) 225.

[17] M. Methippara, S. Kumar, M. Alam, R. Szymusiak, and D. McGinty, *Effects on sleep of microdialysis of adenosine A1 and A2a receptor analogs into the lateral preoptic area of rats,* Am. J. Physiol-Reg. I. **289** (2005) R1715.

[18] S. Chikahisa and H. Séi, *The role of ATP in sleep regulation,* Front. Neurol. **2** (2011) 87.

[19] C. Möller-Levet, S. Archer, G. Bucca, E. Laing, A. Slak, R. Kabiljo, J. Lo, N. Santhi, M. von Schantz, C. Smitth, and D.-J. Dijk, *Effects of insufficient sleep on circadian rhythmicity and expression amplitude of the human blood transcriptome,* Proc. Natl. Acad. Sci. USA **110** (2013) E1132.

[20] S. Archer, E. Laing, C. Möller-Levet, D. Van Der Veen, G. Bucca, A. Lazar, N. Santhi, A. Slak, R. Kabiljo, M. von Schantz, C. Smith, and D.-J. Dijk, *Mistimed sleep disrupts circadian regulation of the human transcriptome,* P. Natl. Acad. Sci. USA **111** (2014) E682.

[21] K. Knutson, *Sleep duration and cardiometabolic risk: a review of the epidemiologic evidence,* Best Pract. Res. Cl. En. **24** (2010) 731–743.

[22] T. S. L.S. Nielsen, K. Danielsen, *Short sleep duration as a possible cause of obesity: critical analysis of the epidemiological evidence,* Obes. Rev. **12** (2011) 78–92.

[23] F. Luyster, P. S. Jr, P. Zee, and J. Walsh, *Sleep: a health imperative,* Sleep **35** (2012) 727.

[24] M. Thase, *Depression and sleep: pathophysiology and treatment,* Dialogues Clin. Neurosci. **8** (2006) 217.

[25] J. Mann and D. Kupfer, *Biology of Depressive Disorders. Part B: Subtypes of Depression and Comorbid Disorders,* Springer, 1993.

[26] S. Patel, A. Malhotra, D. Gottlieb, D. White, and F. Hu, *Correlates of long sleep duration,* Sleep **29** (2006) 881.

[27] A. Naska, E. Oikonomou, A. Trichopoulou, T. Psaltopoulou, and D. Trichopoulos, *Siesta in healthy adults and coronary mortality in the general population,* Arch. Intern. Med. **167** (2007) 296.

[28] C. Thompson, E. Larkin, S. Patel, N. Berger, S. Redline, and L. Li, *Short duration of sleep increases risk of colorectal adenoma,* Cancer **117** (2011) 841.

[29] C. Thompson and L. Li, *Association of sleep duration and breast cancer OncotypeDX recurrence score,* Breast Cancer Res. Tr. **134** (2012) 1291.

[30] L. S. et. al. J. R. Rider, E. Schernhammer, C. A. Czeisler, L. Launer, T. Harris, M. J. Stampfer, and others, *Sleep disruption among older men and risk of prostate cancer,* Cancer Epidem. Biomar. **22** (2013) 872.

[31] F. Cappuccio, F. Taggart, N.-B. Kandala, A. Currie, E. Peile, S. Stranges, and M. Miller, *Meta-analysis of short sleep duration and obesity in children and adults,* Sleep **31** (2008) 619.

[32] S. Schmid, M. Hallschmid, and B. Schultes, *The metabolic burden of sleep loss,* Lancet Diabetes Endo. **3** (2015) 52.

[33] H. Piéron, *Le problème physiologique du sommeil,* (1913).

[34] W. Flanigan, *Behavioral states and electroencephalograms of reptiles,* The sleeping brain. Perspectives in the brain sciences **14** (1972).

[35] I. Tobler, *Evolution of the sleep process: A phylogenetic approach,* Exp. Brain Res. Suppl. **8** (1984) 207.

[36] R. Peraita-Adrados, *Electroencephalography, polysomnography, and other sleep recording systems,* The physiologic nature of sleep **1** (2005) 103.

[37] B. Fisch and R. Spehlmann, *Fisch and Spehlmann's EEG primer: basic principles of digital and analog EEG,* Elsevier Health Sciences, 1999.

[38] E. Niedermeyer and F. da Silva, *Electroencephalography: basic principles, clinical applications, and related fields,* Lippincott Williams & Wilkins, 2005.

[39] G. Pfurtscheller and F. D. Silva, *Event-related EEG/MEG synchronization and desynchronization: basic principles,* Clin. Neurophysiol. **110** (1999) 1842.

[40] A. Loomis, E. Harvey, and G. Hobart, *Potential rhythms of the cerebral cortex during sleep,* Science **81** (1935).

[41] A. Loomis, E. Harvey, and G. Hobart, *Further observations on the potential rhythms of the cerebral cortex during sleep,* Science **82** (1935) 198.

[42] A. Loomis, E. Harvey, and G. Hobart, *Electrical potentials of the human brain,* Journal of experimental Psychology **19** (1936) 249.

[43] A. Loomis, E. Harvey, and G. Hobart, *Cerebral states during sleep, as studied by human brain potentials,* J. Exp. Psychol. **21** (1937) 127.

[44] R. McCarley, *Neurobiology of REM and NREM sleep,* Sleep Med. **8** (2007) 302.

[45] A. Rechtschaffen, *A manual of standardized terminology, techniques and scoring system for sleep stages of human subjects,* Public health service(1968).

[46] H. Schulz, *Rethinking sleep analysis: Comment on the AASM manual for the scoring of sleep and associated events,* J. Clin. Sleep Med. **4** (2008) 99.

[47] P. Maquet, V. Sterpenich, G. Albouy, T. Dang-Vu, M. Desseilles, M. Boly, P. Ruby, S. Laureys, and P. Peigneux, *Brain imaging on passing to sleep,* The Physiologic Nature of Sleep **1** (2005) 123.

[48] T. Åkerstedt, M. Billiard, M. Bonnetl, G. Ficca, L. Garma, M. Mariotti, P. Salzarulo, and H. Schulz, *Awakening from sleep,* Sleep Med. Rev. **6** (2002) 267.

[49] R. Dahl, *The regulation of sleep and arousal: Development and psychopathology,* Dev. Psychopathol. **8** (1996) 3.

[50] A. Scher, *Infant sleep at 10 months of age as a window to cognitive development,* Early Hum. Dev. **81** (2005) 289.

[51] A. Hupbach, R. Gomez, R. Bootzin, and L. Nadel, *Nap-dependent learning in infants,* Developmental Sci. **12** (2009) 1007.

[52] A. Bernier, S. Carlson, S. Bordeleau, and J. Carrier, *Relations between physiological and cognitive regulatory systems: Infant sleep regulation and subsequent executive functioning,* Child Dev. **81** (2010) 1739.

[53] K. Spruyt, R. Aitken, K. So, M. Charlton, T. Adamson, and R. Horne, *Relationship between sleep/wake patterns, temperament and overall development in term infants over the first year of life,* Early Hum. Dev. **84** (2008) 289.

[54] T. Roenneberg, T. Kuehnle, P. Pramstaller, J. Ricken, M. Havel, A. Guth, and M. Merrow, *A marker for the end of adolescence,* Curr. Biol. **14** (2004) 1038.

[55] M. Basner, K. Fomberstein, F. Razavi, S. Banks, J. William, R. Rosa, and D. Dinges, *American time use survey: sleep time and its relationship to waking activities,* Sleep **30** (2007) 1085.

[56] T. Roenneberg, *Chronobiology: the human sleep project,* Nature **498** (2013) 427.

[57] M. Hirshkowitz, K. Whiton, S. Albert, C. Alessi, O. Bruni, L. DonCarlos, N. Hazen, J. Herman, E. Katz, and L. Kheirandish-Gozal, *National Sleep Foundation's sleep time duration recommendations: methodology and results summary,* Sleep Health: J. Natl. Sleep Fdn. **1** (2015) 40.

[58] A. Skeldon, A. Phillips, and D.-J. Dijk, *The effects of self-selected light-dark cycles and social constraints on human sleep and circadian timing: a modeling approach,* Sci. Rep. UK **7** (2017) 45158.

[59] M. Bonnet, *Performance and sleepiness following moderate sleep disruption and slow wave sleep deprivation,* Physiol. Behav. **37** (1986) 915.

[60] E. Haus and M. Smolensky, *Shift work and cancer risk: potential mechanistic roles of circadian disruption, light at night, and sleep deprivation,* Sleep Med. Rev. **17** (2013) 273.

[61] C. Cajochen, S. Frey, D. Anders, J. Späti, M. Bues, A. Pross, R. Mager, A. Wirz-Justice, and O. Stefani, *Evening exposure to a light-emitting diodes (LED)-backlit computer screen affects circadian physiology and cognitive performance,* J. Appl. Physiol. **110** (2011) 1432.

[62] H. Thorne, K. Jones, S. Peters, S. Archer, and D.-J. Dijk, *Daily and seasonal variation in the spectral composition of light exposure in humans,* Chronobiol. Int. **26** (2009) 854.

[63] G. Yetish, H. Kaplan, M. Gurven, B. Wood, H. Pontzer, P. Manger, C. Wilson, R. McGregor, and J. Siegel, *Natural sleep and its seasonal variations in three pre-industrial societies,* Curr. Biol. **25** (2015) 2862.

[64] X. Yuan, C. Zhu, M. Wang, F. Mo, W. Du, and X. Ma, *Night Shift Work Increases the Risks of Multiple Primary Cancers in Women: A Systematic Review and Meta-analysis of 61 Articles,* Cancer Epidem. Biomar. **27** (2018) 25.

[65] M. Wittmann, J. Dinich, M. Merrow, and T. Roenneberg, *Social jetlag: misalignment of biological and social time,* Chronobiol. Int. **23** (2006) 497.

[66] C. Winget, C. DeRoshia, C. Markley, and D. Holley, *A review of human physiological and performance changes associated with desynchronosis of biological rhythms,* Aviat. Space Envir. Med.(1984).

[67] C. Comperatore and G. Krueger, *Circadian rhythm desynchronosis, jet lag, shift lag, and coping strategies,* Occup. Med-C. **5** (1990) 323.

[68] Entrain - Reducing jetlag through mobile tracking, *http://entrain.math.lsa.umich.edu/*, Accessed: 12-06-2018.

[69] K. Serkh and D. Forger, *Optimal schedules of light exposure for rapidly correcting circadian misalignment,* PLoS Comput. Biol. **10** (2014) e1003523.

[70] Sleep as Android, *https://sleep.urbandroid.org/*, Accessed: 12-06-2018.

[71] P. Gringras, B. Middleton, D. Skene, and V. Revell, *Bigger, Brighter, Bluer-Better? Current Light-Emitting Devices–Adverse Sleep Properties and Preventative Strategies,* Front. Public Health **3** (2015).

[72] A.-M. Chang, D. Aeschbachl, J. Duffy, and C. Czeisler, *Evening use of light-emitting eReaders negatively affects sleep, circadian timing, and next-morning alertness,* P. Natl. Acad. Sci. USA **112** (2015) 1232.

[73] f.lux: Software to make your life better, *https://justgetflux.com/*, Accessed: 12-06-2018.

[74] R. Kronauer, C. Czeisler, S.F.Pilato, M.C.Moore-Ede, and E.D.Weitzman, *Mathematical model of the human circadian system with two interacting oscillators,* Am. J. Physiol-Reg. I. **242** (1982) R3.

[75] S. Strogatz, *Human sleep and circadian rhythms: a simple model based on two coupled oscillators,* J. Math. Biol. **25** (1987) 327.

[76] R. McCarley and J. Hobson, *Neuronal excitability modulation over the sleep cycle: a structural and mathematical model,* Science **189** (1975) 58.

[77] R. McCarley and S. Massaquoi, *A limit cycle mathematical model of the REM sleep oscillator system,* Am. J. Physiol-Reg. I. **251** (1986) R1011.

[78] A. Borbély, *A two process model of sleep regulation,* Hum. Neurobiol.(1982).

[79] S. Daan, D. Beersma, and A. Borbély, *Timing of human sleep: recovery process gated by a circadian pacemaker,* Am. J. Physiol-Reg. I. **246** (1984) R161.

[80] A. Borbély, F. Baumann, D. Brandeis, I. Strauch, and D. Lehmann, *Sleep deprivation: effect on sleep stages and EEG power density in man,* Electroen. Clin. Neuro. **51** (1981) 483.

[81] A. Borbély and P. Achermann, *Sleep homeostasis and models of sleep regulation,* J. Biol. Rhythm. **14** (1999) 559.

[82] P. Achermann and A. Borbély, *Mathematical models of sleep regulation,* Front. Biosci. **8** (2003) s683.

[83] P. Achermann and A. Borbély, *Simulation of human sleep: ultradian dynamics of electroencephalographic slow-wave activity,* J. Biol. Rhythm **5** (1990) 141.

[84] P. Achermann, D.-J. Dijk, D. Brunner, and A. Borbély, *A model of human sleep homeostasis based on EEG slow-wave activity: quantitative comparison of data and simulations,* Brain Res. Bull. **31** (1993) 97.

[85] D. Beersma and P. Achermann, *Changes of sleep EEG slow-wave activity in response to sleep manipulations: to what extent are they related to changes in REM sleep latency?,* J. Sleep Res. **4** (1995) 23.

[86] S. Folkard and T. Åkerstedt, *A three-process model of the regulation of alertness-sleepiness,* Sleep, arousal and performance(1992) 11.

[87] S. Folkard, T. Åkerstedt, I. MacDonald, P. Tucker, and M. Spencer, *Beyond the three-process model of alertness: estimating phase, time on shift, and successive night effects,* J. Biol. Rhythm. **14** (1999) 579.

[88] C. Saper, T. Scammell, and J. Lu, *Hypothalamic regulation of sleep and circadian rhythms,* Nature **437** (2005) 1257.

[89] Y. Tamakawa, A. Karashima, Y. Koyama, N. Katayama, and M. Nakao, *A quartet neural system model orchestrating sleep and wakefulness mechanisms,* J. Neurophysiol. **95** (2006) 2055.

[90] A. Phillips and P. Robinson, *A quantitative model of sleep-wake dynamics based on the physiology of the brainstem ascending arousal system,* J. Biol. Rhythm. **22** (2007) 167.

[91] C. Diniz Behn, E. Brown, T. Scammell, and N. Kopell, *Mathematical model of network dynamics governing mouse sleep-wake behavior,* J. Neurophysiol. **97** (2007) 3828.

[92] S. Postnova, K. Voigt, and H. Braun, *A mathematical model of homeostatic regulation of sleep-wake cycles by hypocretin/orexin,* J. Biol. Rhythm. **24** (2009) 523.

[93] C. D. Behn and V. Booth, *Simulating microinjection experiments in a novel model of the rat sleep-wake regulatory network,* J. Neurophysiol. **103** (2010) 1937.

[94] R. Kumar, A. Bose, and B. Mallick, *A mathematical model towards understanding the mechanism of neuronal regulation of wake-NREMS-REMS states,* PLoS ONE **7** (2012) e42059.

[95] M. Puckeridge, B. Fulcher, A. Phillips, and P. Robinson, *Incorporation of caffeine into a quantitative model of fatigue and sleep,* J. Theor. Biol. **273** (2011) 44.

[96] A. Phillips, P. Robinson, D. Kedziora, and R. Abeysuriya, *Mammalian sleep dynamics: how diverse features arise from a common physiological framework,* PLoS Comput. Biol. **6** (2010) e1000826.

[97] A. Skeldon, D.-J. Dijk, and G. Derks, *Mathematical models for sleep-wake dynamics: comparison of the two-process model and a mutual inhibition neuronal model,* PLos ONE(2014).

[98] A. Skeldon, G. Derks, and V. Booth, *Nonsmooth maps and the fast-slow dynamics of sleep-wake regulation: part II,* Extended Abstracts Spring 2016: Nonsmooth Dynamics **8** (2017) 171.

[99] A. Phillips, P. Chen, and P. Robinson, *Probing the mechanisms of chronotype using quantitative modeling,* J. Biol. Rhythm. **25** (2010) 217.

[100] D. Beersma, S. Daan, and D.-J. Dijk, *Sleep intensity and timing: a model for their circadian control,* Math. Q. Biol. - Circ. Rhythm. **19** (1987) 39.

[101] M. Hilaire, E. Klerman, S. Khalsa, K. W. Jr, C. Czeisler, and R. Kronauer, *Addition of a non-photic component to a light-based mathematical model of the human circadian pacemaker,* J. Theor. Biol. **247** (2007) 583.

[102] R. Wever, *Virtual synchronization towards the limits of the range of entrainment,* J. Theor. Biol. **36** (1972) 119.

[103] M. Jewett, R. Kronauer, and C. Czeisler, *Phase-amplitude resetting of the human circadian pacemaker via bright light: a further analysis,* J. Biol. Rhythm. **9** (1994) 295.

[104] D. Forger, M. Jewett, and R. Kronauer, *A simpler model of the human circadian pacemaker,* J. Biol. Rhythm. **14** (1999) 533.

[105] M. Jewett and R. Kronauer, *Refinement of Limit Cycle Oscillator Model of the Effects of Light on the Human Circadian Pacemaker,* J. Theor. Biol. **192** (1998) 455.

[106] R. Kronauer, D. Forger, and M. Jewett, *Quantifying human circadian pacemaker response to brief, extended, and repeated light stimuli over the phototopic range,* J. Biol. Rhythm. **14** (1999) 501.

[107] M. Nakao and M. Yamamoto, *Bifurcation properties of the two process model,* Psychiat. Clin. Neuros. **52** (1998) 131.

[108] M. Nakao, H. Sakai, and M. Yamamoto, *An interpretation of the internal desynchronizations based on dynamics of the two-process model,* Method. Inform. Med. **36** (1997) 282.

[109] V. Arnold, *Cardiac arrhythmias and circle mappings,* Chaos **1** (1991) 20.

[110] B. Romeira, J. Figueiredo, C. Ironside, and T. Slight, *Chaotic dynamics in resonant tunneling optoelectronic voltage controlled oscillators,* IEEE Photonic. Tech. L. **21** (2009) 1819.

[111] L. Glass, M. Guevara, A. Shrier, and R. Perez, *Bifurcation and chaos in a periodically stimulated cardiac oscillator,* Physica D **7** (1983) 89.

[112] H. Poincaré, *On curves defined by differential equations,* GITTL, Moscow-Leningrad(1947).

[113] M. Herman, *Une méthode pour minorer les exposants de Lyapounov et quelques exemples montrant le caractère local d'un théorème d'Arnold et de Moser sur le tore de dimension 2,* Comment. Math. Helv. **58** (1983) 453.

[114] R. Devaney, *An introduction to chaotic dynamical systems: second edition,* Addison-Wesley, 1989.

[115] F. Rhodes and C. Thompson, *Rotation numbers for monotone functions on the circle,* J. Lond. Math. Soc. **34** (1986) 360–368.

[116] J. Palis and W. D. MeloJ. Palis and W. De Melo. *Geometric theory of dynamical systems: An introduction (Translated from the Portuguese by A.K Manning),* .

[117] J. Keener, *Chaotic behaviours in piecewise continuous difference equations,* Am. Math. Soc. **261** (1980) 589.

[118] A. Granados, L. Alsedà, and M. Krupa, *The period adding and incrementing bifurcations: from rotation theory to applications,* SIAM Rev. **59** (2017) 225.

[119] C. Budd, *Grazing in impact oscillators,* Real and Complex Dynamical Systems **1** (1995) 47.

[120] I. Dobson, *Stability of ideal thyristor and diode switching circuits,* IEEE T. Circuits-I. **42** (1995) 517.

[121] G. Maggio, M. D. Bernardo, and M. Kennedy, *Nonsmooth bifurcations in a piecewise-linear model of the Colpitts oscillator,* IEEE T. Circuits-I. **47** (2000) 1160.

[122] G. Yuan, S. Banerjee, E. Ott, and J. Yorke, *Border-collision bifurcations in the buck converter,* IEEE T. Circuits-I. **45** (1998) 707.

[123] P. Jain and S. Banerjee, *Border-collision bifurcations in one-dimensional discontinuous maps,* Int. J. Bifurcat. Chaos **13** (2003) 3341.

[124] A. Kumar, S. Banerjee, and D. Lathrop, *Dynamics of a piecewise smooth map with singularity,* Phys. Lett. A **337** (2005) 87.

[125] M. Bailey, G. Derks, and A. Skeldon, *Circle maps with gaps: Understanding the dynamics of the two-process model for sleep-wake regulation,* Eur. J. Appl. Math.(2018).

[126] L. Menna-Barreto, A. Benedito-Silva, N. Marques, M. de Andrade, and F. Louzada, *Ultradian components of the sleep-wake cycle in babies,* Chronobiology international **10** (1993) 103.

[127] T. Åkerstedt and M. Gillberg, *The circadian variation of experimentally displaced sleep,* Sleep **4** (1981) 159.

[128] R. Mackay and C. Tresser, *Transition to topological chaos for circle maps,* Physica D **19** (1986) 206.

[129] A. Psomas, A. Hogben, M. Gerkhema, R. Winsky-Sommerer, and D. Van der Veen, *On ultradian rhytmicity in the rest/ activity cycles of the common vole,* In preparation(2018).

[130] M. Gerkema and F. V. D. Leest, *Ongoing ultradian activity rhythms in the common vole, Microtus arvalis, during deprivations of food, water and rest,* J. Comp. Physiol. A **168** (1991) 591.

[131] S. Hasan, D. Van Der Veen, R. Winsky-Sommerer, A. Hogben, E. Laing, F. Koentgen, D.-J. Dijk, and S. Archer, *A human sleep homeostasis phenotype in mice expressing a primate-specific PER3 variable-number tandem-repeat coding-region polymorphism,* FASEB J **28** (2014) 2441.

[132] A. Borbély, F. Baumann, D. Brandeis, I. Strauch, and D. Lehmann, *Sleep deprivation: effect on sleep stages and EEG power density in man,* Electroen. Clin. Neuro. **51** (1981) 483.

[133] D.-J. Dijk, D. Brunner, D. Beersma, and A. Borbély, *Electroencephalogram power density and slow wave sleep as a function of prior waking and circadian phase,* Sleep **13** (1990) 430.

[134] P. Franken, D. Chollet, and M. Tafti, *The homeostatic regulation of sleep need is under genetic control,* J. Neurosci. **21** (2001) 2610.

[135] M. Gerkema, S. Daan, M. Wilbrink, M. Hop, and F. van der Leest, *Phase control of ultradian feeding rhythms in the common vole (Microtus arvalis): the roles of light and the circadian system,* J. Biol. Rhythm. **8** (1993) 151.

[136] M. Guillaumin, L. McKillop, N. Cui, S. Fisher, R. Foster, M. de Vos, S. Peirson, P. Achermann, and V. Vyazovskiy, *Cortical region–specific sleep homeostasis in mice: effects of time of day and waking experience,* Sleep **28** (2018) 31.

[137] G. Hall, *Resonance zones in two-parameter families of circle homeomorphisms,* SIAM J. Appl. Math. **15** (1984) 1075.

[138] M. Gerkema, G. Groos, and S. Daan, *Differential elimination of circadian and ultradian rhythmicity by hypothalamic lesions in the common vole, Microtus arvalis,* J. Biol. Rhythm. **5** (1990) 81.

[139] D. Van Der Veen, N. L. Minh, P. Gos, M. Arneric, M. Gerkema, and U. Schibler, *Impact of behaviour on central and peripheral circadian clocks in the common vole, Microtus Arvalis, a mammal with ultradian rhythms,* Neuroscience **103** (2006).

[140] A. Skeldon, G. Derks, and D.-J. Dijk, *Modelling changes in sleep timing and duration across the lifespan: changes in circadian rhythmicity or sleep homeostasis?,* Sleep Med. Rev. **28** (2016) 92.

[141] R. Kronauer, *A quantitative model for the effects of light on the amplitude and phase of the deep circadian pacemaker, based on human data,* Sleep **90** (1990) 306.

[142] M. Jewett, D. Forger, and R. Kronauer, *Revised limit cycle oscillator model of human circadian pacemaker,* J. Biol. Rhythm. **14** (1999) 493.

[143] C. Cajochen, J. Zeitzer, C. Czeisler, and D.-J. Dijk, *Dose-response relationship for light intensity and ocular and electroencephalographic correlates of human alertness,* Behav. Brain Res. **115** (2000) 75.

[144] K. W. Jr, A. McHill, B. Birks, B. Griffin, T. Rusterholz, and E. Chinoy, *Entrainment of the human circadian clock to the natural light-dark cycle,* Curr. Biol. **23** (2013) 1554.

[145] T. Roenneberg, A. Wirz-Justice, and M. Merrow, *Life between clocks: daily temporal patterns of human chronotypes,* J. Biol. Rhythm. **18** (2003) 80.

[146] T. Roenneberg, S. Daan, and M. Merrow, *The art of entrainment,* J. Biol. Rhythm. **18** (2003) 183.

[147] S. Archer, D. Robilliard, D. Skene, M. Smits, A. Williams, J. Arendt, and M. von Schantz, *A length polymorphism in the circadian clock gene Per3 is linked to delayed sleep phase syndrome and extreme diurnal preference,* Sleep **26** (2003) 413.

[148] Y. Park, K. Matsumoto, Y. Seo, M. Kang, and H. Nagashima, *Changes of sleep or waking habits by age and sex in Japanese,* Percept. Motor Skill. **94** (2002) 1199.

[149] J. Duffy and C. Czeisler, *Age-related change in the relationship between circadian period, circadian phase, and diurnal preference in humans,* Neurosci. Lett. **318** (2002) 117.

[150] D.-J. Dijk, J. Duffy, and C. Czeisler, *Contribution of circadian physiology and sleep homeostasis to age-related changes in human sleep,* Chronobiol. Int. **17** (2000) 285.

[151] D.-J. Dijk and C. Czeisler, *Contribution of the circadian pacemaker and the sleep homeostat to sleep propensity, sleep structure, electroencephalographic slow waves, and sleep spindle activity in humans,* J. Neurosci. **15** (1995) 3526.

[152] S. Pring and C. Budd, *The dynamics of a simplified pin-ball machine,* IMA J. Appl. Maths **76** (2011) 67.

[153] T. Lynne Barone, *Is the siesta an adaptation to disease?,* Hum. Nature **11** (2000) 233.

[154] A. Ekirch, *At day's close: a history of nighttime,* W.W. Norton & Company, 2005.

[155] B. Galland, B. Taylor, D. Elder, and P. Herbison, *Normal sleep patterns in infants and children: a systematic review of observational studies,* Sleep Med. Rev. **16** (2012) 213.

[156] A. Phillips, C. Czeisler, and E. Klerman, *Revisiting spontaneous internal desynchrony using a quantitative model of sleep physiology,* J. Biol. Rhythm. **26** (2011) 441.

[157] P. Achermann, *Interaction of homeostatic and circadian process: a modeling approach,* J. Sleep Res. **5** (1996).

[158] P. Achermann and A. Borbély, *Combining different models of sleep regulation,* J. Sleep Res. **1** (1992) 144.

[159] A. Borbély, S. Daan, A. Wirz-Justice, and T. Deboer, *The two-process model of sleep regulation: a reappraisal,* J. Sleep Res. **25** (2016) 131.

[160] A. Skeldon and G. Derks, *Nonsmooth maps and the fast-slow dynamics of sleep-wake regulation: part I,* Extended Abstracts Spring 2016: Nonsmooth Dynamics **8** (2017) 167.

[161] G. Derks, P. Glendinning, and A. Skeldon, *Transitions to gaps and non-monotonicity in circle maps,* In preparation(2018).